

DEVELOPMENT OF SMART E-TEXTILE
WEARABLES BY ADVANCED TECHNICAL
EMBROIDERY

A thesis submitted to the University of Manchester for the degree of

Doctor of Philosophy

in the Faculty of Science and Engineering

2022

Yan Zheng

Department of Materials, School of Natural Sciences

CONTENT

Content	2
List of figures	7
List of tables	11
Abbreviations	13
Publications	14
Abstract	15
Declaration	17
Copyright statement	18
Acknowledgement	19
Chapter 1. Introduction	21
1.1 Research background	21
1.2 Objectives and methodologies	23
1.2.1 Sewing ability of silver coated conductive yarns for lock-stitch embroidery.....	24
1.2.2 Flexible and stretchable highly conductive tracks for interconnects in e-textiles. ..	24
1.2.3 Embroidered electrodes on knitted fabrics for real time ECG signal monitoring in body static situation and the impact of wearing pressure.	25
1.2.4 The embroidered strain sensor with combination of conductive yarns and elastic threads to monitor respiratory rate.....	25
1.2.5 A smart band prototype that integrating embroidered electrodes and strain sensors for physiological signal monitoring in static and dynamic situations.....	25
1.3 Significance and originality	26
1.4 Outline of thesis	27
Chapter 2. Literature review	29
2.1 Introduction.....	29
2.2 Mechanisms of machine embroidery	33
2.2.1 Chain-stitch embroidery.....	33

2.2.2	Lock-stitch embroidery	34
2.2.3	Tailored fibre placement (TFP) method.....	36
2.3	Commercial conductive yarns and sewing ability in embroidery process.....	37
2.3.1	Types of conductive yarns and evaluation method for physical properties	37
2.3.2	The sewing ability of conductive yarns for embroidery	39
2.3.3	Performance evaluation of embroidered conductive stitches	40
2.3.4	Challenges in lock-stitch embroidery with conductive yarns	42
2.4	Embroidered connectors and interconnects for integrations.....	43
2.4.1	Embroidered connectors and interconnects	43
2.4.2	Flexible and stretchable interconnects design.....	44
2.4.3	Research gaps in stretchable interconnects by embroidery	47
2.5	Smart e-textile electrodes and sensors fabricated by embroidery.....	47
2.5.1	Embroidered electrodes	48
2.5.2	Embroidered sensors.....	50
2.5.3	Research gaps in embroidered electrodes and sensors	54
2.6	Summary.....	55
Chapter 3. Evaluation of conductive yarns sewing ability on knitted fabrics by lock-stitch embroidery technique.....		57
3.1	Techniques of conductive yarns embroidery on knitted fabrics	57
3.1.1	Introduction.....	57
3.1.2	Experimental details.....	60
3.1.3	Results and discussion	66
3.1.4	Conclusion	72
3.2	Performance evaluation of conductive tracks in fabricating e-textiles by lock-stitch embroidery	72
3.2.1	Introduction.....	73
3.2.2	Experimental details.....	75
3.2.3	Results.....	79

3.2.4	Discussion.....	90
3.2.5	Conclusion	95
	Supporting information.....	96
Chapter 4.	Stretchable interconnects with enhanced conductivity using embroidery techniques	100
4.1	Embroidery parameters to produce conductive tracks for interconnects with enhanced conductivity	100
4.1.1	Introduction.....	100
4.1.2	Experimental work.....	103
4.1.3	Results and discussion	105
4.1.4	Summary.....	110
4.2	Fabrication and performance evaluation of flexible and stretchable interconnects.....	111
4.2.1	Introduction.....	111
4.2.2	Experimental.....	113
4.2.3	Results and discussions.....	120
4.2.4	Summary.....	135
4.3	Conclusion	136
Chapter 5.	Embroidered electrodes design and performance evaluation for ECG monitoring in body static situation.....	138
5.1	Introduction.....	138
5.2	Experimental work.....	140
5.2.1	Materials	140
5.2.2	Design and fabrication of embroidered electrodes	141
5.2.3	Skin-electrode impedance measurements	143
5.2.4	Comparison of ECG monitoring performance under various applied wearing pressure	145
5.3	Results and discussion	147
5.3.1	Effects of electrodes fabrication parameters on skin-electrode contact impedance	147

5.3.2	Effects of different types of embroidered patterns on ECG signal quality	151
5.3.3	Effects of applied wearing pressure on performance of embroidered electrodes	156
5.4	Conclusion	160
	Supporting information.....	162
Chapter 6. Embroidered strain sensor design with conductive yarns and evaluation for respiratory monitoring		166
6.1	Introduction.....	166
6.2	Experimental work.....	168
6.2.1	Materials	168
6.2.2	Design and fabrication of embroidered strain sensor	168
6.2.3	Electromechanical characterization and response optimization of embroidered strain sensors.....	170
6.2.4	Respiration measurement test	171
6.3	Results and discussion	172
6.3.1	Effect of design parameters on mechanical and electrical performance of sensors	172
6.3.2	Electromechanical performance and working mechanism of the embroidered strain sensor	175
6.3.3	Respiration measurement test	179
6.4	Conclusion	181
	Supporting information.....	183
Chapter 7. Effects of wearing pressure and body movements on the ECG and respiration pattern detection of embroidered textile electrodes and strain sensors		189
7.1	Introduction.....	189
7.2	Materials and methods	191
7.2.1	Embroidered electrodes and strain sensor.....	191
7.2.2	Prototype development	192
7.2.3	Experimental protocol.....	193
7.2.4	Data analysis	196

7.3	Results and discussion	197
7.3.1	Effects of wearing pressure on respiratory rate measurements.....	197
7.3.2	Effects of wearing pressure on ECG measurements.....	204
7.3.3	Performance of physiological signal monitoring in walking.....	210
7.4	Conclusion	214
	Supporting information.....	216
Chapter 8.	Conclusions and suggestions for future work.....	220
8.1	Conclusions.....	220
8.2	Limitation.....	222
8.3	Suggestions for future work.....	223
References	224
Appendices	239

Word counts: 52,000

LIST OF FIGURES

Figure 1-1. Diagram of thesis outline.	28
Figure 2-1. Main fabrication methods for E-textile applications.....	31
Figure 2-2. ZSK embroidery machines.....	33
Figure 2-3. Chain-stitch embroidery (Ari).....	34
Figure 2-4. Lock-stitch embroidery..	35
Figure 2-5. TFP embroidery technique..	37
Figure 2-6. Image of conductive yarns.	38
Figure 2-7. Forms of electrically conductive stitches.....	42
Figure 2-8. Interconnects in e-textiles fabricated by embroidery.	44
Figure 2-9. Design and FEM of horseshoe shaped interconnects.....	46
Figure 2-10. Fabrication procedures of the knitted fabric sensing network [83].....	47
Figure 2-11. Dry electrodes fabricated with embroidery techniques.....	50
Figure 2-12. Sensors fabricated with embroidery techniques.....	52
Figure 2-13. Embroidery techniques used with stretchable substrates.	54
Figure 3-1. Structures of conductive yarns and 602 chain-stitch.....	62
Figure 3-2. The long groove structure of Groz-Beckert needle.....	63
Figure 3-3. Load extension behaviour of different threads.....	66
Figure 3-4. The appearance of 602 chain-stitch with conductive yarns as looper thread.....	69
Figure 3-5. Regression analysis of yarn diameters and needle blade diameters.....	71
Figure 3-6. The images of needle cut in fabric.	72
Figure 3-7. Embroidery test pattern with the studied stitch directions.	77
Figure 3-8. Optical microscope images of sample surface.	81
Figure 3-9. Floated stitch numbers analysis in embroidered conductive tracks.....	83
Figure 3-10. Size shrinkage (%) of embroidered tracks.	85
Figure 3-11. Electrical resistance of embroidered conductive tracks.	87
Figure 3-12. Overlaid contour plot of minimum number of float stitches and the lowest	

electrical resistance per 10 cm.	89
Figure 3-13. Illustration of lock-stitch embroidery mechanism and conductive yarns' characteristics.....	93
Figure 3-14. SEM and EDX analysis of conductive yarns before and after embroidery.....	94
Figure 4-1. Schematic of the types of stitch used in study.....	104
Figure 4-2. Factor influence on resistance of conductive tracks embroidered.	106
Figure 4-3. Effects of Factors A versus B with threads (a) HC 12, and (b) HC 40.	107
Figure 4-4. Schematic illustration of electrical circuit model.....	109
Figure 4-5. Schematic illustration of interconnects pattern designs.	115
Figure 4-6. Schematic drawings of interconnects fabrication techniques.	117
Figure 4-7. Testing instruments for stretchable interconnects.	119
Figure 4-8. Typical curve line to show (a) the tensile force change and (b) resistance change of an interconnect.....	120
Figure 4-9. Tensile main effects analysis of zigzag shaped interconnects.....	122
Figure 4-10. Tensile main effects analysis of horseshoe shaped interconnects.	123
Figure 4-11. Resistance analysis of interconnects.	125
Figure 4-12. Schematic illustration of designs with the relevant segments and dimensions indicated.....	126
Figure 4-13. Electromechanical properties of the embroidered interconnects.	129
Figure 4-14. Mechanical and electronic model of selected zigzag shaped interconnects.	131
Figure 4-15. The electromechanical curve and stress simulated diagram of best performed horseshoe-shaped interconnects.....	132
Figure 4-16. Dynamic stretching endurance test results in 500 cycles.....	134
Figure 4-17. Demonstration of wearability with a LED circuit that maintained conductivity.	135
Figure 5-1. Diagram of filling stitch in electrodes.....	142
Figure 5-2. Optical microscope images of embroidered electrodes.	142

Figure 5-3. Double time constant skin-electrode interface and electrical equivalent circuit [161].	143
Figure 5-4. Two-electrode configuration for skin-electrode impedance measurement.	144
Figure 5-5. The ECG monitoring method.	146
Figure 5-6. Measurement details for wearing pressure.	147
Figure 5-7. Factorial analysis of electrodes design effects on measured impedance at 1 Hz.	149
Figure 5-8. Plot of the skin-electrode contact impedance magnitude versus frequency.	151
Figure 5-9. Prototype of band for ECG measurement.	152
Figure 5-10. Analysis of ECG signal quality.	153
Figure 5-11. Comparison of ECG waveforms measured by EP2 electrode and Ag/AgCl electrode with wearing pressure.	156
Figure 5-12. Skin-band pressure and blood flow analysis.	157
Figure 5-13. Experiment details to measure friction force.	158
Figure 5-14. Factorial analysis of SCF and DCF.	160
Figure 6-1. Process of the strain sensor embroidery combined with two techniques.	169
Figure 6-2. Factorial analysis of the sensor's design effects on GF and EC.	174
Figure 6-3. Electro-mechanical behaviour of the HESS.	177
Figure 6-4. Image and schematic diagram of HESS.	178
Figure 6-5. Respiratory signal from HESS (colour in red) and pressure sensor (colour in black).	181
Figure 7-1. Image of the embroidered electrode and strain sensor.	192
Figure 7-2. Image of the smart band and accessories.	193
Figure 7-3. Images of the subject test.	195
Figure 7-4. Respiratory waveform and frequency spectrum of Subject 1 in sitting and standing	199
Figure 7-5. Respiratory rate value statistics in static measurement of (a) Subject 1, (b) Subject	

2, (c) Subject 3.	200
Figure 7-6. Respiratory waveform and frequency domain of Subject 1 started waving arms with 0.5 kPa WP.	201
Figure 7-7. Respiratory waveform and frequency domain of Subject 1 started waving arms with 1.5 kPa WP.	202
Figure 7-8. Respiratory waveform and frequency domain of Subject 1 started waving arms with 2.5 kPa WP.	203
Figure 7-9. Respiratory rate value in dynamic measurement of (a) Subject 1, (b) Subject 2, and (c) Subject 3.	204
Figure 7-10. Representative ECG signals of Subject 1 in sitting and standing with different wearing pressure.	205
Figure 7-11. Sensitivity of QRS detection in static measurement condition.	206
Figure 7-12. Representative ECG signals of Subject 1 in dynamic measurement conditions at 0.5 kPa wearing pressure.	207
Figure 7-13. Representative ECG signals of Subject 1 in dynamic measurement conditions at 1.5 kPa wearing pressure.	208
Figure 7-14. Representative ECG signals of Subject 1 in dynamic measurement conditions at 2.5 kPa wearing pressure.	209
Figure 7-15. Difference of QRS detection in static measurement condition (a) sensitivity and (b) accuracy.	210
Figure 7-16. Representative plots of raw ECG waveforms from the smart band while the subject is standing stationary, walking on a treadmill.	212
Figure 7-17. The body-clothing microclimate temperature(°C) and relative humidity (%) during the walking test with the participant wearing (a) T-shirt and (b) fleeced hoodie.	212
Figure 7-18. Plots of the filtered resistance changes measured from the smart band while the subject is standing stationary, walking on the treadmill.	214

LIST OF TABLES

Table 2-1. Smart e-textile fabrication techniques	32
Table 2-2. A list of suppliers of conductive yarns.....	38
Table 2-3. Physiological signals that may be measured using textile-based sensors [92].....	48
Table 3-1. The type of commercial conductive yarns and physical properties.....	61
Table 3-2. The characteristics of the knitted fabric used.	64
Table 3-3. Point types of GROZ-BECKERT needle for embroidery [111]	65
Table 3-4. Needle cut test variables and levels	65
Table 3-5. Mean values of mechanical properties of threads.....	67
Table 3-6. Results of calculated maximum diameters of conductive yarns could be used with GROZ-BECKERT needles	70
Table 3-7. The diameter of conductive yarn and suitable needle size	71
Table 3-8. Physical properties of silver-coated polyamide yarns	76
Table 3-9. Properties of the knitted fabric used.	76
Table 3-10. Factorial design of selected embroidery parameters and levels for the experiment.	78
Table 3-11. Samples and corresponding experimental specifications.	78
Table 3-12. Multi-linear regression equations based on significant factors.	88
Table 3-13. Multiple response prediction of embroidery parameters	89
Table 3-14. Validated results of embroidery parameters.....	90
Table 4-1. Physical properties of silver coated polyamide threads.....	103
Table 4-2. Factors and levels used in full-factorial experimental design	105
Table 4-3. Summary of ANOVA response for full-factorial experimental design.....	105
Table 4-4. Resistance comparasion of conductive interconnets embroidered with HC 12 ...	108
Table 4-5. Resistance comparasion of conductive interconnets embroidered with HC 40 ...	108
Table 4-6. Physical properties of conductive yarns	114
Table 4-7. Experimental factors and levels for interconnects design	116

Table 4-8. Statistical analysis of tensile properties of interconnects	121
Table 4-9. Statistical analysis of electrical properties of interconnects	124
Table 4-10. Statistical analysis of electromechanical properties of interconnects.....	127
Table 5-1. Factors and levels used in full-factorial experimental design	142
Table 5-2. Electrodes design variables and impedances in the second step experiment.	150
Table 6-1. Factors and levels used in strain sensors design.....	170
Table 6-2. Patterns of respiration of this study	172
Table 6-3. Solution and multiple response prediction for requested optimization.	175
Table 7-1. Demographic information and body measurements of participants	194
Table 7-2. Design of selected evaluation parameters and levels for the experiment.....	197

ABBREVIATIONS

ECG	Electrocardiogram
EEG	Electroencephalogram
EMG	Electromyography
TFP	Tailored fibre placement
DOE	Design of experiment
PDMS	Polydimethylsiloxane
LED	Light-emitting diode
RRI	Interval times of two adjacent R peak of ECG waveforms
QRS	QRS complexes of ECG waveforms
PH	Height of P wave in an ECG waveform
RH	Height of R wave in an ECG waveform
SCF	Static coefficient of friction
DCF	Dynamic coefficient of friction
PVA	Polyvinylalcohol
GF	Gauge factor
EC	Elasticity coefficient
FFT	Fast Fourier transformation

PUBLICATIONS

Yan Zheng, Lu Jin, Jing Qi, Zekun Liu, Lulu Xu, Steven Hayes, Simeon Gill, and Yi Li. “Performance Evaluation of Conductive Tracks in Fabricating E-Textiles by Lock-Stitch Embroidery.” **Journal of Industrial Textiles**, 2020,7. doi.org/10.1177/1528083720937289.

Zekun Liu, **Yan Zheng**, Lu Jin, Kaili Chen, Heng Zhai, Qiyao Huang, Zhongda Chen, Yangpeiqi Yi, Muhammad Umar, Lulu Xu, Gang Li, Qingwen Song, Yi Li. “Highly Breathable and Stretchable Strain Sensors with Insensitive Response to Pressure and Bending,” *Advanced Functional Materials*, 2021,14,2007622(1-9). doi: 10.1002/adfm.202007622.

Yan Zheng, Lu Jin, Ze-Kun Liu, Jing Qi, Yi Li, Embroidery Parameters to Produce Conductive Tracks with Enhanced Conductivity. The 13th Textile Bioengineering and Informatics Symposium Proceedings, July 7-10, 2020, webinar, 107-113.

ABSTRACT

Applications of wearable electronic textiles (e-textiles) in smart clothing have attracted considerable attention on account of their immense potential to monitor vital signals, such as electrocardiogram (ECG) and respiratory rate. Embroidery is one of the most preferred ways to create e-textiles because the technique allows for flexible patterns, dimensional accuracy, mass production, and cost-effective production. However, the parameter design of embroidery with conductive yarns not only affects the aesthetics of the product but also results in incompetent electrical performance, such as short out of interconnects because the jammed stitches. This thesis proposes embroidery techniques for the design and construction of stretchable interconnects, electrodes and strain sensors used for ECG and respiration signals monitoring.

The thesis focuses on several key aspects for design and fabrication of smart e-textile wearables. 1) After comparing needle thread loop formation performance of various commercial conductive yarns, the analysis of conductive tracks with multi-direction lock-stitch embroidery indicated embroidery direction and stitch length significantly affect size shrinkage, stitch length and embroidery speed significantly affect resistance of conductive tracks. Stretchable interconnects are designed with zigzag and horseshoe shaped structures, which fabricated by lock-stitch and TFP embroidery techniques, respectively. The horseshoe-shaped interconnect proposed in this study ($R = 5\text{mm}$ and $\theta = 45^\circ$) shows significant elongation over 130% and maintain stable resistance during stretching. 2) The electrodes are embroidered by silver-coated conductive yarns with different embroidery patterns, filling density and sizes. The skin contact impedance at 1 Hz, and signal quality of ECG monitoring compared with Ag/AgCl electrodes are evaluated. The EP2 pattern electrode shows the lowest surface resistance under 2.5 kPa wearing pressure since the conductive threads overlapped in filling stitch structures. 3) The embroidered strain sensors combining conductive yarns and elastane threads are designed in conjunction with lock-stitch and TFP embroidery techniques. The electromechanical

performance of optimal sensor shows 32.4 GF at 40% elongation, less electro-mechanical hysteresis and stable stretching-releasing performance within 1000 cycles. The sensor has sufficient capability to clearly detect normal breathing and deeply slow breathing patterns. 4) Based on the design concept of embroidered electrodes and strain sensors, a wearable smart band prototype for physiological signal monitoring is developed. Wearing pressure at 1.5 kPa can ensure the quality of ECG and respiratory signals in body static and dynamic measurement conditions. Additionally, the walking tests demonstrate that the smart band under 1.5 kPa wearing pressure was able to measure representative respiratory and ECG waveform features, body temperature and humidity at various levels of treadmill speed.

The outcome from this research provides guidelines for development and fabrication of tailored smart e-textiles wearables for health care with highly efficient embroidery techniques.

DECLARATION

No portion of the work referred to in this thesis has been submitted in support of an application for another degree or qualification of this or any other university or other institutes of learning.

COPYRIGHT STATEMENT

- i. The author of this thesis (including any appendices and/or schedules to this thesis) owns certain copyright or related rights in it (the “Copyright”) and s/he has given The University of Manchester certain rights to use such Copyright, including for administrative purposes.
- ii. Copies of this thesis, either in full or in extracts and whether in hard or electronic copy, may be made only in accordance with the Copyright, Designs and Patents Act 1988 (as amended) and regulations issued under it or, where appropriate, in accordance with licensing agreements which the University has from time to time. This page must form part of any such copies made.
- iii. The ownership of certain Copyright, patents, designs, trademarks and other intellectual property (the “Intellectual Property”) and any reproductions of copyright works in the thesis, for example graphs and tables (“Reproductions”), which may be described in this thesis, may not be owned by the author and may be owned by third parties. Such Intellectual Property and Reproductions cannot and must not be made available for use without the prior written permission of the owner(s) of the relevant Intellectual Property and/or Reproductions.
- iv. Further information on the conditions under which disclosure, publication and commercialization of this thesis, the Copyright and any Intellectual Property and/ or Reproduction described in it may take place is available in the University IP Policy (See <http://www.campus.manchester.ac.uk/medialibrary/policies/intellectual-property.pdf>), in any relevant Thesis restriction declarations deposited in the University Library, The University Library’s regulations (see <http://www.manchester.ac.uk/library/aboutus/regulations>) and in The University’s policy on presentation of Thesis.

ACKNOWLEDGEMENT

I would like to express my sincere gratitude to my chief supervisor, Prof. Yi Li, for the endless support of my Ph.D. study. He has guided me in design of experiment, the methodology to carry out the experiment and the effective way to present the research work. He gave me advice, inspirations, encouraged me to explore a new area. Working with him, I learnt not only for the knowledge of research, but also the ways of thinking and living.

I would also thank my co supervisors, Dr. Simeon Gill and Dr. Steven Hayes, for their guidance and encourage on my work. My special thanks are given to Dr. David Hall, Dr. Xiaogang Chen, Dr. Celina Jones, Dr. Lisa Taylor, Dr. Jiashen Li, Prof. Rantong Liu, Prof. Bo'an Ying, and Prof. Xin Zhang for their valuable advices on my study. My great thanks go to Mr. Tim Jun Li from Digital Clothing Ltd, and Mr. Hai Guo from the HDWTECH company, Ltd. for the coordinating the development of the prototype products. I am also grateful to Mrs. Fiona Colton, Mr. Mark Chadwick and Mr. Stuart Morse for training me for samples fabrication and testing. I am grateful to Ms. Melanie Hoerr, Ms. Britta Sanders and Mr. Paul Tood from ZSK Machines, Ltd. for their assistance in embroidery. Thanks also go to Mr. Lu Chen and Mr. Kaosheng Deng from Shenzhen Smart Clothing Technology Ltd. for their help and design advises on e-textiles.

I am very thankful to my group members, including Dr. Lu Jin, Dr. Zekun Liu, Dr. Lulu Xu, Dr. Zhangchi Liu, Ms. Sirui Yao, Dr. Yangpeiqi Yi, Dr. Heng Zhai, Mr. Qinghong Huang, Dr. Yangyang Fan, Dr. Muhammad Umar, and Dr. Zhongda Chen for their kind help, insightful comments and collaborations. My special thanks are directed to Ms. Jing Qi, Ms. Yan Ren, and Ms. Qingwen Song from Xi'an Polytechnic University; Prof. Luoyan Hu, Ms. Yan Wang, Ms. Qi Zhen, Miss Xiaoxiao Hao, Mr. Yongliang Liu, Mr. Yazhou Zhang, Dr. Fan Xiong, and Ms. Qian Zheng from Zhongyuan University of Technology for their kind help to my research.

My special thanks are given to my parents, Shuwu Zheng and Shulan Chen, for their unconditional love, encouragement, patience and continuing support to complete my Ph.D.

study successfully.

My Ph.D. research is funded by Zhongyuan University of Technology, and supported by the EU Horizon 2020 program- project code 644268 - ETEXWELD - H2020-MSCA-RISE-2014, and the Cotton Textiles Research Trust for the “Protective Efficiency of Respiratory Protective Equipment against Byssinosis for Cotton Workers” project R119938. Also, I would like to thank Digital Clothing Ltd. and Xi’an Polytechnic University to provide support in developing the prototype product for the study. I would like to express my grateful to those funding sources that give me this great opportunity for carrying out this research in the University of Manchester.

CHAPTER 1. INTRODUCTION

1.1 Research background

Over the last few decades, wearable electronics integrated into textiles has undergone a rapid revolution toward flexible and stretchable electronics with superior mechanical compatibility with the human body and human-machine interactions [1–5]. Within recent years, research and development have been carried out on creating textile-based physiological signal monitoring sensors and electrodes to monitoring firefighter’s physiological signals without skin irritation [6–8]. The methods of integrating electrodes, sensors, interconnects and electronic modules into flexible fabric pieces were important since they have significant influence on wearing comfort and durability of smart wearables [9].

Among the different methods for creating e-textiles, embroidery is one of the most preferred ways because the technique allows for flexible patterns [10, 11], dimensional accuracy, mass production, and cost-effective production. Therefore, embroidery has been widely used to create high-performance textile electrodes [12–15], circuits [16, 17] and sensors [18–21]. This fabrication method could be effectively used to obtain a low-cost performance tailored e-textile wearables as well. However, the deformation of the fabric during sewing increases the unevenness of the stitch tracks and causes size discrepancies between the embroidered element and the digital design. This not only negatively affects the aesthetics of the product but also results in inconsistent levels of electrical resistance, which severely reduces the performance of smart wearables.

For wearable technology, and generally for smart garment development, electronic systems with stretchable interconnects are designed in conformity to soft 3D surfaces in order to maintain the original mechanical properties of textile substrate, which make them accommodate body movement [22]. Therefore, strategies are required to efficiently develop customized stretchable interconnects and preferably integrate into smart garments with other

electronic components during the fabrication process. Numerous researchers have demonstrated fabrication techniques during the fabric formation processes such as weaving and knitting [23, 24], or pattern conductive polymer (or nanomaterials) into elastic fabrics [25–27] to maintain its inherent properties. Unlike knitting techniques that only allow interconnects in the length and/or cross directions, embroidery techniques provide extraordinary and sophisticated capabilities for multi-directional interconnect design and have been successfully used in circuit integration of wearable electronics [28–30]. However, the stretchability and electrical properties of stretchable interconnects via embroidery techniques were not investigated.

The embroidered electrodes can minimize skin irritation and discomfort, particularly when used over prolonged time periods[13, 31]. Previous studies have shown that the embroidered electrodes were reliable and demonstrated applications in electrocardiogram (ECG), electroencephalogram (EEG) and electromyography (EMG) monitoring [12–14, 31]. Compared with knitted and woven electrodes, embroidered electrode has a good contact with the skin and well suited for measuring ECG especially in dry skin condition [32]. Moreover, pressures exerted on the electrodes could reduce the motion artefact hence helping achieve higher signal quality [33]. However, different embroidery patterns, which were structured by various contact methods of conductive yarns, could have effects on the contact impedance of electrodes. Moreover, the higher contact pressure may have influence on the wearing comfort.

A wearable strain sensor can detect the relative change in electrical resistance according to human motions to monitor the pulse, joint movements, walking, and breathing [34–36]. Recent studies on textile strain sensors explored the uses of polyurethane (PU), poly styrene-butadiene-styrene (SBS), polydimethylsiloxane (PDMS) and spandex for the stretchable component. Knitting [37, 38], printing [39], and dip coating [40, 41] are applied to fabricate the textiles with the integrated strain sensor. Although these strain sensors show excellent characteristics stretchability and sensitivity, they can cause skin irritation due to their low air-permeability, which is the natural character of polymeric compounds [42, 43]. Stitch-based strain sensors

have an advantage in that they are comfortable to wear and can detect human motion over a long measurement period because they have better wearability and air-permeability than other materials [44, 45]. However, the strain of sensors was limited by elasticity of textile substrates, structures of stitches, and conductive yarns used. The structure of stitch-based strain sensors that can be directly integrated to smart wearables needs to be developed. Therefore, the application of embroidering conductive yarns with elastic threads for strain sensors still needs exploring.

Based on studies mentioned above, a smart band that integrate electrodes, strain sensors to monitor ECG and respiratory rate will be developed. Cardiovascular events are the leading cause of death among firefighters [46]. The ECG is a widely studied physiological signal and long-term ECG measurements can be used for the examination of all electrical processes in the heart [47, 48]. Respiratory monitoring has been widely applied in healthcare settings as a vital sign, and it can be measured by wearing a strain gauge on the chest [49]. The final smart band prototype will integrate electrodes, strain sensors and stretchable interconnects by combining lock-stitch and tailored fibre placement (TFP) embroidery techniques. This hybrid fabrication methods can be used in garment industry for tailored and mass production.

1.2 Objectives and methodologies

The aim of this research is to fill the research gaps for developing a detachable smart band for ECG and respiratory rate monitoring by embroidering silver coated conductive yarns to construct electrodes and strain sensors. To fulfil the research aim, the following objectives have been identified:

- 1) To evaluate the sewing ability of silver coated conductive yarns for lock-stitch embroidery.
- 2) To develop flexible and stretchable highly conductive tracks for interconnects in e-textiles.
- 3) To develop embroidered electrodes on knitted fabrics for real time ECG signal monitoring in body static situation and to investigate the impact of wearing pressure.

- 4) To develop an embroidered strain sensor with combination of conductive yarns and elastic threads to monitor respiratory rate.
- 5) To develop a smart band prototype that integrating embroidered electrodes and strain sensors for physiological signal monitoring in static and dynamic situations.

To achieve the objectives, the following research methodologies are adopted:

1.2.1 Sewing ability of silver coated conductive yarns for lock-stitch embroidery.

The needle thread loop formation performance of various conductive yarns will be evaluated by tensile test and 602 stitch sewing. The needle size and safety of needle cutting for knitted fabrics will be determined. The selected conductive yarns will be embroidered to study the appearance quality, dimensional stability and electrical resistance of conductive tracks in different directions. The influence of the embroidering speed, stitch length, needle thread pre-tension and embroidering direction as well as their interactions will be evaluated via factorial design of experiment (DOE). According to the results of DOE analysis, an optimal parameter combination for the conductive tracks with balanced appearance quality and lower electrical resistance is to be sought.

1.2.2 Flexible and stretchable highly conductive tracks for interconnects in e-textiles.

The electrical resistance of conductive tracks is to be evaluated by embroidering with parameters including three types of stitch, the position of conductive threads and sewing repeated times of stitches. The result with variables to reach highly conductive tracks will be used for further stretchable interconnects study. Stretchable conductive tracks will be designed with zigzag and horseshoe shaped structures, and fabricated by lock-stitch and TFP embroidery techniques, respectively. The influence of the arm length and opening angle of a zigzag structure, the inner radius and turning angle of a horseshoe structure on the tensile property of interconnects are to be evaluated. According to the results of design of experiment analysis, the electromechanical performance of interconnects with different design parameters are to be investigated.

1.2.3 Embroidered electrodes on knitted fabrics for real time ECG signal monitoring in body static situation and the impact of wearing pressure.

The electrodes with design parameters including embroidery pattern, filling density and size will be prepared. The effects of electrodes' design parameters on skin contact impedance at 1 Hz are to be compared to find optimal structures with lower impedance. The relationship between the embroidered structures and the contact impedance, ECG signal quality will be investigated using two channel ECG measurement module (BN-ECG2) in BIOPAC MP160 to compare with Ag/AgCl electrodes. The consistency will be evaluated by Pearson product-moment correlation coefficient, time intervals and peak height of ECG waveforms. The influence of three levels of wearing skin pressure on the ECG signal quality will be evaluated by the signal's consistency and changes of blood flow index.

1.2.4 The embroidered strain sensor with combination of conductive yarns and elastic threads to monitor respiratory rate.

A novel textile-based strain sensor that combining conductive yarns and elastane threads are to be proposed by embroidery techniques. The strain sensors with different width of conductive area, filling density of conductive yarns and density of elastane threads will be prepared via surface response DOE. The relationship between design parameters and mechanical and electrical characteristics of sensor will be investigated. Then the gauge factor and elasticity coefficient will be used to determine the optimal fabrication conditions for sensors to monitor human respiration. A comparative experiment with a commercial airbag pressure sensor (AMI 9002) will be performed to evaluate the respiratory measurement performance for three breathing patterns.

1.2.5 A smart band prototype that integrating embroidered electrodes and strain sensors for physiological signal monitoring in static and dynamic situations.

A novel design strategy was adopted to fabricate a smart band using embroidered electrodes,

strain sensor to monitor physiological signals including ECG, respiratory rate, body temperature and humidity. The electronic module of the smart band, which can wirelessly collect and send data will be developed by the 3rd cooperation partner. The relationship between wearing pressure and signal quality will be explored in static and dynamic conditions by subject tests. In addition, the smart band prototype will be used to detect changes of physiological signals via wear trials on a treadmill with various speed.

1.3 Significance and originality

- 1) The study provides a simple and accessible method to evaluate the possibility of conductive yarns used in the machine embroidery. The optimal embroidery parameters guide successful embroidery with conductive yarns in industry. Part of this work has been published on *Journal of Industrial Textiles* (DOI: 10.1177/1528083720937289) entitled “Performance evaluation of conductive tracks in fabricating e-textiles by lock-stitch embroidery”.
- 2) A circuit model for the embroidered conductive tracks to develop interconnects is developed. The embroidered pattern provided stretchability of interconnects is designed and fabricated, and can be tailored for smart clothing. Part of this work has been published on *Textile Bioengineering and Informatics Symposium Proceedings (2020)* (DOI: 10.3993/tbis2020) entitled “Embroidery parameters to produce conductive tracks with enhanced conductivity”.
- 3) This study designs embroidered patterns for electrodes, and presents subject test protocols to study influence of real-time wearing pressure on signal quality of ECG and blood flow under static and dynamic conditions. This can guide further research on textile-based dry electrodes development and application on smart clothing for physiological monitoring.
- 4) This research develops an embroidered strain sensor, which is air-permeable and can directly sew into a clothing. The proposed smart band has integrated electrodes, a strain

sensor and electronic temperature and humidity sensor. This band provide a wireless E-textile wearables to measure physiological signals in field, including ECG, respiration patterns, body temperature and humidity.

1.4 Outline of thesis

This thesis consists of eight chapters, as shown in Figure 1-1. Chapter 1 introduces the research background, objectives, and methodologies. Chapter 2 reviews the applications of embroidery techniques on smart e-textiles research and development to draw important knowledge gaps. Chapter 3 explores sewing ability of conductive yarns and find proper technique parameters for lock-stitch embroidery on knitted fabrics. Chapter 4 investigates an optimal embroidery design to achieve enhanced conductivity of interconnects, and stretchable performance of interconnects embroidered with zigzag shape and horseshoe shaped pattern respectively. Chapter 5 fabricates electrodes with four types of patterns, the performance of dry electrodes for ECG signal monitoring in static condition. Chapter 6 focuses on designing a hybrid embroidered strain sensor for respiration signals measurement. Chapter 7 demonstrates a developed smart band was used for ECG and respiratory rate monitoring in static and dynamic measurement using embroidered electrodes and strain sensor. Chapter 8 presents conclusions and suggestions for future work.

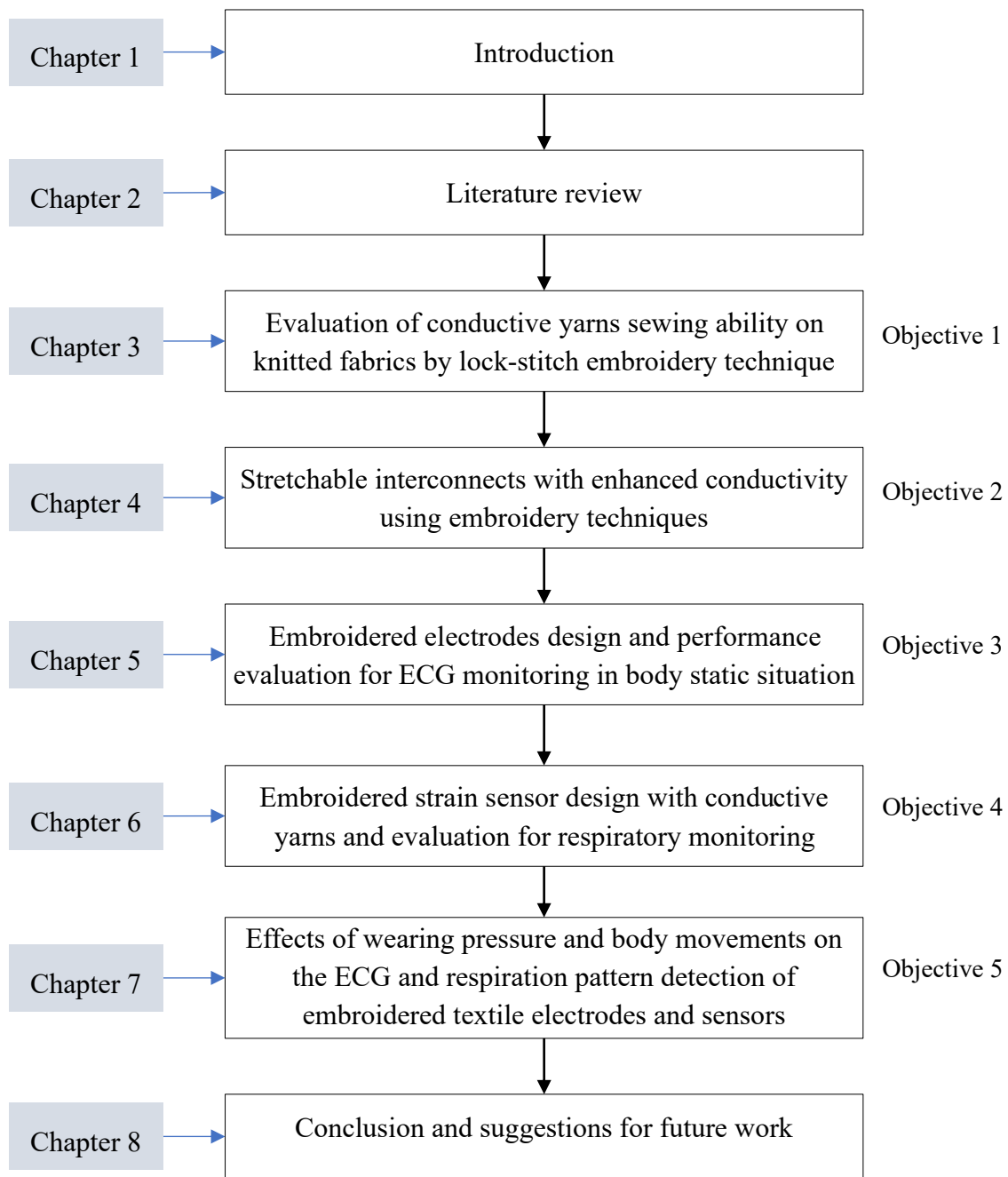


Figure 1-1. Diagram of thesis outline.

CHAPTER 2. LITERATURE REVIEW

2.1 Introduction

The smart e-textiles can be made with several materials using different fabrication methods. The selected materials and fabrication methods are always related to the final application [9]. Depending upon the different approaches adopted, e-textiles are also called smart textiles, intelligent textiles, wearable electronics, and wearable computers. Over the past decade, it has been proved that traditional fabrication methods that are used to produce conventional textiles could be used in e-textiles production too [50]. Thanks to the development of flexible conductive yarns and conductive nanoparticles inks, the sensing conductive materials integration processes into conventional textiles can be done automatically through weaving [51–53], knitting [24, 54, 55], printing [26, 56, 57] and embroidery [12, 58, 59], examples of which are shown in Figure 2-1.

The process of embroidering allows threads to be arranged on a flat substrate in any direction, thus enabling the production of any desirable textile form [10]. As opposed to weaving, where threads are arranged at rigid angles, embroidery also enables rounded patterns. Additionally, made-up embroidery goods are dimensionally stable — unlike knitted fabrics. Modern embroidery machines are equipped with automatic thread change devices, enabling switching from one material component to another during the course of production. Table 2-1 compares weaving, knitting, printing and embroidery as smart e-textile fabrication methods.

Embroidery is a very versatile, fast, and effective way to fabricate e-textile wearables; however, it may suffer friction between the threads and the needles, causing yarn breaks and discontinuities at higher level of embroidery speed and pretension of thread [60]. Nevertheless, some researches and commercial products have been developed and launched using current technologies. A Swiss company, *Forster Rohner*, has been supplying the market with integrated LEDs by embroidery techniques such as e-broidery[®] illuminated textiles since 2013 [61]. The

company *ZSK Stickmaschinen GmbH* and the research institute *TITV Griez* demonstrated the automatic manufacturing of light-emitting textiles via embroidery and LEDs[60]. The following sections review the progress and research gaps of research and development in e-textiles with embroidery techniques.

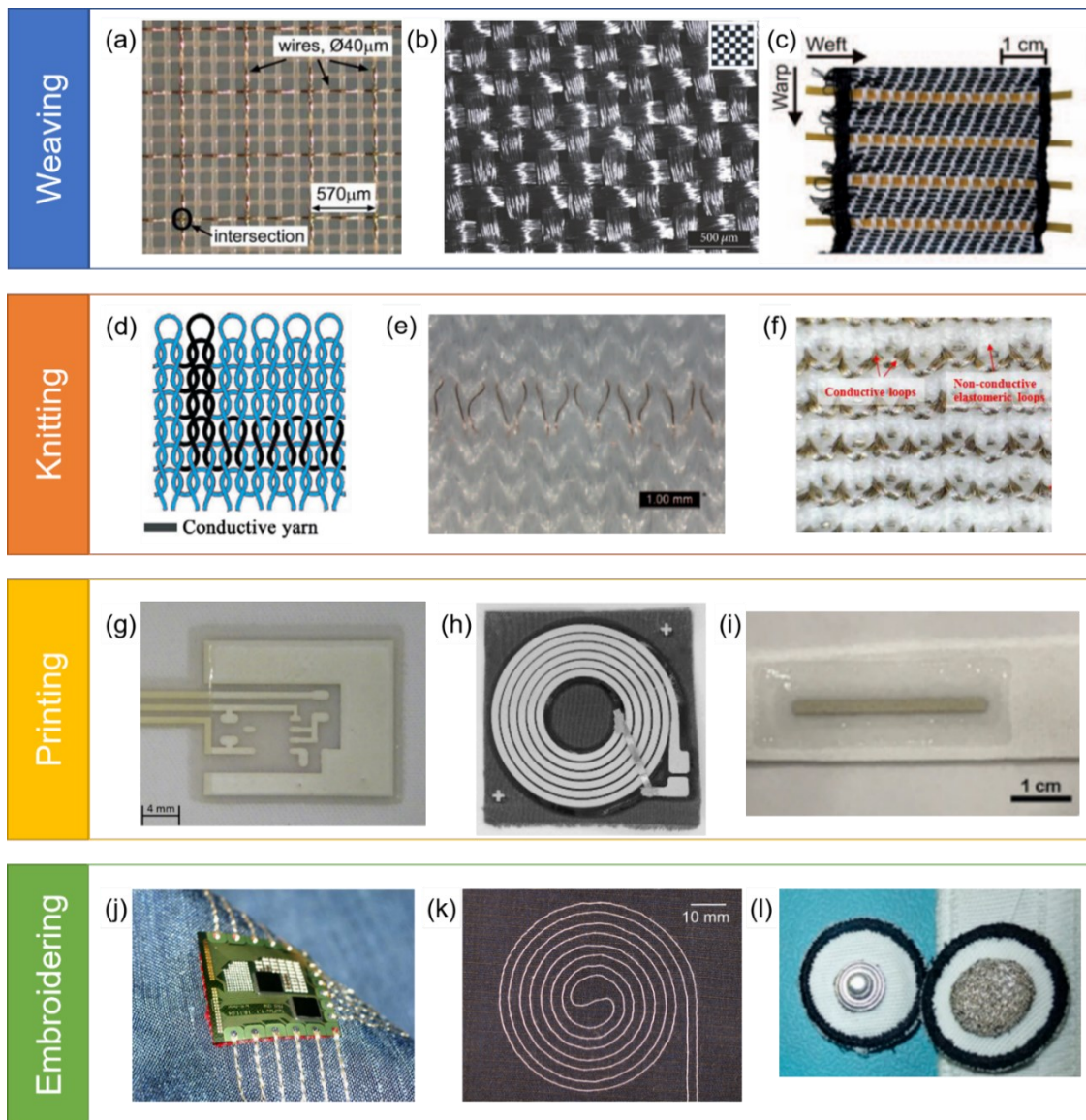


Figure 2-1. Main fabrication methods for E-textile applications. (a) PETEX hybrid fabric[51]; (b) Plain woven fabric with pure conductive yarns used as electrodes [52]; (c) Woven textile band with integrated flexible plastic strips [53]; (d) Design of turning routing with intarsia knitting technique [54]; (e) Interlaced interconnect for three-dimensional curvilinear surfaces [24]; (f) Technical face of sensor design includes conductive & elastomeric yarns [55]; (g) The screen printed base for a printed active electrode[56]; (h) Printed coil for inductive power transfer[57]; (i) Screen printing of Ag paste for textile electrode[26]; (j) Flexible substrate with metalized contact pads interconnected with embroidery[58]; (k) Embroidered temperature sensor[59]; (l) Removable embroidery electrodes[12].

Table 2-1. Smart e-textile fabrication techniques

	Advantages	Disadvantages	Key challenges
Weaving	<ul style="list-style-type: none"> • Produce conductive structures simultaneously during the fabric making process; • Can be automated, or made in a hand loom to create a two-layer electrical design [58]; • More stable size [52]; • Conductive yarns traverse through different layers; • Less demand on the thread stability [58]. 	<ul style="list-style-type: none"> • Limited in the freedom of routing the conductive thread. The conductive connections need to follow the warp and/or weft structure direction and is not suitable for coil geometries[57]; • Stiff and brittle soldered connectors with other components. 	<ul style="list-style-type: none"> • The mechanical durability of the woven fabric.
Knitting	<ul style="list-style-type: none"> • Produce conductive structures during the fabric making process; • Feasible to ‘ knit’ stretchable interconnectors with a more complex arbitrary route; • High level stretchability with high comfort. 	<ul style="list-style-type: none"> • Additional yarn requirements to form loops leading to a larger resistance. • Stiff and brittle soldered connectors with other components. 	<ul style="list-style-type: none"> • Pre-design of pattern; • The resistance changes when knitted fabric was stretched.
Printing	<ul style="list-style-type: none"> • Precisely specify the circuit, connections and sensors; • Flexible and versatile. 	<ul style="list-style-type: none"> • Nozzle clogging occur in inkjets; • High costing; • Rough surface of fabric has negative impact. 	<ul style="list-style-type: none"> • Conductive materials used; • Technique settings help transfer of conductive paste.
Embroidery	<ul style="list-style-type: none"> • Precisely specify the circuit layout and stitch patterns; • Control and integrate of yarns with different linear density, twist and electrical properties; • Easy to set up, and make tailoring design [58]; • Adapt to almost all types of conductive yarns in tailored fibre placement embroidery; • Eco-friendly process. 	<ul style="list-style-type: none"> • Stretchable performance relied on the pattern design; • Thread and needle diameters affect the accuracy; • Failed mechanically and electrically within 20–30 % strain in standard embroidery[9]. 	<ul style="list-style-type: none"> • Suitable embroidery parameter settings according to the application.

2.2 Mechanisms of machine embroidery

Three types of embroidery methods are currently used in the market, i.e., chain-stitch embroidery, lock-stitch embroidery and tailored fibre placement (TFP). All three classes of embroidery are typically used when attempting to increase productivity in automated manufacturing[62]. There are various machine configurations available, including up to 11 parallel embroidery heads for TFP, and more than 56 parallel heads for lock-stitch embroidery. Figure 2-2 shows typical embroidery machines from ZSK Stickmaschinen GmbH, Krefeld, Germany.



Figure 2-2. ZSK embroidery machines. (a) Chain-stitch embroidery/ K-Head series; (b) Multi-head standard embroidery/ F-Head series; (c) Tailored fibre placement/ W-Head series [63].

Potential applications of the technology range from decorative embroidery in carpeting and tablecloths to TFP embroidery for resistive automotive seat heating systems[64]. Due to this productivity performance, embroidery technology is poised to further functionalise e-textiles.

2.2.1 Chain-stitch embroidery

The chain-stitch, also known as the Ari stitch, has been found to be particularly interesting in the construction of textile-based sensors. It is generally used for constructions such as kettle and moss embroidery because its surface structures were highlighted onto substrate textiles [62]. As shown in Figure 2-3(a), chain-stitch embroidery is created by a single-thread system. In this system, the needle goes through the carrier material and pulls the thread out from under the needle, plate side up. Then, a loop is created by a rotary motion of the needle on the upper side of the carrier material. Repeating this pattern frequently, and with tight density, produces

a moss-like surface [62].

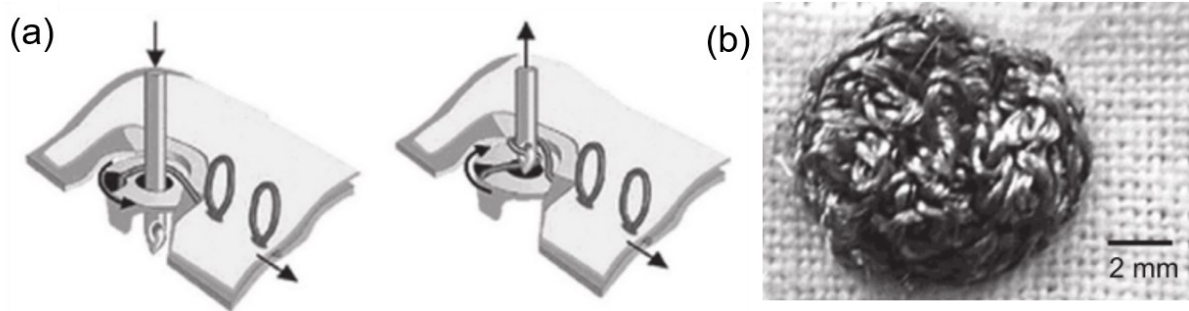


Figure 2-3. Chain-stitch embroidery (Ari). (a) Principle of moss embroidery; (b) Textile electrode obtained by moss embroidery [65].

Chain-stitch embroidery is particularly important when creating textile-based contact sensors. When the single-thread system utilises a conductive thread, the moss embroidery can be used to build a three-dimensional structure like the electrodes shown in Figure 2-3(b) [65]. These electrodes can be used as sensor electrodes for body signal monitoring such as ECG, EEG or EMG. The disadvantage of this method is that because of the inherent mechanical properties of the one-thread system, the embroidering can behave like a knitted textile. This is particularly undesirable in sensor technology, because a break in the conductive thread could lead a break in the entire sensor unit, causing failure of the sensor [65].

2.2.2 Lock-stitch embroidery

Lock-stitch embroidery is the standard embroidery technique the same as a double lock stitch sewing, which is a two-thread system, as shown in Figure 2-4(a). In this system, the needle, or upper thread, is stored on a conical spool. When the tip of the needle passes through the fabric, it pulls a small loop of thread through with it. A hook mechanism under the needle plate pulls this loop and wraps it around another piece of thread, which is reeled from the bobbin. The two threads interlock around the fabric, forming a stitch, and the needle is pushed up and slightly forward before it goes through the fabric again [66]. The thread tension is the essential factor to locate the two-thread interlock in embroidery process. In general, 2/3 upper thread and 1/3 bobbin thread are visible on the back of the embroidery to hidden the interlock knot, as shown

in Figure 2-4(b) [67].

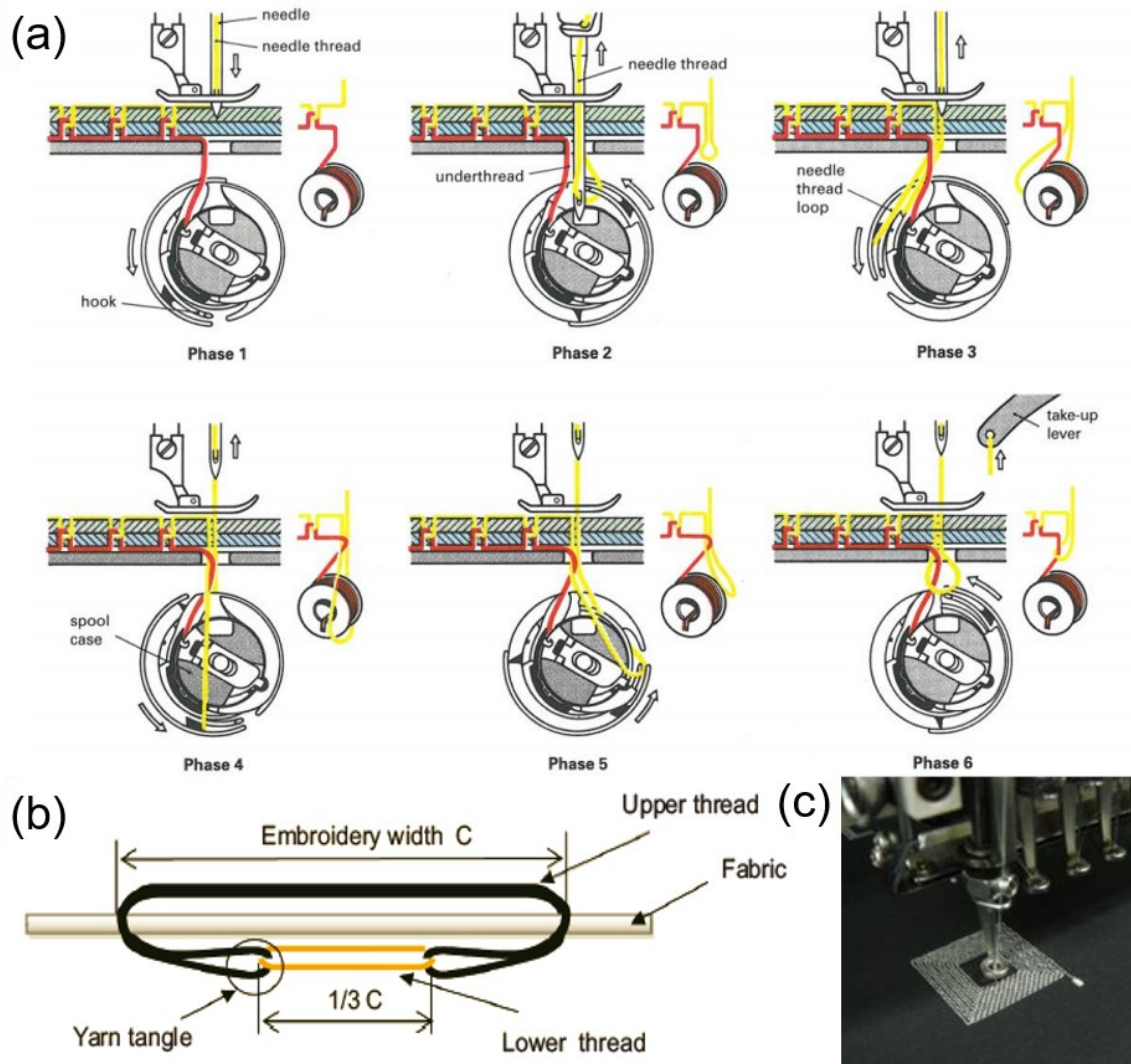


Figure 2-4. Lock-stitch embroidery. (a) Principle of lock stitch formation [66]; (b) Embroidery process with regular thread tension [67]; (c) Embroidered inductors [68].

During the embroidery process, the frame that secures the substrate fabric is controlled by a computer and moved in the x-and y-directions in order to create the programmed pattern. The lock-stitch embroidery can be particularly well suited to creating electro-conductive pads due to the inclusion of electro-conductive yarns as upper and/or lower threads, allowing for more control to fit the desired application [58]. The desired type of sensor and its ability to output relevant data depends on the yarn material, the pattern and the method of signal processing. Figure 2-4(c) shows an embroidered inductor obtained by lock-stitch embroidery. The circuits

proposed are applicable to various smart interactive textile systems, such as wireless communications for real time health and security monitoring [68]. The advantage of the lock-stitch embroidery is that these sensors can be produced on standard multi- or single-head embroidery machines. By using a multi-head embroidery machine, the functional parts (electrodes or sensors) and the design parts of a pattern can be embroidered in one step [65]. This efficient and low-cost embroidery enables more customization in the design and shape of the electrodes and thus the ability to adapt to different application and monitoring scenarios.

2.2.3 Tailored fibre placement (TFP) method

Another embroidery technique is called the TFP method, which consists of a three-thread system. TFP technique allows for continuous placement of a selected textile material in a highly controlled geometry [64]. This procedure has traditionally been used in the composite industry for the optimization of materials to fit customized loading conditions. The fibrous material that acts as the roving is fixed by an upper and lower stitching thread onto a substrate material. This step 'locks' the selected third fibre into a geometry and further preserves that geometry by the use of an upper and lower stitch. Figure 2-5(a) shows the principle of the TFP technique [62]. A variety of fibres, such as carbon, glass, basalt, aramid, natural, thermoplastic, ceramic fibres, and also metallic threads, can be applied and combined within one design application for sensors or electronics [65]. Figure 2-5(b) shows the embroidered flexible plastic optical fibre for realization of the textile display in luminescent smart photonic clothing [69].

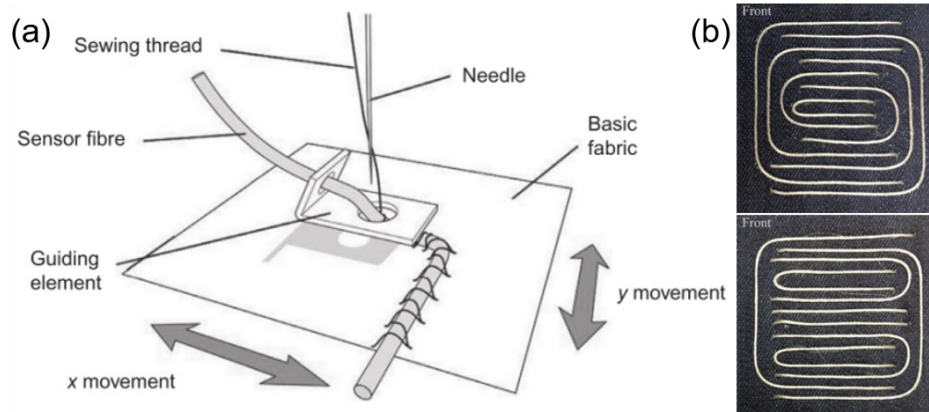


Figure 2-5. TFP embroidery technique. (a) Basic principle driving TFP technologies [62]. (b) Different geometries of TFP embroidered flexible plastic optical fibre samples [69].

The method of TFP is extremely versatile, and less material dependent than other forms of conductive yarns embroidery since the yarn fixed by conventional threads stitching. Conductive materials that usually cannot be embroidered directly can now be placed on a textile due to the fibre placement and fixation provided by TFP.

2.3 Commercial conductive yarns and sewing ability in embroidery process

2.3.1 Types of conductive yarns and evaluation method for physical properties

Conductive yarns can be either based on non-metallic conductive materials, such as carbon fibres, or metallic materials, such as stainless-steel fibres. By twisting a fine metal wire around a multifilament fibre, as shown in Figure 2-6(a), the electrical conductivity of the yarn is achieved with an improvement of the mechanical stability [70]. Figure 2-6(b) shows the spiral-shape of the metal wire allowing a flexibility of the whole yarn and the metal wire is able to follow the deformation when the yarn is stretched [71]. Another method of achieving conductivity is coating yarns with a metal layer. Adopting an electrochemical process, a fine metal layer such as copper (Cu), silver (Ag), or gold (Au) can be deposited on the surface of the fibres, as shown in Figure 2-6(c) [72]. Metallic coating produces highly conductive fibres; however, corrosion resistance and mechanical propriety can present problems because the

metallic coating is sensitive to breakage during the deformation of the yarn or during the textile production process.

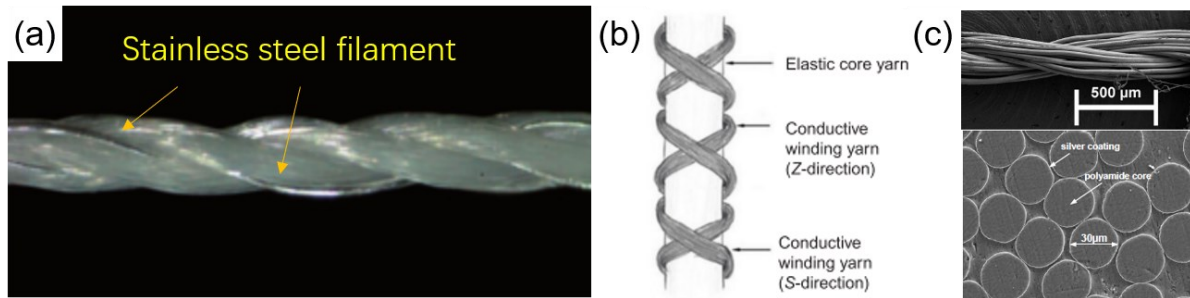


Figure 2-6. Image of conductive yarns. (a) Polyester filament twist stainless steel filament[70]. (b) Spiral-shape yarn with elastic core[71]. (c) Silver coated yarn with polyamide core[72].

Conductive yarns of all sorts are commercially available and mainly used for technical and smart e-textile wearables [60]. Table 2-2 gives a list of suppliers of conductive yarns.

Table 2-2. A list of suppliers of conductive yarns

Material	Conductive yarn suppliers
Copper	Syscom Advanced Materials; R.Stat
Silver	Statex (Shieldex); Sauquoit Industries; TITV Greiz (Elitex); Syscom Advanced Materials; Textronics; Swiss Shield; Nobel Biomaterials (coating); Quigdao Hengtong; R-Stat (coating); Micro-Coax, Inc; Weixing Technology; Microcoax
Gold	Microcoax; Syscom Advanced Materials
Nickel	Electro Fiber Technologies; Syscom Advanced Materials; Micro-Coax, Inc
Stainless Steel	Bekaert Textiles; Schoeller; Epitropic Fibers; Kings Metal Fiber Technologies; R.Stat; Créafibers; IMATTEC International; TibTech Innovation; Koolon; W. Zimmermann GmbH & Co. Kuraray; Teijin Monofilament; Ascend Performance Materials;
Carbon Black	Shakespeare Conductive Fibers; Unitika Fibers; Barnet; Resistat Fiber Collection; Epitropic Fibers
Carbon Nanotubes	Kuraray and Mitsui
Conductive Polymers	Sterling Fibers; Eeonyx Corporation

When evaluate the physical properties of conductive yarns, the morphologies, strength and electrical properties are main factors to consider. The physical and electrical properties of two types of conductive yarns (developed by wrapping and twisting superfine metal filaments with

polyester filaments, called metal conductive embroidery yarns, MCEYs) were investigated by Roh [19]. SEM and a video microscope system were used to observe the surface morphologies and cross-sectional images. Tensile tests of the MCEYs were conducted on a universal testing machine (Instron 5543) according to ASTM D 2256 with a gauge length of 250 mm. The electrical resistance of the MCEYs and the embroidered circuits were measured with a multimeter (Agilent 4293B, Miliohmmeter). Oh *et al.* [73] adopted the conductivity (S/cm) variation as an electrical parameter in relation to elongation. The changes of mechanical properties of the conductive fabric prepared by in situ chemical polymerization were investigated with a tensile testing machine by a standard test method (ASTM D 751-95) coupled with a digital multimeter. For calculating and predicting the properties of the elastic and conductive yarns, Schwarz [74] designed an electrical circuit model based on Kirchhoff's voltage and current law on electrical models with junction points in a circuit.

2.3.2 The sewing ability of conductive yarns for embroidery

The electrical and mechanical properties of conductive yarns and threads need to be fit for the e-textile applications, and these properties must be stable in high-speed embroidery processes. During embroidery processes, threads are affected by dynamic loads, multiple bending, friction, abrasion, and so on [75], and the conductive yarns should exhibit suitable flexibility and strength so as not to be broken by the high tensions generated in the high-speed embroidery.

The first embroidery technique with conductive yarns, called e-broidery was systematically analysed in design and fabrication of textile-based computing [16]. The sewing ability of various stainless-steel yarns used in woven fabrics with lock-stitch embroidery was compared. Stainless steel threads were chosen for their strength, resistance to corrosion, biological inertness, and ready availability in textile forms at low cost.

All- steel continuous fibre thread used to form component leads cannot be sewn by machine because they were too stiff to form a small radius circle, and tensions rapidly mount during the needle repeatedly punching, resulting in bunching of the thread as it feeds through the sewing

machine. Some of the bunched threads will eventually twist into an obstruction that will not pass through the sewing needle's eye, and the entire process will grind to a halt. In contrast, composite yarns of short steel fibres and polyester were able to accommodate this variation in tension by stretching. Orth [76] described machine sewing and embroidery as one of the most stressful textile manufacturing processes. In sewing conductive threads on fabric substrates, the threads encounter various levels of stresses and friction. This requires an embroidery thread to have relatively high strength and flexibility because of the stresses due to bending and shear and the tortuous path it has to traverse to form a secure stitch. Grabham [57] described the key parameters that affect the suitability of the conductive thread or wire for standard embroidery as following:

- 1) Diameter: The thread or wire must be a compatible in size with the needles used.
- 2) Breaking strain: The thread or wire needs to be strong enough to withstand the tension applied during the sewing process.
- 3) Thread surface texture/roughness: The surface roughness affects how the thread or wire feeds through the embroidery machine. Excessive surface fibres of yarns increased the friction and can cause jams and snags in the machine.
- 4) Abrasion resistance / fraying: If the thread or wire has a tendency to fray, it may bunch up and then jam in the needle, causing incomplete embroidery and/or thread breaks.

2.3.3 Performance evaluation of embroidered conductive stitches

Conductive yarns in embroidery processes allow design and integration of yarns with different electrical properties. The level of stitch control and yarn variety brings up the possibility of replacing discrete components such as capacitors, resistors, and inductors with specific combinations of thread and stitch pattern.

- 1) The electrical property evaluation of embroidered conductive yarns

Once the conductive yarns are characterized then it is easier to find techniques to embroider

the e-textile component, such as conductor for circuit and resistor for sensing pattern. Roh [19] used conductive yarns twisted with Ag-coated copper filaments and polyester filaments to test the physical and electrical properties of embroidered zig-zag type circuits. Figure 2-7(a) shows the conductive yarns were embroidered on a cotton woven fabric at four different directions. The appearance of stitches was various even though they were designed as the same straight line. The electrical resistance of them were significantly different since the structure of conductive stitches were disturbed because of the stress of substrates were not even in wale and course. Post [16] compared the usability and performance of conductive stainless steel yarns, BK 50/2, combining used as needle thread and bobbin thread in embroidery process. Stitched traces combining runs of needle and bobbin threads with BK 50/2 dramatically increased the conductivity, which was about 100 times greater than that of the all-steel yarn. The electrical property of conductive traces by sewing was influenced by the combination of each conductive stitches, and the stress of substrates has influences on the shape of stitches structures.

2) The evaluation of embroidery failure and defects

Failure and appearance defects of embroidered elements means the substrate fabric was damaged by needle punching, or the embroidery element did not match the digitally designed pattern. These issues occur due to choosing improper technological parameters or not considering structure properties of substrate. Some researches focus on the embroidery accuracy, defects and ends-down rate with common sewing thread because high accuracy is required to maintain the design and functionality of the product in woven and knitted fabrics [77–79]. The factors of needle size, embroidery thread type, stitch length, type and weight of fabric impacts on the quality and manufacture productivity were studied [79]. The results show for heavy knitted fabrics, embroidery by viscose fine yarn using small gauge needle at less stitch length were optimal parameters specification to obtain least thread cuts during processing. Shafti et al. [14] proposed imprecisions in digital embroidery of EMG sensors led to high electrode impedance and low manufacturing consistency. To investigate influence of

technological parameters on the electrical conductivity of embroidery, Juchnevičienė [80, 81] designed a square shaped closed-circuit, shown in Figure 2-7(b), to embroider on different fabric substrates. The results showed that the width of the embroidered element in the corners of the square is bigger than in the centres of the segments [80]. The electrical conductivity of the square is bigger than in the centres of the segments [80]. The electrical conductivity of the embroidered element was found to differ depending on the filling type of stitch density, and the physical characteristics of the fabric [81].

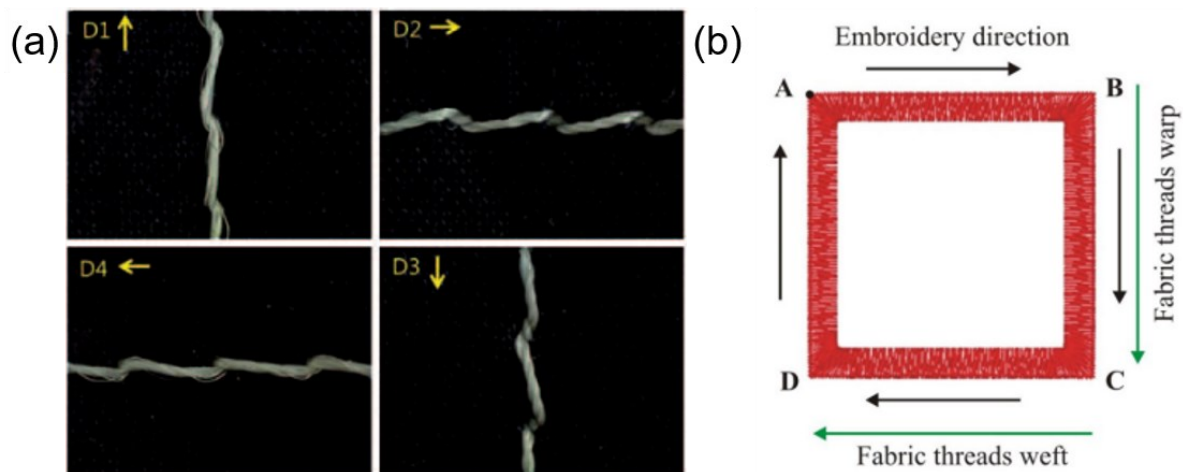


Figure 2-7. Forms of electrically conductive stitches. (a) running stitches in four directions [19], and (b) closed-circuit embroidery chain [81].

2.3.4 Challenges in lock-stitch embroidery with conductive yarns

Previously, the factors of conductive yarns like diameter, breaking strain, thread surface roughness and fraying are investigated in standard embroidery technique, but most of the chosen conductive yarns were used in the bobbin thread. The mechanical demands on the upper needle thread were much complicated than on the bobbin thread according to the lock stitch sewing mechanism. In order to evaluate if conductive yarns can be used in upper needle thread in lock stitch, the features of conductive yarns such as twist, liner density which is vital to the upper thread for loop formation need to be investigated as well. Since the conductive yarns, interaction of fabric type and needle size are the most significant factors which affect the appearance quality of embroidery, there are challenges to figure out proper embroidery parameters on the knitted fabric substrate with conductive yarns.

2.4 Embroidered connectors and interconnects for integrations

Connectors should provide reliable electric connections between other electronic components. When applied in smart e-textile wearables field, the connectors and interconnects that are in direct contact with the soft, three-dimensional and extensible human body should meet the ergonomic movement without electrical resistance changes. Such next-to-skin electronic connectors and interconnects require comfort, flexible and stretchable performance that work in repeated large deformation in three dimensions in the tensile, bending and shear modes [82]. The easy approach is to make largely deformable interconnects thus the electrodes and/ or sensors can be linked by stretchable electric connectors as comparing to that make stretchable electronic devices [83].

2.4.1 Embroidered connectors and interconnects

For the construction of textile-based connectors and interconnects, embroidery of conductive yarns on textile substrates is an attractive approach due to the freedom of circuit design and ease of fabrication interconnection of the wires with electronics.

Post *et al.* [16] developed a multilayer e-broidery circuitry for the plastic threaded chip carrier. Figure 2-8(a) shows the embroidery technique that was used to develop stitched vias. Linz *et al.* [28, 58] systematically characterised embroidery as a means for interconnecting conductive yarn with electronics modules. As shown in Figure 2-8(b), an embroidered wiring and embroidered interconnects was developed. The embroidered conductive thread served as an electrical contact and mechanical fixation simultaneously. The reliability of the assembly and its encapsulations were assessed by standardized tests. The tighter this needle stitches loop is the better the contact. A prototype of an all-fabric touch sensor with multilayer structures was developed using the one-stop electronic textile embroidery process based on all-fabric interconnection [29]. As shown in Figure 2-8(c), both sensing pattern and circuit patterns are embroidered on a woven base layer by metal composite conductive yarns.

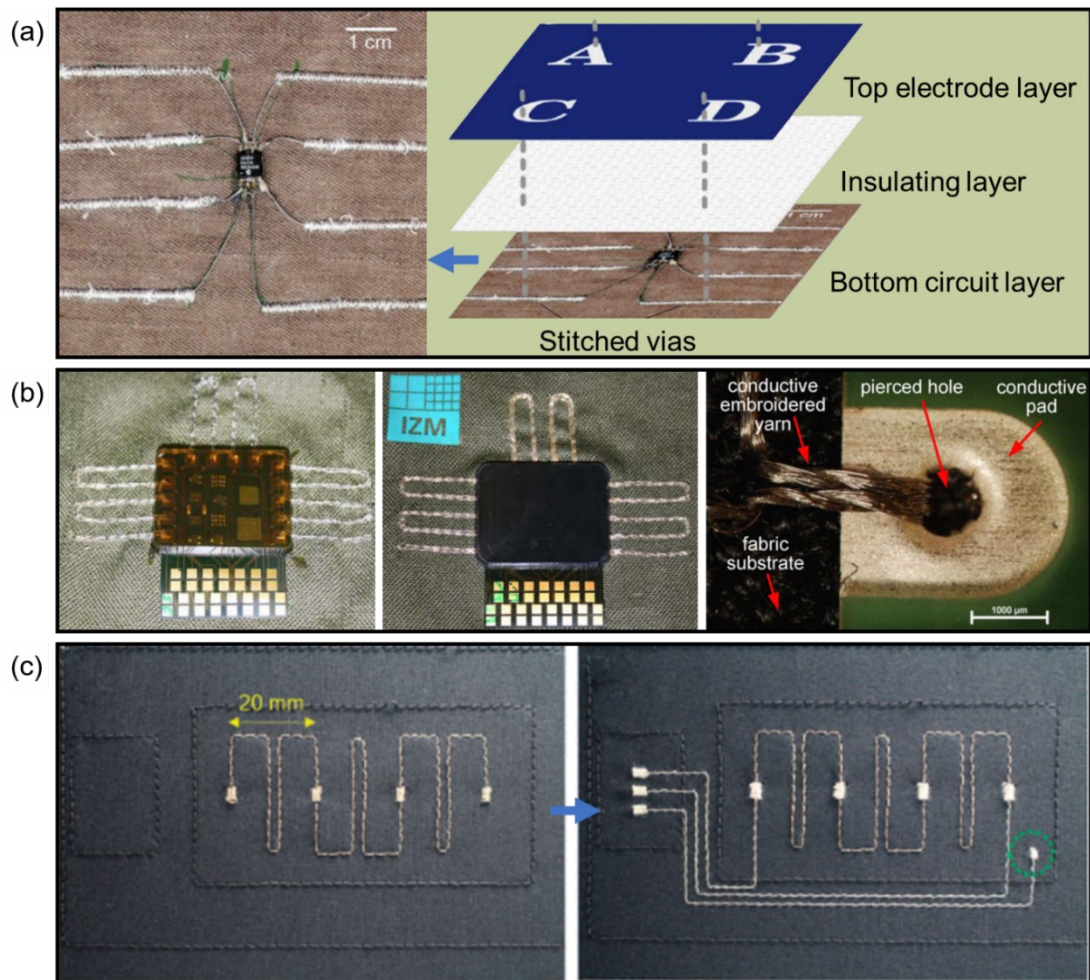


Figure 2-8. Interconnects in e-textiles fabricated by embroidery. (a) Prototype chip carrier package couched onto fabric substrate, left view image showing stitched vias [16]. (b) Metalized contact pads interconnected with embroidery [58] (c) The potentiometric resistive embroidery for the sensing pattern (left) and embroidered circuit interconnection (right) [29].

2.4.2 Flexible and stretchable interconnects design

In addition to the accessibility, comfort, and durability, the flexibility and stretchability of e-textiles are extremely important [9, 84]. Indeed, with high-frequency signal of smart wearables, the interconnection have to be stretchable and therefore the substrate and the conductors have to be stretchable as well [85].

In most cases sinuous electroplated metallic wires were integrated with a stretchable substrate material [86, 87]. Figure 2-9(a) presents a stretchable interconnection structure, called ‘horseshoe-shape’, able to accommodate large deformation in response to a mechanical stress,

preserving the electrical properties [88]. Usually, a polymeric material is chosen as encapsulating substrate, because it can be stretched and it is biocompatible. Figure 2-9(b) showed the interconnect made by conductive metal coupled with PDMS [89]. Stretchability of the electrical interconnects is a requirement in wearable products, and it that can be satisfied with different designs [87, 90, 91]. The design optimization is done by Gonzalez *et al.* [88] using FEM modelling and other tests. The ‘horseshoe-shape’ was evaluated to be the optimal solution for interconnects to achieve stretching performance, as shown in Figure 2-9(c). They demonstrated that in case of multiple and narrow metallisation, the stretchability of the circuit reaches 100% of the deformability. The conductive paths will peel off or broken with bending of interconnects over larger deformation, which result in the lack of robustness in e-textiles circuit.

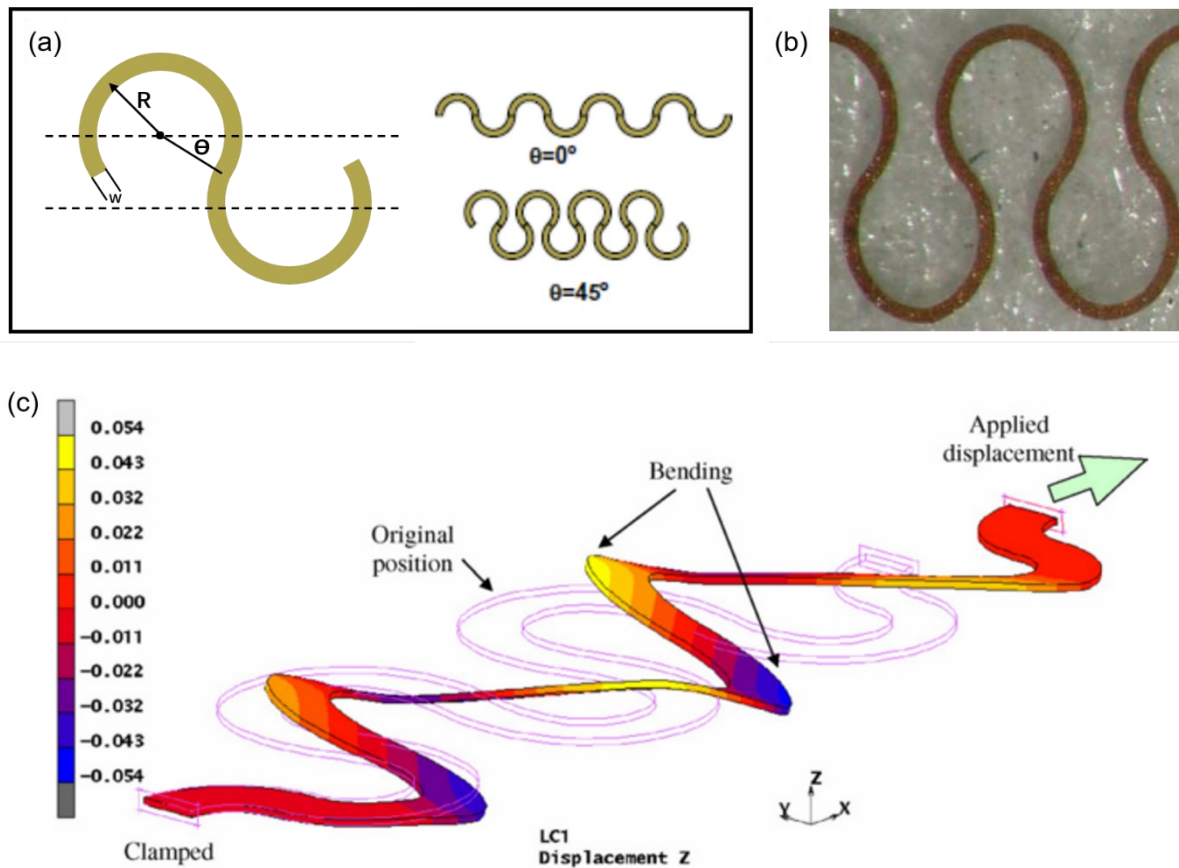


Figure 2-9. Design and FEM of horseshoe shaped interconnects. (a) Notable measures of a horseshoe design: inner radius (R), joining angle (θ) and width of the metal track (w) [88]; (b) Horseshoe metal interconnects embedded into a PDMS matrix [89]. (c) Out of plane deformation of an unconstrained copper meander stretched 20% [88].

Li *et al.* [83] presented the state-of-the-art intarsia knitting technique with out-of-plane loops that withstand strain in both transversal and longitudinal directions to develop fabric circuit boards (FCBs). Their stretchable textile allowed building electronic systems on textile that are permeable, comfortable and stretchable. The conductive fibres were copper wires with $50 \mu\text{m}$ diameter and $3 \mu\text{m}$ polyurethane coating. Authors reported that a 300% stretched textile with conductive paths exhibited less than 1% of relative change in resistance. The fabrication procedure of the sensing system is shown in Figure 2-10. The knitted FCBs have shown reliability during the ballistic impact deformations as all 35 sensor network assembly samples performed well without mechanical and electrical failure and received reliable electrical signals.

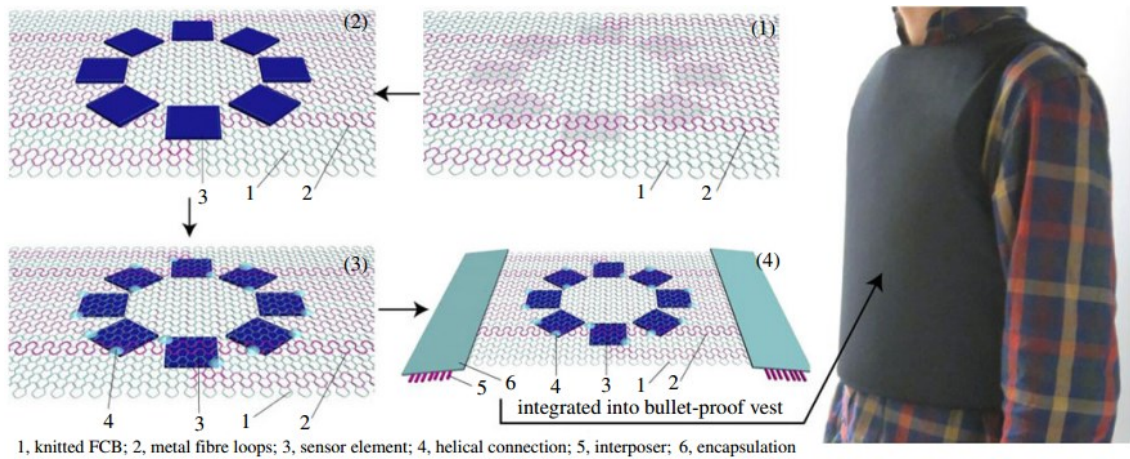


Figure 2-10. Fabrication procedures of the knitted fabric sensing network [83].

2.4.3 Research gaps in stretchable interconnects by embroidery

E-textile connectors and interconnects remain an open research field due to the diversity of application environments where each solution is customized and is almost unique. Most of the researches on embroidered connectors and interconnects by conductive yarns are mainly focus on the integration techniques and electrical conductivity functions, the stretchable performance and electric characteristic changes in wear scenario, like bending, compressing, sweating is rare. Since all the techniques will serve the smart clothing of the next step, the design and development of embroidered interconnects can be stretched to fit the daily body motion still needs to investigate.

2.5 Smart e-textile electrodes and sensors fabricated by embroidery

Textile electrodes can be used to detect electric signals from the body, such as ECG from the heart and EMG from skeletal muscles. Textile strain gauges and pressure sensors can detect body movements, such as breathing movements and foot pressure [92]. Wearable chemo-sensors can monitor the composition of body fluids, such as sweat, saliva, tears, and urine. There are also potential biomarkers from gaseous samples in breath and perspiration. Table 2-3 lists some physiological parameters that have been widely studied using textile-based electrodes and sensors.

Table 2-3. Physiological signals that may be measured using textile-based sensors [92]

Physiological measurement	Textile-integrated sensors	Signal source	Typical sensor placement
Breathing patterns	Piezoresistive stretch sensors, inductive plethysmography, impedance plethysmography, optical fibres	Expansion and contraction of ribcage during breathing	Thoracic-abdominal region
Heart activity	Woven/ knitted electrodes	Electrical activity of heart	Thoracic region
Muscle activity	Woven/ knitted electrodes	Electrical activity of muscles	Skin surface overlying relevant muscles
Blood oxygen saturation	Optical sensing components, plastic optical fibres	Light absorption of haemoglobin in blood	Regions with good blood perfusion, e.g. fingertip, earlobe
Blood pressure	Features of the photoplethysmography signal	Arterial pressure pulsations	Finger, wrist, and earlobe
Body movement, posture	Piezoresistive strain/ pressure sensors, accelerometers, gyroscopes, optical fibre sensors	Body kinematics	Dependent on motion to be analysed
Electrodermal activity	Woven electrodes	Skin electrical conductivity	Fingertips
Composition of body fluids	Electrochemical sensors, colorimetric pH fabric	Composition of sweat, saliva, urine	Fluidic sampling system necessary

2.5.1 Embroidered electrodes

Electrodes are devices that can conduct an electrical current and thus can be used to measure potential differences. Commonly, electrodes used in a medical environment are rigid metal plates in all types of shapes and sizes with electrolytic gel. The usage of textile electrodes in home and personal health care systems has been increasingly investigated in recent years [93]. Integrated into garments, belts or caps, they are more suitable for long-term monitoring and are

being used extensively in textile-based health monitoring systems such as cardiac, muscle or brain activity.

Most researches select lock-stitch embroidery to fabricate textile electrodes since it can simply integrate electrodes into finished garments at suitable locations on clothes. The embroidered electrodes were used to measure ECG [12, 13, 94] and EMG [14]. Apart from embroidering individual electrodes, as shown in Figure 2-11(a), lock-stitch embroidery techniques were employed to fabricate connectors together with electrodes. Weder [31] developed an embroidered textile electrode from polyethylene terephthalate (PET) yarn which is plasma-coated with silver for electrical conductivity and with an ultra-thin titanium layer on top for passivation. As shown in Figure 2-11(b), two of these electrodes are embedded into a breast belt. They are moisturized with a very low amount of water vapour from an integrated reservoir. The same coated yarn as used for the electrode is also used for an embroidered connection between the electrodes and the press-studs for the fixation of the data logger. Study in [95] embroidered a band for long term ECG monitoring using silver coated yarns, made from Madeira, to fabricate electrodes and conductive lines with lock-stitch embroidery. After protecting conductive lines by embroidering nonconductive yarn, as shown in Figure 2-11(c), the band can measure cardiac waves clearly after 50 washing cycles.

Figure 2-11(d) shows a round shape ECG electrode fabricated with the prepared Ag/AgCl multifilament yarn on polyester plain fabric by chain-stitch embroidery technique [96]. This “brush” structure, shown in Figure 2-11(e), can increase the effective contact area with electrolyte compared to plate electrode, in turn, decreases the contact impedance [97]. ECG testing confirmed that the embroidered electrodes made from treated fibre can acquire high quality signal better than woven and knitted electrodes.

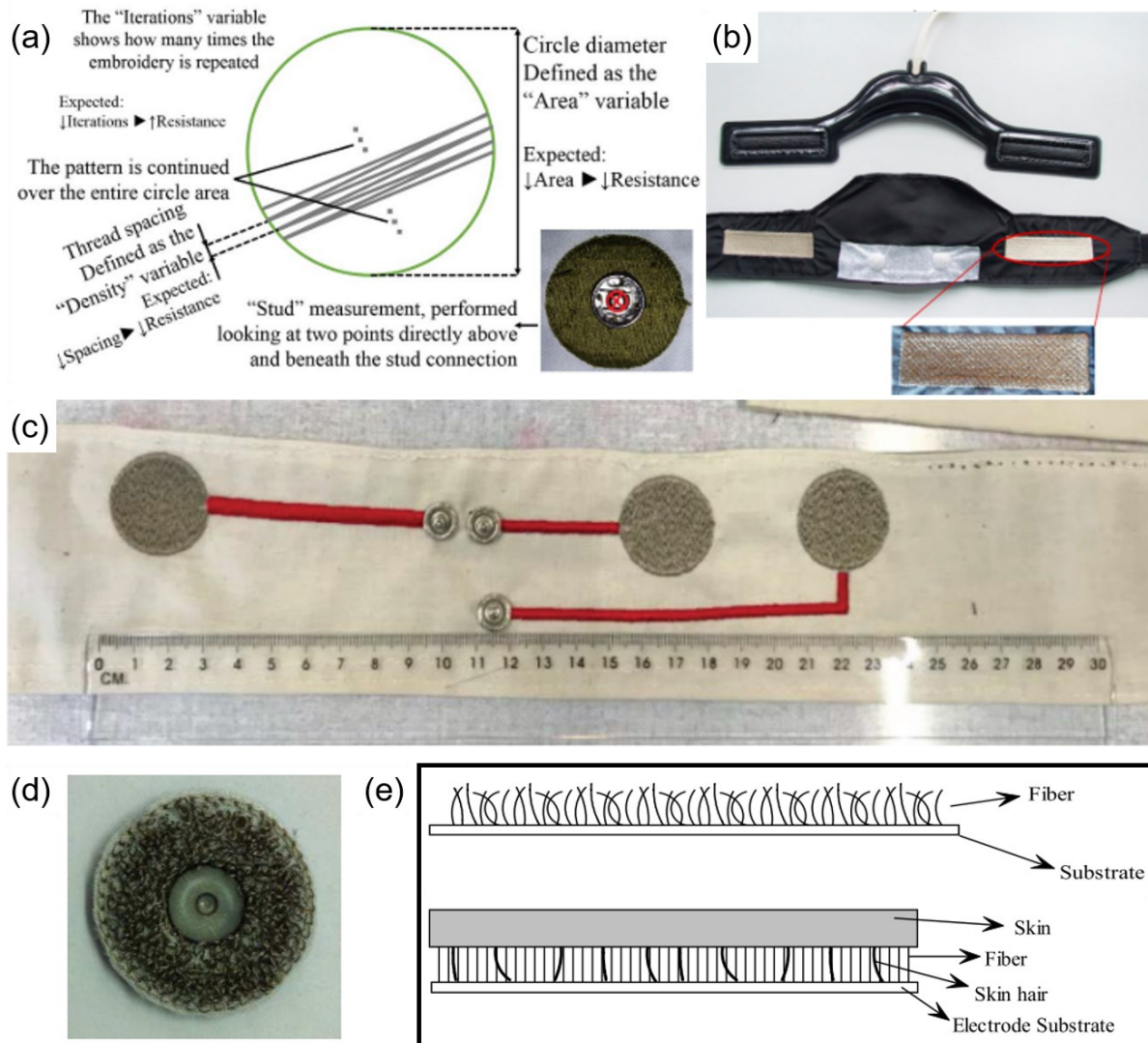


Figure 2-11. Dry electrodes fabricated with embroidery techniques. (a) Design variables for a circular electrode during embroidery [14]. (b) Prototype of the wetting pad (above) and the ECG belt with embroidered electrodes (below) [31]. (c) Band with lines protected by nonconductive yarn (red yarn) [95]. (d) Illustration of the electrode embroidered with chain-stitch [96]. (e) Fabric structure and electrode-skin contact with skin hair [97].

2.5.2 Embroidered sensors

Sensors based on changes in electrical resistance are the most common, the resistive change is obtained by physical changes such as stretching, bending, pressure, deformation, and friction [60]. The resistive sensing method of a potentiometer as an accurate positional indicator was chosen to make simple prototypes of metal composite embroidery yarns embroidered touch sensors [19]. As shown in Figure 2-12(a), the rounded rectangle area of this resistive

embroidery was effectively filled with about 2.5mm stitches which run from side to side with up to 8mm width movement and 0.4mm forward movement without a short between the adjacent embroidered lines. These minimal fabrication technologies may be highly valued in the smart textile field thanks to their simplified interconnects, customizability and tailorability on double curvature surfaces. Embroidery textile humidity sensors has been studied by embroidery on non-woven fabrics using Liberator® nickel and silver cladded conductive yarns [98]. Figure 2-12(b) shows the appropriate pattern designed with meander structure for a fast response sensor and easy automatized production. To develop a three-layer structure textile pressure sensor, an array of individually connected electrodes were embroidered and simultaneously the interconnection to each electrode was fabricated [99], as shown in Figure 2-12(c). With embroidery techniques, an textile capacitive sensor for moisture sensing was investigated [18]. Figure 2-12(d) shows the interdigitated structures of the sensor embroidered on a high hygroscope woven fabric. A electrochemical sensor on gauze via a unique embroidery fabrication process for quantitative measurements of uric acid, a biomarker for wood severity and healing [100]. Figure 2-12(e) shows the sensor has three electrodes embroidered using ink-coated polyester thread. Carbon-coated thread was used for the WE and CE, and Ag/AgCl coated thread was used for the RE. Several embroidery parameters, such as the stitch length and stitch density, were optimized to enhance the electrical properties of the electrodes for improved signal consistency. A fabric-based chemical gas sensor was developed to use as wearable electronic nose [101]. As shown in Figure 2-12(f), the interdigitate electrodes were embroidered with conductive thread to produce comb-like patterns as a sensing area. Conductive threads were connected to snap fasteners, in which external devices can be plugged to fulfil the measurement.

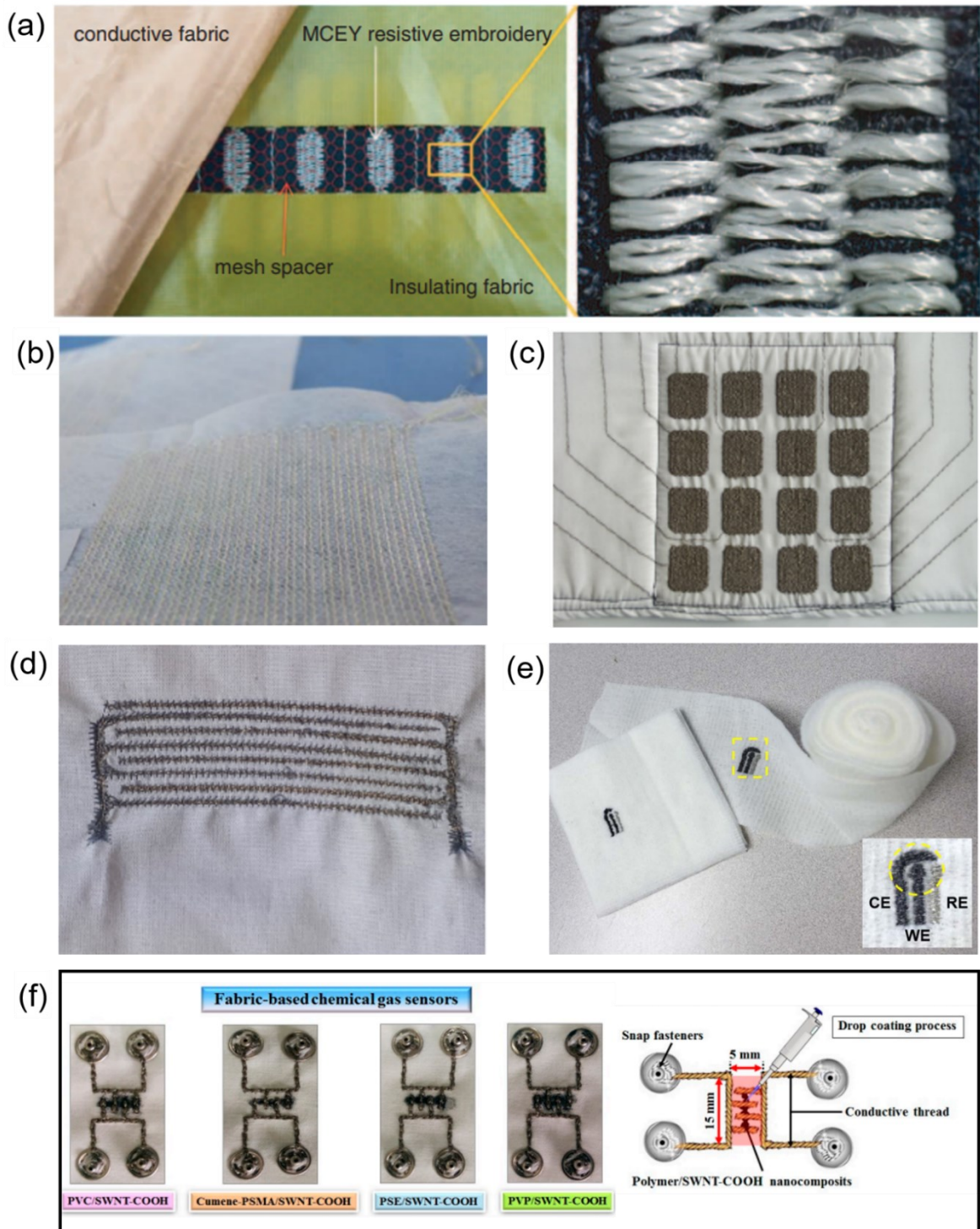


Figure 2-12. Sensors fabricated with embroidery techniques. (a) Photograph of an embroidered potentiometer [19]. (b) Meander structure on the non-woven material to form humidity sensor [98]. (c) Textile pressure sensor with embroidered sensing elements [99]. (d) Interdigitated structures of embroidered textile moisture sensor [18]. (e) Embroidered electrochemical sensors on gauze and wound dressing. Inset shows a close-up image of the sensor [100]. (f) Comb-like pattern of fabric-based chemical gas sensors [101].

Another attractive approach to produce sensors is to embroider conductive yarns on stretchable fabrics. The conductive stitches in embroidered structures were capable for the strain and the tensile force applied to the substrate fabrics, which achieve various electrical properties. A 2-D chipless strain sensor for wireless structural deformation monitoring was fabricated by embroidering two resonant scatterers on stretchable fabrics with conductive threads [102]. As shown in Figure 2-13(a), two scatterers with 90° rotated rectangular split ring resonator, the backscattered response, as a function of frequency, is detected with the help of frequency- stepped continuous wave radar technique. The radar performs the detection by scanning the two orthogonal polarizations. A textile-based, embroidered planar coupling feed UHF RFID tag antenna was used as a displacement sensor for human activities tracking [103]. Figure 2-13(b) shows the antenna structure consists of a dipole arm and a coupling loop mounted with an RFID chip. When a displacement occurs between the loop and dipole arm, the impedance of the antenna is changed and consequently modulate the backscattered signals from the RFID chip to the reader. An alternative embroidered method to develop textile strains sensors has been proposed [104]. The sensor resistive can measure up to 65% of elongation, which corresponds to the maximum elongation of elastic substrate. Figure 2-13(c) shows the sensor was based on a crossed zig-zag embroidered structure. When the structure is stretched the relative distance of contact points increases and thus, the effective length of the sensor increases. Therefore, the sensor resistance is increased. Three lock-stitching patterns of conductive yarns were sewn on elastic fabrics to obtain strain sensors for precisely monitoring complex motions of the human body [44]. Figure 2-13(d) shows the schematics of the lock-stitching process of an integration of stretchable textile substrate with stretchable yarn, and the process of pre-stretching of the textile substrate. Furthermore, a wearable strain sensor to monitor human respiration by lock-stitching stretchable conductive yarn was developed [45]. As shown in Figure 2-13(e), the conductive yarn twisted around a Lycra fibre with a lock wrinkle structure that could stretch after sewing, a snap button was attached to tighten the conductive yarn on the top and bottom of the stretchable textile. This wearable textile sensor

could output respiratory signals corresponding to breathing motions.

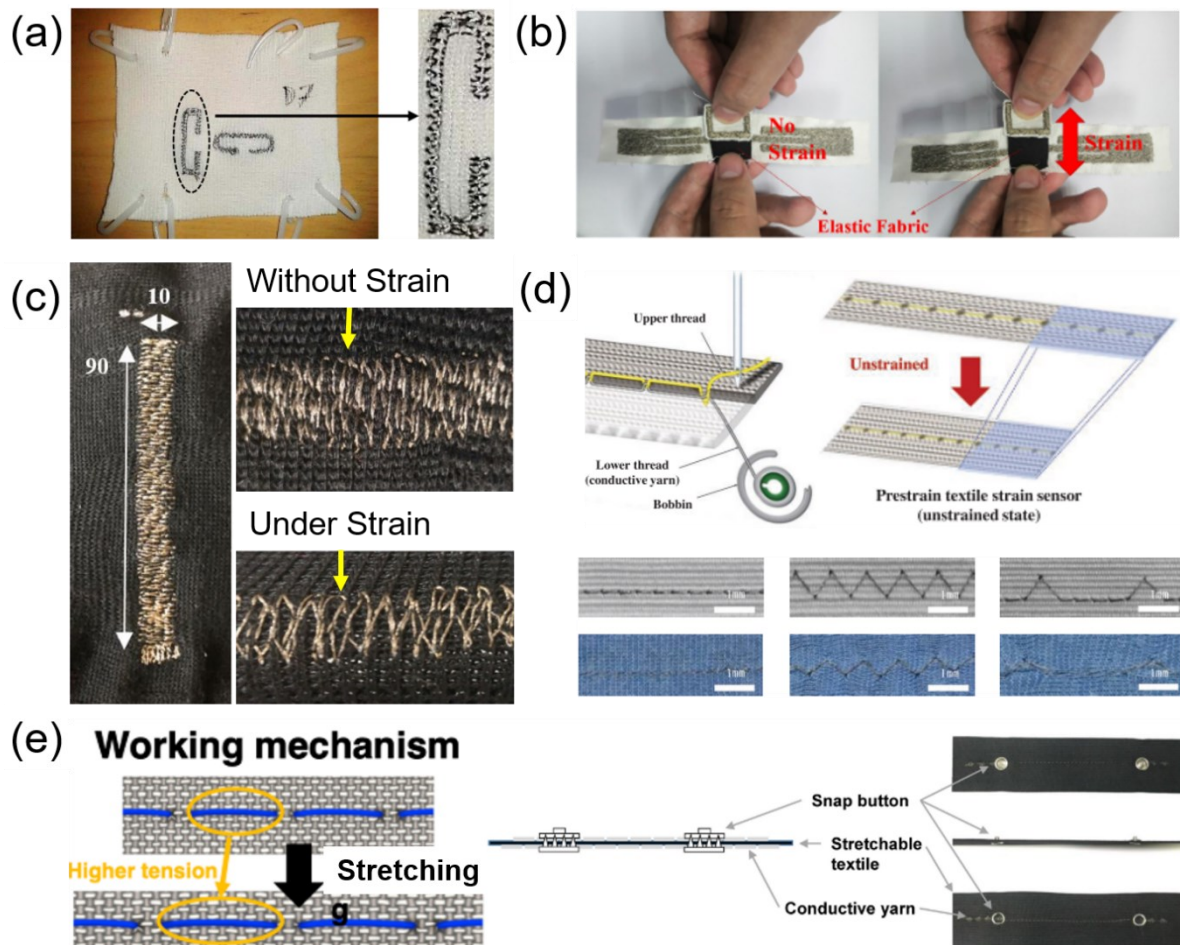


Figure 2-13. Embroidery techniques used with stretchable substrates. (a) 2-D scatterer design based on orthogonal arranged rectangular split ring resonator [102]. (b) Embroidered planar coupling feed antenna as a strain sensor [103]. (c) Layout of the embroidered sensor and the pattern without or under strain [104]. (d) Textile strain sensor fabricated by lock stitching over pre-strained textile substrate [44]. (e) Integrating the conductive yarn with the stretchable textile substrate [45].

2.5.3 Research gaps in embroidered electrodes and sensors

A variety of physiological and behavioural measurements smart e-textile wearables have been enabled through the integration of embroidered electrodes and sensors within a fabric substrate. In these applications, signal quality has generally been the primary consideration while user comfort and sensor integration implemented on an industrial standard have become secondary. The effect of human body and moisture in the substrate are not quantitatively studied in most

researches as well. The standard evaluation methods are necessary and need to be developed to realize mass production.

The inaccuracies of embroidery manufacturing on knitted fabrics to digital design should be taken into account. If the embroidery machine is not entirely accurate at low dimensions and spacing, it will lead to manufacturing errors. These errors will result in higher overall resistance values than expected [14]. Prior studies have not been able to account for all aspects of manufacturability of e-textile wearables embroidered with conductive yarns. The next issue to consider is how consistently the digital embroidery machine can manufacture a particular design variable set.

However, these studies were mainly focused on the conductive yarns and product function evaluation, the embroidery technique parameters, like stitch density and interface impedance of skin-electrode are not well investigated. Furthermore, dry electrodes suffer from very high electrode-skin impedance and thus are more vulnerable to noise and motion artefacts compared to the wet electrodes. Applied external pressure could reduce the impact of noise and motion artefacts by reducing the electrode-skin impedance. The influence of wearing pressure on bio-signal qualities measured by textile electrodes need to be investigated. Embroidered sensors were fabricated on woven or non-woven fabrics, which was stiff without stretchability. Embroidery onto stretchable fabric, such as knitted fabric with elastane yarns, still need to be investigated. Moreover, performance of strain sensors by embroidery techniques needs to be improved.

2.6 Summary

Embroidery techniques are used in smart e-textile wearables' connectors and interconnect, electrodes and sensors. Some of smart clothing were made to integrate all the electronic components by embroidering conductive yarns. From the literature review, the knowledge gaps of developing smart e-textile wearables by embroidery are listed below:

1) The conductive yarns performance used in upper needle thread in lock stitch and the influence of different embroidery parameters on the embroidery traces of knitted fabrics is not well studied.

2) The stretchable performance and electric characteristic changes of embroidered flexible interconnects need to study.

3) The effect of wearing pressure on ECG monitoring by embroidered electrodes are unclear.

4) Textile-based strain sensors for respiratory monitoring needs to be developed by embroidery process.

CHAPTER 3. EVALUATION OF CONDUCTIVE YARNS SEWING ABILITY ON KNITTED FABRICS BY LOCK- STITCH EMBROIDERY TECHNIQUE

This chapter focuses on completing objective 1, which has two sections written with the paper format. The section 1 focuses on how to embroidery conductive tracks on knitted fabric, which has been published on peer reviewed conference paper. The section 2 focuses on optimization of embroidered conductive tracks performance, which has been published in Journal of Industrial Textiles.

3.1 Techniques of conductive yarns embroidery on knitted fabrics

Authors: Yan Zheng, Lu Jin, Simeon Gill, Steven Hayes, and Yi Li

Conference: Textile Bioengineering and Informatics Symposium Proceedings (Sep. 5-8, 2022), accepted.

Statement of own contributions: Main research idea, conductive yarns testing, embroidery techniques design and fabrication of samples, data analysis, and preparation of manuscript.

Statement of co-author contributions: Lu Jin supports in conductive yarns mechanical property tests. Simenon Gill and Steven Hayes support in techniques design of lock-stitch embroidery. Yi Li initiated project idea and provided supervision and guidance in research methodology, the design of experiment, data analysis and interpretation, and paper revision.

3.1.1 Introduction

Embroidery technique is relatively simple and mature in fabrication wearable electronic textiles (e-textiles) to create high-performance textile electrodes [12–15], circuits [16, 17] and sensors [18–21] because the technique allows for flexible patterns, dimensional accuracy, mass production, and cost-effective production [10, 11]. Lock-stitch is the main stitch type in

embroidery techniques, combining a two-thread system from needle and bobbin. The tip point of the needle passes through the fabric, it pulls a small loop of thread through with it. A hook mechanism under the needle plate pulls this loop and wraps it around another piece of thread, which is reeled from the bobbin [66]. The two threads interlock under the fabric to form a stitch, and the needle is pushed up and went through the fabric again for the next stitch. The key step for the lock-stitch formation is the needle thread loop formation, which is caught by the point of the hook. In order to form the thread loop, the twist direction and bending rigidity property of thread are important. The twist direction of the thread for the lock-stitch embroidery should be Z twist because the stitch-forming devices enter the needle loop from the right-hand side, and this reduces the untwisting of the thread during sewing [105]. Kinetics of the sewing process deals with the influence of the force acting on thread movement in the stitch forming process, and bending of the thread with small curvature radius is very important [106]. The thread should bend and form a loop with the needle movements, so the thread perform suitable bending rigidity characteristics is critically important.

With the rapid development of materials science, the technology of conducting yarn is relatively mature from lab to market. As there exist many types of conductive yarns with different qualities and properties in market, selecting high-quality conductive yarns is vitally important for embroidery. Conductive yarns can be either based on non-metallic conductive materials (such as carbon fibres) or metallic materials, including a set of metal filaments. As an example, stainless steel filaments can be twisted around each other to form a conductive yarn. Another method of achieving conductivity is coating yarns with a metal layer, such as copper (Cu), silver (Ag), or gold (Au) which can be deposited on the surface of the fibres [72]. Conductive threads used in e-textile wearables should keep suitable electrical property for applications in fabrication process. Apart from conductivity of yarns, they must strong and flexible enough to be sewn at high speeds without breaks. Post et al. [16] compared different types of conductive stainless steel yarns and fabricated multilayer textile circuitry. They found pure steel continuous fiber thread cannot be sewn by machine, and short steel fibers in steel-

composite threads is easily extend from the body of the thread, which make short circuits between sewn traces. Orth [76] evaluated mechanical properties of conductive threads that are used for producing embroidered circuit fabrics by a 'Curl test' , which was developed to observe if the conductive threads are permanently deformed. The bending and tensile properties measurement of cotton/metal wire complex conductive yarns was performed to investigate yarn behavior in textile manufacturing stages [107]. Based on the analysis of mechanisms of lock-stitch embroidery [66], the conductive yarn with sewing ability should be: (1) Flexible with appropriate bending rigidity to form loops. (2) Balanced twist with Z direction. (3) Appropriate tensile strength and elongation. However, the mechanical performance of different types of conductive threads to forming needle threads in lock-stitch formation were undefined. The simple method to verify the feasibility of applying conductive threads in the needle of lock-stitch embroidery is necessary.

The needle cutting damage in knitted fabrics is a type of mechanical damage made by needle in sewing process, and this damage is a fault that includes yarns being broken by the penetration/ withdrawal of the sewing needle [108]. Needle size is the prime variable affecting mechanical damage. A large diameter needle requires greater force to penetrate the fabric than a fine needle, leading to increased heat generated and increased mechanical damage [109]. The sharp needle point will damage the fibres of the knitted fabric as well and ball-point needles can push the knitted loops apart without damaging the fibres in the material[110]. Since the size and physical property of conductive threads are different compared with common threads, there were technique challenges for the knitted fabric embroidery under high-speed fabrication to avoid needle cutting damage.

In this paper, various conductive yarns, classified according to the conductive materials including silver, stainless stain, copper and carbon were selected to compare the performance of loop formation used as needle thread in lock-stitch embroidery. A simple sewing stitch, 602, was employed to estimate the loop formation ability of the conductive threads. Moreover, an equation is proposed to calculate the needle size corresponding to the size of conductive threads.

Through experiments and embroidery technique parameters setting, the needle cutting damage to knitted fabric through embroidery was studied.

3.1.2 Experimental details

3.1.2.1 Physical properties of conductive yarns

The commercial conductive yarns selected for the research were listed in Table 3-1. The structure of each commercial conductive yarns by optical microscope were shown in Figure 3-1(a). The machine sewing ability of four types of conductive yarns were tested and compared with two traditional sewing threads, made with polyester and viscose respectively.

Table 3-1. The type of commercial conductive yarns and physical properties

Thread code	Supplier and product code	Thread types	Line density (tex)	Electrical resistance (Ω/m)	Twist (tpm)	Twist direction	Twist balance (revolutions number)
A1	Madeira HC12	Silver coated embroidery thread-2 ply	61	80	467	Z	0
A2	Madeira HC40	Silver coated embroidery thread-2 ply	29	270	633	Z	0
A3	Tibtech Silverpam S95	Silver coated thread-single ply	9.5	400	417	S	0
B1	Tibtech N30	Stainless steel thread-2 ply	231	30	233	S	5
B2	Adafruit FLORA P603	Short fibre hybrid Stainless steel thread-3 ply	269	40	400	S	32
B3	Adafruit FLORA P640	Stainless steel conductive thread-2 ply	187	52	333	S	0
B4	Adafruit FLORA P641	Stainless steel conductive thread-3 ply	357	33.2	400	Z	5
C1	Tibtech 4Cu-0.1	Cu wire and cotton-2 ply	331	3	267	Z	1
D1	Tibtech Carbon Tenax	Carbon yarn-2 ply	140	213	250	Z	6
E1	Madeira Polyneon No.40	Polyester thread-2 ply	27	-	633	Z	0
E2	Madeira Classic No.40	Viscose thread-2 ply	27	-	600	Z	0

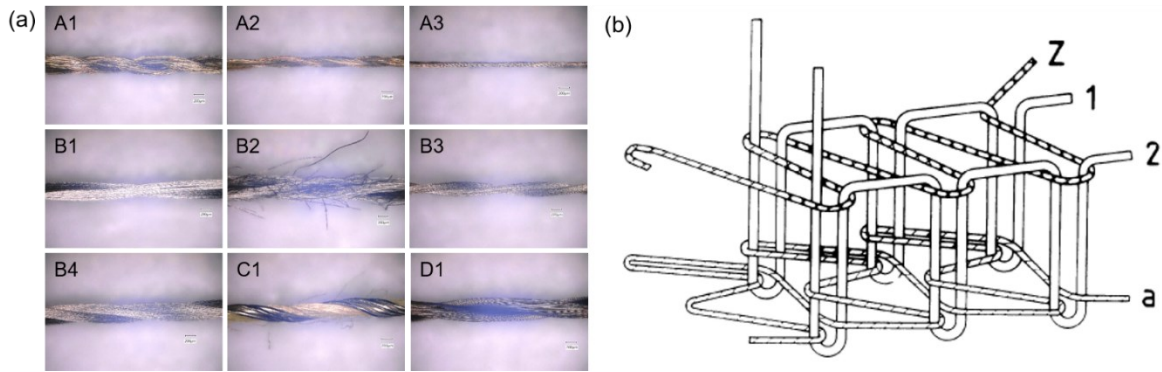


Figure 3-1. Structures of conductive yarns and 602 chain-stitch. (a) Structures of commercial conductive yarns. (b)The structure of 602 chain-stitch [66].

The twist balance of conductive yarns was tested based on ASTM Test Method D204-02. This method was used to predict the kinking and snarling tendency of thread during actual sewing operation. The tensile strength of conductive yarns was measured according to ASTM D2256-10, describes the measurement of breaking force and elongation of yarns, together with the calculation of breaking tenacity, initial modulus, chord modulus and breaking toughness. Two types of ordinary insulated embroidery thread composed of polyester and viscose were listed respectively for comparison. These tests were carried out in the lab with stable ambient air condition, which were 22 °C and 60% RH humidity.

When using the conductive thread directly in the needle of the embroidery machine, the thread is more prone to get stuck with the mechanical parts of the machine and to get damaged. Knowing the bending rigidity before feeding the conductive yarns into the embroidery machine would be useful to protect the machine and make embroidery more successful. In this paper, the bending rigidity of conductive thread was tested by putting conductive thread in curved needle of 602 covering chain stitches sewing. The 602 stitches are formed with two-needle threads, one looper thread on the bottom, and one cover thread Z on the top, as shown in Figure 3-1(b). The looper thread was formed by the curved needle and the angle of thread is similar to the loop formed in the needle thread of lock-stitch.

3.1.2.2 Selection of needle size

The needle size is based on the diameter of the blade (in 1/100 mm) at a point just above the scarf [66]. The long groove is the hollow along the blade designed to take the needle thread as it passes from the thread take-up lever to the eye. Dimensions of the groove should ideally exceed those of the sewing thread and the thread in scarf side is retarded by friction with the fabric so a loop is formed during the upstroke of needle in the embroidery process. The vertical movements of the needle are extremely rapid, so the efficient functioning of the long groove is critically important.

The GROZ-BECKERT needles from Groz-Beckert KG Germany were used in ZSK embroidery machine. Its unique Loop Control[®] needle geometry secure loop formation minimizes skipped stitches and ensures maximum care of the sewing thread [111]. Figure 3-2 shows the long groove structure of a needle, and the cross section of the long groove can be regarded as a trapezoid shape. The width and depth of the long groove in different needle size were measured by optical microscope KEYENCE VH-Z100R.

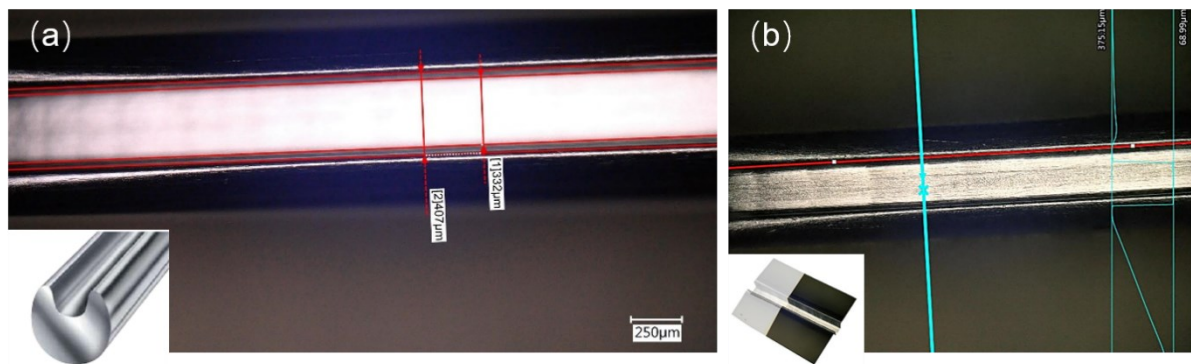


Figure 3-2. The long groove structure of Groz-Beckert needle. (a) Width of the long groove measurement; the inset is cross section illustration of a needle [111]; (b) Measurement of the depth of a long groove; the inset is 3D image for the measurement.


Based on the lock-stitch formation mechanism, the needle size could be determined by the diameter of the conductive threads used. The width and depth of long groove is in proportion to the diameter of blade [111]. The cross section of the conductive thread could be regarded as a circle and the area is equal to the long groove cross section area, then the needle size could

be calculated.

3.1.2.3 Tests of needle cutting damage






During the embroidery process, the frame that secures the substrate fabric is controlled by a computer and moved in the x-and y-directions in order to create the programmed pattern. The repeated punching of needles during high-speed embroider may damage the yarns in substrates leading to broken holes, which are a serious quality issue in embroidery. In this paper, the standard of BS EN ISO 11612:2015 was used as reference for the requirement of fabric used as firefighter’s T-shirt. The substrate knitted fabric for the research was supplied by KIVANC GROUP from Turkey, which is the qualified supplier for firefighter uniforms in EU. The properties of the knitted fabric were listed in Table 3-2. The wale and course counts were tested as directed in ASTM Test Method D8007 [112].

Table 3-2. The characteristics of the knitted fabric used

Fabric image	Structure	Content	Wale count per inch	Course count per inch	Weight (g/m ²)
	Single jersey	78% FR viscos 20% Para-aramid 2% antistatic	28±1	35±1	200±10

Needles are made with a wide variety of needle points to fit for sewing with the different properties of fabric. The needle point should avoid cutting the yarns in the fabric during embroidery process. Round points are used for sewing fabrics and the ball points needles are particular used for the knitted fabric sewing[109]. The tips of ball-points needles are slightly dulled and GROZ-BECKERT needles used in embroidery machine were classified as light, medium and heavy ball points (Table 3-3). The ball tips tend to push yarns in the fabric aside more readily other than cut them directly in sewing procedure.

Table 3-3. Point types of GROZ-BECKERT needle for embroidery [111]

Needle point type	Regular round point	Round point with slightly rounded tip	Light ball point	Medium ball point	Heavy ball point
Product code	R	RG	FFG	FG	G
Needle point diagram					

The embroidery speed has an effect on the penetrating force of the needle when sewing, and the higher speed would cause bigger force to penetrate the fabric. The needle cutting test was carried out based on the variables and levels shown in Table 3-4. The knitted fabric was embroidered 10 cm long under each specific condition using 100% viscos thread in needle and bobbin. There were 24 test samples and each sample were repeated three times.

Table 3-4. Needle cut test variables and levels

Variables	Levels		
Needle size	70#	100#	
Needle point shape	RG	FFG	FG
Stitch length	1mm	3mm	
Embroidery speed	400RPM	800RPM	

In attempts to simulate the situation of wearing for each stitch, the stitched fabric samples were tested for tensile properties with 100% longer stretch with Instron tensile testing instrument at speed 300 mm/min. After 10 cycles of stretch, the thread structure of the yarns was inspected around each needle hole. The viscose thread tensile strength is low and will broke in the first stretch.

The test to measure the ‘needle-related damage due to sewing in woven fabric’ was made according to ASTM D1908-89. The needle cutting damage could be valued with needle cut index (NCI). NCI can be calculated using the Equation 3-1 [113]:

$$NCI = \frac{N_{cut}}{N_{fabric}} \quad (3 - 1)$$

where N_{cut} means number of yarns cut per cm, and N_{fabric} means number of yarns in fabric per cm.

3.1.3 Results and discussion

3.1.3.1 Needle thread loop formation performance evaluation of conductive yarns

1) Tensile properties of conductive yarns

The tensile properties test of four types of conductive yarns and two types of ordinary embroidery thread were tested on a universal testing machine (Instron 5543) with a gauge length of 25cm, according to the standard ASTM D2256.

Figure 3-3 compared the load extension curve for the four types of conductive yarns and two types of general embroidery thread. It was observed that carbon conductive yarns exhibit the highest initial modulus followed by stainless steel conductive yarns and cooper-cotton hybrid yarns. The breaking elongation for silver coated single ply yarn was maximum (over 50%). The 2-ply silver coated conductive yarns and ordinary embroidery thread show similar breaking elongations, which were more than 20%. The tensile properties of these threads were displayed in Table 3-5.

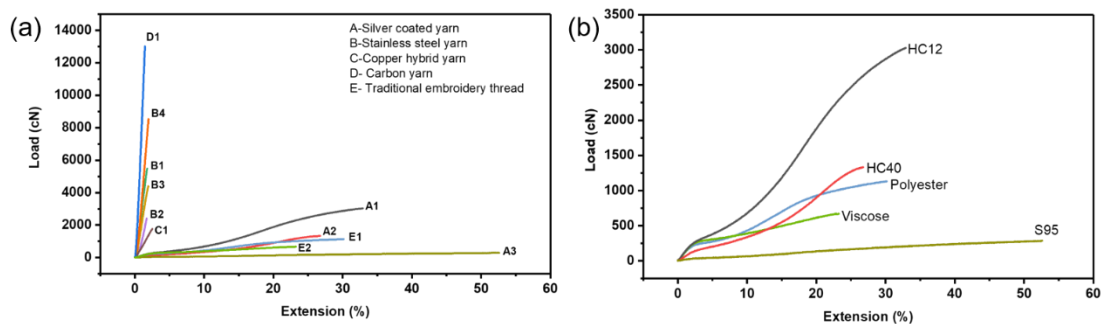


Figure 3-3. Load extension behaviour of different threads. (a) Comparisons of all the threads. (b) The comparison of threads can be extended over 20%.

The initial modulus of the thread was a symbol of tenacity and was an important criterion

to evaluate sewing performance in embroidery machine. Table 3-5 shows that the initial modulus for carbon conductive yarn was the highest. The initial modulus of pure stainless-steel yarns were higher than the metal-cotton hybrid yarns. The 2-ply silver coated polyamide yarns show similar initial modulus with the normal polyester embroidery thread and the single ply silver coated yarn was similar to the viscose embroidery thread. The initial modulus results were respective to the break elongation performance.

Table 3-5. Mean values of mechanical properties of threads

	Thread types	Breaking load (cN)	Breaking elongation (%)	Breaking tenacity (cN/tex)	Initial modulus (cN/tex)
A1	Silver coated embroidery thread-2 ply	2998±51.7	32.9±0.73	49.15	165.5
A2	Silver coated embroidery thread-2 ply	1330±7.2	26.33±0.38	45.86	172.0
A3	Silver coated thread-single ply	283.8±8.3	52.52±2.24	29.87	56.6
B1	Stainless steel thread-2 ply	5453±62.5	1.73±0.03	23.61	1425.2
B2	Short fibre hybrid Stainless steel thread-3 ply	2460±183.8	1.71±0.15	9.15	542.5
B3	Stainless steel conductive thread-2 ply	4163±428.2	1.84±0.15	22.26	1319.8
B4	Stainless steel conductive thread-3 ply	8523±141.4	1.91±0.09	23.88	1291.0
C1	Cu wire and cotton-2 ply	1789±173.7	2.62±0.28	5.4	220.4
D1	Carbon yarn-2 ply	12843±1384.5	1.4±0.13	91.73	6677.5
E1	Polyester-2 ply	1134±12.3	30.85±0.73	41.99	141.3
E2	Viscose-2 ply	669.3±3.2	23.36±0.27	24.79	83.6

The tensile stress test of the conductive yarns could be used as a method to estimate the

needle thread bending performance, which need small curvature radius deformation to form thread loop. Based on the analysis of bending rigidity, twist direction and balance, and tensile stress test, the silver coated polyamide threads HC 12 and HC 40, which was brought from MADEIRA[®], are proper to be used as needle thread in e-textiles embroidery.

2) Bending rigidity evaluation of conductive yarns

The bending rigidity of the conductive yarns is the main factor to affect the needle thread loop formation in embroidery [66]. The ‘Curl test’ [76] and ‘ring-loop method’ [114] are indirect methods to evaluate the bending performance of the yarns in force condition. The force to form needle thread loop in sewing process is a combination force of needle going upward and friction between the thread and fabric. The indirect bending rigidity test method is static simulation of the force condition, and the bending angle in the test was larger than the real needle thread loop formation during sewing.

The selected four types of conductive yarns were sewed with 602 covering chain stitches and they were only used as looper thread. The final seam appearance sewn with traditional sewing threads and different types of conductive yarns scanned by optical microscope KEYENCE VH-Z100R were shown in Figure 3-4. It is clear that the silver coated yarns, HC12 and HC40, used as looper thread can follow the uniform deformation, while the other types threads, such as the carbon yarn and stainless-steel looper thread were irregular and cannot form curved lines with small angle. These findings were consistent with the initial modulus of conductive yarns in tensile test. The initial modulus of the carbon yarn and stainless-steel threads were higher than silver-coated yarns, and the looper threads in 602 stitch sewing were irregular, as shown in B2, B3, B4 and D1 in Figure 3-4.

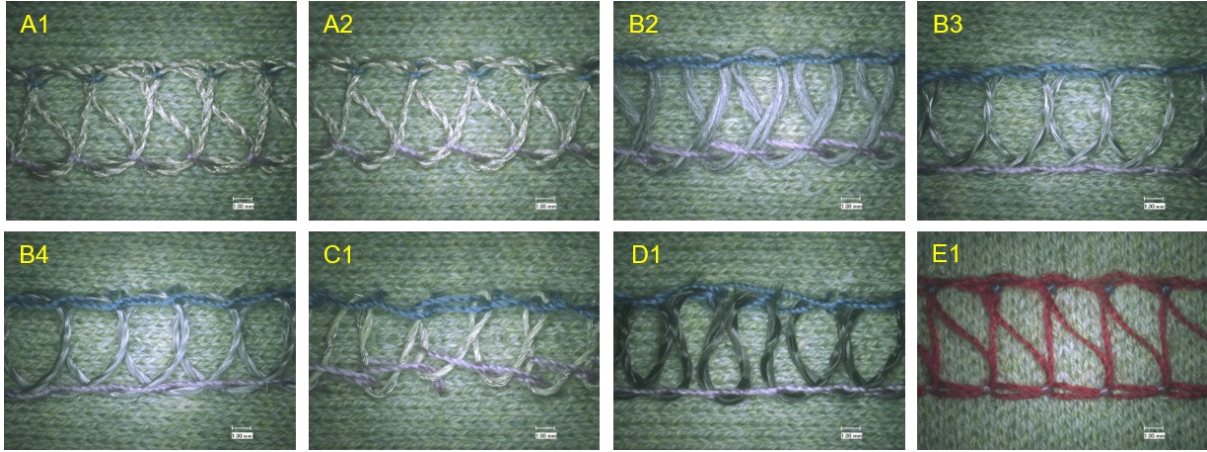


Figure 3-4. The appearance of 602 chain-stitch with conductive yarns as looper thread. A1 and A2 are silver coated yarns HC12 and HC40, respectively. B2, B3 and B4 are stainless steel yarns, C1 is Cu wire and cotton yarn, D1 is Carbon yarn. E1 is traditional sewing thread.

Putting conductive thread in the loop of 602 covering chain stitch sewing machine was easier to test and the sewing performance can be evaluated immediately after sewing. This method can be used to estimate the bending performance of conductive yarns instead of complicated indirect mechanical test.

3.1.3.2 Needle size for conductive yarns embroidery

The first step to choose the needle for embroidery relates to its size, which the long groove can hold the thread pass through the needle and form the loop [66]. The cross section of the needle was shown in Figure 3-2(a), which could be looked as ‘trapezoidal’ shape. The silver-coated conductive threads were soft and flexible, they could change the cross-section shape when passing through the needle. But the cross-section area of the yarns would keep the same value as the circle shape. The cross-section area of the needle’s long groove can be estimated with Equation (3-2), and the cross-section area of the yarn can be estimated by Equation (3-3). The maximum diameter of conductive yarn used based on the long groove cross section area could be roughly estimated with Equation (3-4) with the condition of S_1 equals S_2 .

$$S_1 = (TW + BW) \times \frac{D}{2} \quad (3 - 2)$$

$$S_2 = \pi \times \left(\frac{d}{2}\right)^2 \quad (3-3)$$

$$d = \sqrt{\frac{(TW + BW) \times 2D}{\pi}} \quad (3-4)$$

where S_1 is the cross-section area of long groove in a needle, S_2 is the cross-section area of the yarn, TW is the top width of the long groove, BW is the bottom width of the long groove, D is the depth of the long groove. d is the diameters of thread used through the needle.

The cross section of the conductive thread was assumed to be circle shape and the long groove of the needle is in proportion to the diameter of the needle blade, which represents the needle size. K5 series GROZ-BECKERT needles, from 60# to 110# with RG needle head were used to calculate the cross-section area of the long groove. Five new needles were selected from each size and to measure the bottom width, top width and depth of the needle long groove with the 3D measurement function in optical microscope system, shown in Figure 3-2(b). Table 3-6 shows the calculated maximum diameters of conductive yarns could be used with needles. Linear regression analysis was carried out to study the relationship between yarn diameters and needle blade diameters, the results of which is shown in Figure 3-5.

Table 3-6. Results of calculated maximum diameters of conductive yarns could be used with GROZ-BECKERT needles

Needle Size	60#	65#	70#	75#	80#	85#	90#	100#	110#
Needle blade diameter (μm)	600	650	700	750	800	850	900	1000	1100
Calculated the maximum conductive yarn diameter could be used (μm)	262.1	281.2	291.7	307.8	328.4	371.3	373.3	418.2	443.0

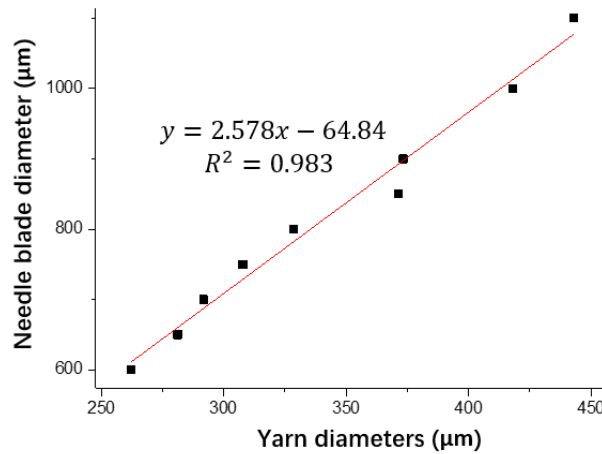


Figure 3-5. Regression analysis of yarn diameters and needle blade diameters.

According to the analysis before, the GROZ-BECKERT needle size used for conductive yarn embroidery could be calculated by Equation (3-5) (unit: μm):

$$NB = 2.578 \times d - 64.84 \quad (3 - 5)$$

where NB is the diameter of a needle blade, d is the diameter of threads. Based on the equation, the needle sizes for the HC12 and HC 40 embroidery were selected as shown in Table 3-7. The diameter of the yarns was measured according to the ASTM D204-2 standard method with optical microscope KEYENCE VHX-5000.

Table 3-7. The diameter of conductive yarn and suitable needle size

Conductive yarn types	Diameter of conductive yarns (μm)	Needle size
HC12	388.3±28.92	90#-100#
HC14	283.4±35.29	70#-75#

3.1.3.3 Analysis of needle cutting damage

The needle passed through the center of fabric structures, an opening is formed and the fibers are pushed to accommodate the thickness of the needle, as shown in Figure 3-6(a). Only 1 stitch damage was found in the knitted fabric after high speed at 800 RPM and 1 mm length stitching, using 100 RG needle. Figure 3-6(b) shows the yarn of the knitted fabric was cut by the needle

punching. The embroidery technique was friendly with knitted fabric because there was no needle cutting damage on substrates after ordinary fabrications.

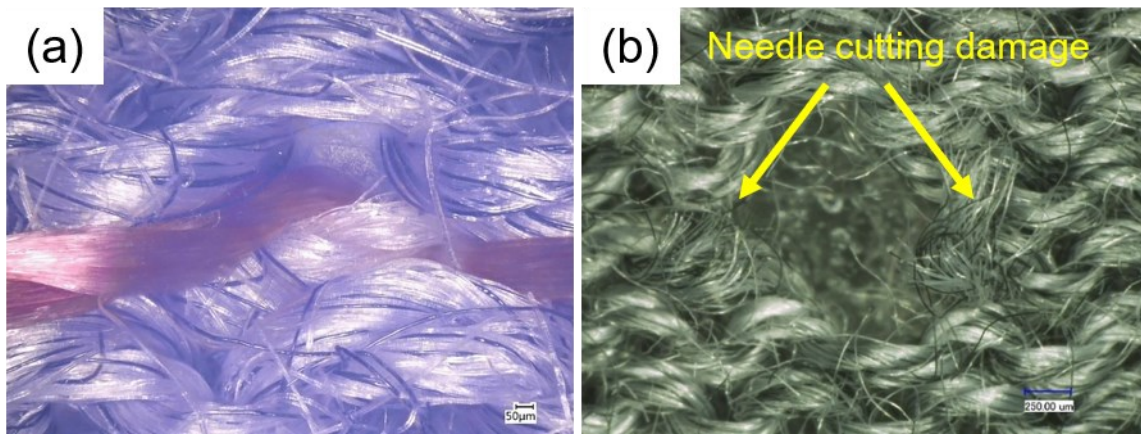


Figure 3-6. The images of needle cut in fabric. (a) Appearance of the needle hole formed with 100 FG needle embroidered in 400 RPM; (b) Appearance of the yarn broken in the fabric with 100 RG needle embroidered in 800 RPM.

3.1.4 Conclusion

Compared to silver coated polyamide threads, the stainless-steel yarns, copper-cotton hybrid yarns and carbon yarns show higher initial modulus and higher bend resistance in small diameter circle tested by 602 stitch type sewing. The silver coated polyamide threads were fit for embroidery through needle thread of lock-stitch formation. Based on the stitch development mechanism of lock-stitch embroidery, the calculation equation for selection of needle size for silver coated conductive yarns were achieved. The analysis of needle cutting damage showed needle punching of embroidery processes were safe for knitted fabrics, but higher speed of 800 RPM embroidery with thicker and medium ball point needle are not proper for knitted fabric fabrication.

3.2 Performance evaluation of conductive tracks in fabricating e-textiles by lock-stitch embroidery

Authors: Yan Zheng, Lu Jin, Jing Qi, Zekun Liu, Lulu Xu, Steven Hayes, Simeon Gill, and Yi Li

Journal: Journal of Industrial Textiles

DOI: 10.1177/1528083720937289

Statement of own contributions: Main research idea, conductive tracks fabrication and evaluation, data analysis; Preparation of tables, figures, and the manuscript.

Statement of co-author contributions: Lu Jin, Jing Qi and Zekun Liu supports in conductive tracks samples evaluation. Lulu Xu, Simenon Gill and Steven Hayes support in embroidery techniques for conductive tracks. Yi Li initiated project idea and provided supervision and guidance in research methodology, the design of experiment, data analysis and interpretation, and paper revision.

3.2.1 Introduction

Applications of wearable electronic textiles (e-textiles) in smart clothing have attracted considerable attention on account of their immense potential to monitor vital signs in health care situations [115, 116], physical performance during sporting activities [117, 118], the safety and wellbeing of soldiers and firefighters [119–121], and treatment processes and rehabilitation [92], as well as their role in providing interactive entertainment [122]. Among the different methods to create e-textiles, embroidery is one of the most preferred ways because the technique allows for flexible patterns [10, 11], dimensional accuracy, mass production, and cost-effective production. Therefore, embroidery has been widely used to create high-performance textile electrodes [12–15], circuits [16, 17] and sensors [18–21].

During the embroidery process, the fabric substrate is held under tension by an embroidery frame that is moved in the x-and y-directions, and an embroidery needle repeatedly pierces the fabric to form stitches. However, the deformation of the fabric during sewing increases the unevenness of the stitch tracks and causes size discrepancies between the embroidered element and the digital design. This not only negatively affects the aesthetics of the product but also results in inconsistent levels of electrical resistance, which severely reduces the performance

of wearable e-textiles. A number of studies have therefore investigated the factors that are associated with the accuracy of embroidery pattern elements on woven fabric with digital designs [67, 80, 81, 123, 124]. However, while they have shown that the shape and dimensions of the embroidered element fail to conform to the designed digital image in most cases, they use non-conductive embroidery threads. Moreover, even though their work examines embroidery technology, the accuracy of the wearable embroidered devices with conductive yarns has been largely ignored.

Since there is a research gap in fabricating wearable embroidered devices with conductive yarns, it is important to have a good understanding of the type of conductive yarns used for such devices. In the literature, some studies have examined the use of conductive yarns for fabricating wearable devices. For instance, Chui et al. [125] examined silver-coated polyamide yarns for wearable electronic product applications as they are light in weight, and flexible with high mechanical stability as opposed to metal and carbon yarns. They are also widely used in smart clothing as they do not irritate the wearer and are bacteriostatic [126]. Therefore, silver-coated yarns will be examined in this study. However, Chui et al. [125] and de Kok et al. [127] also reported that silver-coated yarns become damaged as the silver is delaminated after stitching during the manufacturing process. The coating of the conductive yarn is damaged after stitching and the damage to the yarns increases in severity from the applied mechanical stresses. That is, conductive thread is subjected to mechanical stresses and strains at different guides, regulated tensions, take-up levers and needle eye sizes during embroidery process. As such, the yarn is damaged that interferes with the electrical resistance performance of the embroidery elements. Therefore, the impact of the fabrication process on the functional performance of silver-coated yarns should be well understood before advancing to the development of e-textiles because it is crucial to preserve the silver that is coated on the yarns during the production process.

As for the type of fabric, knitted fabrics are a good option for e-textiles as they have high extensibility and air permeability. However, embroidering precise wearable devices with

conductive yarns on knitted fabric is still challenging. The fabric structure becomes unstable with the application of tensile force, such as when a needle penetrates the fabric [128], which leads to the deformation of the fabric. In turn, this can lead to the nonconformity of the embroidery elements with respect to the designed digital image. Therefore, woven and nonwoven fabrics are usually used in developing electronic wearable devices [13, 31, 95] in order to produce robust embroidery elements. Nevertheless, even though the effects of the stitch type, stitch length and number of embroidered conductive threads on the resistance of the embroidered lines were compared in [129], little attention has been paid to the impact of the embroidery parameters on the performance of the conductive tracks on knitted fabrics.

Herein, we explore the impacts of the design and fabrication parameters on the embroidery process in terms of the appearance quality, dimensional stability and electrical resistance of conductive tracks. The significance and interactive impacts of the stitch length, needle thread pre-tension, and embroidering speed and directions on the performance of conductive tracks are then evaluated. Also, optimized parameter settings that balance both appearance quality and enhanced conductivity of the conductive tracks are determined. The findings have importance for the embroidery parameter settings of wearable e-textiles, such as electrodes and circuits, which integrate silver-coated conductive yarns into knitted fabrics.

3.2.2 Experimental details

3.2.2.1 Materials

Two-ply silver-coated polyamide threads (HC 12 and HC 40) were purchased from MADEIRA[®][130], and used to investigate the impacts of the embroidery parameters on the performance of conductive tracks. The threads are twisted into 2-ply yarns (see Figure S1 in Supporting Information). The physical properties of these yarns are listed in Table 3-8. They were tested in accordance with standard ASTM Test Method D204-02.

Table 3-8. Physical properties of silver-coated polyamide yarns

Thread name	Thread types	Linear density (tex)	Electrical resistance (Ω/m)	Breaking strength (cN)	Breaking elongation (%)	Silver content (wt%)	Twist (tpm)	Twist direction
HC 12	Shieldex [®] 235/36-2 ply	61±1.5	80±9.6	2998±51.7	32.9±0.7	22.95±2.5	467±1	Z
HC 40	Shieldex [®] 117/17-2 ply	29±0.6	270±11.2	1330±7.2	26.3±0.4	19.31±2.1	633±1	Z

The knitted fabric substrate is certified for producing the T-shirts of firefighters, and supplied by KIVANC GROUP (Istanbul, Turkey). The properties of the fabric substrate are listed in Table 3-9. The wale and course counts were tested in accordance with ASTM D8007. A cold water soluble film known as Avalon (made of polyvinyl alcohol, 20 g/m²) was placed over the fabric surface to improve stability of knitted fabrics during the embroidery process.

The embroidery machine, JCZA 0109-550 (ZSK Stickmaschinen GmbH Germany) was used with DBX K5 ball-point needles (Groz-Beckert KG Germany), which meant that the needles would not cut fibres and yarns of the fabric substrate.

Table 3-9. Properties of the knitted fabric used.

Structure	Composition	Wale count per 2.5 cm	Course count per 2.5 cm	Surface density (g/m ²)
Single jersey	78% FR viscose, 20% Para-Aramid, 2% carbon	28±1	35±1	200±10

3.2.2.2 Methods

A rectangular shaped embroidery pattern that used polylines lines with different angles was designed by using an embroidery software called EPCwin (ZSK Stickmaschinen GmbH). The embroidered tracks were produced along a designed pattern, which contained the wale and course direction, and four bias angles of 15°, 30°, 45° and 60° respectively. They are symmetric angles based on the course direction as shown in Figure 3-7. The embroidering process began

at the ‘Start’ point in the counter-clockwise direction and after stitching based on shape of the embroidery tracks, and ended at the ‘Finish’ point. Selected embroidered samples are presented in Figure S3-2 (Supporting Information).

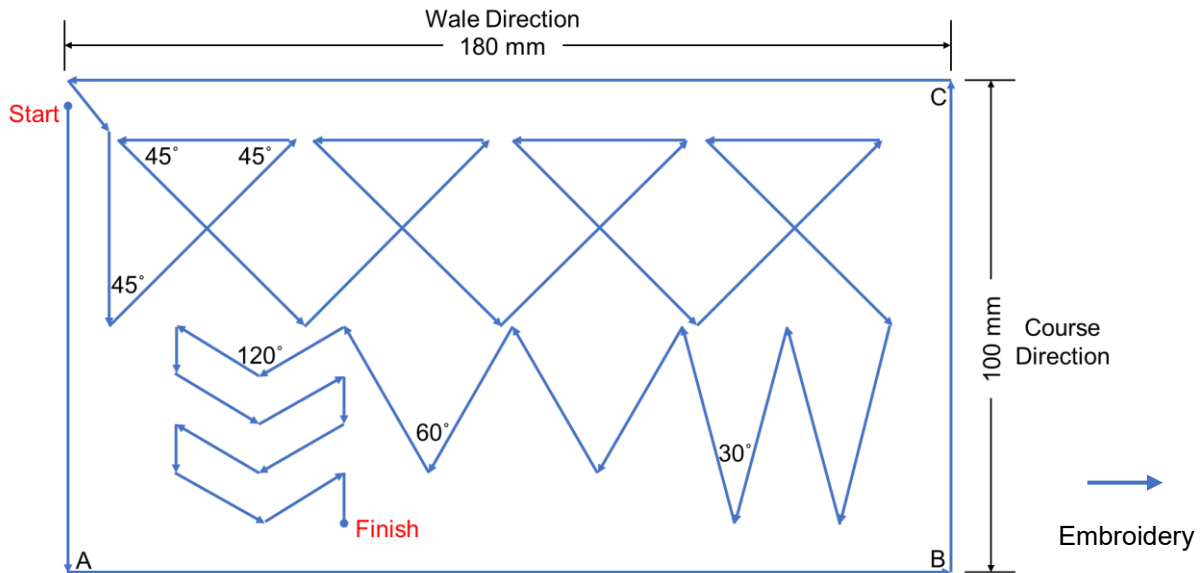


Figure 3-7. Embroidery test pattern with the studied stitch directions.

The fabrication parameters, including the embroidering speed (ES), stitch length (SL), needle thread pre-tension (NTP) and embroidery direction (ED), were examined for their influence on the conductive tracks. Therefore, a four-factor two-level experimental factorial design was used to consider all combinations of the input parameters (see Table 3-10 and Table S1 in Supporting Information). Sixteen runs were carried out for each set of experiments. For accuracy and repeatability of the results, the experiments were repeated three times. Therefore, 48 runs were conducted. To determine if there were any data variations in the fabrication process, additional centre points were added in the course and wale directions and repeated four times separately with the following settings: ES (400 RPM), SL (2.75mm), NTP (40 gf for HC 12 and 30 gf for HC 40) and ED (wale and course). In total, 56 runs were conducted.

The NTP of HC 12 and HC 40 was set differently because the latter has a lower tensile stress (see Figure S3, Supporting Information). An ordinary polyester thread was placed into the bobbin and the NTP was fixed at 40 gf. The maximum NTP was set in accordance with the

stitch formation which kept the interlacing of the needle thread and bobbin thread just below the fabric.

Table 3-10. Factorial design of selected embroidery parameters and levels for the experiment

Level \ Factor	ES (rpm)	SL (mm)	NTP (gf) ^A		ED
			HC 12	HC 40	
Low	200	1.5	30	20	Wale
High	600	4	50	40	Course

^A 1 gf=0.98 cN

Since the designed embroidery pattern consists of the wale and course directions, the samples were fabricated by using 3 combined input technical parameters. Table 3-11 presents the simplified embroidery parameters of the 2³+1 conductive track samples fabricated with HC 12 and HC 40.

Table 3-11. Samples and corresponding experimental specifications

Sample No.	ES (rpm)	SL (mm)	NTP (gf) ^A	
			HC 12	HC 40
1	200	1.5	30	20
2	600	1.5	30	20
3	200	4	30	20
4	600	4	30	20
5	200	1.5	50	40
6	600	1.5	50	40
7	200	4	50	40
8	600	4	50	40
9	400	2.75	40	30

^A 1 gf=0.98 cN

3.2.2.3 Characterization of conductive tracks

The performance of the conductive tracks embroidered with silver-coated polyamide thread was evaluated by their appearance quality, dimensional stability and electrical resistance of the running stitch tracks in the wale and course directions respectively. Points A to B in Figure 3-7

denotes the measured value in the wale direction. Points B to C is the measured value in the course direction.

The appearance quality was subjectively assessed by examining the stitch continuity and uniformity in different directions. The floated stitch numbers at every 10 cm in the wale and course directions on the back side of the sample was used for the statistical (objective) analysis.

The dimensional stability was evaluated by percentage of shrinkage of the embroidered tracks in the wale and course directions, which is calculated by using the following equation:

$$\text{Size shrinkage (\%)} = (L_1 - L_0) / L_0 \times 100\% \quad (3-6)$$

where L_1 is the length of the conductive tracks after stabilized for 24 hours. L_0 is the software designed length of the conductive tracks, which is 180 mm in the wale direction and 100 mm in the course direction.

A scanning electron microscope (SEM, Philips Quanta 200) and an optical microscope (KEYENCE VHX-500F) were used to examine the morphology of the conductive yarns and for the shape image of conductive tracks. A multi-meter (Keithley 2000) was used to measure the electrical resistance of conductive tracks. The length of the embroidered conductive tracks was measured by using a soft tailor tape.

3.2.2.4 Statistical analysis

Minitab-19 software was used to create the experimental design and carry out the statistical analysis. The influence of the investigated variables was assessed by using the p-value of the two-way analysis of variance (ANOVA) results, in which $p < 0.05$ shows the significance of each independent variable and the interaction between them.

3.2.3 Results

3.2.3.1 Evaluation of appearance quality of conductive tracks

All of the conductive tracks were found to be continuous with no broken threads. Figure 3-8(a)

to (l) show the surface morphology of Sample 6 which is embroidered with bias angles in different directions. The figure shows that the appearance of the stitches changed with the embroidering direction. Figure 3-8(a) and(g) show the conductive tracks in the wale direction adhere the most to the design pattern, while the conductive tracks in the course direction are observed to have serious drift, as shown in Figure 3-8(b) and (h). The appearance of embroidered conductive tracks can be ordered from uniform to irregular based on the stitch uniformity as follows: wale direction > 60° bias angle > 45° bias angle > 30° bias angle > 15° bias angle > course direction.

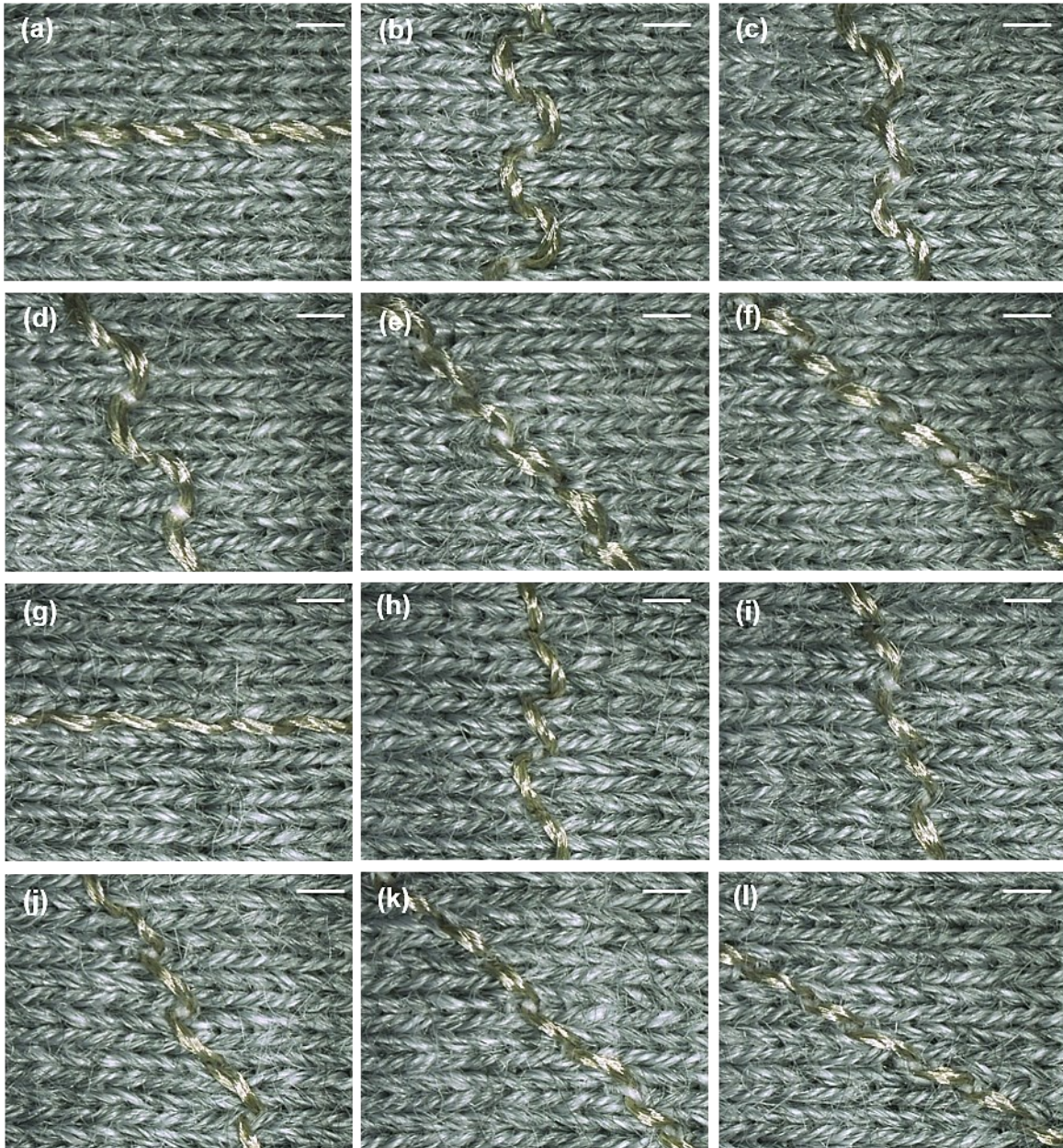


Figure 3-8. Optical microscope images of sample surface. Scale bars are 1 mm. (a-f) Conductive tracks embroidered with HC 12 thread in the wale direction, course direction, with 15°, 30°, and 60° bias angles respectively. (g-l) Conductive tracks embroidered with HC 40 thread in the wale direction, course direction, with 15°, 30°, 45° and 60° bias angles respectively.

The float stitches were defective as they were obviously loose and twisted on the fabric after the embroidering was carried out, which is the result of the unbalanced thread tension of the needle and bobbin threads. Figure 3-9(a) and (b) show the mean floated stitch numbers on

the back side of the samples, and the factors that contribute to the defects was shown in Figure 3-9(c) to (f). As shown in Figure 3-9(a) and (b), the floated stitch numbers in the course direction in most cases is higher than that in the wale direction. Samples 1 to 4 with an SL of 1.5 mm have most of the defective stitches. There are a larger number of floated stitches in the conductive tracks embroidered with HC 12 than in the conductive tracks that use HC 40. Figure 3-9(c) and (f) show the ranking of the influential factors that affect the float stitches of the conductive tracks embroidered with HC 12 and HC 40 threads, respectively. The number of floated stitches is significantly reduced (from over 3 to 0) with a longer SL and increase in the NTP, as shown in Figure 3-9(d) and (g). However, Figure 3-9(e) and (h) show the SL has less influence when the NTP is high. As for the HC 12 thread, the number of floated stitches embroidered in the wale and course directions is also fewer when using a higher NTP and longer SL, as shown in Figure 3-9(e).

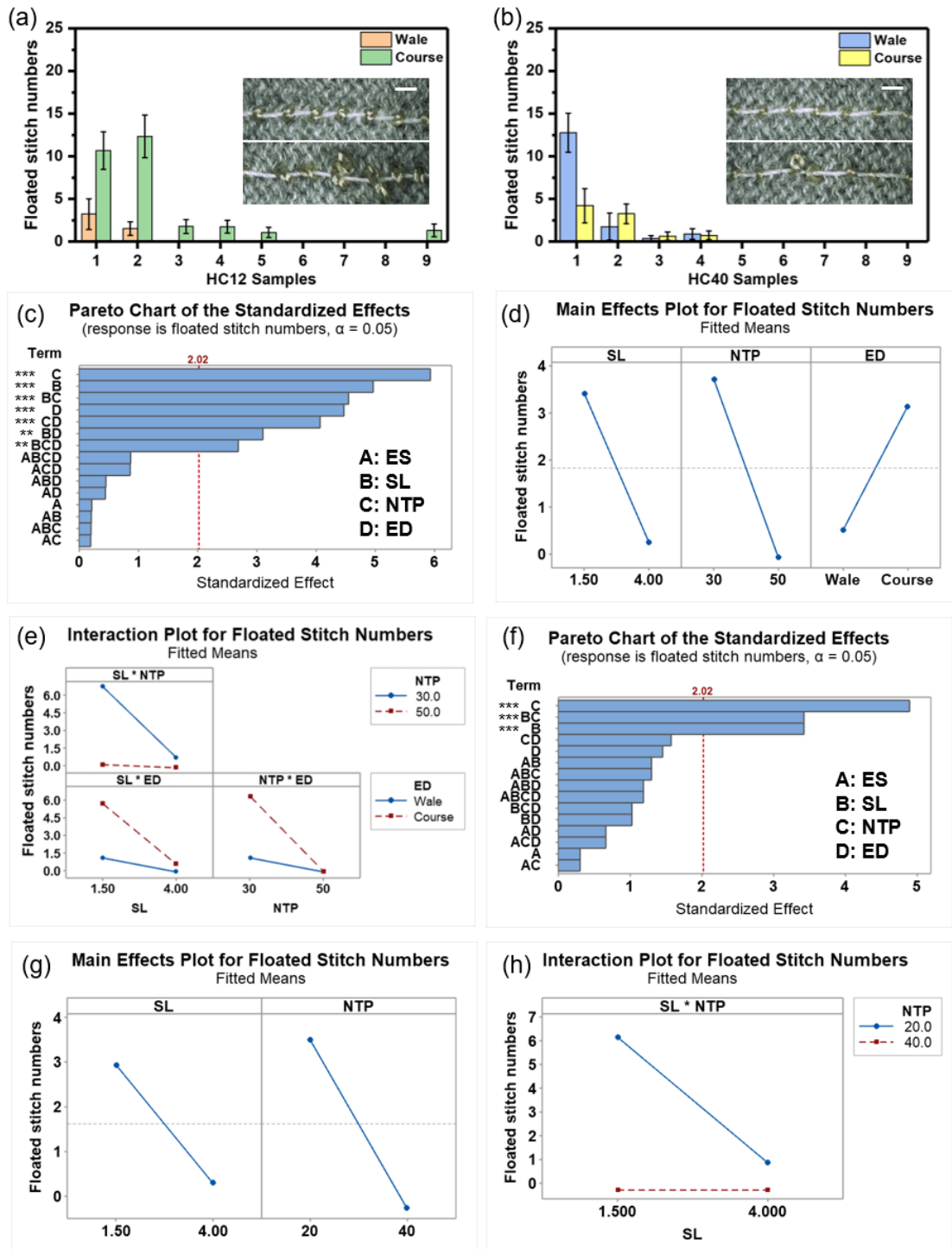


Figure 3-9. Floated stitch numbers analysis in embroidered conductive tracks. (a, b) Mean of floated stitch numbers on back side for every 10 cm of conductive tracks with HC 12 and HC 40 threads respectively. The upper inset shows a uniform stitch and the float stitch is shown below. Scale bars are 2 mm. (c- e) Statistic results for number of floated stitches of samples embroidered with HC 12 thread. (f- h) Statistic results for number of float stitches of samples embroidered with HC 40.

3.2.3.2 Evaluation of dimensional stability of conductive tracks

The deformation of embroidered fabric increases the nonconformity of the conductive tracks and cause size discrepancies. In order to evaluate the dimensional stability of the embroidered element, the shrinkage (%) of conductive tracks in the wale and course directions was determined. The results can be used to maintain accuracy of the size of embroidered elements through a comparison with the pattern. Figure 3-10(a) and (b) show the average shrinkage (%) of samples in the wale and course directions, and the factors that contribute to this issue was shown in Figure 3-10(c) to (f). It can be observed that there is less shrinkage in the wale direction than in the course direction for all of cases. The shrinkage (%) is significantly influenced by the ED and SL, as shown in Figure 3-10(c) and (e). However, there is no interaction between any of the parameters. Figure 3-10(d) and (f) show that with a longer SL, the percentage of shrinkage increases albeit not very significantly (from 4 % to over 5 %). Note that the lowest percentage of shrinkage of the embroidery in the wale direction is about 3 %, while that in the course direction is higher than 6 %. Furthermore, longer SL results in an increase in the percentage of shrinkage.

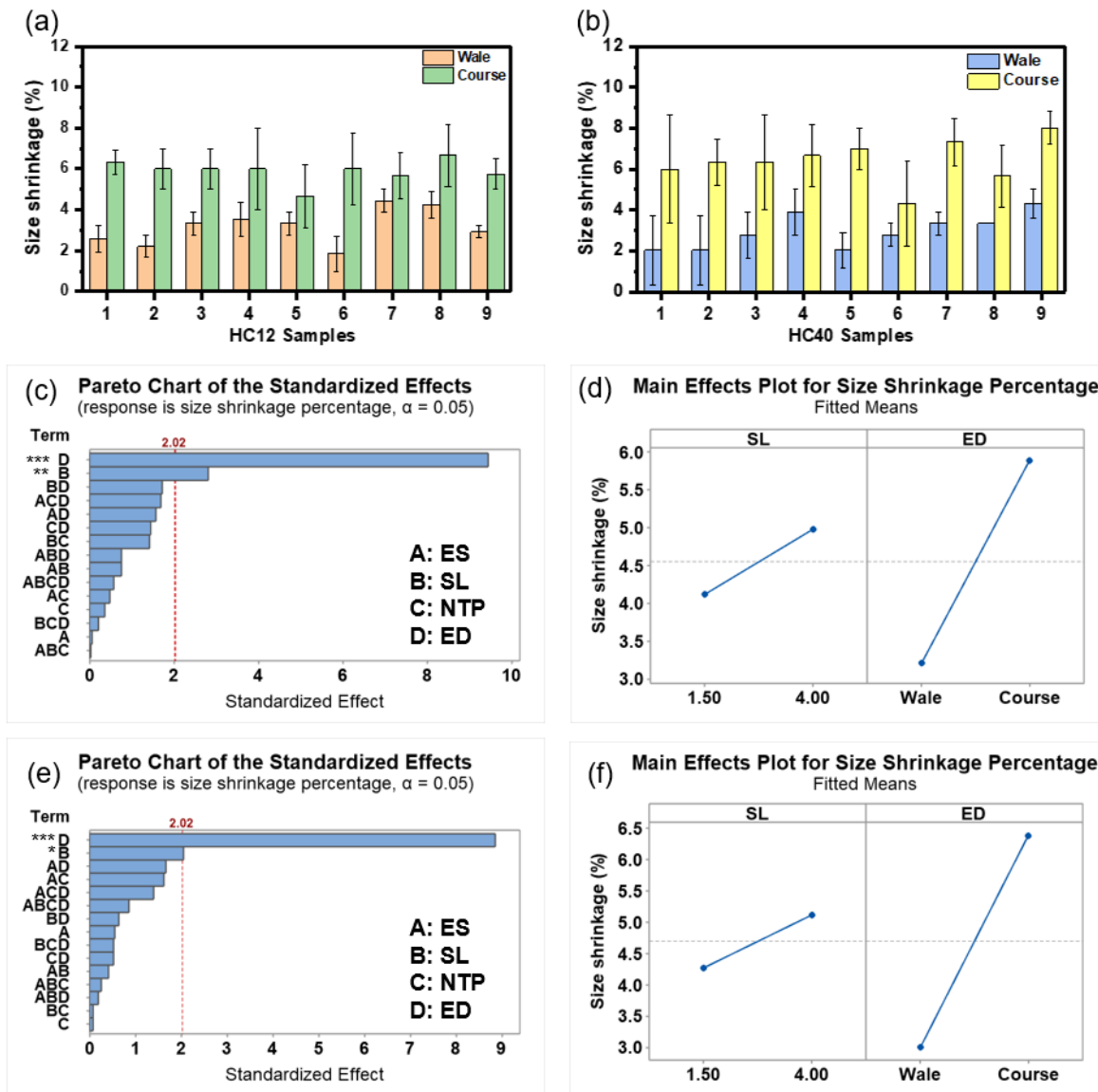


Figure 3-10. Size shrinkage (%) of embroidered tracks. (a-b) Shrinkage (%) in wale and course directions of tracks embroidered with HC 12 and HC 40. (c-d) Statistic results of samples embroidered with HC 12. (e-f) Statistic results of samples embroidered with HC 40.

3.2.3.3 Evaluation of electrical resistance of conductive tracks

It is crucial to maintain optimum electrical conductivity when incorporating conductive yarns in the embroidery process. Figure 3-11(a) and (b) show the average electrical resistance for each 10 cm of embroidered conductive tracks, and the factors that affect the electrical resistance was shown in Figure 3-11(c) to (f). There is no difference in the electrical resistance in the wale and course directions of the embroidered conductive tracks, which was shown in Figure 3-11(a)

and (b). Among all of the test samples, the highest electrical resistance is found with Sample 6, which has an SL of 1.5 mm, the fastest ES and highest NTP. The lowest electrical resistance is found with Samples 3 and 4, which use HC 12, and Sample 7 that uses HC 40 respectively. All of these samples have an SL of 4 mm. Figure 3-11(c) and (e) show that the SL and ES significantly influence the electrical resistance of embroidered conductive tracks that use HC 12 and HC 40. The NTP also impacts the electrical resistance as of the embroidered conductive tracks that use HC 12. A longer SL significantly reduces the electrical resistance of embroidered conductive tracks, from about 23 $\Omega/10$ cm to 13 $\Omega/10$ cm with the use of HC 12, as shown in Figure 3-11(d), and 94 $\Omega/10$ cm to 68 $\Omega/10$ cm with the use of HC 40, which were recorded in Figure 3-11(f). In addition, the electrical resistance increases with a faster ES and higher NTP with the use of HC 12.

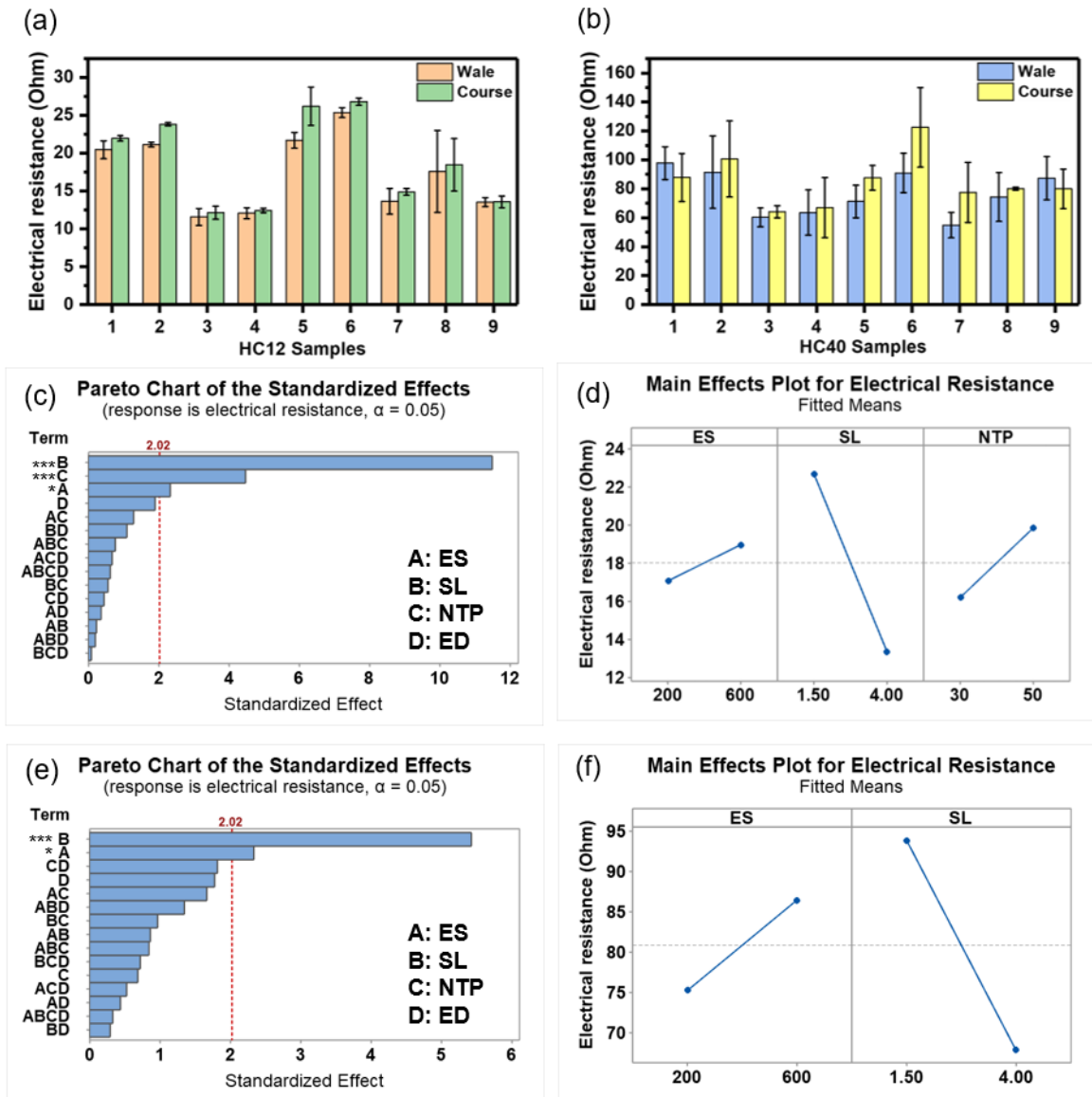


Figure 3-11. Electrical resistance of embroidered conductive tracks. (a-b) Mean of electrical resistance for each 10 cm of conductive tracks embroidered with HC 12 and HC 40. (c-d) Statistic results of samples embroidered with HC 12. (e-f) Statistic results of samples embroidered with HC 40.

3.2.3.4 Trade-off between appearance quality and electrical resistance

The study results show that the appearance quality of the conductive tracks vary in different embroidered directions on the knitted fabric. The number of float stitches increase with a lower NTP and shorter SL. Embroidering in the wale direction not only increases the uniformity of the stitches of conductive tracks, but also reduces the percentage of shrinkage. The electrical

resistance of conductive tracks is reduced with a longer SL and slower ES. Based on the analysis of variance, the statistically significant effects were selected to develop a first-order response surface model for the process [131]. Regression equations that involve the parameters of the significant factors and their interactions with the performance of conductive tracks were subsequently established and provided in Table 3-12. The regression coefficients (R^2) are also listed.

Table 3-12. Multi-linear regression equations based on significant factors

Evaluation target	Thread name	Multi-linear regression equation	R^2 (%)
Number of floated stitches	HC 12	24.4-5.59 B-0.47 C+8.19 D+0.11BC-1.52 BD-0.14 CD+0.02 BCD	92.29
	HC 40	28.69-7.44 B-0.72 C+0.19 BC	88.58
Percentage of shrinkage	HC 12	6.3-0.51 B+5.73 D	93.58
	HC 40	3.01-0.09 B-0.2 D	89.79
Electrical resistance	HC 12	20.26+0.007 A-2.62 B+0.16 C	94.62
	HC 40	150.2-0.08 A-22.4 B	85.6

Notes: A: ES; B: SL; C: NTP; D: ED.

To determine the appropriate embroidery parameters that would allow for conditions of good appearance quality and lower electrical resistance, an overlay plot analysis [132] was carried out. The SL and NTP were set as the decisive factors for the HC 12 and HC 40 threads. The white region of the contour plot shows the best results and related variable values in Figure 3-12. The acceptable range of electrical resistance values for the conductive tracks is set as one to twofold value of the resistance for each 10cm of the original conductive yarns. The optimum number of float stitches ranges from -0.5 to 0. Other optimal embroidery parameters are an ES of 200 rpm and stitching in the wale direction. Figure 3-12(a) shows the optimum range of SL and NTP with the use of HC 12. When embroidering with stitches longer than 3.1 mm, the NTP can be set from 30 gf to 50 gf. An SL that is more than 3.5 mm and NTP setting of 26 gf to 40 gf are suitable with the use of HC 40, which was shown in Figure 3-12(b).

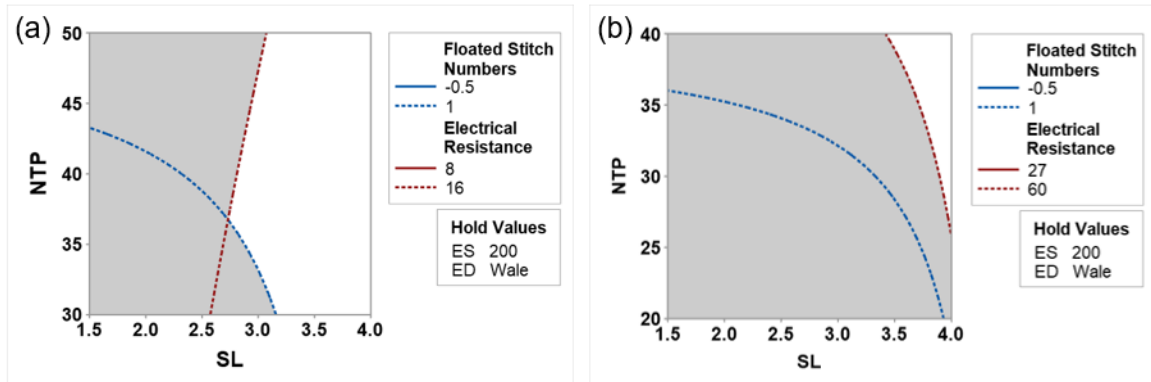


Figure 3-12. Overlaid contour plot of minimum number of float stitches and the lowest electrical resistance per 10 cm. (a) HC 12 thread and (b) HC 40 thread.

Based on the variable ranges obtained from the overlaid contour plot, a multiple response optimization analysis [132] was carried out to establish the factor levels that minimise the electrical resistance value and number of floated stitches. The prediction was carried out by Minitab-19 and the results are shown in Table 3-13 for both the HC 12 and HC 40 threads. The targets for the upper and lower limits of the electrical resistance value and the number of float stitches were set to be the same as those in the contour plot analysis.

Table 3-13. Multiple response prediction of embroidery parameters

Thread name	Variable setting				Electrical resistance For each 10 cm of conductive track (Ohm)		Number of float stitches for each 10 cm of conductive track	
	SL (mm)	ES (rpm)	NTP (gf) ^A	ED	Fit	95 % CI	Fit	95 % CI
HC12	4	200	30	Wale	10.956	(10.25, 11.66)	-0.100	(-0.39, 0.19)
HC40	4	200	31	Wale	44.98	(31.60, 58.36)	-0.243	(-1.26, 0.77)

^A 1 gf=0.98 cN

After the optimization analysis was carried out, the variables and their values were validated by carrying out an embroidery test. Each embroidery parameter was used to fabricate 15 cm of straight tracks along the wale direction, and each embroidery test sample was replicated ten

times. The electrical resistance of conductive tracks was calculated and the results are all in the range of a 95 % confidence interval (CI) of the predicted response results. All of the stitches on the validated samples are uniform with no float stitches. Table 3-14 shows the validated results.

Table 3-14. Validated results of embroidery parameters

Thread name	SL (mm)	ES (rpm)	NTP (gf) ^A	ED	Electrical resistance per 10 cm (Ohm)	Floated stitch numbers per 10 cm
HC 12	4	200	30	Wale	11.46±0.62	0
HC 40	4	200	31	Wale	40.16±3.72	0

^A 1 gf=0.98 cN

3.2.4 Discussion

Knitted fabrics have a slack structure and deform with the application of tensile force, and when used for e-textiles, result in the nonconformity of conductive tracks. Audzevičiūtė-Liutkienė et al. [128] showed that there is less non-uniformities of knitted fabrics in the wale direction as opposed to the course direction. The loops of the knitted fabric in the course direction can easily slip when the needle and bobbin threads interlace to form stitches. Also, this study finds that the loop structure of the knitted substrate can be easily distorted by the force of the interlacing of the needle and bobbin threads when the embroidery angle is 15° and 30°. When the embroidery angle is greater than 45°, the loops in the wale direction are more stable and can endure the force during stitch formation. For example, the stitches are more uniform with an embroidery angle of 60°. The density of the fabric structure in the wale direction (35 counts per 2.5 cm) is higher than in the course direction (28 counts per 2.5 cm); therefore, the stitches in the wale direction are more compact and closer together during the embroidery process. Furthermore, a lower density in the course direction results in a larger elongation in this direction, which increases the shrinkage of the embroidered conductive tracks. These findings are help to fulfil an analysis by Juchnevičienė et al. [80]: it is important to

evaluate the changes in size of substrate materials in different directions in order to produce embroidered elements with more accurate dimensions.

Lock-stitch embroidery is versatile because different materials and techniques can be combined and used together, such as padding and shearing [62]. This technique can produce a ‘two-thread’ structure, and the needle thread passes through the fabric substrate, bends and forms a loop with a small curvature radius when the needle moves upward. This loop is pulled by the rotary hook point, and the bobbin thread is released and wrapped during rotation of the hook mechanism under the needle plate. These two threads interlace below the fabric and form the stitch [66, 106, 133]. The key steps to forming a needle thread loop and lock stitches by the rotary hook are illustrated in Figure 3-13(a). The NTP is the essential factor for determining the interlocking of the needle and bobbin threads. In general, their tension is adjusted so that the bobbin thread is visible on the back side of the embroidery elements [67]. Figure 3-13(b) shows the formation of a 301 lock stitch with the appropriate amount of pre-tension. The electrical resistance of the embroidered conductive tracks is related to the length of the conductive thread. A longer SL reduces the stitch density, thereby reducing the thread consumption per unit. This lower thread consumption is related to the lower final electrical resistance value of conductive tracks.

To validate the bending rigidity of the silver-coated threads, their tensile properties were examined in accordance with standard ASTM Test Method D2256-10 (250 ±3 mm gage length at 300 ± 10 mm/ min operating rate). Compared to an ordinary polyester thread, the silver-coated threads showed a higher initial modulus, as shown in Figure 3-13(c). The thread at higher level initial modulus is stiff, which is easy to result in floated stitches with improper needle thread pre-tension. Therefore, the number of floated stitches on the conductive tracks embroidered with HC 12 is higher than with the use of HC 40. However, a higher NTP can stabilize the stitch formation and solve this problem. Figure 3-13(a) shows the NTP was adjusted by using three disk tensioners during the embroidery process. The conductive thread became elongated and rubbed the mechanical components which increased the friction with

the higher NTP, and subsequently damaged the silver coating on the conductive threads. The silver coating of HC 12 is more sensitive to this abrasion because it is thicker than HC 40, as shown in Figure 3-13(d) and (e). Apart from that, as the conductive thread passed through the take-up lever, the needle underwent greater dynamic loading and more friction cycles as the embroidery process was carried out at a high ES, which resulted in more damage to the silver coating of the conductive threads. Most embroidered wearable e-textiles use conductive thread in the bobbin because the thread is subjected to less stress during the manufacturing process [134, 135]. However, the conductive tracks are hidden by the frame of the embroidery hoop, which makes it difficult to combine different materials and techniques.

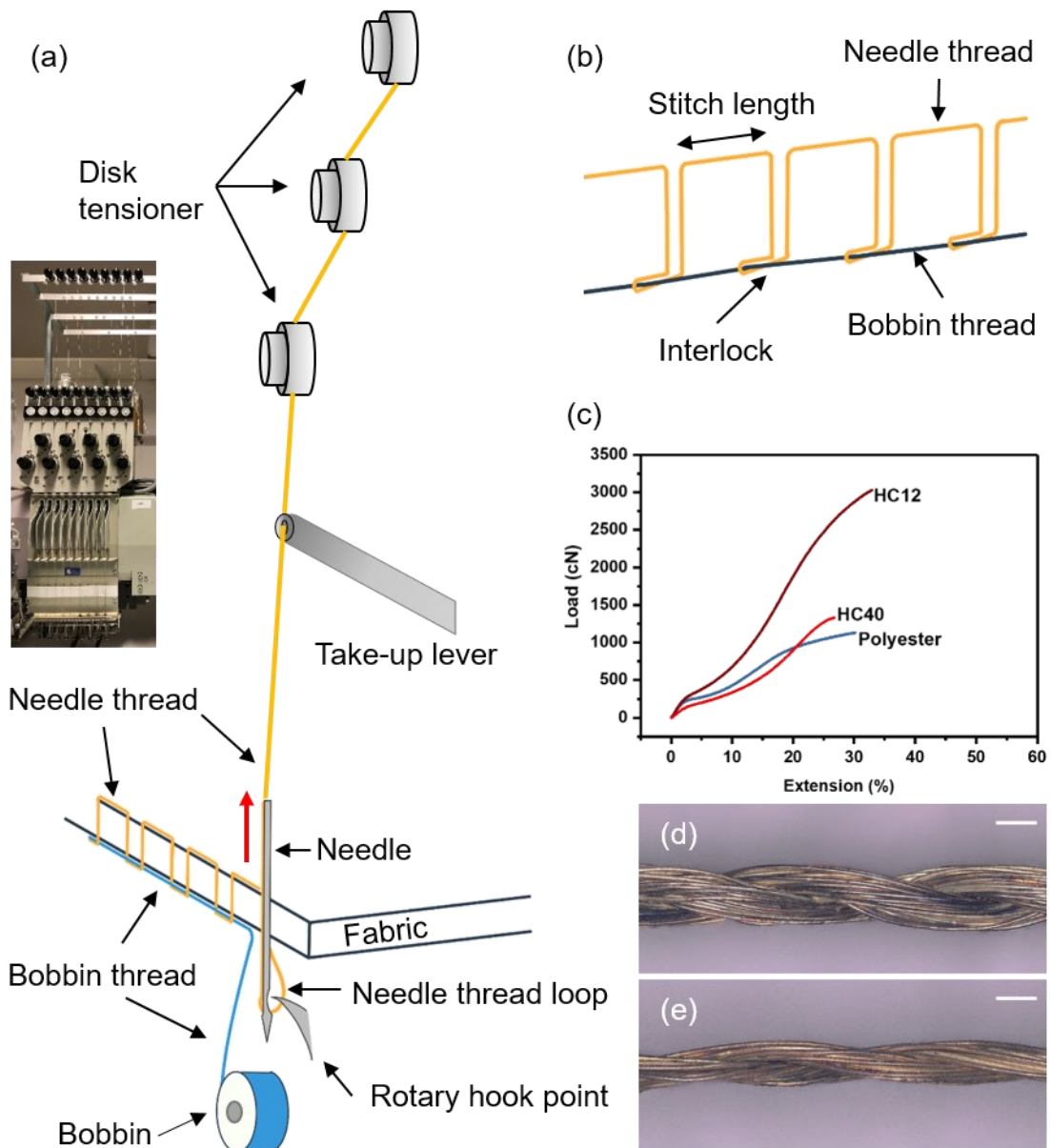


Figure 3-13. Illustration of lock-stitch embroidery mechanism and conductive yarns' characteristics. (a) Mechanical components of stitch formation in lock-stitch embroidery. Inset: photograph of NTP regulator components. (b) Lock-stitch structure in the embroidery. (c) Load extension curve for HC 12 and HC 40. (d) Optical microscope image of HC 12 and (e) of HC 40. Scale bars are 1 mm.

In order to investigate the extent of the damage to the silver coating, Figure 3-14(a) to (d) show the surface morphology of HC 12 before and after the embroidery process analysed by using the SEM. The embroidered conductive track of Sample 6, which has the highest electrical

resistance was examined. Figure 3-14(c) and (d) show that the silver coating on the fibre surface is damaged after the embroidering process, which is also confirmed through energy dispersive X-ray spectroscopy (EDX). There is more than a 20 % reduction, as shown in Figure 3-14(e) and (f), the silver atomic content after the embroidering process which could also be caused by the exfoliation of the silver coating on the conductive fibres due to abrasion.

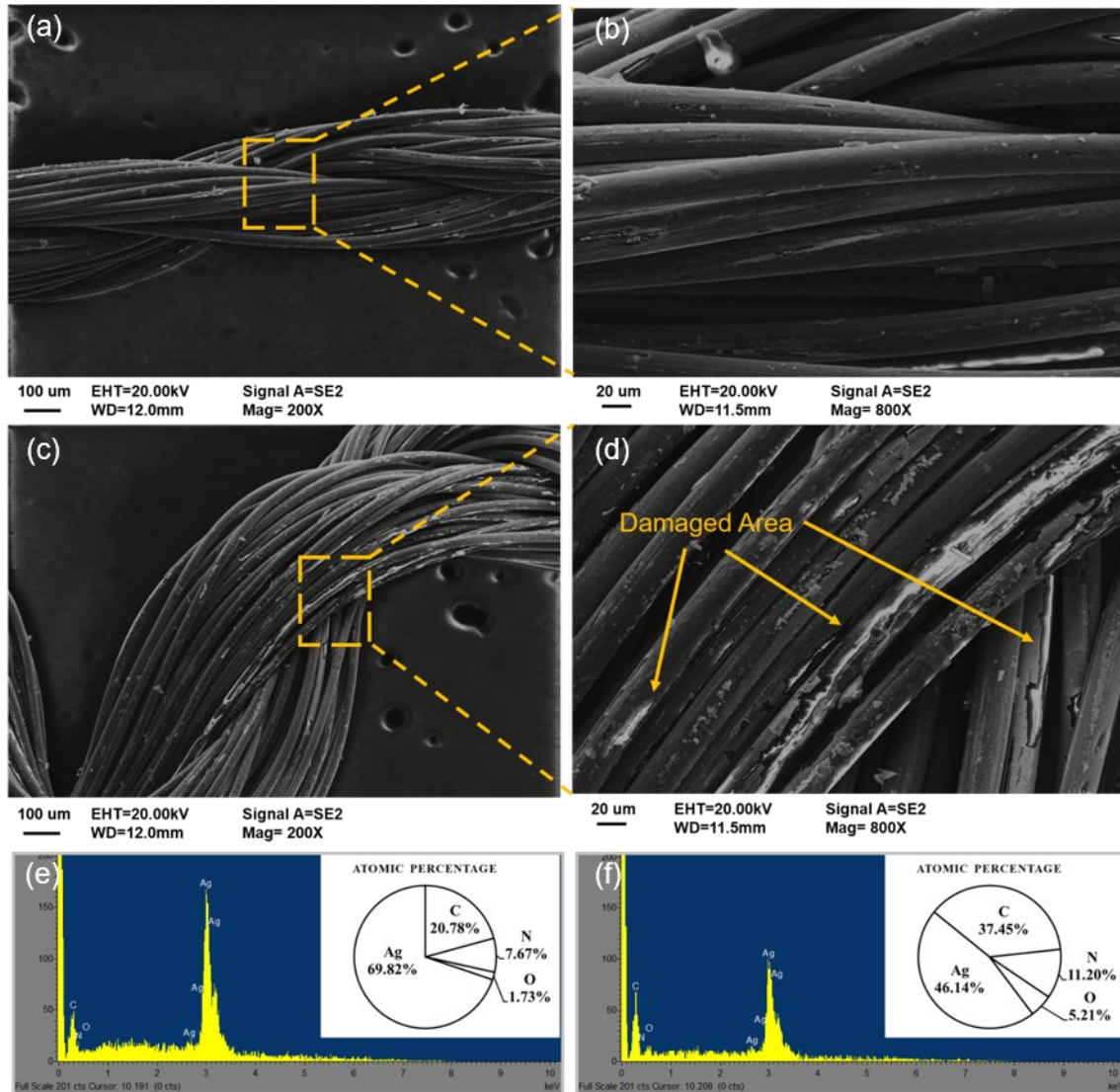


Figure 3-14. SEM and EDX analysis of conductive yarns before and after embroidery. (a,b) SEM images of HC 12 before embroidery processes. (c,d) SEM images of HC 12 after embroidering with 1.5mm stitch, at 600 rpm, and NTP of 50 gf. (e) EDX analysis of HC 12 before embroidery process. (f) EDX analysis of HC12 after embroidery process. The insets in (e) and (f) are atomic percentage results in EDX.

3.2.5 Conclusion

In summary, objective 1 has been achieved with demonstration that a uniform appearance of the conductive tracks in fabricating e-textiles would be more feasible if stitched in the wale direction of a single jersey fabric. An analysis of the stitch balance indicates that the number of floated stitches is higher with an SL of 1.5mm and lower NTP. It was shown that the percentage of shrinkage in the wale direction is less than in the course direction, and the electrical resistance of the conductive tracks is increased with a higher ES and shorter SL. The EDX results indicate that a thicker yarn is more sensitive to the NTP and some of the silver coating is rubbed off with an NTP of 50 gf. In order to optimize the embroidery parameters for excellent appearance quality and lower electrical resistance, we use an overlay plot analysis to predict the appearance quality and electrical resistance. It is found that an SL of 4 mm and lower ES of 200 rpm comprise the optimum combination of factors due to lower consumption of conductive yarns and mechanical force reduction during the embroidery process, which is validated by conducting further embroidery experiments. The results of the new experiments validate the optimised parameters and we obtain the lowest electrical resistance for the conductive tracks embroidered with HC 12 thread ($11.46 \pm 0.62 \Omega/10 \text{ cm}$). These findings have substantial value for the fabrication of e-textiles such as high-performance circuits and other electrically conductive systems and devices.

Supporting information

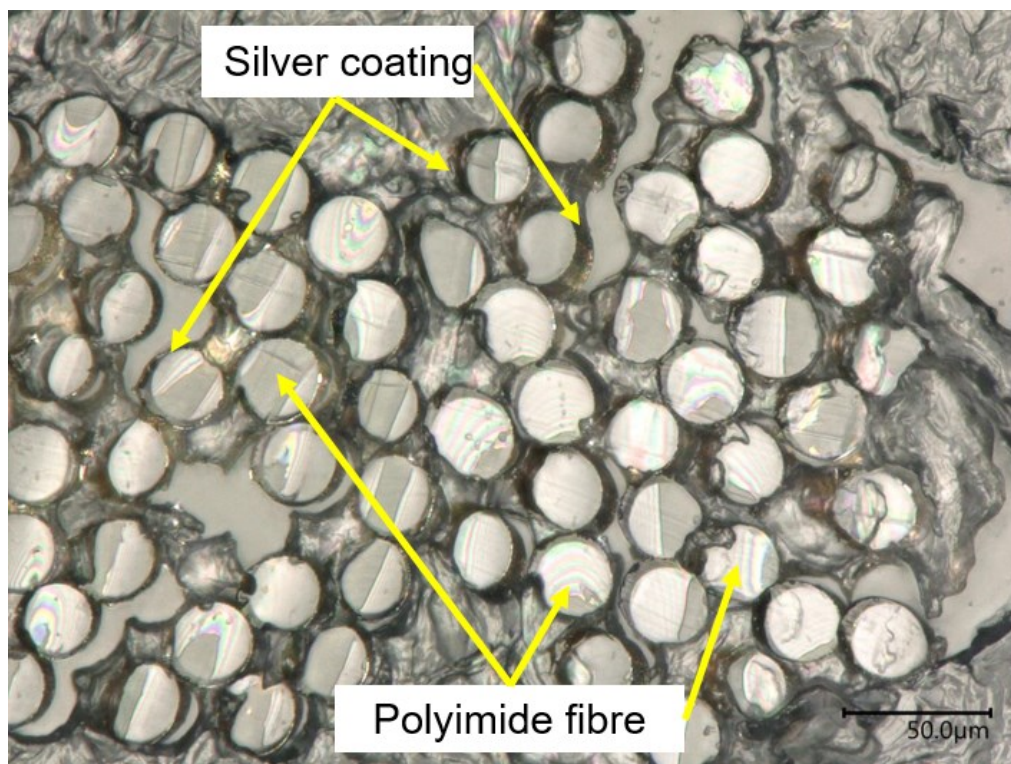


Figure S3-1. Cross section optical microscope image of HC12.

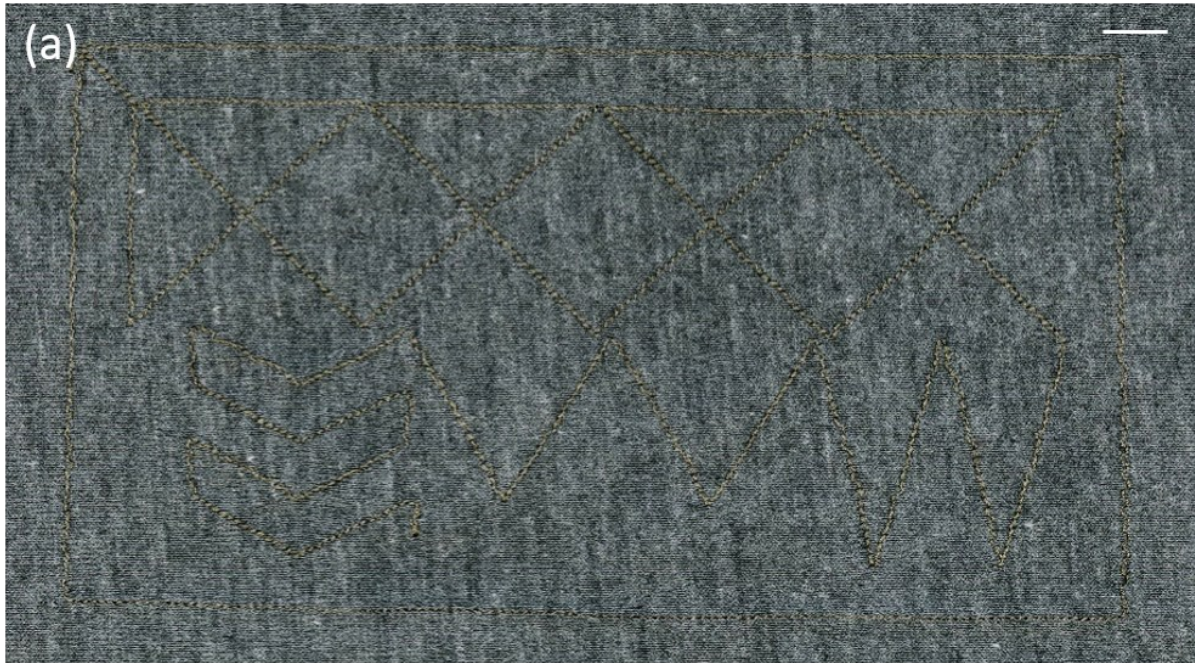


Figure S3-2. Embroidery pattern of sample 6 (a) and sample 8 (b) embroidered with HC 12 thread. Scale bars are 1 cm.



Figure S3-3. Needle thread pre-tension measurement with digital tension gauge.

Table S3-1. Sample numbers and corresponding experimental specifications.

Run No.	Sample No.	ES (rpm)	SL (mm)	NTP (gf)		ED
				HC12	HC40	
1	1W	200	1.5	30	20	Wale
2	1C	200	1.5	30	20	Course
3	2W	600	1.5	30	20	Wale
4	2C	600	1.5	30	20	Course
5	3W	200	4	30	20	Wale
6	3C	200	4	30	20	Course

7	4W	600	4	30	20	Wale
8	4C	600	4	30	20	Course
9	5W	200	1.5	50	40	Wale
10	5C	200	1.5	50	40	Course
11	6W	600	1.5	50	40	Wale
12	6C	600	1.5	50	40	Course
13	7W	200	4	50	40	Wale
14	7C	200	4	50	40	Course
15	8W	600	4	50	40	Wale
16	8C	600	4	50	40	Course
17	9W	400	2.75	40	30	Wale
18	9C	400	2.75	40	30	Course

CHAPTER 4. STRETCHABLE INTERCONNECTS WITH ENHANCED CONDUCTIVITY USING EMBROIDERY TECHNIQUES

This chapter focuses on objective 2, which is to develop flexible and stretchable highly conductive tracks for interconnects in e-textiles. The section 1 of this chapter focuses on embroidery parameters to produce conductive tracks for interconnects with enhanced conductivity, which has been published on a peer reviewed conference paper. The section 2 focuses on flexible and stretchable interconnects fabrication and performance evaluation, which has submitted to the targeted journal.

4.1 Embroidery parameters to produce conductive tracks for interconnects with enhanced conductivity

Authors: Yan Zheng, Lu Jin, Zekun Liu, Jing Qi, and Yi Li

Conference: Textile Bioengineering and Informatics Symposium Proceedings (July 7-10, 2020)

DOI: 10.3993/tbis2020, at pages of 107-113

Statement of own contributions: Main research idea, conductive tracks fabrication, testing and data analysis; preparation of figures, tables and manuscript.

Statement of co-author contributions: Lu Jin, Zekun Liu and Jing Qi support in conductive tracks fabrication. Yi Li initiated project idea and provided supervision and guidance in research methodology, the design of experiment, data analysis and interpretation, and paper revision.

4.1.1 Introduction

In the past 20 years, the significant advancements in electronic textiles (e-textiles) were witnessed including technology adding electrically conductive tracks to textiles which

seamlessly integrates sensors, actuators and controlling units to produce smart garments that are flexible, breathable, durable and have good air/moisture permeability [12, 14, 136]. These textile-based conductive tracks are the electrically conductive part of the textile with a length to width ratio of at least 10:1 in accordance with the standard BS EN 16812. The primary purpose of incorporating conductive tracks is to transmit electrical signals with a minimal loss of signal quality. Therefore, high performance conductive tracks with low resistance are crucial for many related applications.

Textile-based conductive tracks are produced through weaving [53], knitting [24], printing [137], embroidering [28] or sewing [138] electrically conductive materials on a carrier fabric. The integration of conductive tracks in a woven fabric structure requires weaving conductive threads or yarns in the warp or weft direction. Similarly, the conductive tracks are integrated along the wale or course direction in a knitted fabric structure. This standard geometric arrangement of conductive threads however limits the placement and electrical conductivity of the conductive tracks. As such, there have been studies on printing metallic paste or nanoparticle ink to produce conductive tracks onto textiles [27, 137, 139]. However, the precision and durability of such conductive tracks that are directly printed onto fabric still need to be improved. Instead, conductive threads can be directly stitched into fabric by using embroidering and other sewing techniques. Nevertheless, while sewing machines can produce different types of stitches, they need to be manually controlled. The solution proposed in this study is embroidery, which is a numerically controlled automatic sewing machine that can produce lock stitches at high-speed. Embroidery techniques have been widely used to produce the conductive tracks because the conductive threads can be sewn where needed during the e-textiles production stage.

Electrically conductive fibres, threads and yarns are the key components of conductive tracks. Silver coated conductive yarns are usually used to fabricate electrodes and circuits because they are flexible, ductile and do not cause irritation upon contact with the skin. However, different combination of the conductive threads in the formation of stitches will

influence the electrical resistance of the embroidered tracks. For example, the electrical conductivity of conductive paths sewn with different types of stitches was studied [138]. The effects of the type of embroidery stitch, length and number of the stitches on the electrical resistance of embroidered lines were compared [129]. The optimum fabrication approach for incorporating passive and active electronic circuit elements into composite materials was determined [134]. Moreover, the mechanical damage to the silver coating on conductive yarns during the fabrication process was studied [127], and the impact of the stitch length of the conductive yarn on electrical resistance was examined [140]. In all of these studies, conductive threads are embroidered onto woven or non-woven fabrics that are stiff with minimal elasticity. However, the interaction effects of different embroidery parameters on the electrical conductivity of conductive tracks on knitted fabric have been neglected. Moreover, the model of embroidered stitches with conductive threads has not been investigated yet.

In response, this study applied lock-stitch embroidery to fabricate conductive tracks with two types of silver coated polyamide threads. The electrical resistance of conductive tracks embroidered with different parameters were measured. The results are analysed by taking into account the types of stitch, the placement of the conductive thread in a needle or bobbin during stitch formation, and number of embroidered stitches by using a full-factorial design. An analysis of variance (ANOVA) is then carried out, through which the location of the conductive thread was found having a significant impact on the resistance of the conductive tracks. Embroidering with conductive threads in both a needle and bobbin, was observed a substantial reduction in the resistance of the conductive tracks (i.e., a reduction of about 50% in the resistance in comparison to that of the original conductive thread), which is a much larger reduction than using triple embroidered stitches. Furthermore, we propose an electrical resistance model based on lock stitch type 301, which can be used to guide the designing of embroidered conductive tracks for smart garments.

4.1.2 Experimental work

4.1.2.1 Materials

Two types of silver coated polyamide threads, HC12 and HC40, which were purchased from Madeira Garnfabrik GmbH (Freiburg, Germany), were used in this study as the conductive thread. Table 4-1 shows physical properties of them, which have a two-ply structure with a Z twist which means that they can be used as a needle thread in an embroidery machine (the JCZA 0109-550, ZSK Stickmaschine GmbH, Krefeld, Germany). The substrate is knitted fabric, which is a blend of 78% FR viscose, 20% para-aramid, and 2% carbon fibres (200±10 g/m² surface density), and certified by the EU to fabricate T-shirts for firefighters. A cold water-soluble film was applied on the top of the fabric to improve the stability of the fabric during embroidering process.

Table 4-1. Physical properties of silver coated polyamide threads

Thread name	Thread type	Linear density (tex)	Electrical resistance (Ω/m)	Force at break (cN)	Elongation at break (%)	Diameter (μm)
HC 12	Shieldex [®] 235/36-2 ply	61±1.5	80±9.6	2998±51.7	32.9±0.7	388.3±28.9
HC 40	Shieldex [®] 117/17-2 ply	29±0.6	270±11.2	1330±7.2	26.3±0.4	283.4±35.3

4.1.2.2 Methods

Three different types of lock stitches, 301, 304 and 308 defined in ASTM standard D6193 were inputted into the embroidery software program with the same straight length of 15 cm, as shown in Figure 4-1(a). Figure 4-1(b) shows the stitches were embroidered once and repeated three times, respectively. The conductive thread was used in three ways: threaded only in the needle, used only in the bobbin and threaded in both the needle and bobbin. Figure 4-1(c) shows the image of a stitch embroidered three times. The embroidery technique used here is pulling the needle thread, as shown in red colour thread in Figure 4-1(c), three times in a single stitch

unit, which is forward, backward and forward to the next stitch. The bobbin thread, which was golden colour thread shown in Figure 4-1(c) was used to sew forward only and there is no overlapping of the bobbin thread under the fabric.

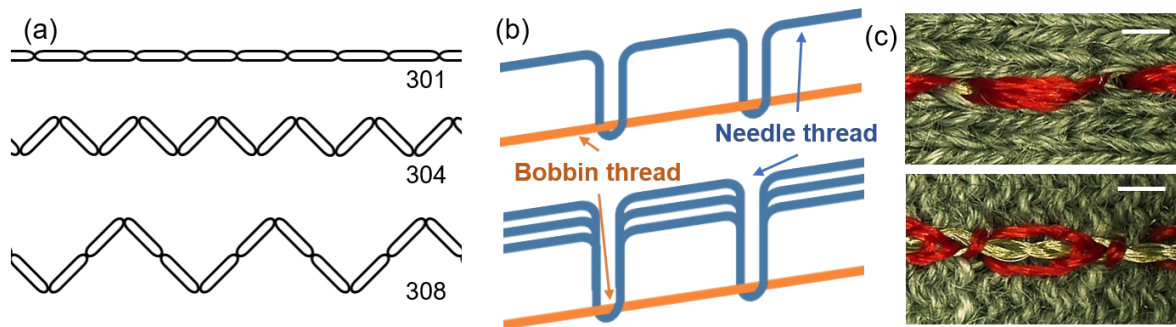


Figure 4-1. Schematic of the types of stitch used in study. (a) Lock stitch types 301, 304, and 308 in accordance with ASTM standard D6193; (b) structure of stitches embroidered once (top) and thrice (bottom); and (c) optical microscope images of thrice embroidered lock stitch type 301 with conductive thread in bobbin only. Front of stitches (top), and back of stitches (bottom). Scale bars are 1 mm.

A full-factorial design was used to examine the main factors and their interactions to determine the resistance of the embroidered tracks. Two variables at three levels and one variable at two levels were used to design the experiment. The factors and the levels used are listed in Table 4-2.

The samples were embroidered with a stitch length of 3.5 mm and the needle thread pre-tension was controlled to form the interlock with the bobbin thread just below the knitted substrates. The samples designed with a straight length of 15 cm were embroidered thrice following the different experimental combinations of input parameters in the wale direction. The resistance of the conductive tracks was measured by using the four-probe method with a multimeter (Keithley 2000) and used as a response value for evaluating the electrical conductivity. Each type of conductive thread was used to fabricate 18×3 (total of 54) test samples. An ANOVA test was carried out to obtain the statistical significance (p -value<0.05) of the resistance.

Table 4-2. Factors and levels used in full-factorial experimental design

Factor	Factor code	Level		
		1	2	3
Type of stitch	A	301	304	308
Placement of conductive thread	B	In needle	In bobbin	Both (in needle and bobbin)
Stitch repeats	C	1	3	-

4.1.3 Results and discussion

4.1.3.1 Statistical results

Table 4-3 presents the ANOVA results including all of the input factors and their interactions. The stitch type (Factor A), placement of the conductive threads (Factor B), and their interactions have a large impact on the resistance, where the number of stitch repeats (Factor C) has a very small effect since it only has a significant effect when considered together with Factor B.

Table 4-3. Summary of ANOVA response for full-factorial experimental design

Source	Tracks fabricated with HC 12					Tracks fabricated with HC 40				
	DF	SS	MS	F-Value	P-Value	DF	SS	MS	F-Value	P-Value
Model	13	43850.3	3373.1	264.03	0.000	13	1341091	103161	108.71	0.000
Linear	5	40532.8	8106.6	634.55	0.000	5	1245699	249140	262.53	0.000
A	2	1714.7	857.4	67.11	<u>0.001</u>	2	15870	7935	8.36	<u>0.037</u>
B	2	38791.3	19395.7	1518.22	<u>0.000</u>	2	1227192	613596	646.58	<u>0.000</u>
C	1	26.8	26.8	2.10	0.221	1	2637	2637	2.78	0.171
2-Way Interactions	8	3317.4	414.7	32.46	0.002	8	95392	11924	12.56	0.014
A*B	4	2880.1	720.0	56.36	<u>0.001</u>	4	39011	9753	10.28	<u>0.022</u>
A*C	2	45.9	23.0	1.80	0.277	2	650	325	0.34	0.729
B*C	2	391.4	195.7	15.32	<u>0.013</u>	2	55731	27866	29.36	<u>0.004</u>

Notes: DF denotes degrees of freedom, SS denotes sum of squares, and MS represents mean squares.

Figure 4-2 shows an analysis on the factor influence which includes all of the input factors and their interactions. The mean of the resistance of the conductive tracks embroidered with HC 12 and HC 40 has a similar value. It can be observed that the samples embroidered with lock stitch type 301 stitch have a lower electrical resistance. Moreover, a lowest resistance is obtained when embroidering the conductive threads through both the needle and bobbin. There is no significant difference in the resistance when the conductive thread is embroidered once or thrice, and specifically, there is almost no difference when embroidering the conductive threads in both a needle and bobbin.

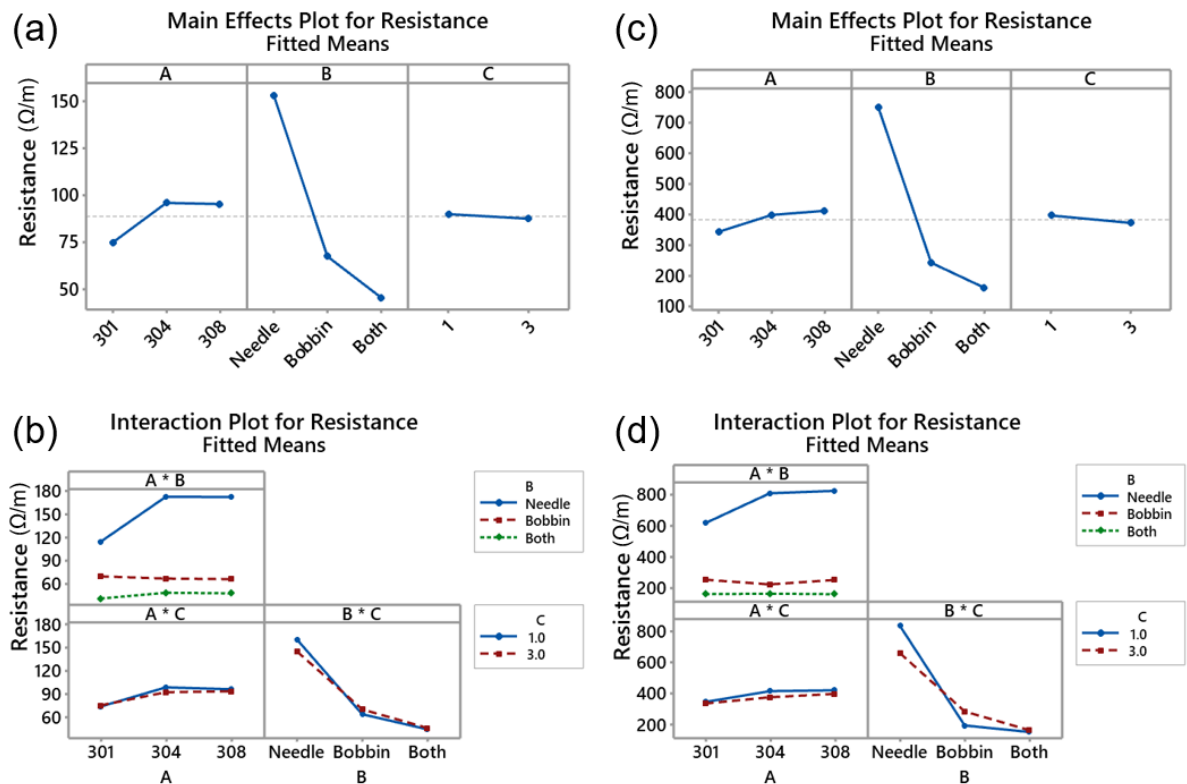


Figure 4-2. Factor influence on resistance of conductive tracks embroidered (a and b) with HC 12 and (c and d) with HC 40.

4.1.3.2 Effects of placement of conductive thread on resistance of embroidered interconnects

Figure 4-3(a) and (b) show the influence of Factors A and B on the resistance of the conductive tracks embroidered with HC 12 and HC 40 respectively. When putting conductive threads in the needle, resistance of the embroidered conductive tracks with lock stitch type 301 is significantly lower than using of other type of stitches. There is also only a small difference in resistance with lock stitch types 304 and 308. When conductive threads only used in a bobbin, the electrical resistance is significantly reduced regardless of the types of stitch. The lowest resistance is obtained when using conductive threads both in the needle and bobbin. The difference in resistance among the three types of stitch also noticeably decrease.

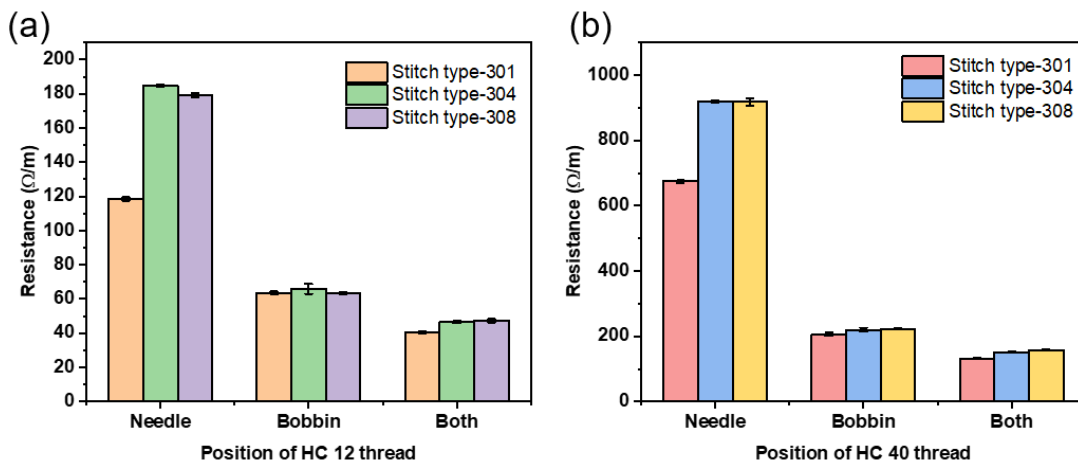


Figure 4-3. Effects of Factors A versus B with threads (a) HC 12, and (b) HC 40.

In order to quantitatively evaluate the reduction of embroidered interconnects' resistance between various stitch type and placement of conductive thread, the percentage of reduction was calculated as follows:

$$Reduction (\%) = \frac{R_{max} - R_{min}}{R_{max}} \times 100 \quad (4 - 1)$$

where R_{max} represents the maximum resistance value in the group; and R_{min} represents the minimum resistance value in the group. The group to compare the effect of Factor A was

calculated with conductive yarns used in needle, bobbin and both respectively. The group to compare the effect of Factor B was calculated with types of stitch forms including 301, 304, and 308 respectively. Table 4-4 lists the mean values of the reduction in resistance with a comparison of Factors A and B for HC 12 thread. The reduction percentage by using conductive threads in various place is considerably higher than embroidery with different stitch types. The maximum reduction, 74.9% was achieved when applying conductive yarns both in needle and bobbin at 304 stitch embroidering. While putting conductive thread in the bobbin, the reduction of resistance was 3.9% between three types of stitch forms. Table 4-5 shows the comparison of interconnects' resistance reduction with HC 40 embroidery. Similar to HC 12, interconnects embroidery with 304 stitch by using conductive yarns both in the needle and bobbin could get 83.5% reduction of resistance. The resistance of the conductive tracks embroidered with the conductive threads in both the needle and bobbin is much lower (about 50% lower in resistance) in comparison to the original conductive thread with the same straight length.

Table 4-4. Resistance comparison of conductive interconnects embroidered with HC 12

Factor A \ Factor B		Placement of conductive thread			
		Needle (Ω/m)	Bobbin (Ω/m)	Both (Ω/m)	Reduction
Types of stitch forms	301	118.5	63.6	40.5	65.8%
	304	184.9	66.0	46.5	74.9%
	308	179.3	63.4	47.4	73.6%
	Reduction	33.9%	3.9%	14.6%	

Table 4-5. Resistance comparison of conductive interconnects embroidered with HC 40

Factor A \ Factor B		Placement of conductive thread			
		Needle (Ω/m)	Bobbin (Ω/m)	Both (Ω/m)	Reduction
Types of stitch forms	301	674.3	206.2	131.7	80.5%
	304	920.2	220.0	151.4	83.5%
	308	917.9	222.3	158.4	82.7%
	Reduction	26.7%	7.2%	16.9%	

The electrical conductivity of the conductive tracks is influenced by the stitch formation of the conductive thread for each stitch unit. Lock stitch type 301, which provides the lowest resistance based on the experiments, is used to illustrate the relationship between resistance and stitch structure, as shown in Figure 4-4(a) to (c). As the point of the interlocking of the stitch is on the back side of the fabric with embroidering, more thread is used through a needle as opposed to a bobbin. The resistance of the conductive tracks is directly proportional to the length of the conductive thread used. When the conductive thread is used in both the needle and bobbin, the stitch lines can be modelled as a parallel electrical circuit.

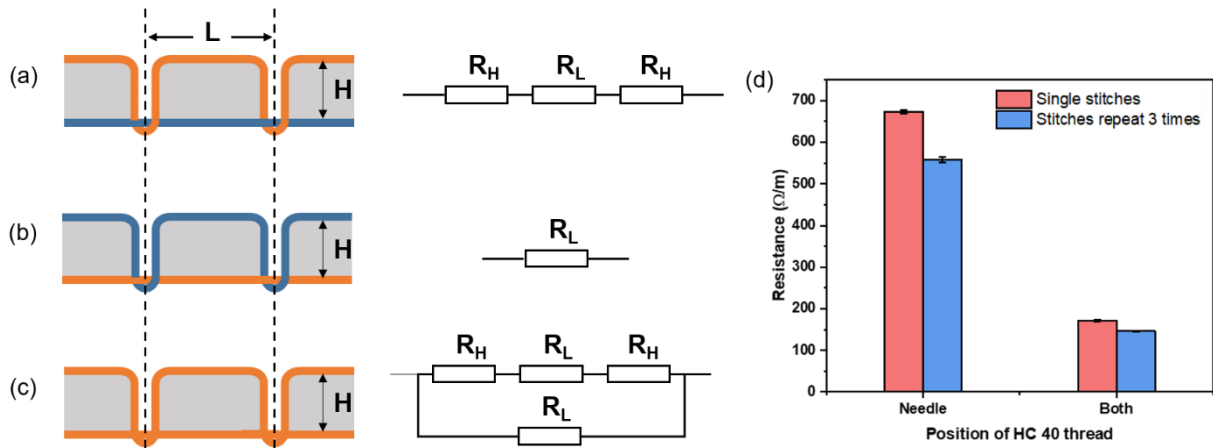


Figure 4-4. Schematic illustration of electrical circuit model. (a-c) Schematic illustration of electrical circuit model as stitch embroidered once with conductive thread in (a) needle, (b) bobbin, and (c) both needle and bobbin. L is the length of each stitch, and H is the thickness of the fabric. The conductive thread is highlighted in orange. (d) Resistance of conductive tracks embroidered with HC 40: embroidered once and thrice.

The resistance of the stitch units with lock stitch type 301 according to the placement of the conductive threads can be calculated by:

$$R_a = R_H + R_L + R_H \quad (4 - 2)$$

$$R_b = R_L \quad (4 - 3)$$

$$R_c = \frac{R_L(2R_H + R_L)}{2(R_H + R_L)} \quad (4 - 4)$$

where R_H is the resistance of the conductive thread with a length related to the thickness of the fabric substrate, and R_L is the resistance of the conductive thread with a length that is related to the stitch length.

Factors B and C have interactive effects on the resistance of the conductive tracks, which shows $p < 0.05$ in Table 4-3. The placement of HC 40 was examined to determine the effects of Factor C on the resistance, and Figure 4-4(d) shows the mean resistance value of embroidered interconnects. When HC 40 is used in both a needle and bobbin, a significant reduction in the resistance is achieved, which can reach up to 75%. However, embroidering thrice can reduce the resistance for about 17% with a needle thread was conductive and only 8.5% with embroidering conductive threads in both needle and bobbin. Embroidering conductive threads with both needle and bobbin shows a remarkable increase in conductivity (that is reduction in resistance) opposed to the use of multiple stitching. Moreover, multiple-needle punching during the embroidering process may potentially cause mechanical damage to the fabric substrates, particularly knitted fabrics.

4.1.4 Summary

In summary, the electrical conductivity of embroidered conductive interconnects was evaluated by fabricating with three type of stitch form, various placement of conductive threads and number of stitch repeats. The ANOVA findings show that:

- When conductive threads are used as needle threads, the resistance of the conductive tracks fabricated with lock stitch type 301 is the lowest because the least amount of conductive thread is used. Stitch repeats during embroidering will increase the conductivity of the conductive tracks since the threads overlap in the same place which increases the thickness of the conductive area.
- There is a sharp decline in the resistance of the conductive tracks when only putting conductive threads in a bobbin. There is less thread used due to the structural characteristics of the embroidered stitches.

- Embroidering with conductive threads used both in needle and bobbin results in the highest conductivity, or the greatest reduction in the resistance (about 50% of that of the conductive thread). There is no major difference in the resistance of the conductive tracks among the three types of stitches used.
- The resistance of the conductive tracks will slightly decrease when the conductive thread is embroidered thrice through only a needle. However, multiple needle punching has limited effects on improving conductivity when using conductive thread in both needle and bobbin.

4.2 Fabrication and performance evaluation of flexible and stretchable interconnects

Authors: Yan Zheng, Lu Jin, Zekun Liu, Simeon Gill, Steven Hayes, and Yi Li

Targeted journal: The Journal of The Textile Institute, submitted

Statement of own contributions: Main research idea, embroidered interconnects fabrication and evaluation; data analysis and modelling; preparation of tables, figures, and manuscript.

Statement of co-author contributions: Lu Jin supports in finite element analysis. Zekun Liu supports in samples testing. Simenon Gill and Steven Hayes support in techniques of embroidery. Yi Li initiated project idea and provided supervision and guidance in research methodology, the design of experiment, data analysis and interpretation, and paper revision.

4.2.1 Introduction

Stretchable interconnects are passive electronic components that connect two or more devices or a conductor to another, and are mechanically and electrically compatible to the stretchable substrates [22]. For wearable technology, particularly a smart garment development, the electronic systems with stretchable interconnects are designed in conformity to soft 3D surfaces and to minimize losing original mechanical properties of textile substrate in order to accommodate body movement. However, stretchable demands are various in accordance with

human body parts and activities of daily life. Therefore, strategies are required to efficiently develop customized stretchable interconnects and preferably integrate into smart garments with other electronic components during the fabrication process.

To develop flexible and stretchable interconnects, numerous researchers have demonstrated fabrication techniques during the fabric making processes such as weaving and knitting, or pattern conductive polymer (or nanomaterials) into elastic fabrics that maintain inherent properties of fabrics. Knitted fabrics are a suitable material for smart garments as they have high softness, air permeability and extensibility, and can significantly improve the comfort of wearers. Direct knitting of metallic wires [23, 24], conductive paste screen/ stencil printing on knitted fabrics [25–27], and metal nanoparticle inkjet printing on elastic fabrics [3, 139] were reported to produce flexible interconnects with up to 100% strain. Even though printed conductive interconnects have demonstrated relatively good stretchability, they have shown limited mechanical durability due to the delamination and fragmentation of the conductive layers occurring at extreme strains. Also, their manufacturing complexity, material cost, and scalability limit their usage in mass production of smart garments. Unlike knitting techniques that only allow interconnects in the length or cross directions, embroidery techniques provide extraordinary and sophisticated capabilities for multi-direction interconnects design and have been successfully used in circuits integration of wearable electronics [28–30]. Embroidered interconnects can be precisely fabricated based on the graphics, the tensile properties can be customized according to the requirements of applications, and can be seamlessly integrated with other sensors and electrodes during fabrication process. However, the stretchable and electrical properties of stretchable interconnects via embroidery techniques were not well investigated.

In order to provide stretchable properties to none-elastic conductive tracks, shape geometric design for stretchable interconnects were widely investigated to modify 2-D meander-shaped tracks during the past 20 years. Zigzag-shaped interconnects deposited metallic film on top of Polydimethylsiloxane (PDMS) substrate have been studied by experimental observations and

numerical analysis [87, 141]. Moreover, a horseshoe-shaped metallic wires interconnection allowing stretchability going up to 100% was simulated through finite element analysis after comparing with sinus, ‘U’ shape, half circles, and elliptical shapes [86, 88, 142]. In addition, kirigami topology structure [143], fractal-based structures [144–147] and serpentine interconnects [91, 148–150] were reported for fabrication of hard-soft materials integration of stretchable electronics. Textile-compatible methods have been demonstrated by sewing and transferring thin zigzag pattern metallic wires onto the wearable materials, after coating with a stretchable elastomer, and the interconnections maintain a constant electrical conductivity for strains up to 50% [151, 152]. However, the design and optimization of stretchable patterns for embroidering conductive tracks on knitted fabrics, and the impact of pattern design parameters on electromechanical properties of interconnects were not analysed thoroughly before.

In this paper, stretchable interconnects were fabricated by lock-stitch and TFP embroidery techniques on elastic knitted fabrics with the zigzag and horseshoe patterns, respectively. The effects of pattern design parameters on electrical resistance, electrical stability and stretchability of embroidered interconnects were evaluated. The usefulness of the stretchable interconnects was demonstrated with light-emitting diode (LED) circuits toward stretching process integrated in a long sleeve T-shirt and skinny pants via human wear trials.

4.2.2 Experimental

4.2.2.1 Materials

A stretchable knitted fabric was selected as the embroidering substrate for interconnects because of its excellent flexibility and stretchability. This fabric was single jersey and composed of 85 % polyester and 15 % Spandex (200 g/m² surface density, 566±8 um thickness). It was commonly used for underwear and sportswear, and purchased from SPEED WIND Textile (Guangdong, China).

Two types of silver coated polyamide yarns purchased from statex GmbH (Bremen, Germany) were used in this study. The Yarn A, highly conductive yarn (Shieldex[®] 235/34 2-

ply), was embroidered by lock-stitches. The Yarn B, thermoplastic polyurethane (TPU) insulated conductive yarn (Shieldex[®] 235/34 2-ply TPU), was fixed with polyester non-conductive thread by tailored fibre placement (TFP) embroidering. The physical properties of these yarns are shown in Table 4-6.

Table 4-6. Physical properties of conductive yarns

Yarn code	Thread types	Linear density (tex)	Electrical resistance (Ω/m)	Strength at break (cN)	Elongation at break (%)	Diameters (μm)	Insulation coating
A	Shieldex [®] 235/36-2 ply	61 \pm 1.5	80 \pm 9.6	2998 \pm 51.7	32.9 \pm 0.7	388 \pm 15	No
B	Shieldex [®] 235/36-2 ply TPU	400 \pm 10	80 \pm 9.6	2320 \pm 40	25.5 \pm 5	1000 \pm 20	Yes

4.2.2.2 Methods

Stretchable properties of conductive materials with limited elasticity can be achieved using special patterning such as triangular/zigzag [87], ‘U’ shape [91] and horseshoe shape [86]. A proper pattern design is crucial to avoid losing structural integrity and electrical functionality during substrate stretching. The horseshoe shape has been proposed to be an optimal design that it has more than 100% elongation and 39.2% reduction in the plastic strain when compared with other patterns [88]. Moreover, the zigzag pattern is the only one shape that can be applied in fine pitch multiple routings because of the geometrical advantage, as shown in Figure 4-5(a), the pitch of zigzag pattern D_z is smaller than that of horseshoe pattern D_h .

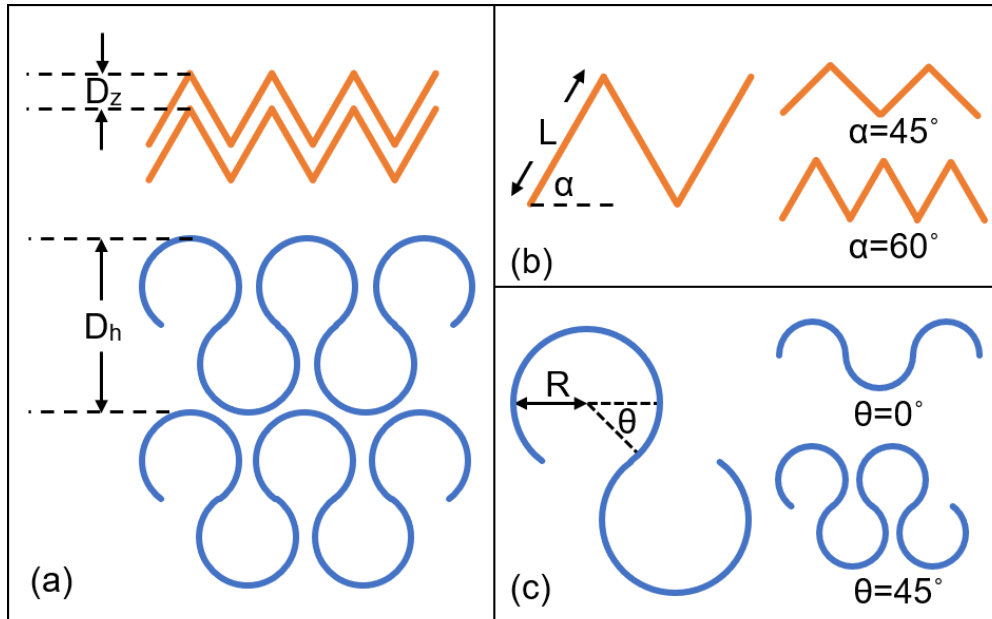


Figure 4-5. Schematic illustration of interconnects pattern designs. (a) The pitch comparison between zigzag and horseshoe interconnects. (b) Geometrical parameters of a zigzag patterned stretchable interconnect; right: pattern with different opening angles ($\alpha=45^\circ$ and 60°). (c) Geometrical parameters of a horseshoe patterned stretchable interconnects; right: pattern with different turning angles ($\theta=0^\circ$ and 45°).

Each unit of zigzag structure interconnects contains one arm (L) and an opening angle (α), as shown in Figure 4-5(b). In order to understand the mechanical relationship between the stress induced by external loading and deformability of the zigzag interconnect, the deformation behaviour of a zigzag structure copper solid on top of a PDMS non-woven substrate during stretching was analysed [141]. The equation of the total displacement of interconnects in loading direction is developed as follows:

$$\delta = n \cdot \left[\frac{PL}{E} \left(\frac{\cos^2 \alpha}{A} + \frac{4 \cdot L^2 \sin^2 \alpha}{A^3} \right) \right] \quad (4-5)$$

where L is the length of the arm, α is the opening angle of each arm, n is the repeating number of arms, P is the applied loading, E is the Young's modulus of the zigzag structure, and A is the cross-section area. The stretchability of zigzag structures, which equals to the total displacement in loading direction as shown in Equation (4-5), increases dramatically with increasing L and α .

The horseshoe pattern is created by joining a series of circular arcs as shown in Figure 4-5(c), where R is the inner radius, and θ is the turning angle, measured clockwise, where the two arcs tangentially connect. Tensile properties of horseshoe shaped interconnects was analysed by electroplating gold layer on a silicone elastomer [88]. The increase of the scale factor R/w (w is the width of the metal track) is translated into a reduction of the induced strain. Elongation up to 100% and more were obtained in the case of $\theta=30^\circ$ and 45° . Moreover, a developed nonlinear mechanics model [145] indicated that the stretchability of the horseshoe microstructure can be well controlled by two geometric parameters, w/R and θ .

In this study, design parameters of zigzag-shaped interconnects focus on L and α because the diameter of conductive yarns are fixed. For the same reason, parameters R and θ are used to design horseshoe-shaped interconnects. To investigate the influence and significance of the pattern design parameters on the tensile and electrical properties of embroidered interconnects, Minitab 19 was used to design 2^2 full factorial experiments for zigzag-shaped and horseshoe-shaped interconnects respectively. Table 4-7 lists the experimental factors and the factor levels. Based on the analysis in Chapter 3, the stitch length has impact on resistance and appearance quality of conductive tracks. The stitch length of 2 mm to 4 mm were selected to compare the stretchability of interconnects. The inner radius of a horseshoe pattern was determined by the width of the final pattern, which should be reasonable narrow because multiple interconnects will be used in wearable scenario to connect electronic modules. 5 mm to 10 mm were selected to develop horseshoe-shaped interconnects.

Table 4-7. Experimental factors and levels for interconnects design

Pattern shape	Factors	Coded level	
		-1	1
Zigzag	Arm length, L (mm)	2	4
	Opening angle, α ($^\circ$)	45	60
Horseshoe	Inner radius, R (mm)	5	10
	Turning angle, θ ($^\circ$)	0	45

4.2.2.3 Fabrication of stretchable interconnects

The zigzag-shape interconnects were embroidered with Yarn A by lock-stitches. Yarn B with TPU insulated coating were employed to fabricate horseshoe-shape interconnects by TFP embroidery. Figure 4-6 illustrates the fabrication techniques of the embroidered interconnects. Yarn A was used as needle thread and bobbin thread to achieve higher conductivity of zigzag-shaped interconnects. As shown in Figure 4-6(a), SL is the stitch length, which is the arm length in experiment design. The thread pre-tension was adjusted to keep interlock points of needle thread and bobbin thread just below the fabric. The zigzag pattern was the same in the face and back side of the fabric. Figure 4-6(b) exhibits the schematic drawing of Yarn B was placed and fixed on the top of the fabric by polyester threads lock stitch embroidery. SL is the stitch length of polyester thread to fix conductive yarns, which is 1 mm in this experiment.

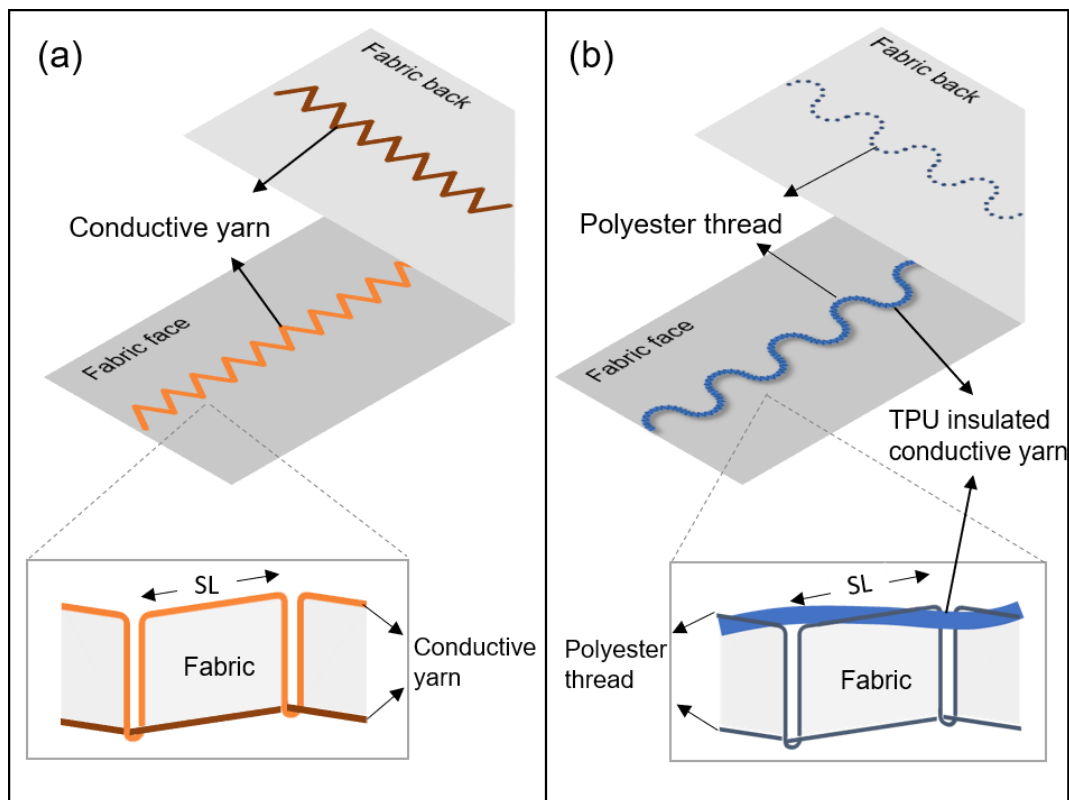


Figure 4-6. Schematic drawings of interconnects fabrication techniques. (a) lock-stitch embroidery for zigzag pattern interconnects fabrication with uninsulated conductive yarns. (b) TFP embroidery for horseshoe pattern interconnects fabrication with TPU insulated conductive yarns.

These interconnects with these two patterns were designed using the EPCwin software and fabricated with the embroidery machine JCZA 0109-550 from ZSK Stickmaschinen GmbH (Krefeld, Germany). The knitted fabric has an anisotropic structure and hence anisotropic strain-stress behaviour. Therefore, the direction of embroidered interconnections affects mechanical performance. To take advantage of the most stretchable property of fabric substrate, interconnects were embroidered along the course direction of the knitted fabric. To examine the stretchable interconnects with the standard tensile instrument for textiles, the straight distance of interconnects was 100 mm. The samples prepared for testing were 40 mm in width and 180 mm in length to hold the embroidered interconnects.

In order to keep the stability of substrate fabric during embroidery, the water-soluble film and lining was placed on the top and bottom of substrate. After embroidery, the water-soluble film and lining was washed away in smooth-running tap water with care without displacing the stitches.

4.2.2.4 Testing methods and data analysis

Tensile properties of embroidered interconnects were tested following ASTM D5034. The conductive interconnects were tested for the breaking force and elongation at a tensile rate of 300 mm/min [153] using a universal testing machine (INSTRON 3344). The distance between the upper and lower gauges is 100 mm, which is the same with the conductive interconnects. Figure 4-7(a) and (b) show embroidered interconnects of zigzag shape and horseshoe shape respectively. Three samples for each design specification were fabricated and tested.

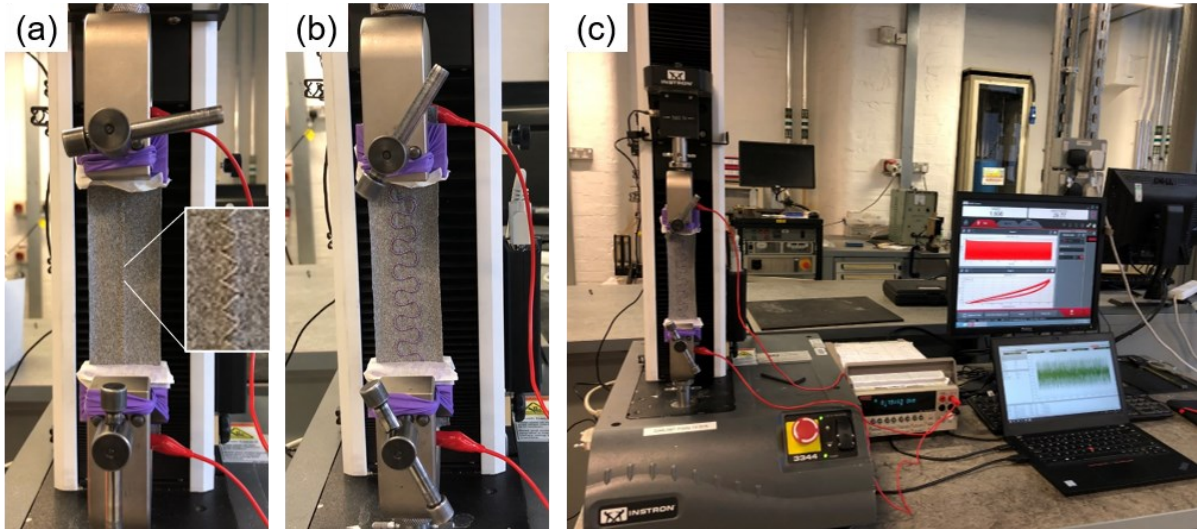


Figure 4-7. Testing instruments for stretchable interconnects. (a) Zigzag-shaped interconnects; (b) Horseshoe-shaped interconnects; (c) Cyclic testing devices.

The electrical resistance of the fabricated interconnects was measured by multimeter instrument (Keithley 2000). The resistance change of the embroidered interconnects was expressed by $\Delta R/R_0$, where $\Delta R=R-R_0$, R_0 is the initial resistance, and R is the resistance measured during stretching. The dynamic stretching endurance tests were performed through 500 consecutive elongation cycles at 25% and 45% for the zigzag-shaped interconnect and horseshoe-shaped interconnect, respectively. During the stretching tests (at 300 mm/min), the electrical resistance of interconnects was measured in real time using Keithley 2000, as shown in Figure 4-7(c).

The slope of the tensile curve line was quantified and termed $E1$ and $E2$, as shown in Figure 4-8(a). $E1$ determines the stable force of interconnects before change during stretching, and $E2$ represent the significant changes of force in interconnects during stretching. ϵ_1 is the strain value at change of force. The slope of the changes of interconnects' resistance was marked as ECR . The stable change rate of the resistance is expressed as $ECR1$, and the remarkable resistance change of interconnects is termed $ECR2$. Figure 4-8(b) shows qualitative simulated slope of the resistance curve line $ECR1$ and $ECR2$. ϵ_2 is the strain point at the change of resistance during stretching.

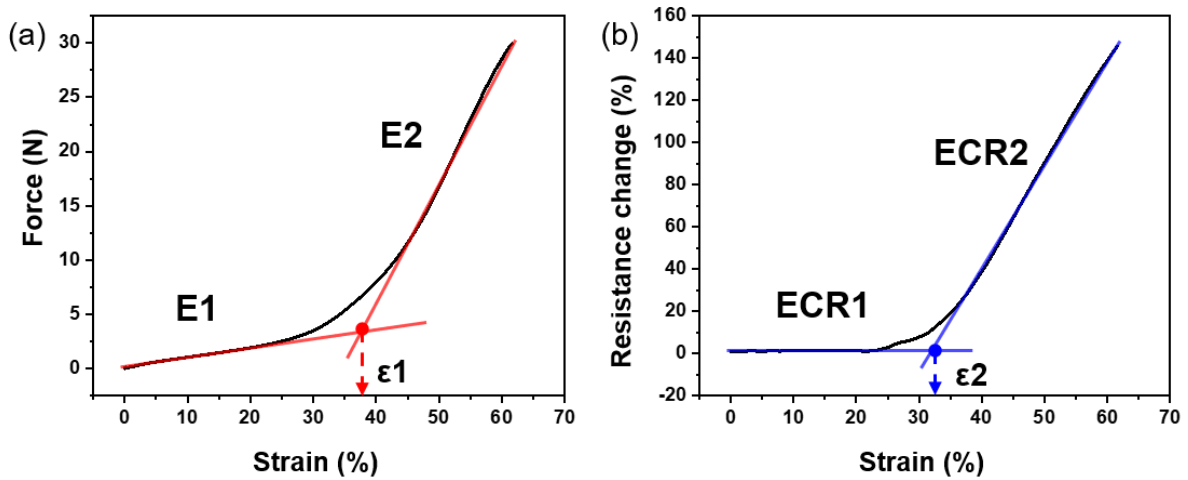


Figure 4-8. Typical curve line to show (a) the tensile force change and (b) resistance change of an interconnect.

All experiment data were presented as mean \pm standard deviations (SD). Statistical analysis was performed using two-way ANOVA with the level of statistical significance set as $P < 0.05$. A light-emitting diode (LED) circuit embroidered with conductive yarns connected with a chip LED was demonstrated as a customized conductive interconnect that would fit for different levels stretchable requirements in the arm and leg during body movements.

4.2.3 Results and discussions

4.2.3.1 Tensile properties of the embroidered interconnects

Table 4-8 shows the ANOVA analysis of tensile properties of interconnects. The design parameters L and α significantly influence the breaking force and elongation percentage for the zigzag pattern at $p < 0.05$. For interconnects fabricated with the horseshoe pattern, the angle θ in design are significantly affect breaking elongation and force of interconnects because $p < 0.05$ and F value is remarkably high.

Table 4-8. Statistical analysis of tensile properties of interconnects

Pattern shape	Factorial parameter	Strain at change of force (%)		Strain at breaking (%)	
		P-Value	F-Value	P-Value	F-Value
Zigzag	L	<u>0.008</u>	12.54	<u>0.007</u>	12.9
	α	<u>0.000</u>	75.73	<u>0.000</u>	66.8
	L* α	0.047	5.53	0.11	3.24
Horseshoe	R	0.183	2.12	0.928	0.01
	θ	<u>0.000</u>	1299.55	<u>0.000</u>	6062.88
	R* θ	<u>0.000</u>	34.35	<u>0.000</u>	212.17

1) Effects of design parameters on tensile properties of zigzag-shaped interconnects

Figure 4-9(a) and (b) show the elongation at breaking of zigzag-shaped interconnects is positive dependent on the L and angle α in the structures. The sample which has an L of 4 mm and an angle α of 60° showed stretchability up to 80%. The samples with minimum resistance, which were fabricated with an angle α of 45° showed 30% to 40% elongation. This findings is consistent with previous studies [141]. Figure 4-9(c) and (d) show the breaking force of zigzag-shaped interconnects designed with L at 2 mm and α at 45° is about only 1N higher than that has an L of 4mm and an angle α of 60°.

The elongation of zigzag-shaped interconnects is proportional to the L and angle α . In the case of low-level angle design ($\alpha=45^\circ$) of zigzag shape interconnects, the lower resistance was obtained but also the smaller elongation. However, the increased α will notably cause the rise of electrical resistance. The breaking force of interconnects is a little bit lower in higher level parameters design.

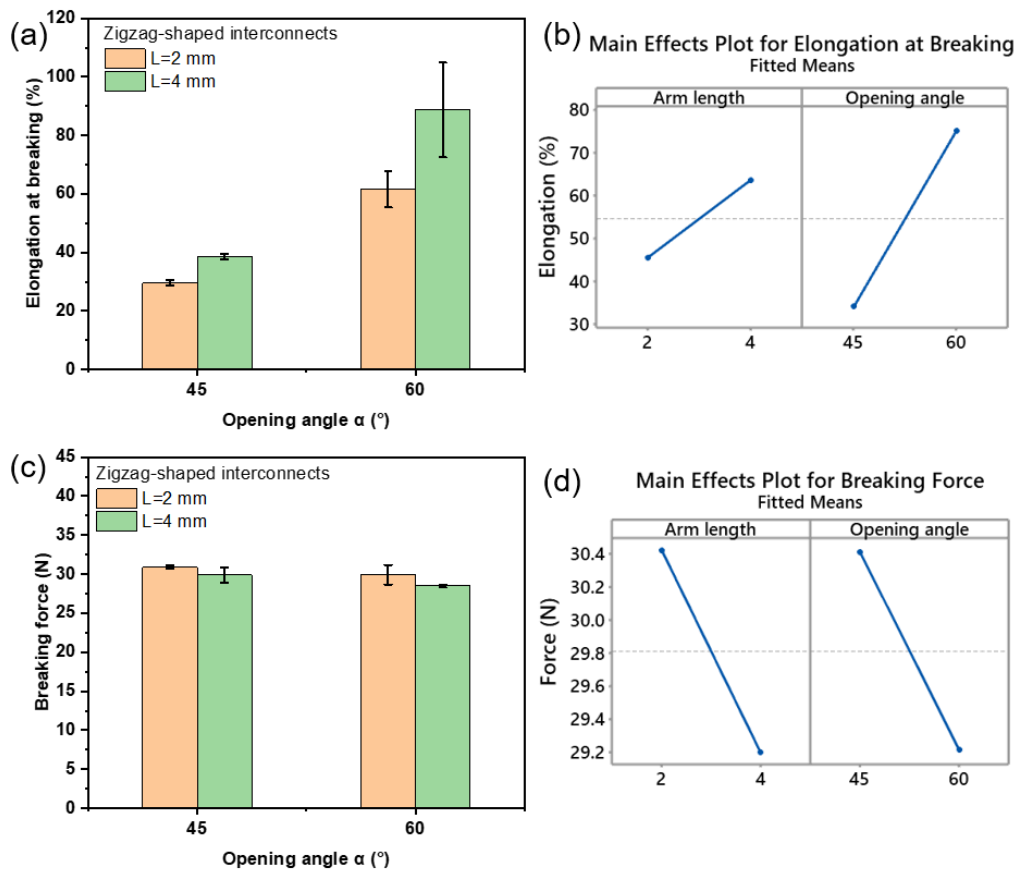


Figure 4-9. Tensile main effects analysis of zigzag-shaped interconnects. (a) The mean value of elongation percentage at breaking and (b) main effects plot analysis. (c) The mean value of breaking force of interconnects and (d) main effects plot analysis of it.

2) Effects of design parameters on tensile properties of horseshoe-shaped interconnects

As listed in Table 4-8, the elongation of horseshoe interconnects is dependent on the angle θ . Figure 4-10(a) exhibits the sample has an R of 5 mm and an angle θ of 45° showed significant stretchability up to 180%. The samples with the lowest resistance (around $80 \Omega/\text{m}$), which were fabricated with an angle of 0° and 5mm radius showed around 75% elongation. Figure 4-10(b) shows the stretchability of horseshoe-shaped interconnects is significantly proportional to the angle θ . This findings are consistent with previous studies [145]. Figure 4-10(c) and (d) show the breaking force of horseshoe-shaped interconnects is notably improved with angle θ , from around 50 N (at $\theta=0^\circ$) to 80 N (at $\theta=45^\circ$).

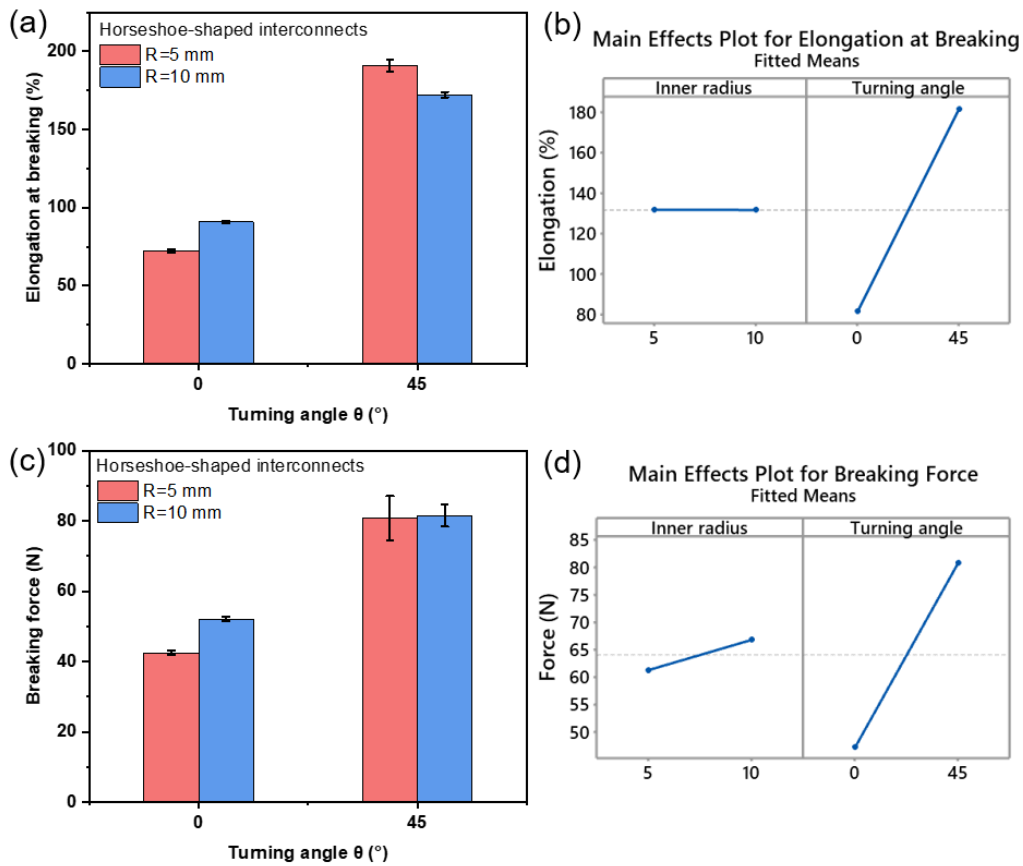


Figure 4-10. Tensile main effects analysis of horseshoe shaped interconnects. (a) The mean value of elongation percentage at breaking and (b) main effects plot analysis of it. (c) The mean value of breaking force of interconnects and (d) main effects plot analysis of it.

The breaking elongation and force of horseshoe-shaped interconnects are significantly proportional to the angle θ . In the case of semicircles designed ($\theta=0^\circ$, $R=5$ mm) interconnects, the smaller resistance was obtained but also the smaller elongation. However, increased angle θ results in the rise of electrical resistance because of the increased conductive yarns consumption.

4.2.3.2 Electrical properties of the embroidered interconnects

Stable electrical conductivity of interconnects during stretching is highly desirable. In this regard, the best working strain ranges that keep stability of the electrical resistance of two patterns' interconnects during stretching were evaluated. The resistance change of

interconnects is expressed by $\Delta R/R_0$ and the value of 5% is determined as the stability criteria of electrical resistances since 0.05 is a value to verify significance in statistical analysis.

Table 4-9 lists the ANOVA analysis of resistance of interconnects. The turning angle α of zigzag-shaped interconnect has significant effect on strain at change of resistance and resistance before change where $p < 0.05$. The opening angle θ of horseshoe-shaped interconnect has remarkable influence on strain at change of resistance and resistance before change.

Table 4-9. Statistical analysis of electrical properties of interconnects

Pattern shape	Factorial parameter	Strain at change of resistance (%)		Electrical resistance before change (Ω/m)	
		P-Value	F-Value	P-Value	F-Value
Zigzag	L	0.063	4.64	0.259	1.48
	α	<u>0.001</u>	29.67	<u>0.000</u>	100.99
	L* α	0.094	3.61	0.097	3.52
Horseshoe	R	0.195	2.00	0.004	16.25
	θ	<u>0.000</u>	292.88	<u>0.000</u>	723.25
	R* θ	0.100	3.47	0.315	1.15

The electrical resistance of the embroidered zigzag-shaped interconnects shows positive relationship with the angle α , as shown in Figure 4-11(a). The lowest resistance (highest conductivity) was obtained for interconnects has an angle α of 45° . The fitted mean resistance in Figure 4-11(b) shows the significantly lower resistance (around $46 \Omega/m$) can be achieved. The samples with 60° angle were shown to obtain higher resistance of around $60 \Omega/m$. Figure 4-11(c) exhibits the measured electrical resistance of horseshoe-shaped interconnects. Main effects plot analysis in Figure 4-11(d) shows the resistance of interconnects has positive relationship with the R and θ . The lowest resistance (highest conductivity) was around $80 \Omega/m$, which was obtained by fabricating with low-level parameters ($R=5 \text{ mm}$, $\theta=0^\circ$). Interconnects designed with an angle θ of 45° shows higher resistance than 0° pattern tracks.

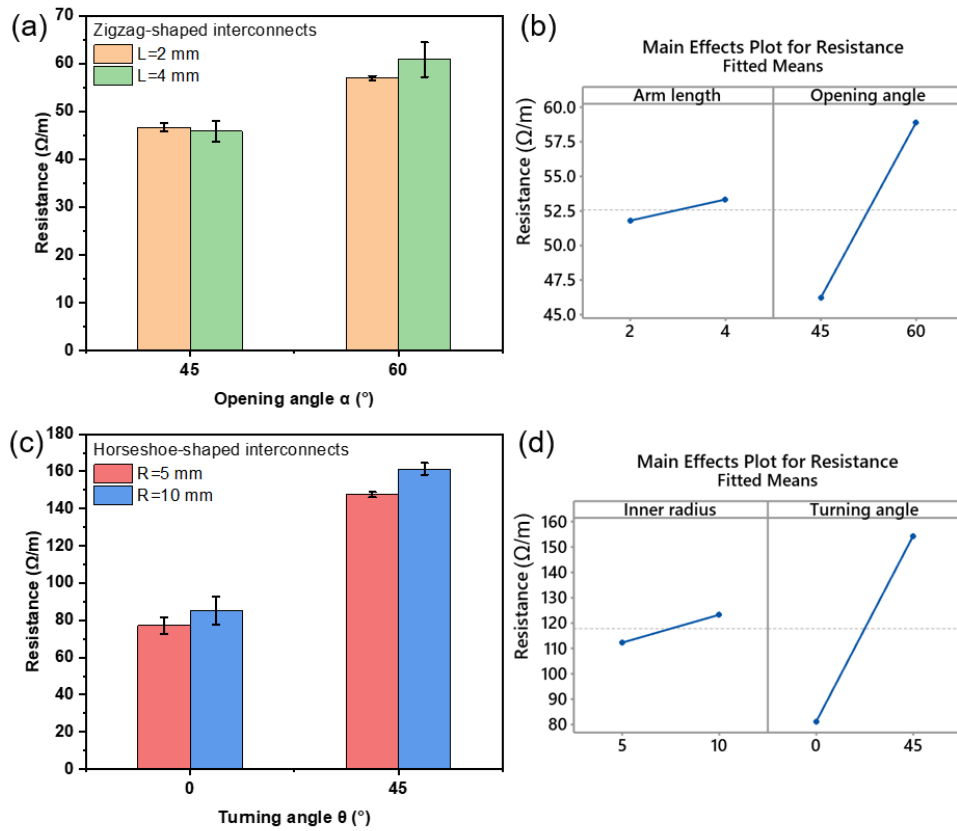


Figure 4-11. Resistance analysis of interconnects. (a) The mean resistance of zigzag-shaped interconnects and (b) main effects plot analysis of it. (c). The mean resistance of horseshoe-shaped interconnects and (d) main effects plot analysis of it.

The relationship of resistance with pattern of interconnects can be explained by the length of conductive yarns consumed in the zigzag and horseshoe shaped conductive tracks, as shown in Figure 4-12.

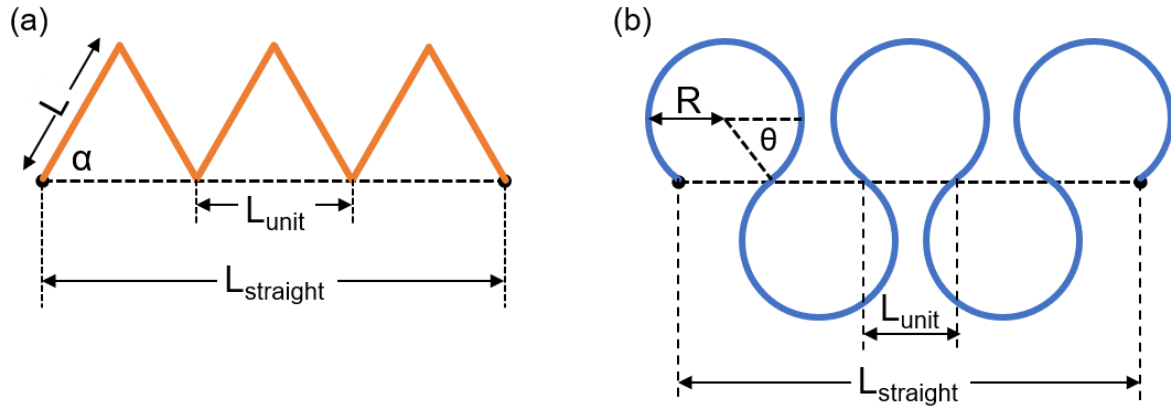


Figure 4-12. Schematic illustration of designs with the relevant segments and dimensions indicated for (a) zigzag-shaped and (b) horseshoe-shaped interconnect sections.

Four variables are required to determine the length of zigzag-shaped interconnects, and they give rise to the following equations for the length of total zigzag-shaped interconnects:

$$L_{total} = n \cdot 2L \quad (4 - 6)$$

$$n = \frac{L_{straight}}{L_{unit}} = \frac{L_{straight}}{2L \cos \alpha} \quad (4 - 7)$$

$$L_{total} = \frac{L_{straight}}{2L \cos \alpha} \cdot 2L = \frac{L_{straight}}{\cos \alpha} \quad (4 - 8)$$

Equation (4-8) exhibits the total length of conductive yarns consumed in the zigzag pattern interconnect is proportional to the angle α , since increasing the angle α adds the number of zigzag unit and total length of the interconnect.

The length of horseshoe pattern conductive interconnect can be defined by four variables, and they were used to calculate the length of total interconnects by the following equations:

$$L_{total} = n \cdot \left(\pi R + \frac{2\theta}{180^\circ} \pi R \right) \quad (4 - 9)$$

$$n = \frac{L_{straight}}{L_{unit}} = \frac{L_{straight}}{2R \cos \theta} \quad (4 - 10)$$

$$L_{total} = \frac{L_{straight}}{2R \cos \theta} \cdot \pi R \cdot \left(1 + \frac{\theta}{90^\circ} \right) \quad (4 - 11)$$

Equation (4-11) explains the total length of conductive yarns consumed in the horseshoe pattern interconnect that is determined by the R and angle θ . Increased value of R and angle θ give rise to the total length of interconnects, which results in the higher resistance.

4.2.3.3 Electromechanical performance of the embroidered interconnects

Table 4-10 shows design parameters L and α are significantly responsible for E1 in zigzag-shaped interconnects. The effect of the opening angle α in zigzag pattern to ECR1 of interconnects are significant. For interconnects fabricated with the horseshoe pattern, design parameters θ , and interaction of R and θ have significant effects on E1. There was no significant effect of design parameters to ECR1 of horseshoe-shaped interconnects.

Table 4-10. Statistical analysis of electromechanical properties of interconnects

Pattern shape	Factorial parameter	E1		ECR1	
		P-Value	F-Value	P-Value	F-Value
Zigzag	L	<u>0.001</u>	25.69	0.452	0.63
	α	<u>0.003</u>	16.75	<u>0.010</u>	11.30
	L* α	0.045	5.66	0.309	1.18
	R	0.602	0.29	0.071	4.32
Horseshoe	θ	<u>0.020</u>	8.30	0.804	0.07
	R* θ	<u>0.019</u>	8.52	0.208	1.87

The best performance samples within each of pattern design groups were selected for the electromechanical performance evaluation, and Figure 4-13 show the electromechanical properties of the embroidered interconnects. As shown in Figure 4-13(a) and (b), electrical resistance of all the zigzag-shaped interconnects showed a stability within limited elongation range (from about 10% to 80%) and started to increase monotonically with strain, which is consistent with typical force-elongation curve. The highly conductive interconnect which designed with an angle α of 45° shows a stable resistance at 17.8% elongation, and the interconnect breaks at 38.6% strain. The highest tensile strain (mean of 88.7%) of the zigzag-shaped interconnect is fabricated with an L of 4 mm, and an angle α of 60° , which achieved stable resistance at around 80%. The electrical resistance of zigzag-shaped interconnects is

lower than the value of original conductive yarns. This is the result putting conductive yarns in needle and bobbin together, which developed a parallel circuit during lock-stitch embroidering. The resistance is lower by connections of two conductive interconnects.

Figure 4-13(c) and (d) show the horseshoe-shaped interconnects fabricated with Yarn B exhibited a stable resistance change within a certain elongation level (from about 60% to 120%), after which the resistance rose sharply with stretching. The elongated range with stable resistance is consistent with the linear scope in typical force-elongation curve of horseshoe-shaped interconnects. In addition, the horseshoe-shaped interconnects designed with an angle θ of 45° shows significantly stretchability over 130% with stable resistance. The elongation of horseshoe-shaped interconnect which has an R of 10 mm is lower than 5mm radius pattern. This difference in stretchability according to R may be due to embroidery stitches limited the stretchability of fabric substrate with larger R design, which limited performance of stretchable interconnects in large area fabrication with TFP.

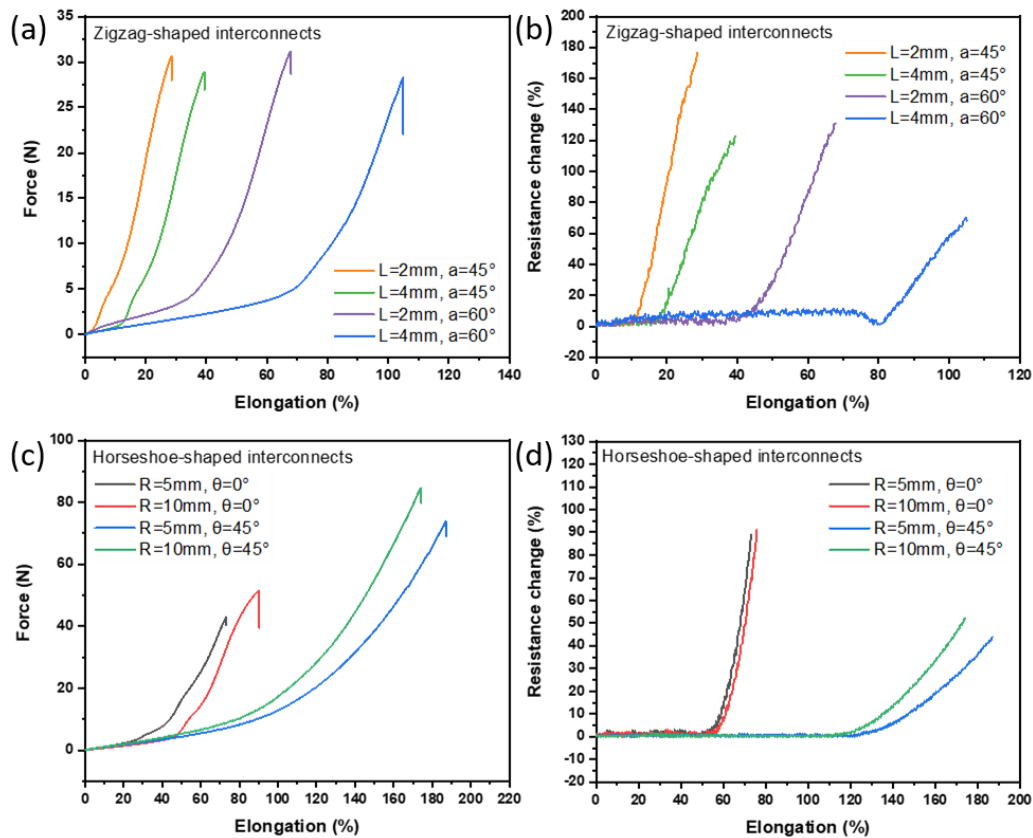


Figure 4-13. Electromechanical properties of the embroidered interconnects. (a) Force-strain Zigzag shaped interconnects under tensile strain to break. (b) Electrical resistance changes of zigzag shaped interconnects during stretching. (c) Horseshoe shaped interconnects under tensile strain to break. (d) Electrical resistance changes of horseshoe shaped interconnects during stretching.

Results of the best sample of zigzag shaped interconnects were selected to analyse the electromechanical performance. Figure 4-14(a) shows the change of force during stretching. This zigzag pattern was embroidered into the elastic substrate, the linear increment in the force was mainly due to the elasticity of the Spandex fibres and knit structures in initial period. The mechanical model of zigzag-shaped interconnect was developed according to a rheological model. E_1 indicates the elastic deformation of fabric during stretching. The friction between fabric and embroidered stitches (β_1) is stable since the pattern can contribute this stretching capability. The sharp force increase from a tightening of the knitting structure and the stitches in zigzag-shaped interconnects were stretched (after ϵ_1). This process can be described by three

deformation processes operating simultaneously: Spandex fibres' elastic deformation (E_2), fibres' viscoelastic deformation (η) and friction between fabric and embroidered stitches (β_2).

Figure 4-14(b) shows the resistance changes of conductive stitches from initial period to final broken part. Before elongation of ϵ_2 , these stitches became increasingly packed together to create more compact parallel electrical circuits. Each stitch unit can be estimated as a conductive element that the resistance corresponded to the length of threads in the structure, as shown in the left inset figure. The interconnect can be regarded as a parallel circuit created with resistance of conductive thread at length of needle thread (L_1), bobbin thread (L_2) and depth of fabric (L_3). The resistance of each conductive unit in the circuit can be calculated as following:

$$\frac{1}{R_{unit}} = \frac{1}{R_1 + \left(\frac{R_3}{2}\right)} + \frac{1}{R_2} \quad (4 - 12)$$

$$R_{unit} = \frac{[R_1 + \left(\frac{R_3}{2}\right)] \times R_2}{R_1 + R_2 + R_3} \quad (4 - 13)$$

where R_{unit} is the resistance of each stitch unit in embroidered interconnect before stretching, R_1 and R_2 is the resistance of conductive yarns at L_1 length, and L_2 length respectively. R_3 is the resistance of conductive yarns at L_3 length.

After stretched over elongation of ϵ_2 , the resistance increased rapidly under higher forces since the stitches separated to form similarly series circuit. The resistance of each conductive unit in the circuit can be calculated as Equation 4-14. The circuit pattern changed from parallel to series results in the increase of resistance.

$$R'_{unit} = \frac{R_2 \times (R_1 + 2R_3)}{R_1 + R_2 + 2R_3} \quad (4 - 14)$$

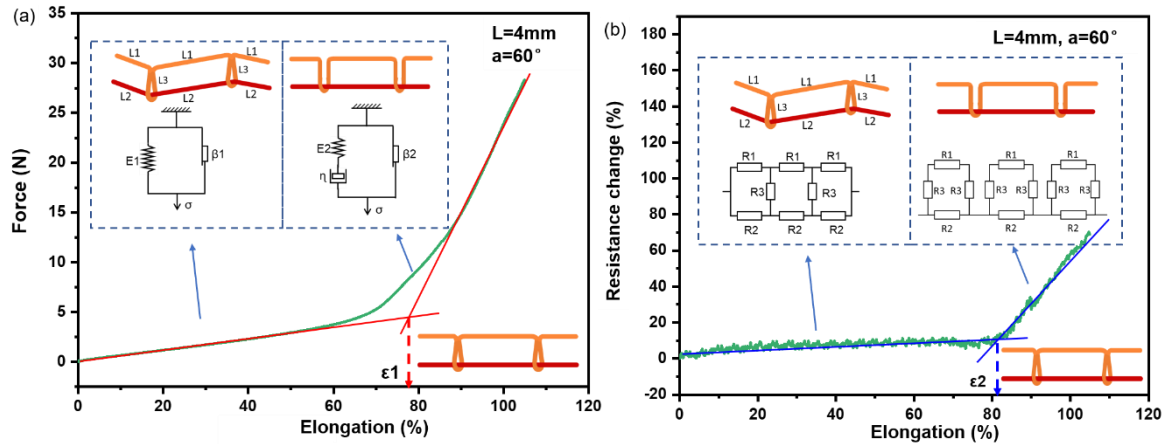


Figure 4-14. Mechanical and electronic model of selected zigzag shaped interconnects. (a) Mechanical model, and (b) electronic model.

The horseshoe shaped pattern interconnects are fabricated with insulated conductive threads. These threads were fixed with common polyester threads by lock stitches. There were no direct contact of conductive yarns. The fixed threads broken under higher tensile force, even though the conductive threads still in good condition. But the conductive threads were stretched over 100% stretching, which results in the increase of resistance because the threads were attenuated. Figure 4-15(a) and (b) show the changes of force and resistance during stretching of interconnects with horseshoe shape. Finite element simulations further reveal the detail distribution of stress applied to interconnects. When stretched, localized von Mises stress concentration was observed on the radius of the horseshoe shape, as shown in Figure 4-15(c) and (d). Figure 4-15(e) shows such tension stress built up with the increase in the stretching, the failure was determined by breakage of fixed polyester threads instead of fractures of conductive threads. The breakage of fixing threads in arc part of the pattern was overserved in high tension stress, as shown in Figure 4-15(f). As a result, the conductive threads with TPU coating in horseshoe shaped interconnects possess electromechanical stability under stretching, while the fixing threads broke in high tension stress.

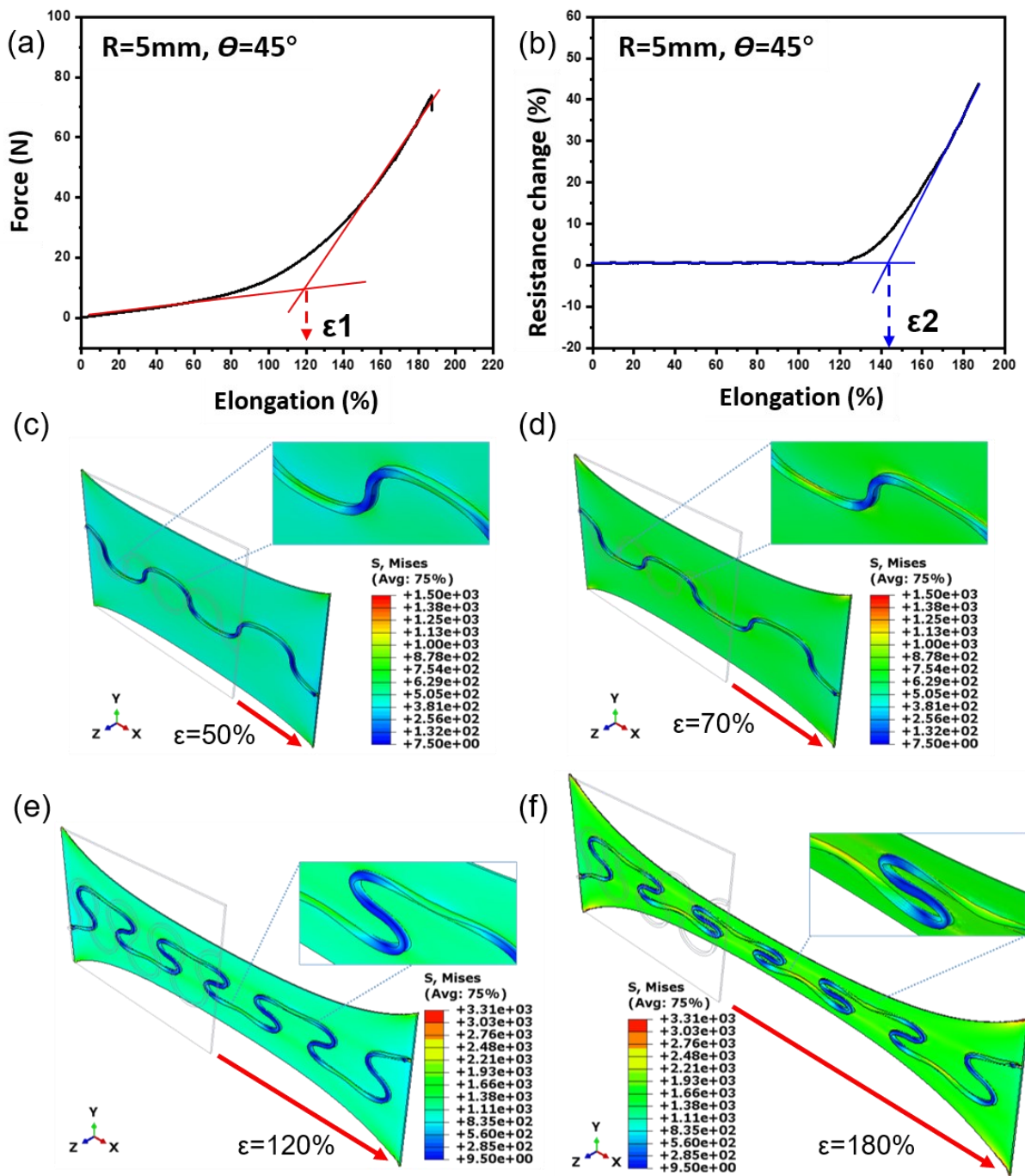


Figure 4-15. The electromechanical curve and stress simulated diagram of best performed horseshoe-shaped interconnects. (a) Force-strain curve, and (b) electrical resistance changes during stretching. Simulated diagrams of the distribution of von Mises stress in the stretched thread at the elongation of (c) 50%, (d) 70%, (e) 120%, and (f) 180%.

4.2.3.4 Durability and application

The human use case scenario for wearables requires the electrical resistance to be retained over

multiple activity cycles. The cyclic tensile test at 300 mm/min was employed to evaluate the stability of the resistance of interconnects during 500 repeated stretching process. The zigzag and horseshoe shaped interconnects with the highest elongation performance were evaluated at 25% and 45% strain, respectively. Figure 4-16 presents the resistance of zigzag-shaped interconnect changes less than 9% during 25% stretching. This may due to the silver coating was peeled off by mechanical abrasion from textile deformation during repeated stretching. However, the horseshoe-shaped interconnect showed significantly lower resistance changes, which is less than 2% under 45% strain. Since Yarn B used in horseshoe-shaped interconnects has a TPU coatings, which can protect the conductive layer on the fibres during dynamic stretching.

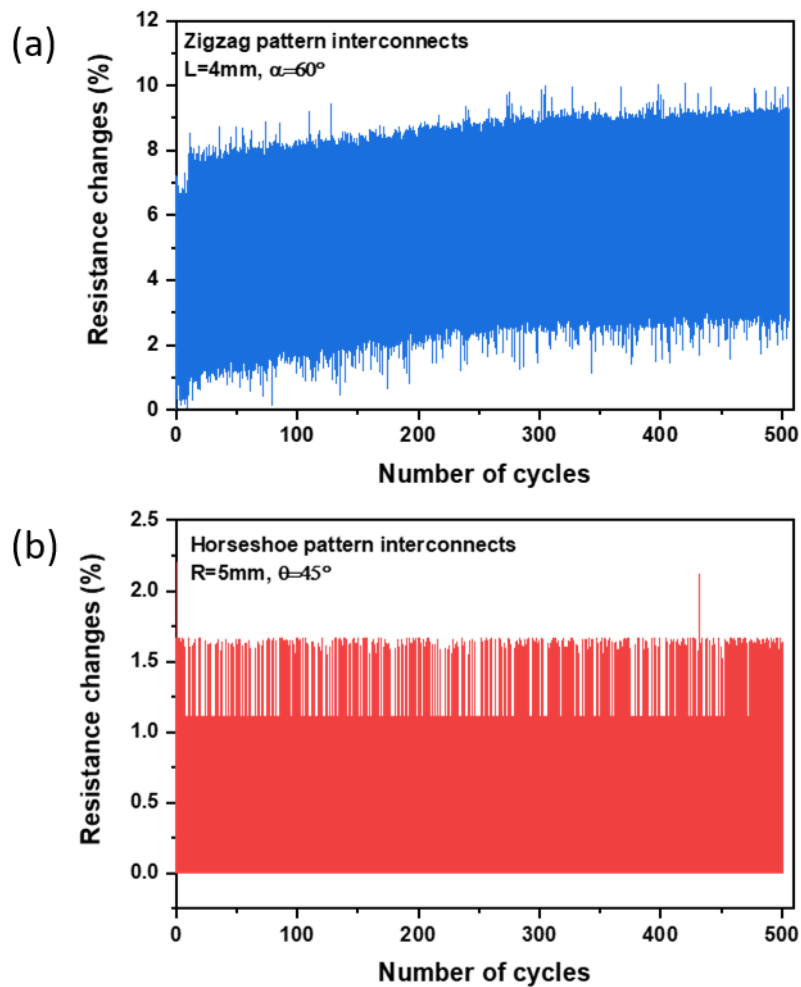


Figure 4-16. Dynamic stretching endurance test results in 500 cycles. (a) The zigzag pattern at an elongation of 25%. (b) The horseshoe pattern at an elongation of 45%.

As a demonstration of applicability of the embroidered interconnects in e-textiles, two lines of embroidered samples were sewn with a commercial LED to develop circuits by horseshoe structures ($R=5\text{ mm}$, $\theta=45^\circ$). The embroidered samples were able to maintain a stable conductive tracks to the LED illumination during the arm and leg movement, as shown in Figure 4-17(a) to (e). As a wearable conductive tracks in smart garments, the LED and embroidered interconnects was demonstrated that allowing retention of lighting over strain cycles. The pattern of interconnects was selected according to the elongation requirement of movement across joint.

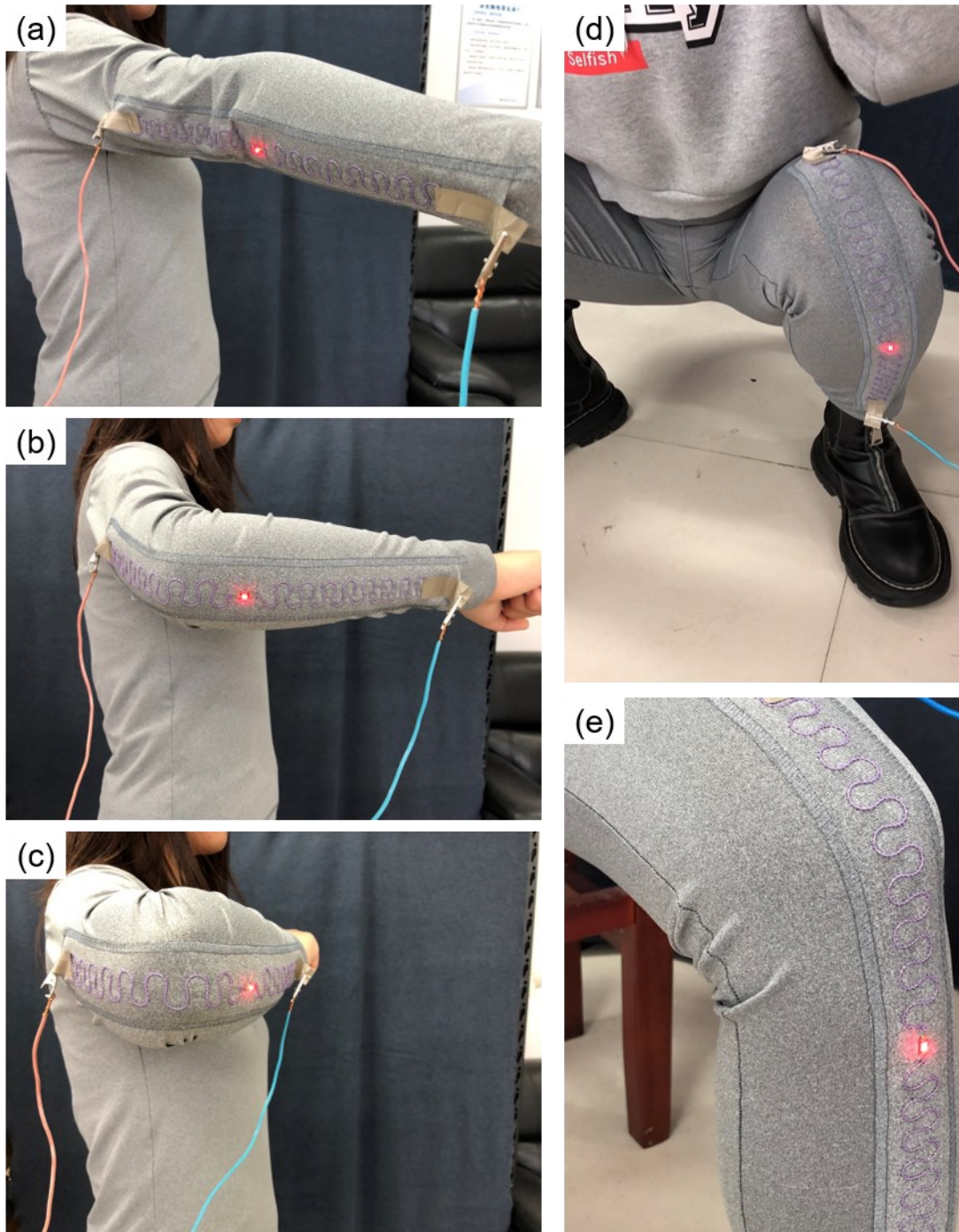


Figure 4-17. Demonstration of wearability with a LED circuit that maintained conductivity. During (a) the arm in straight, (b) bending the arm with 90° and (c) 45° ; (d) squatting and (e) sitting.

4.2.4 Summary

In summary, zigzag-shaped interconnect (fabricated with $L=4\text{mm}$ and $\alpha=60^\circ$) has stable

resistance up to 80% elongation, and the resistance changes less than 10% during 500 repeated 25% tensile strain. The horseshoe-shaped interconnect proposed in this study ($R = 5\text{mm}$ and $\theta = 45^\circ$) shows significant elongation over 130% remaining resistance stability during stretching. The changes of resistance is less than 2% during 500 cyclic 45% elongation stretching. Finally, the embroidered interconnects were applied as conductive tracks in smart garments fitting arm and leg movement requirements. Thus, the diverse stretchable properties of zigzag and horseshoe shaped interconnects can be applied in smart garments in accordance with daily activities' requirements.

4.3 Conclusion

In this chapter, the objective 2 to develop flexible and stretchable highly conductive tracks for interconnects has been achieved. The electrical conductivity of embroidered interconnects was studied first. When conductive threads are used as needle threads, the resistivity of the conductive tracks fabricated with lock stitch type 301 is the lowest because the least amount of conductive thread is used. Embroidering with conductive threads used both in needle and bobbin results in the highest conductivity, or the greatest reduction in the resistivity (about 50% of that of the conductive thread). However, multiple needle punching has limited effects on improving conductivity in this fabrication situation.

Moreover, two embroidery techniques for stretchable interconnects have been performed using silver-coated conductive yarns (with and without TPU insulation) designed with zigzag and horseshoe patterns respectively. The impact of design parameters, which is L and α for zigzag, R and θ for horseshoe pattern to stretchability of interconnects have been thoroughly studied. Results show that the zigzag shaped interconnects have lower electrical resistance but a lower strain level than the horseshoe structures. Moreover, the electromechanical properties of interconnects are examined in order to determine a strain range with stable electrical resistances. Results indicate that zigzag-shaped interconnect (fabricated with $L = 4\text{mm}$ and $\alpha = 60^\circ$) has stable resistance up to 80% elongation, and the resistance changes less than 5%

during 500 repeated 25% tensile strain. The horseshoe-shaped interconnect proposed in this study ($R = 5\text{mm}$ and $\theta = 45^\circ$) shows significant elongation over 130% remaining resistance stability during stretching. The change of resistance is less than 2% during 500 cyclic 45% elongation stretching. Finally, the embroidered interconnects were applied as conductive tracks in smart garments fitting arm and leg movement requirements. Thus, the diverse stretchable properties of zigzag and horseshoe shaped interconnects can be applied in smart garments in accordance with daily activities' requirements.

CHAPTER 5. EMBROIDERED ELECTRODES DESIGN AND PERFORMANCE EVALUATION FOR ECG MONITORING IN BODY STATIC SITUATION

This chapter focuses on objective 3 to develop embroidered electrodes for ECG monitoring by collaborating with external research partners.

Authors: Yan Zheng, Lu Jin, Jing Qi, Zekun Liu, Zhangchi Liu, and Yi Li

Targeted journal: Journal of the Textile Institute, submitted

Statement of own contributions: Main research idea, embroidered electrodes fabrication and ECG monitoring performance evaluation, subject tests protocol and implement; data analysis and modelling; preparation of prototype, tables, figures, and manuscript.

Statement of co-author contributions: Lu Jin supports in impedance measurement. Jing Qi supports in wearing pressure measurement. Zekun Liu and Zhangchi Liu support in carrying out ECG measurement experiment. Yi Li initiated project idea and provided supervision and guidance in research methodology, the design of experiment, data analysis and interpretation, and paper revision.

5.1 Introduction

Cardiovascular events are the leading health issue among firefighters [46]. The electrocardiogram (ECG) is a widely studied physiological signal and long-term ECG measurements that can be used for the examination of all electrical processes in the heart. These signals are generated in different parts of the heart and the function of electrodes is to convert ionic flow into electric current [154, 155]. Thanks for the versatility of embroidery technique and now it is a major contributor to e-textiles fabrication. The embroidered electrodes can minimize skin irritation and discomfort, particularly when used over prolonged time periods. Previous studies have identified the embroidered electrodes were reliable and demonstrated

application in ECG, EEG and EMG monitoring [12–14, 31]. Pola [32] compared knitted, weaved and embroidered electrodes for ECG measurement, and embroidered electrode has a good contact with the skin and well suited for measuring ECG especially in dry skin condition. Zhang [97] developed an embroidered ‘brush-like’ electrode with silver-silver chloride treatment and used in wearable biopotential signals acquisition systems. Ankhili [95] assessed the performance of embroidered electrodes for ECG long term monitoring before and after 50 cycles of washing. These researches show the performance of embroidered electrodes was over weaving and knitting textile structure for ECG long term monitoring and they are resistant to dry abrasion and normal home laundering. As for the whole smart wearable products development, the embroidery technique not only used as electrodes fabrication, but also to realize the interconnectors that integrate into the garment directly [156, 157]. The breast belt integrated an reservoir into embroidered electrodes was developed and that they were moisturized with low amount of water vapour [31]. Even some system realized the connection lines with embroidery techniques, the connections need to be insulated after the fabrication. With the development of silver coated conductive yarns, there were TPU insulated silver coated conductive yarns in the market. The embroidery techniques that can combine electrodes and insulated connection lines need to be investigated.

In details, the relationships between textile electrodes properties and ECG signal quality were studied as well. The optimum knitted electrodes size for ECG measurement was determined at 20mm×40mm [158]. The silver plated nylon thread sewn electrodes were compared [159]. This study found decreasing area of textile electrodes decreases fidelity of registered ECG signals at 0-250Hz frequency, and the electrodes with an area greater than 4 cm² will not cause significant distortions to ECGs’ low frequency spectrum content. Beckmann [160] designed the electrode test setup that could investigate the electrical properties of textile electrodes and the skin-electrode contact behaviour. The relation between pressures exerted on the electrode and the observed motion artefact, and on the padding application were investigated [33]. In general, the paddings could reduce the motion artefact and pressure is

strongly affect signal quality when measure electrode impedance at 100 kHz. Taji [161] found that skin-electrode impedance of dry electrodes decreases with the initial application of the 4kPa pressure, and applied pressure has larger effect on dry electrodes than wet electrodes. The research [162] about electrodes locations in smart clothing determined the optimal locations of the ECG electrodes that can keep the electrode contact to skin with body motion.

Different embroidery patterns, which were structured by different contact methods of conductive yarns, may have effects on the contact impedance of electrodes. The influence of the 304 lock stitch embroidery processes on the electrical conductivity of embroidery elements was analysed [81]. The research demonstrated that to achieve high quality embroidery systems with precise electrical conductivity, a filling type of thicker stitch density should be applied. Because the solid filling of the embroidery area most successfully guarantees an integral electrical conductivity of different forms. However, the effects of other embroidery stitch type filling in electrodes, the embroidery layers and filling density on the electrodes performance for ECG monitoring still need to be studied.

Thus, the effect of embroidered electrodes' design including size, filling layer and density, and stitch types of on the skin-electrode impedance were investigated through DOE. In addition, morphology of ECG signals detected by electrodes with various stitch patterns were compared under three levels of wearing pressure were studied to determine proper electrodes and wearing pressure for ECG signal monitoring in body static situation. More importantly, the mechanism of surface friction of embroidered electrodes on skin was also discussed.

5.2 Experimental work

5.2.1 Materials

The silver coated polyamide thread, named as HC12, purchased from MADEIRA (Madeira Garnfabrik GmbH, Freiburg, Germany) was used as needle thread during embroidering. The thread is highly conductive (with resistance at $80\pm 9.6 \Omega/m$) and thicker than common

conductive yarns (with diameter at 388.3 ± 28.9 μm) that has better contact between skin and electrode. The regular non-conductive polyester thread was used as bobbin thread. The substrate fabric is single jersey and application for firefighters' T-shirt in EU (composed of 78% FR viscose, 20% Para-Aramid, and 2% carbon with 200 ± 10 g/m^2 surface density). The elastic band (composed by polyester and rubber, width at 45 mm) were prepared to fix the electrodes with stable pressure (1 ± 0.2 kPa). In order to quantify the performance of embroidered electrodes, the commercial disposable Ag/AgCl electrodes used for ECG monitoring in clinic (3M Red Dot™ 2238) were used as the benchmark.

5.2.2 Design and fabrication of embroidered electrodes

The skin-electrode impedance decreases when increasing the electrode size[163]. However, the area size of electrodes is limited by available skin area for ECG monitoring application. In embroidered electrodes, the combination structure of conductive threads in the patterns have different electrical properties. Here, the characteristics of embroidered electrodes were evaluated in two steps to determine the optimum size, fabrication parameters, and filling patterns for lower skin-electrode impedance.

In the first step, the area size of electrodes and embroidering parameters include filling layer, filling density (distance between two filled lines), and stitch types were used to analyse the main factors and their interactions effects on skin-electrodes impedance of embroidered electrodes. In this study, four factors at two levels were used to design the experiment (listed in Table 5-1, detailed experiment plan can be found in Supporting Table S5-1). The samples were embroidered with stitch length at 3.5 mm and the diagram of conductive thread combination methods were shown in Figure 5-1. The conductive thread was used as needle thread and regular polyester thread was used as bobbin thread.

Table 5-1. Factors and levels used in full-factorial experimental design

Factor codes	Factors	Levels	
		Level 1	Level 2
A	Area size of electrodes	20×20 mm ²	20×40 mm ²
B	Filling layer	1	2
C	Filling density	1 mm	2 mm
D	Stitch types	301	304

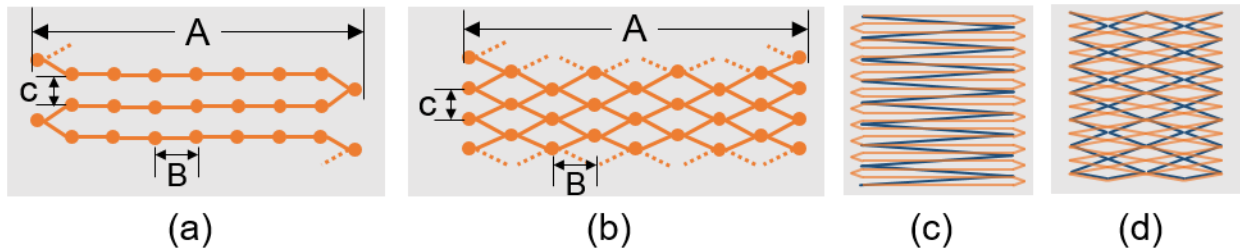


Figure 5-1. Diagram of filling stitch in electrodes. (a) 301 and (b) 304: A- the width of the electrodes; B-the length of the stitch (3.5mm); C-filling density. The formation scheme of two layers electrodes filled with 301 (c) and 304 (d). The lines in dark blue are the under layer, and the lines in orange is the upper layer.

The second step aims to compare different filling pattern impact on the contact impedance. Four types of filling pattern that composed by different conductive thread contact combinations were developed and named EP1, EP2, EP3 and EP4. Figure 5-2 shows the electrodes were filled with 301, 304, 45° intersected 301 stitch and cross lock stitch, respectively. The results from the first step, which is the optimised fabrication parameters to achieve lower impedance will be used to prepare samples.

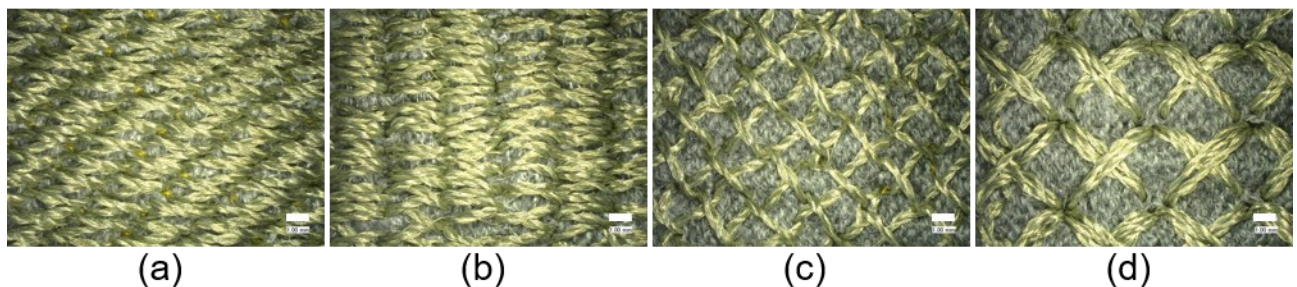


Figure 5-2. Optical microscope images of embroidered electrodes. (a) EP1- filled with 301 lock stitch; (b) EP2-filled with 304 lock stitch; (c) EP3-filled with 45° intersected 301 lock stitch; (d) EP4-filled with cross lock stitch. The scale bar is 1 mm.

5.2.3 Skin-electrode impedance measurements

ECG signal is the spectrum recording of the heart bioelectricity, which pass through the body electrolyte and human skin to reach the electrode [97]. The double-time-constant model for the skin-electrode impedance [164] exhibits more accurate results in terms of ECG measurement and frequency response. As depicted in Figure 5-3, it is composed of two stages of the single-time-constant model. The first stage represents the electrode-electrolyte interface. The second stage represents the electrolyte-skin interface.

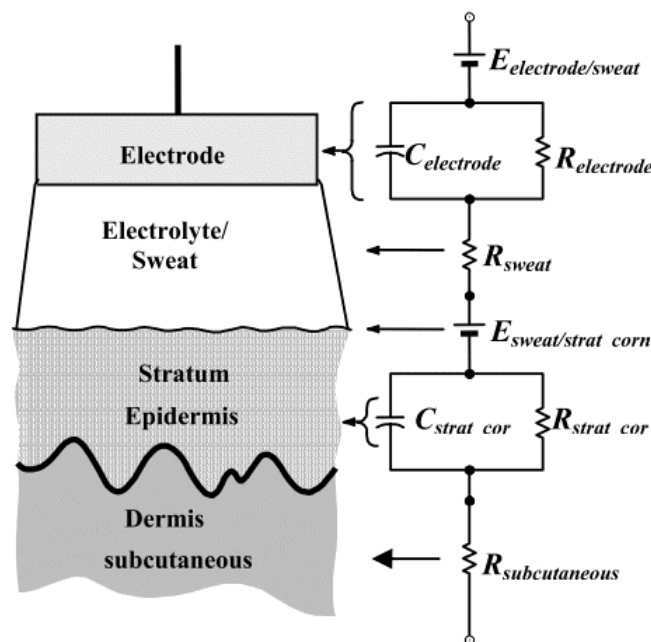


Figure 5-3. Double time constant skin-electrode interface and electrical equivalent circuit [161].

Skin-electrode impedance is an important factor in biopotential signal quality. Many researches have discussed measurement methods for the skin-electrode impedance and methods to improve the measurement accuracy [56, 97, 165, 166]. A double-electrode structure measuring method and equivalent circuit [167] were shown in Figure 5-4.

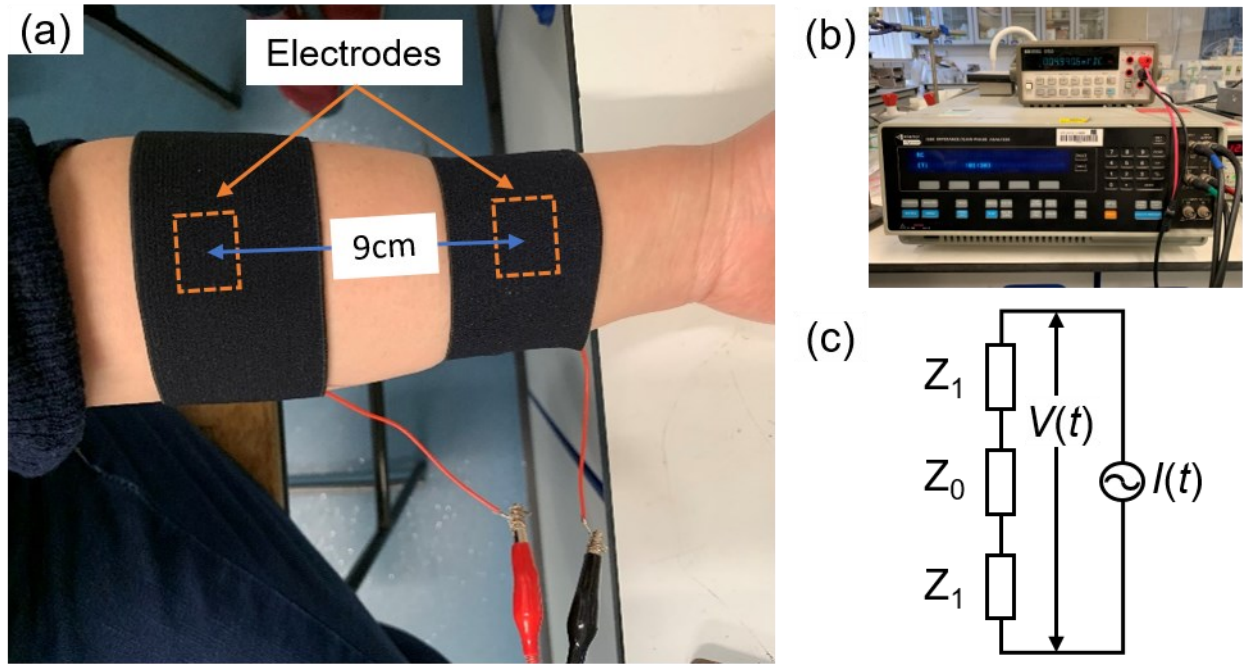


Figure 5-4. Two-electrode configuration for skin-electrode impedance measurement. (a) Measurement methods. (b) Solartron impedance analyser instruments. (c) Equivalent measurement circuit [167]. Z_1 is the impedance of skin-electrode, Z_0 is the impedance of body.

As presented in Figure 5-4(a), two polyester elastic bands were used to stable embroidered electrodes on the inside of left forearm without any skin preparation. The pressure between skin and the band was kept at 1 ± 0.2 kPa. The centre of two electrodes was 9 cm apart and the participant was asked to sit and relax. To avoid errors caused by individual differences, the experiments only use one female volunteer as a test subject. The skin-electrode contact impedance was measured by the impedance analyser (Solartron 1260), as shown in Figure 5-4(b) at frequency from 0.1Hz to 10 kHz at 100mV signal amplitude. The impedance at 1Hz was used as response value to evaluate the main factors and their interactions effects on skin-electrodes impedance of embroidered electrodes. The record began when the signal was stable. Two electrodes are used to inject the current, and the same electrodes are used to sense the resulting voltage. The general bipolar configuration equivalent electrical circuit was shown in Figure 5-4(c), where $I(t)$ is the constant current, $V(t)$ is the voltage obtained from the differential amplifier. In this setup, the skin-electrode impedance (Z_1) of both electrodes plus

body impedance (Z_0) was measured. Assuming the skin-electrode impedances were approximately equal, the measured impedance Z_m can be expressed in terms of its equivalent electrical circuit equation, as shown in Equation (5-1).

$$Z_m = \frac{V(t)}{I(t)} = \frac{I(t)(2Z_1 + Z_0)}{I(t)} = 2Z_1 + Z_0 \quad (5 - 1)$$

Assuming the body impedance Z_0 ($\approx 55\Omega$) is negligible [161], the impedance for one electrode is shown in Equation (5-2).

$$Z_1 = \frac{Z_m}{2} \quad (5 - 2)$$

The skin-electrode impedance measured begin with each pair of textile electrodes and then that of standard Ag/AgCl electrode. There was 5 minutes interval between each pair of textile electrodes test in order to avoid the possible sweat influence. The test was performed in the standard lab environment with stable temperature and humidity, which is 22°C and 65% RH, and without any skin preparation or conductive gel used during the test.

To study the impact of filling patterns on the impedance of electrodes, the fabrication parameters of electrodes with low contact impedance were selected to prepare electrodes samples with four types of filling stitches. The skin-electrode impedance of samples with different filling patterns were measured with the same methods and compared with Ag/AgCl electrodes.

5.2.4 Comparison of ECG monitoring performance under various applied wearing pressure

Three electrode samples with each filling patterns were used to carry out ECG monitoring subject test. Figure 5-5(a) shows electrodes are placed on the fifth intercostal space at the intersection with the left and right anterior axillary lines, which is the V4 position of a standard 12 lead ECG monitoring placement. The third electrode is placed in the centre of left and right electrodes as reference. Three Ag/AgCl electrodes were used to collect ECG signal

simultaneously to compare the signal quality detected by embroidered electrodes. The snap buttons were used to connect electrodes to the two channel ECG detection BioNomadix wireless module, as shown in Figure 5-5(b) and (c). The ECG signal was recorded by BIOPAC wireless data acquisition system (Model: MP160, Biopac Systems inc., USA) shown in Figure 5-5(d).

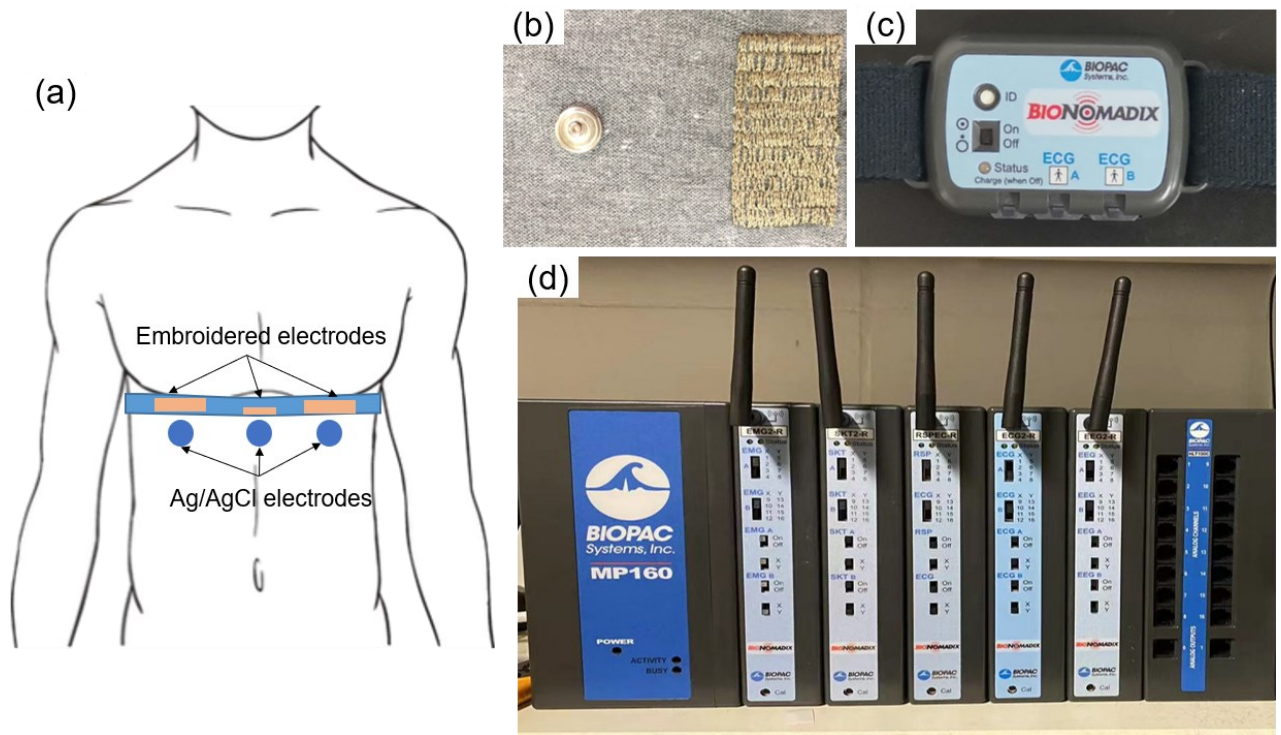


Figure 5-5. The ECG monitoring method. (a) Electrodes set up. (b) Embroidered electrodes. (c) Wireless module for synchronous ECG recording. (d) Wireless Biopac instruments.

The prototype band for ECG measurement was developed with the commercial elastic band (Huamei textile, Guangdong, China). The length of band can be adjusted that could bring three levels of pressure during test, which were 0.5 kPa, 1.5 kPa and 2.5 kPa. Three points, P1, P2 and P3 shown in Figure 5-6(a), were selected to measure the skin-band pressure, which is the experiment separated from ECG measurement. P1 is the body side area above the ribs, P2 is the position of electrodes, and P3 is the centre of the body in front. Skin-electrode contact pressure was measured by a clothing pressure air measure system (AMI-3037, AMI Techno Co., LTD, Japan) with two air bag sensors, as shown in Figure 5-6(b) to (d). The air bag sensors

were filled with air to measure pressure, and an integrated laser tissue blood flowmetry to measure blood flow mass in P2. According to the standard ASTM F2668, three male participants (aged at 20 to 40, mass between 65 to 100 kg and body height between 1.70 to 1.95 m) were recruited. They were asked to wear each of the test band with 3 levels of pressure and test only in sitting static situations. The ECG signal was monitored with a sample rate of 1000 Hz. The characterization of the ECG signal was recorded 200 seconds. The research protocol is approved by the Proportionate UREC of the University of Manchester (2019-5112-12512) and participants provide their informed consent before tests.

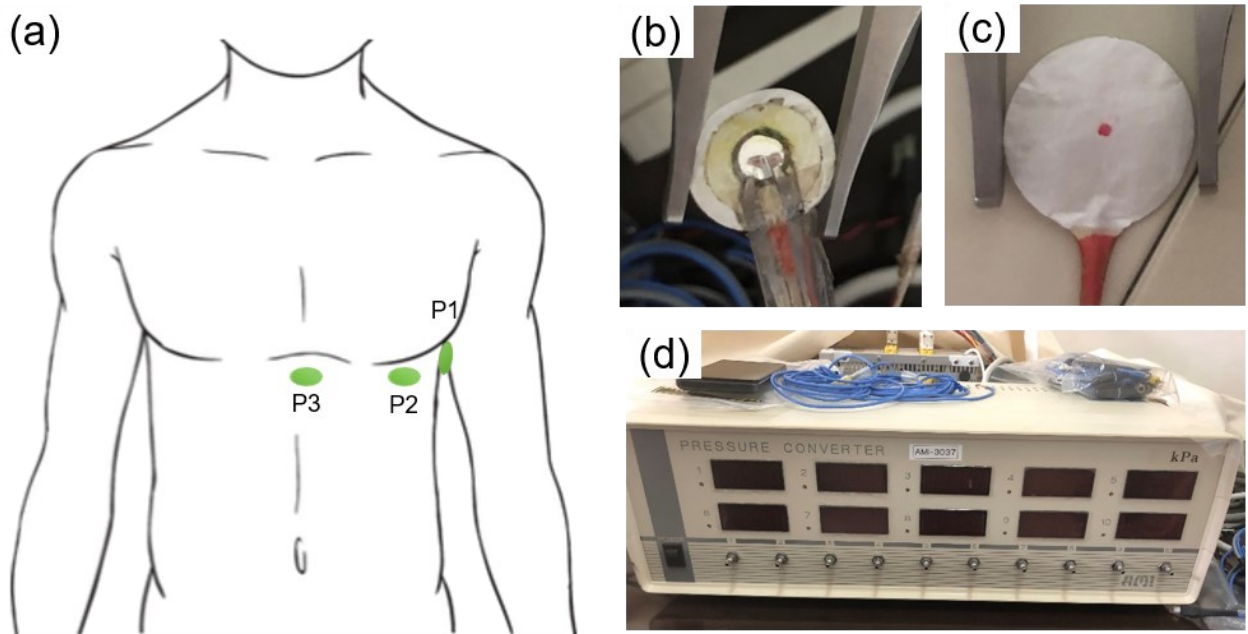


Figure 5-6. Measurement details for wearing pressure. (a) Positions of skin-band pressure measurement. (b) An air bag with blood flow measurement sensor. (c) An air bag for pressure measurement. (d) The instrument for wearing pressure measurement.

5.3 Results and discussion

5.3.1 Effects of electrodes fabrication parameters on skin-electrode contact impedance

Skin-electrode contact impedance directly influenced the reliability of collected signals, low contact impedance resulting in less noise and a higher quality ECG signal [168]. Supporting Table S5-2 shows the statistical significance ($p < 0.05$) of the contact impedance at 1 Hz of

ANOVA analysis. The embroidery area size (factor A), fill density (factor B), fill layer (factor C) and stitch types (factor D) were significant influence the contact impedance of the electrodes. The interaction effects of factor A and C, factor C and D on impedance were significant as well.

Figure 5-7 shows the influence of area size, fill density and fill layers of embroidered electrodes on the skin-electrode impedance at 1 Hz frequency. From Figure 5-7(a), it can be seen that large area size, which is 8 cm² could get the lower impedance. The close density with 1mm distance of two filling lines is better for the low impedance, while the multiply layer embroidery would make the impedance higher than single layer embroidery. The electrode embroidered with stitch type 304 showed slightly lower contact impedance than 301 stitch embroidery, but the multilayer embroidery of 304 stitch could increase the skin-electrode contact impedance significantly, as shown in Figure 5-7(b) to (c). Figure 5-7 (d) to (e) present electrodes embroidered with 301 and 304 stitch types to compare mean of contact impedance at 1 Hz frequency.

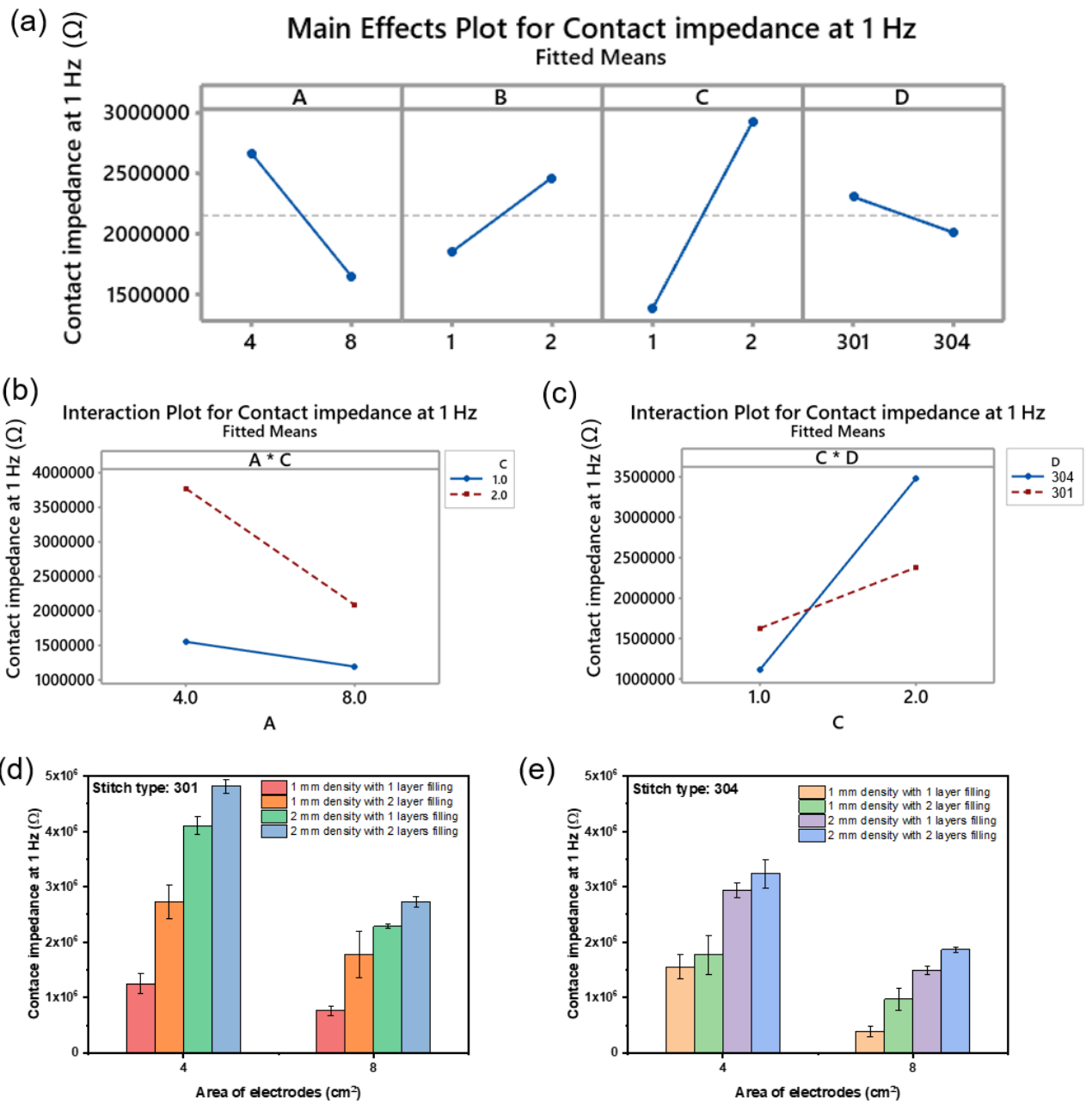


Figure 5-7. Factorial analysis of electrodes design effects on measured impedance at 1 Hz. (a) Main effects plot. Interaction effects plot of factor (b) A×C and (c) C×D. Mean of contact impedance at 1 Hz of electrodes embroidered with stitch type of (d) 301 and (e) 304.

Based on the factorial analysis of embroidered electrodes impedance in the first step, the electrodes designed with 20 mm×40 mm, single layer filling with 1mm density stitch could receive the lower contact impedance at 1 Hz frequency. The second step was to compare contact impedance with different filling patterns, which presented in Figure 5-2. Ag/AgCl electrode

(3M Red Dot™ 2238) was selected to compare contact impedance. The designed experiment variables and values were shown in Table 5-2. At a frequency of 1 Hz, the mean impedances of the embroidered electrodes EP1, EP2, EP3 and EP4 are 23.8 MΩ, 18.8 MΩ, 32.1 MΩ and 36.1 MΩ, respectively. The impedance of Ag/AgCl wet electrode is 1.91 MΩ.

Table 5-2. Electrodes design variables and impedances in the second step experiment

Electrode code	Fill pattern	Area size (mm)	Filling density (mm)	Contact impedance at 1 Hz (Ω)	
				Mean	SD
EP1	301 stitch	20×40	1	2.38E+07	2.04E+06
EP2	304 stitch	20×40	1	1.88E+07	3.45E+06
EP3	45° intersected 301 stitch	20×40	2	3.21E+07	2.98E+06
EP4	Cross 301 stitch	20×40	3.5	3.61E+07	3.53E+06
Ag/AgCl	-	-	-	1.91E+06	1.72E+05

Figure 5-8 shows the mean contact impedance plot of embroidered electrodes (EP1, EP2, EP3 and EP4) compared with the clinical Ag/AgCl electrodes from 0.1 Hz to 10 kHz. It was shown that the impedance decreased strongly with increasing frequency for both embroidered electrodes. The values of the impedance obtained from the embroidered electrodes were significantly higher than that of the wet Ag/AgCl electrodes, which may be a result of no conductive gel was used. Based on a comparison of the various pattern electrodes, the EP3 and EP4 were found has higher impedance. However, the EP1 and EP2 showed lower and very similar impedance in the results, which is consistent with analysis in the first step experiment.

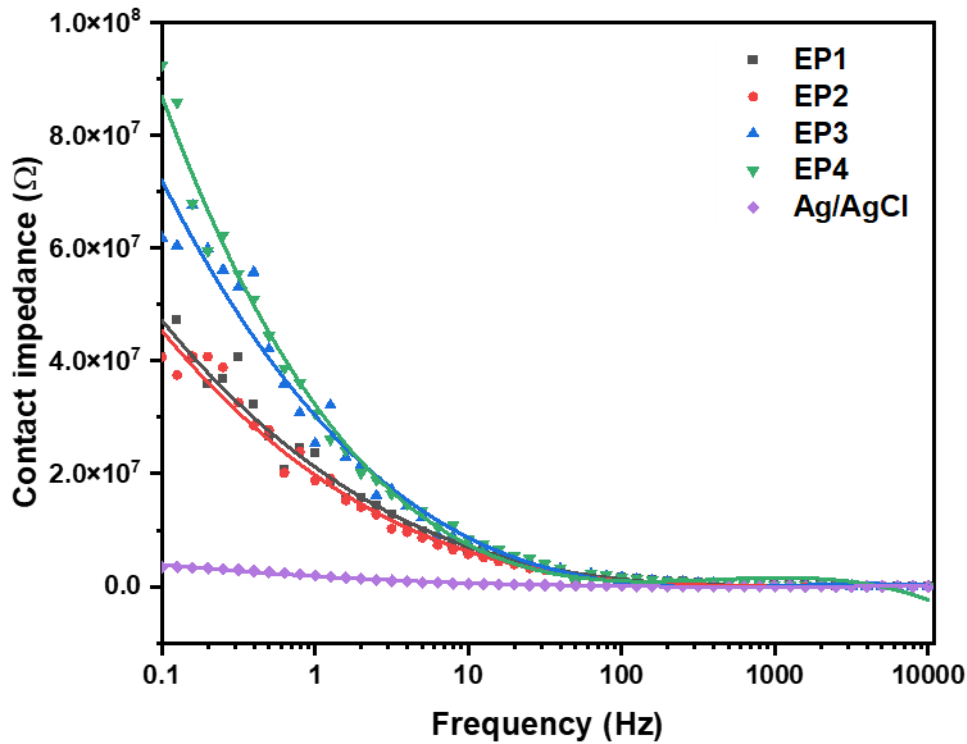


Figure 5-8. Plot of the skin-electrode contact impedance magnitude versus frequency.

5.3.2 Effects of different types of embroidered patterns on ECG signal quality

The prototype of band for ECG signal detection was developed according to the impedance measurement results. The filling pattern A and D were employed to embroidery and the electrodes size was 20 mm×40 mm with close density. The band was designed with III-lead electrode method [155]. The left arm lead was placed in the middle of the 4th and 5th rib in the body left, and the right arm lead was in the symmetry right side of the body. The distance between these two electrodes were determined by the subject participant body size, which was 18 cm to 20 cm. The right leg lead was designed in the middle of the band. The connection line was used TPU insulated 235/36-2ply silver coated thread and one lead embroidered with electrodes fabrication process by combined techniques in one step. The other lead connected to the snap button manually. The final one-step embroidered electrodes in prototype for ECG monitoring was presented in Figure 5-9.

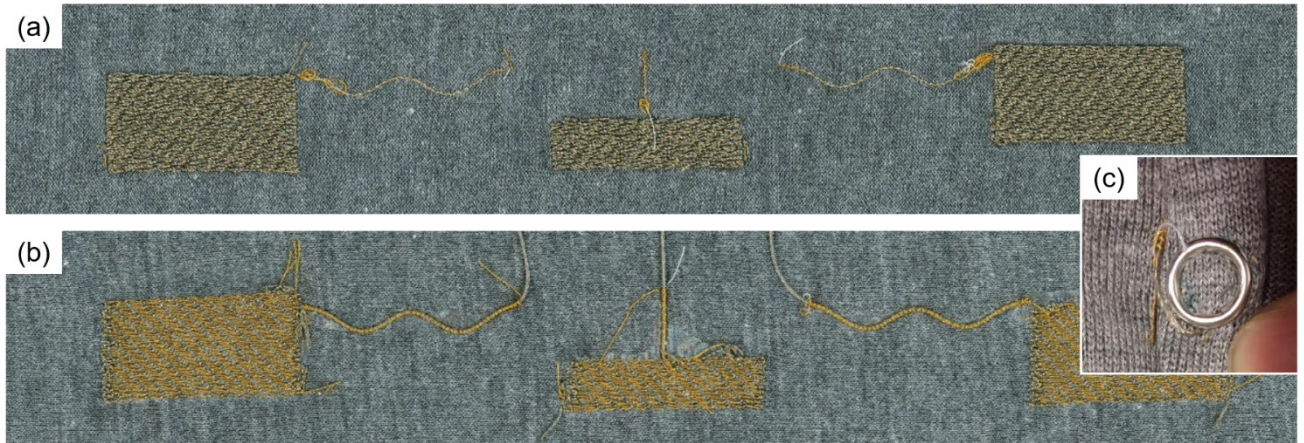


Figure 5-9. Prototype of band for ECG measurement. (a) Electrodes inside part contact to skin, (b) electrodes outside part, and (c) connection to the snap button.

Pearson product-moment correlation coefficient (CC value) [169] was used to evaluate the consistency of ECG signals measured by embroidered electrodes and Ag/AgCl electrodes. The CC value can be obtained using the following equation [170]:

$$r = \frac{n \sum xy - \sum x \sum y}{\sqrt{[n \sum x^2 - (\sum x)^2][n \sum y^2 - (\sum y)^2]}} \quad (5 - 3)$$

where r is CC value, n is the number of samples, x and y are ECG values of points from embroidered electrodes and Ag/AgCl respectively.

The ECG signal monitored by wireless BIOPAC system was analysed and results were shown in Figure 5-10. The ANOVA result shown in Figure 5-10(a) to (b) illustrate the wearing pressure and electrodes pattern affect the CC value, and this value increased by the wearing pressure. The EP2 has the highest CC value compared to other electrode patterns. Table S5-3 shows the summary of ANOVA response for CC value. Figure 5-10(c) shows mean of CC value of three participants calculated from three participants under three levels of wearing pressure. This results was agree with the study of [161]. The CC value increased rapidly when wearing pressure increased from 0.5 kPa to 1.5 kPa, and this increase continuous slightly rise after the wearing pressure adjusted to 2.5 kPa. Figure 5-10(d) shows the representative ECG cycle of one participant detected from the embroidered electrodes could get ECG signal similar to the

Ag/AgCl clinical electrodes. The CC value of ECG signals could reach as high as 0.959 detected by EP2 with 2.5 kPa wearing pressure. There was little ECG waveform difference caused by the ECG measurement position since the CC value measured by Ag/AgCl electrodes from upper and lower was 0.996, as shown in Figure 5-10(e).

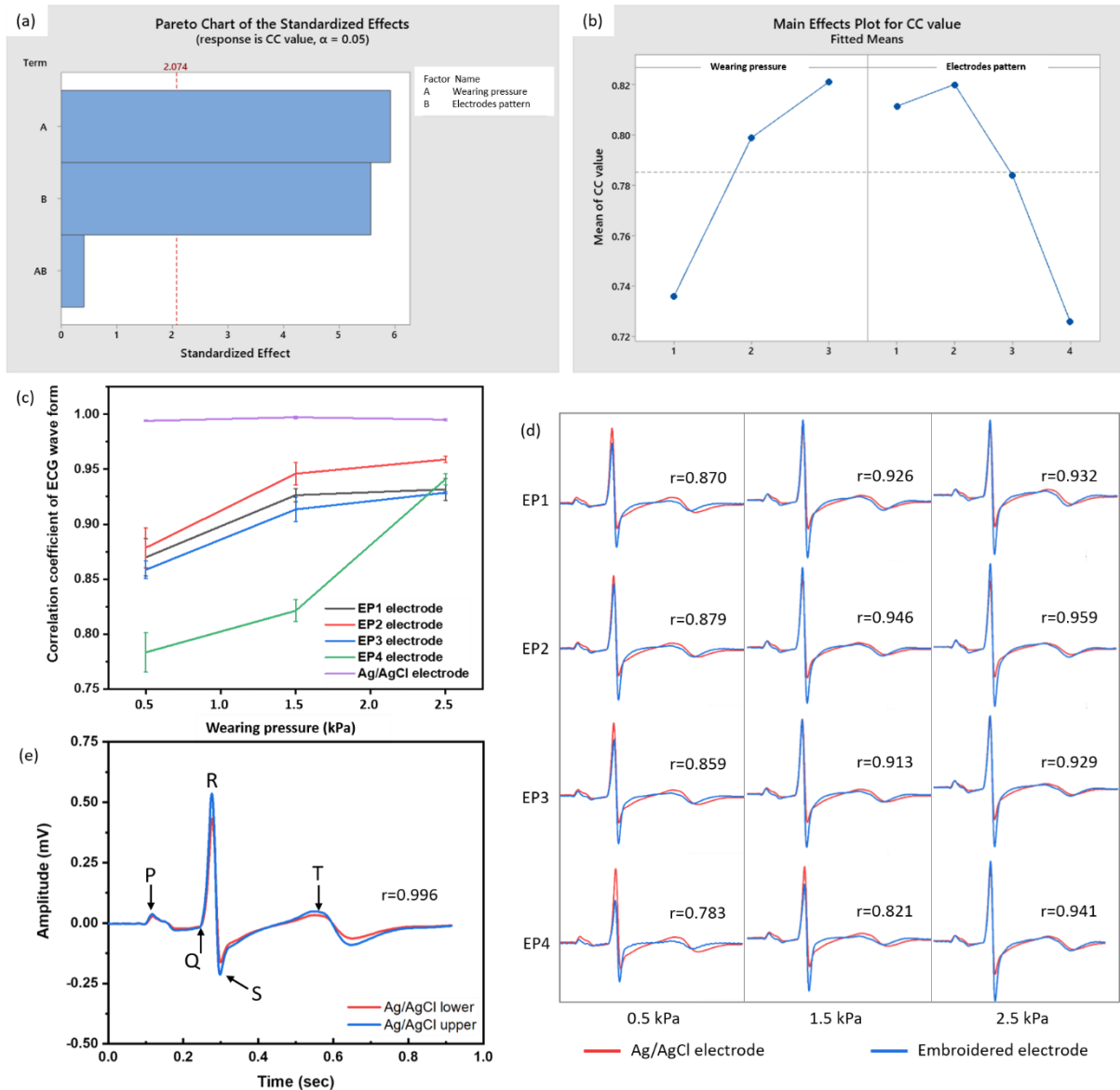


Figure 5-10. Analysis of ECG signal quality. (a) ANOVA significance of two factors; (b) Main effects plot for CC value. (c) Mean of CC value calculated from three participants' wearing trial under three levels of wearing pressure. (d) Comparison of representative ECG cycles measured from embroidered electrodes and Ag/AgCl electrodes, calculated CC values of this cycle was inserted. (e) A representative ECG cycle and CC value measured by Ag/AgCl from different position.

Each ECG cycle contains significant P peak, QRS wave form and T peak, as marked in Figure 5-10(e). The R peak is the highest and easy to recognised in long time ECG waveforms. The time between R peaks of two adjacent cycles is called RR intervals (RRI). Figure 5-11 shows the comparison of ECG waveforms measured by EP2 electrodes and Ag/AgCl electrodes. The interval of R peaks measured with EP2 electrodes were the same with the Ag/AgCl electrodes. Figure 5-11(a) shows the amplitude of R peak measured by EP2 was lower under 0.5 kPa wearing pressure, and there were noises shown in the wave patterns. With the wearing pressure increased to 1.5 kPa and 2.5 kPa, the noises in ECG waveforms measured by EP2 electrodes were gradually decay and the amplitude of R peaks were increased, as shown in Figure 5-11(b) and (c). In addition to objectively evaluate consistency of ECG signals measured from two channels, times of RR intervals and QRS intervals, height of P peak and R peak of each ECG cycle was calculated. QRS intervals was the time duration of QRS waveform. 200 seconds heart beats signals measured by EP2 electrodes and Ag/AgCl electrodes under 2.5 kPa wearing pressure were analysed by comparison of interval times and amplitudes of ECG morphology peaks. Figure 5-11(d) shows the RR intervals and QRS interval times measured by EP2 were perfectly kept pace with that from Ag/AgCl electrodes. Figure 5-11(e) shows the height of R peak and P peak measured by embroidered EP2 were similar to the waveform of Ag/AgCl measurement. The minor difference of QRS interval times and height of R peak and P peak were caused by the position of ECG measurement. This can be explained by the signal detected with the same Ag/AgCl electrodes through different measurement position. Support figure S5-1 illustrates this difference.

The EP2 pattern embroidered electrodes were the best electrodes for ECG signal monitoring, and the higher wearing pressure over 1.5 kPa could help to combat the distractions of chest movements during breathing. The pattern of electrodes with interspace or gaps of conductive yarns, such as EP3 and EP4, could be used for ECG signals detection. However, the CC value compared with Ag/AgCl electrodes to measure ECG wave patterns was lower.

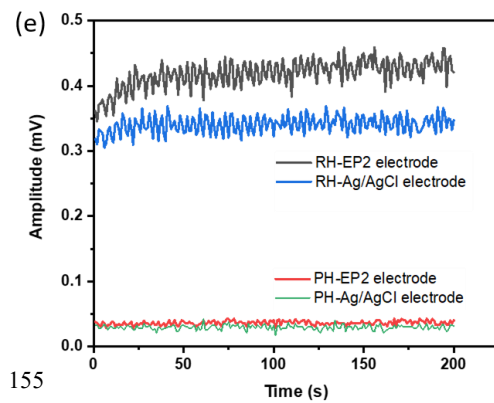
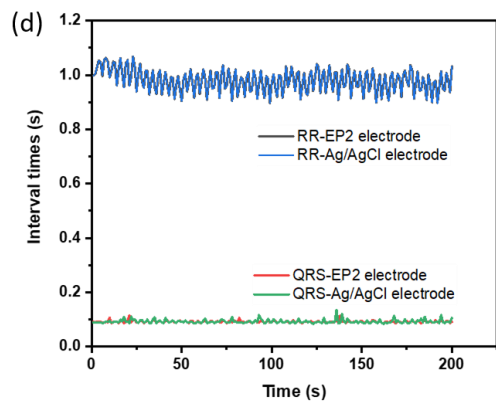
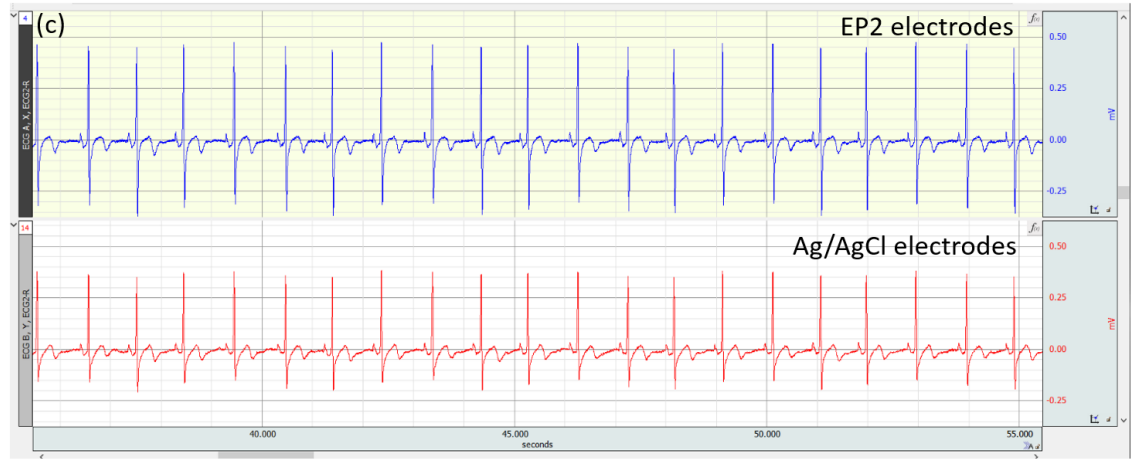
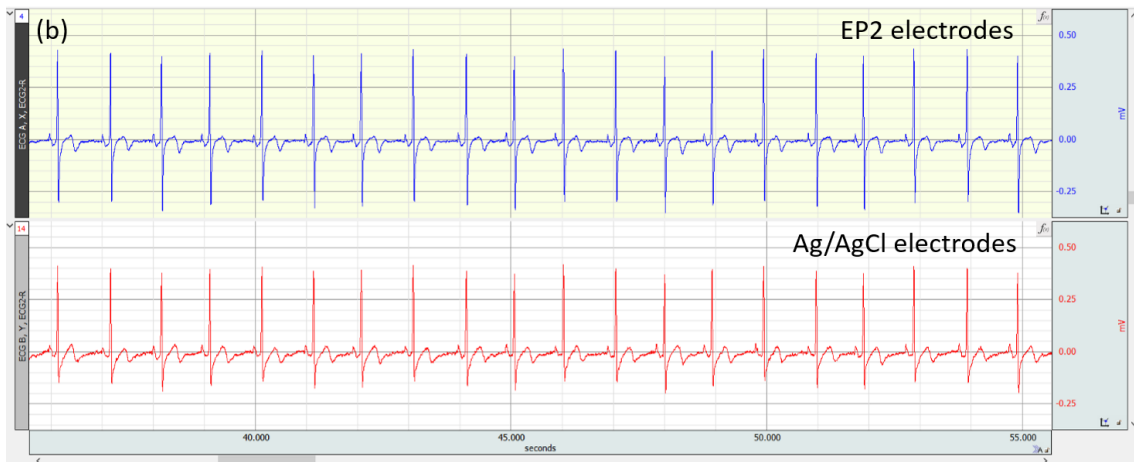


Figure 5-11. Comparison of ECG waveforms measured by EP2 electrode and Ag/AgCl electrode with wearing pressure. (a) 0.5 kPa, (b) 1.5 kPa, and (c) 2.5 kPa. (d) The interval times of RR peaks and QRS waveform and (e) amplitudes of R peak height and P peak height comparison of ECG morphology peaks during 200 seconds measurement with 2.5 kPa wearing pressure.

5.3.3 Effects of applied wearing pressure on performance of embroidered electrodes

Many researches have observed the skin-electrode impedance of textile electrodes was decreased with increasing of the applied pressure [33, 161, 171, 172]. Studies showed a pressure between 15 to 20 mmHg to provide the best signal quality and more stability against motion artifact [33]. However, most of the researches only measure electrode-skin pressure on the arms, the real wearing pressure on the body for ECG measurement may not the same. The impact of applied pressure to the body's physiological parameters, such as blood flow were not clear yet. The surface friction of electrodes under different level of forces needs to be studied since it has impact on the stability of electrodes during body activities.

Figure 5-12 shows the skin-band pressure of three measured positions and situation of blood flow under wearing pressure of 0.5 kPa, 1.5 kPa and 2.5 kPa. The pressure was measured in position of P1, P2 and P3, as shown in Figure 5-6(a). From Figure 5-12(a), the skin-band pressure was different at body position, which the pressure in P1 is the highest and changes significantly. The pressure of P2 and P3 increased slowly with the elongation of elastic band, and the pressure in P3 was changed slightly after the band elongated over 25%. This difference was caused by the body content and body shape difference in various positions. P1 and P2 were over the ribs, and P3 was above the curved body surface covered with subcutaneous fatty tissue. Figure 5-12(b) to (d) show changes of blood flow in P1, P2 and P3 under various wearing pressure. With the increase of wearing pressure, the blood flow mass declined, and this descend fell sharply when wearing pressure increased to 1.5 kPa. The blood flow volume and velocity decreased when applied wearing pressure to 0.5 kPa, however, the velocity of blood flow increased significantly when the wearing pressure increased to 1.5 kPa. This could be the nature body's physiological response to the higher-level applied pressure. Even though the increased

wearing pressure could bring contact impedance descend of electrodes, and this would increase the signal quality of ECG monitoring. But the higher pressure in wearing may lead to body physiological issues, such as limited the blood flow mass in pressure applied area.

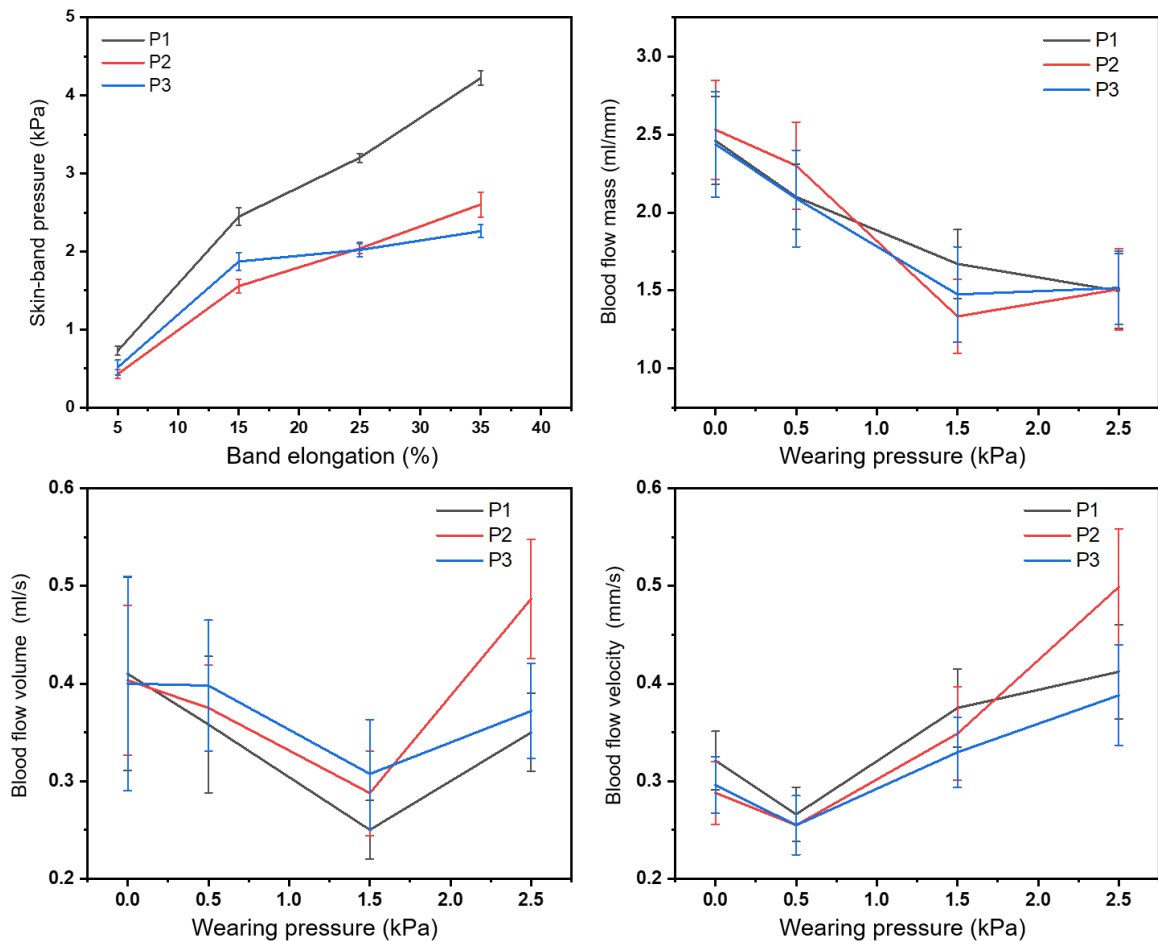


Figure 5-12. Skin-band pressure and blood flow analysis. (a) Skin-band pressure of three measured positions. (b) Blood flow mass, (c) blood flow volume, and (d) blood flow velocity at different wearing pressure level.

Wearing pressure could help to reduce the motion-induced artifacts in ECG measurements as well[33]. Tradition Ag/AgCl electrodes use adhesive conductive gel to improve the contact at the skin interface. Textile based electrodes do not comprise any form of adhesive layer, the coefficient of friction of the electrode can help to determine its surface properties and identify the tendency to slide of electrodes [173]. The coefficient of friction was calculated by Equation

5-4 [174]:

$$\mu = \frac{f}{N} \quad (5 - 4)$$

where f represents the friction force and N is the normal force exerted by the sled. The static coefficient of friction (SCF) corresponds to the force necessary to initiate a motion of the upper electrodes against the skin mimic substrate. The dynamic coefficient of friction (DCF) is the force required to maintain the motion[175]. Figure 5-13 illustrate the instruments to measure the static and dynamic force of embroidered electrodes proposed in this paper. Figure 5-13(a) shows the stage covered with PU fabric to simulate human skin, and a tensile gauge to measure friction force during keep electrodes moving on the surface of stage. Electrodes were put on the stage with face done and measure the force when pulling electrodes 10 cm, as shown in Figure 5-13(b). Figure 5-13(c) shows the surface resistance of embroidered electrodes was measured under different applied force with four external electrodes connected to a multimeter. As shown in Figure 5-3, the resistance of electrodes was part of contact impedance value. The analysis of electrodes' resistance could help to figure out the impact of different embroidered pattern on the contact impedance under pressures.

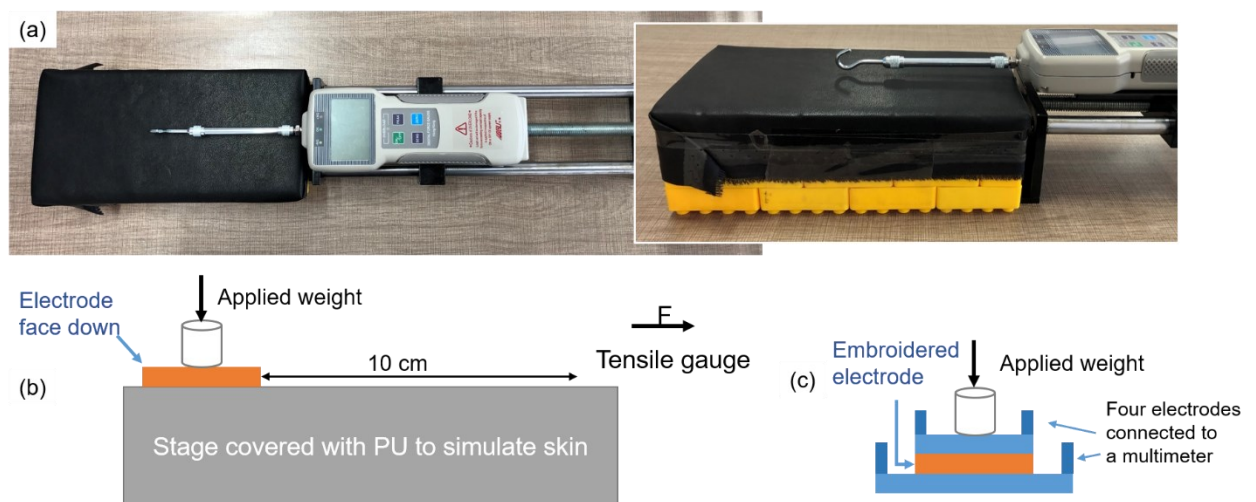


Figure 5-13. Experiment details to measure friction force. (a) Image of stage and a tensile gauge to measure friction force. (b) Schematic representation of the electrodes and applied weight for the measurement. (c) Schematic diagram for the surface resistance measurement of electrodes applied with weight.

As for the coefficient friction of electrodes proposed in this paper, Figure 5-14 (a) presents the effects of applied force and embroidered patterns on the SCF, which decreased significantly with increased applied weight. Figure 5-14 (b) shows the order of SCF for different patterns of electrodes was EP4>EP3>EP2>EP1. The impact on the DCF was shown in Figure 5-14 (c) and (d), where the DCF showed similar trend to SCF, except the DCF of EP3 was lower than EP2. These results explained the textile-based electrodes were compressed and the surface of electrodes tend to smooth under applied pressure. Thanks for the compressive contact of conductive yarns in embroidered electrodes, the surface resistance of electrodes descended when the pressure applied from 0.5 kPa to 1.5 kPa, as shown in Figure 5-14(e). The EP2 electrode was significantly sensitive to the applied weight, and this type of embroidered pattern electrodes could reach the lowest surface resistance with applied pressure compare to 2.5 kPa, which can be found in Figure 5-14(f). The EP2 embroidered electrodes with 304 stitch pattern could get better quality ECG signal under 1.5 kPa wearing pressure level. These be because there were some conductive threads overlapped in filling stitch structure of this pattern.

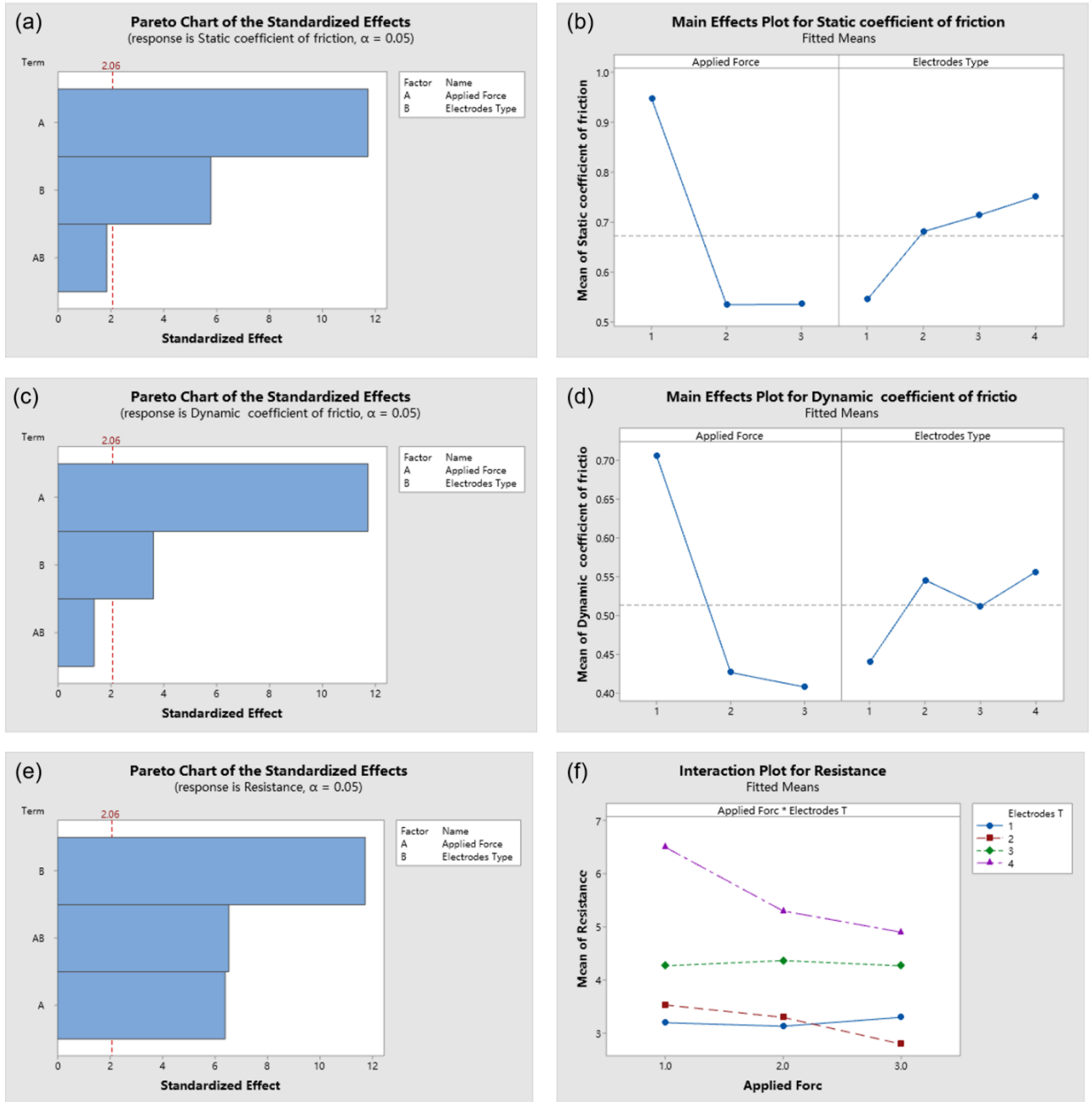


Figure 5-14. Factorial analysis of SCF and DCF. (a) Significant factors for SCF and (b) main effects plot for SCF. The results of (c) significant factors for DCF and (d) main effects plot for DCF. (e) The significant effects for surface resistance of electrodes, and (f) interaction plot for surface resistance of electrodes.

5.4 Conclusion

When using embroidery electrodes to monitor ECG signal, the area size, filling density and layers have significant effects on the skin-electrodes contact impedance at 1 Hz frequency.

After compare with different filling pattern embroidered electrodes, the electrodes filling with parallel 304 lock stitch and cross stitch in size 2cm×4cm could reach the lower impedance that could provide good quality of ECG signal.

The prototype band for ECG monitoring in static situation was developed with combined embroidery technique, which using TPU insulated silver conductive thread as connection lines. The electrodes and the connection lines were embroidered in one step and the snap button was employed to connect the wireless BIOPAC MP160 system to record 200 seconds ECG signals. The developed embroidered electrodes could detect ECG signal and the quality was equal to the clinical Ag/AgCl electrodes. The peak-to-peak ECG signal amplitude analysis in different pressure level revealed that the electrodes with 304 stitch embroidery could display high quality ECG wave form in lower pressure level.

This work investigated different embroidery design parameters influence on the contact impedance of electrodes and compare ECG monitoring quality with different filling pattern under various applied pressure level. The design combined different embroidery techniques into one step manufacture process, and could be used in the automatic manufacture for the smart wearable products. It is the important fundamental study for the tailored and low-cost e-textiles fabrication method as well.

Supporting information

Table S5-1. Detailed full-factorial experimental design

Sample No.	Area Size	Fill Layer	Fill Density (mm)	Stitch Type
1	20×20	1	1	301
2	20×40	1	1	301
3	20×20	2	1	301
4	20×40	2	1	301
5	20×20	1	2	301
6	20×40	1	2	301
7	20×20	2	2	301
8	20×40	2	2	301
9	20×20	1	1	304
10	20×40	1	1	304
11	20×20	2	1	304
12	20×40	2	1	304
13	20×20	1	2	304
14	20×40	1	2	304
15	20×20	2	2	304
16	20×40	2	2	304

Table S5-2. Summary of ANOVA response for skin-electrode impedance at 1 Hz

Source	DF	Adj SS	Adj MS	F-Value	P-Value
Model	10	6.13366E+13	6.13366E+12	31.05	0.000
Linear	4	4.71503E+13	1.17876E+13	59.68	0.000
A	1	1.24873E+13	1.24873E+13	63.22	<u>0.000</u>
B	1	4.53236E+12	4.53236E+12	22.95	<u>0.000</u>
C	1	2.90845E+13	2.90845E+13	147.25	<u>0.000</u>
D	1	1.04613E+12	1.04613E+12	5.30	<u>0.027</u>
2-Way Interactions	6	1.41863E+13	2.36438E+12	11.97	0.000

A*B	1	12023154653	12023154653	0.06	0.806
A*C	1	5.25407E+12	5.25407E+12	26.60	<u>0.000</u>
A*D	1	4.74317E+11	4.74317E+11	2.40	0.130
B*C	1	2.96869E+11	2.96869E+11	1.50	0.228
B*D	1	3.59845E+11	3.59845E+11	1.82	0.185
C*D	1	7.78915E+12	7.78915E+12	39.43	<u>0.000</u>
Total	47	6.86449E+13			

Table S5-3. Summary of ANOVA response for CC value of ECG monitoring

Source	DF	Adj SS	Adj MS	F-Value	P-Value
Model	13	0.379378	0.029183	27.24	0.000
Blocks	2	0.279221	0.139610	130.30	0.000
Linear	5	0.095913	0.019183	17.90	0.000
Wearing pressure	2	0.046855	0.023427	21.86	<u>0.000</u>
Electrodes pattern	3	0.049058	0.016353	15.26	<u>0.000</u>
2-Way Interactions	6	0.004244	0.000707	0.66	0.682
A*B	6	0.004244	0.000707	0.66	0.682
Error	22	0.023573	0.001071		
Total	35	0.402950			

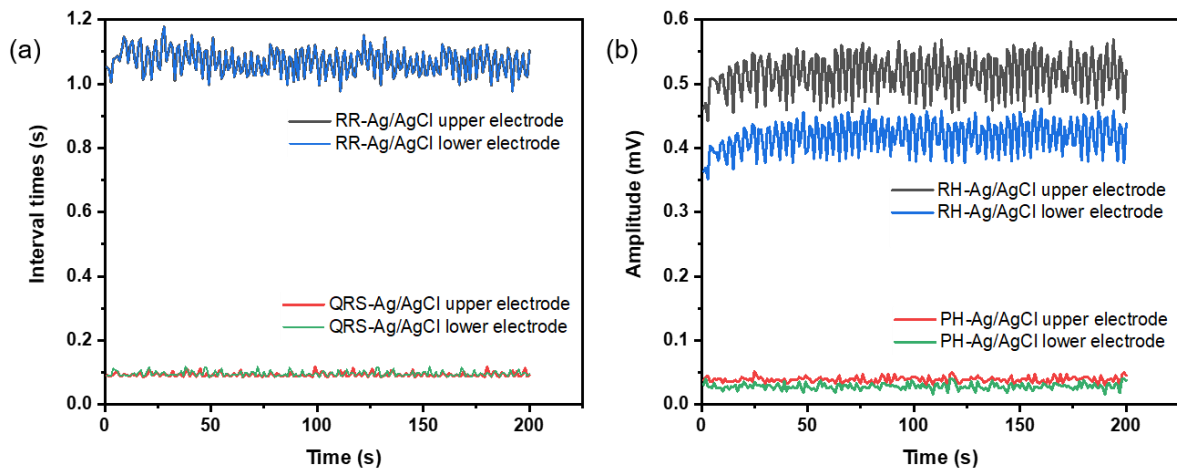


Figure S5-1. Comparison of the interval times and amplitudes of ECG morphology peaks measured by Ag/AgCl electrodes in upper and lower body position during 200 seconds measurement.

Table S5-4. Summary of ANOVA response for static coefficient of friction

Source	DF	Adj SS	Adj MS	F-Value	P-Value
Model	11	1.63846	0.148951	33.24	0.000
Linear	5	1.57881	0.315762	70.47	0.000
Applied Force	2	1.36114	0.680570	151.88	0.000
Electrodes Type	3	0.21767	0.072557	16.19	0.000
2-Way Interaction	6	0.05965	0.009941	2.22	0.076
Applied Force*Electrodes Type	6	0.05965	0.009941	2.22	0.076
Error	24	0.10754	0.004481		
Total	35	1.74600			

Table S5-5. Summary of ANOVA response for dynamic coefficient of friction

Source	DF	Adj SS	Adj MS	F-Value	P-Value
Model	11	0.77954	0.070868	20.29	0.000
Linear	5	0.74542	0.149084	42.68	0.000
Applied Force	2	0.67071	0.335353	96.01	0.000
Electrodes Type	3	0.07471	0.024905	7.13	0.001

2-Way Interactions	6	0.03412	0.005687	1.63	0.183
Applied Force*Electrodes Type	6	0.03412	0.005687	1.63	0.183
Error	24	0.08383	0.003493		
Total	35	0.86338			

Table S5-6. Summary of ANOVA response for dynamic coefficient of friction

Source	DF	Adj SS	Adj MS	F-Value	P-Value
Model	11	38.9789	3.5435	93.11	0.000
Linear	5	35.8250	7.1650	188.28	0.000
Applied Force	2	1.9106	0.9553	25.10	0.000
Electrodes Type	3	33.9144	11.3048	297.06	0.000
2-Way Interactions	6	3.1539	0.5256	13.81	0.000
Applied Force*Electrodes Type	6	3.1539	0.5256	13.81	0.000
Error	24	0.9133	0.0381		
Total	35	39.8922			

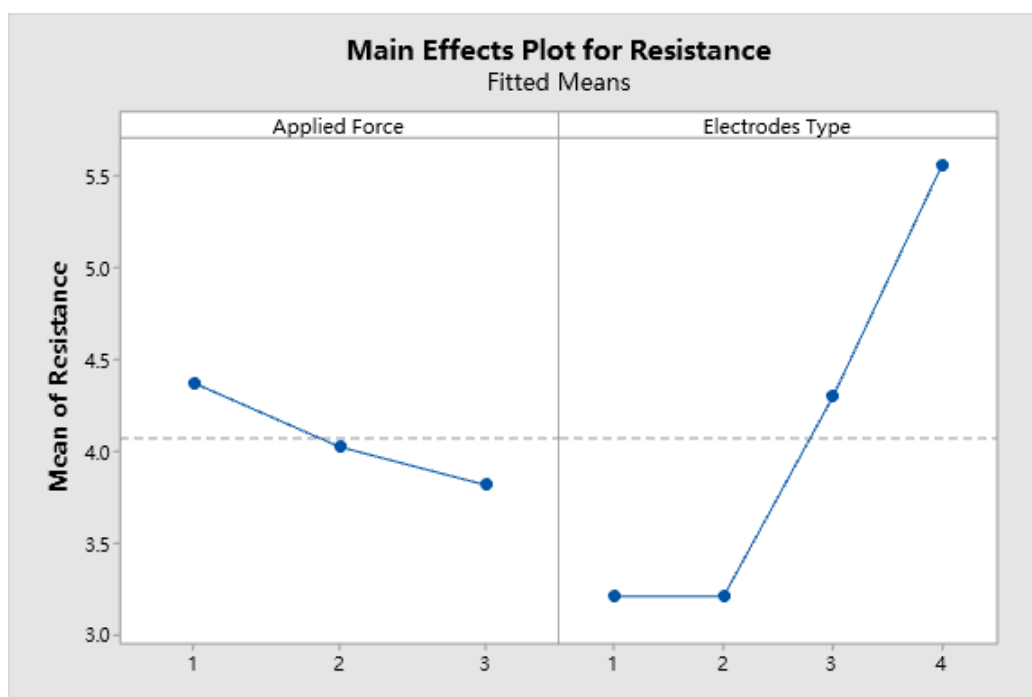


Figure S5-2. Main effects plot for resistance of four types of electrodes under applied force 0.5 kPa, 1.5 kPa and 2.5 kPa.

CHAPTER 6. EMBROIDERED STRAIN SENSOR DESIGN WITH CONDUCTIVE YARNS AND EVALUATION FOR RESPIRATORY MONITORING

This chapter focuses on completing objective 4 by collaborating with external research partners.

Authors: Yan Zheng, Zekun Liu, Lu Jin, Jing Qi, Zhangchi Liu, and Yi Li

Targeted journal: Smart Materials and Structures, submitted

Statement of own contributions: Main research idea, the embroidered strain sensor design and fabrication, breath rate monitoring performance evaluation, subject tests protocol and implement; data analysis and modelling; preparation of prototype, tables, figures, and manuscript.

Statement of co-author contributions: Zekun Liu supports in electromechanical characterization measurement. Lu Jin, Jing Qi and Zhangchi Liu support in carrying out breath rate measurement experiment. Yi Li initiated project idea and provided supervision and guidance in research methodology, the design of experiment, data analysis and interpretation, and paper revision.

6.1 Introduction

Respiration signals are vital in health care for chronic respiratory disease, such as asthma and chronic obstructive pulmonary disease. The significant progress of smart e-textiles and wearable electronics for respiration measurements has been demonstrated, including strain sensors [37, 38, 45, 176, 177], pressure sensors [178, 179], inductive sensors [180–182], air flow sensors [183, 184], and bioelectronic devices [185]. To assess respiratory health within a clinical setting, continuous monitors are needed to track a patient's respiration so that any measured changes in breathing patterns can be used as markers for intervention or as data for diagnoses [186]. Textile-based strain sensors embedded in smart clothing or wearables could

continuously monitor respiratory state by detecting changes of chest or abdominal circumference during inhale and exhale under normal daily environments for long term use.

High performance textile based strain sensors can be made by directly knitting with conductive yarns [37, 38], or sewing or embroidery conductive yarns on the elastic fabrics[44, 45, 104]. But the stretchable scopes of sensors are limited by the elastic performance of fabrics or the sewing patterns of conductive yarns. Coating conductive components onto fabrics [36], carbonized fabric [43], or electrostatic spinning nanoparticle [176] with polydimethylsiloxane (PDMS) or natural rubber latex substrates were used to develop high performance strain sensors. However, they are not able to be assembled with clothing directly, which cannot conveniently used in daily life. Embroidery is a versatile technique not only can combine various types of yarns, but also to develop diversiform patterns for strain sensors with desired stretchability. There are technique challenges to improve stretch performance and sensitivity of strain sensors, and also can be directly sewn into clothing.

The main criteria to evaluation performance of wearable strain sensors is gauge factor (GF), which is the changes of electrical characteristics according to the strain of sensors [34]. The GF can reach greater than 85,000 with high mechanical resilience [187]. But for respiration measurement, the quick response strain sensor needs to be activated under lower external mechanical force. Therefore, the strain sensor should show great balance with high GF and low mechanical resilience. Placement of the sensors for respiration measurement needs to be based on physiological markers and ensure the placement is correct and consistent. To ensure the durability of sensors during stretching and achieve a high sensitivity for respiration monitoring, the structures of sensors and methods to wear still need to be studied.

This paper aims to study the performance of hybrid embroidered strain sensors (HESS) fabricated with three design parameters setting at three levels. Using tailored fibre placement (TFP) embroidery, the double polyamide fibre covered elastane yarns was fixed onto a water-dissolvable substrate to provide stretchability of HESS. Nonconductive polyester threads and

silver coated conductive yarns were embroidered by lock stitch techniques to form the frame and sensing sections of HESS. To our best knowledge, this is the first tailored strain sensor fabricated through such a versatile, convenient, scalable, and cost-effective method. The HESS is then tested to investigate the influence of width of conductive area, filling density of conductive yarns and elastane yarns on the sensitivity and stretchability. The electromechanical performance of HESS with good trade-off between gauge factor and elasticity coefficient was tested. The working mechanism of HESS was further investigated. Moreover, the HESS with highly GF to detect respiration signals of human was demonstrated. Taking advantage of the high porosity structure of HESS, highly precious and versatile design of embroidery techniques, strain sensors can be customised in smart clothing with highly wearing comfort.

6.2 Experimental work

6.2.1 Materials

The silver coated polyamide thread, coded as HC40, purchased from MADEIRA (Madeira Garnfabrik GmbH, Freiburg, Germany) was used as needle thread and bobbin thread for conductive area of HESS. The thread is conductive (with resistance at $270 \pm 11.2 \Omega/\text{m}$) and has diameter of $283.4 \pm 35.3 \mu\text{m}$ that fit for hybrid embroidery with non-conductive threads. The regular non-conductive polyester thread was used to embroider non-conductive part of HESS which is needed for sewing. The type of elastomeric yarn affected the sensing properties of textile-based strain sensors, and stronger elastomeric yarns produced knitted sensors with higher gauge factor values [55]. An elastomeric yarn, 800 dtex core LYCRA[®] with double polyamide 66 covering yarns (D 963B from WYKES), was used to provide stretchable frame for the sensor. A water-soluble polyvinylalcohol (PVA) nonwoven fabric was used to embroider the strain sensor. The same PVA threads was use to fix the elastomeric yarns by TFP method.

6.2.2 Design and fabrication of embroidered strain sensor

Since the embroidery techniques are versatile, flexible and highly precious in e-textiles

fabrication, the strain sensor proposed here were fabricated with combination of TFP and lock-stitch embroidery techniques. The embroidery machine, JCZA 0109-550 (ZSK Stickmaschinen GmbH Germany) was used. Figure 6-1(a) shows the elastane yarns were fixed by PVA threads onto the PVA substrate by TFP embroidery. Then the machine can change to lock stitch embroidery automatically following the design in EPC win software, which the polyester threads then started to be embroidered exactly cross over the fixed elastane yarns, as shown in Figure 6-1(b). After that, Figure 6-1(c) shows the conductive yarns, HC40, then started to be embroidered over the elastane yarns in desired area where interlacing with polyester thread passing boundary. Figure 6-1(d) shows the embroidered strain sensor was taken down from the hooks, the sample would rebound because the elasticity of elastane yarns. The PVA fabric and threads dissolved after the sample was gently washed in deionized water, the embroidered sensor could get the stretchability and the conductive yarns were closely attached and separated with applied force, as shown in Figure 6-1(e) and (f). The high elasticity of elastane yarns, and the silver coated conductive yarns give the sensing ability of stretchable embroidered samples.

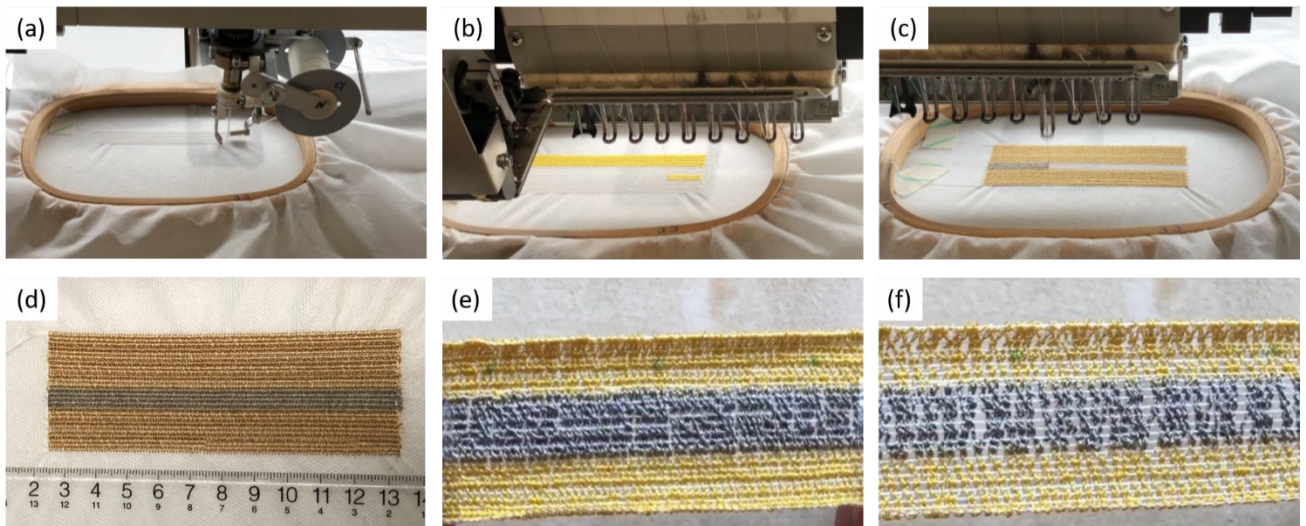


Figure 6-1. Process of the strain sensor embroidery combined with two techniques. (a) Fix of elastane yarns by tailored place PVA threads on PVA substrates. (b) Polyester threads lock-stitch embroidery to form substrate of the strain sensor. (c) HC 40 conductive yarns embroidery to develop conductive area in the strain sensor. (d) The surface image of the embroidered strain sensor before washing. After dissolving PVA threads and nonwoven fabric, the strain sensor was (e) porous and (f) stretchable.

From the structure character of proposed strain sensor, the density of conductive yarns determined the sensor's electrical conductivity during stretching. The density of elastane yarns could affect the force to pull the sensor. Because this sensor was designed speciality for respiration monitoring, the sensitivity and working range of the sensor was important. In this study, the impact of design parameters, including width of conductive area (WCA), filling density of conductive yarns (DCY) and density of elastane threads (DLT) were investigated. Box-Behnken design method [188] was used to set up experimental plan in Minitab 19 software. Table 6-1 presents the manufacturing parameters for the embroidered strain sensors. Detailed experiment plan can be found in Supporting Table S6-1. Three samples of each experimental design were fabricated.

Table 6-1. Factors and levels used in strain sensors design

Factors Levels	A-WCA (mm)	B-DCY (mm)	C-DLT (mm)
Low (-1)	5	0.3	1.5
Centre (0)	10	0.5	2
High (+1)	15	0.7	2.5

6.2.3 Electromechanical characterization and response optimization of embroidered strain sensors

Mechanical tests and electrical properties of HESS were simultaneously acquired using an Instron universal testing system (Model 3344, Instron, USA) and a multimeter (Keithley 2000, Keithley instrument, USA) respectively. There were two conductive tapes as electrodes at both ends of the sensor to connect with the multimeter for signal collection, and the gauge length was 30 mm. All tests were carried out under room temperature (20°C) and relative humidity of 65% RH.

Strain sensing performance of HESS has been characterised by parameters including stretchability, gauge factors (the sensitivity to strain), linearity, hysteresis, response and recovery time, durability[49]. To evaluate the mechanical behaviour of stretchability, the embroidered strain sensors were stretched to 200% at a speed of 1 mm/s. The resistance of

strain sensors was measured at the same time. Slope of the relative change of the resistance versus applied strain was used to calculate GF (given by $GF_s = (\Delta R/R_0)/\varepsilon$, where R is resistance and ε is strain) and linearity of strain sensors. Elasticity coefficient (k), given by $k = F/\varepsilon$, was used to present the external force needed to active the strain sensor. The maximum working strain was the response strain scope of the maximum GF. The time in this strain scope was used to present response time. To detect respiratory signals, which was measurements of body surface strain changes according to inhale and exhale, a balance between sensitivity and EC is required for strain sensors. The response optimization was investigated by the balance of high sensitivity with low EC. Due to the viscoelasticity of the fibre assembly itself, the yarn-based strain sensors inevitably exhibit relatively high electro-mechanical hysteresis in response to external strain stimuli, which leads to low accuracy, poor repeatability and non-stability of flexible sensors [189]. After calculate the parameters for the optimized HESS, the tensile hysteresis of this sensor was measured under strain of 5%, 10%, 15%, 20% and 25% respectively at a speed of 3 mm/s to investigate proper working range with lower electro-mechanical hysteresis. The durability of this optimised sensor was measured 1000 cycles at 0.5 Hz with 30% strain at a speed of 9 mm/s.

6.2.4 Respiration measurement test

The optimised HESS with a balance of GF and EC was chosen to evaluate its respiratory monitoring performance by a comparative experiment with a commercial air bag pressure gauge (AMI 9002 made in Japan). As reference sensor to measure respiration, the air bag sensor of pressure gauge was placed above the rib in the left side of the body. The proposed HESS was sewn onto a customised elastic band, which was adjusted according to body size of participants to provide stable supporting. The sensor was placed on the right side of the body and connected to the multimeter to record the resistance changes of HESS during measurement. Five participants were recruited based on the specification in ASTM F2668-2016 (Standard Practice for Determining the Physiological Responses of the Wearer to Protective Clothing Ensembles). Table 6-2 shows three respiration patterns for the real time respiration

measurement. Each participant was measured at sitting position with nature normal breathing for 300 seconds. The resistance and pressure changes during breathing was measured simultaneously and repeated three times. After that, participants were asked to breathe deeply at slow rate of 12 bpm for 150 seconds. For shallow breathing, participants were asked to breath at high rate of 30 bpm for 150 seconds. A metronome was used in time to instruct purpose breathe. The prototype band was adjusted to maintain wearing stable of band with wearing pressure at the range of 1 to 1.5 kPa according the comfort feeling of participants. The personal information of participants was listed in Supporting Table S6-2. This experimental protocol was approved by the ethics committee of University of Manchester (2019-5112-12512). Prior informed consent form was obtained from all participants.

Table 6-2. Patterns of respiration of this study

Respiration patterns	Descriptions
Normal breathing	Normal breathing in daily life
Deep breathing (slow rate)	Instruct to breathe deeply at 12 bpm
Shallow breathing (fast rate)	Instruct to breathe shallow at 30 bpm

The measured respiratory signal may include respiratory-independent noise as a motion artefact. In this study, a high-pass filter with a 0.005 Hz cut off was used to remove the dynamic noise, and then the respiratory component was filtered using a bandpass frequency at 0.05-1 Hz. The fast Fourier transformation (FFT) was used to calculate the respiratory rate in natural peace breath measurement.

6.3 Results and discussion

6.3.1 Effect of design parameters on mechanical and electrical performance of sensors

The electromechanical properties of HESS samples were measured and sensing performance was evaluated by resistance-strain and tension-strain curves of samples. The typical electromechanical curves of HESS were illustrated in Supporting Figure S6-1. The significant influence of WCA, DCY, and DLT on gauge factor was shown in Figure 6-2(a). The main effects plot for GF in Figure 6-2(b) indicates that the sensor designed with increased conductive

area, 0.3 mm tightly conductive yarns embroidering could gain higher gauge factors, which supplied sensitivity of strain sensors. For density of elastane threads impacts, there was a small increase of gauge factor from 1.5 mm to 2 mm distance embroidery, then the GF trend declined significantly. Figure 6-2(c) shows the elasticity coefficient has significant impact with factor C, which the increased distance of elastane threads embroidery in substrate of sensors slow down the elasticity coefficient, as shown in Figure 6-2(d). The analysis of design parameters impact on maximum strain of sensors, and response time can be found in Figure S6-2. The Factor B has significant effects on working strain and response time of sensors. The 0.5 mm spacing embroidery of conductive yarns has the maximum working strain and response time for sensors. Summary of ANOVA response analysis for these response index can be found in Supporting from Table S6-3 to Table S6-6. Figure 6-2(e) shows gauge factor, elasticity coefficient, and linearity of each sensor samples. Sample 6 has the highest GF, it has the highest EC as well. When it was applied for respiratory signal monitoring, it may hard to catch the strain changes of body during inhale and exhale since the higher EC needs more force to active sensors. Each sensor sample also exhibits high linearity, which was 0.96 ± 0.038 at average. Figure 6-2(f) shows he distribution of maximum working strain and response time of samples were similar, and they were similar to the GF and EC as well. Performances of these embroidered strain sensors were reliable and design parameters of sensors can be tailored for various application scenarios through versatile embroidery techniques.

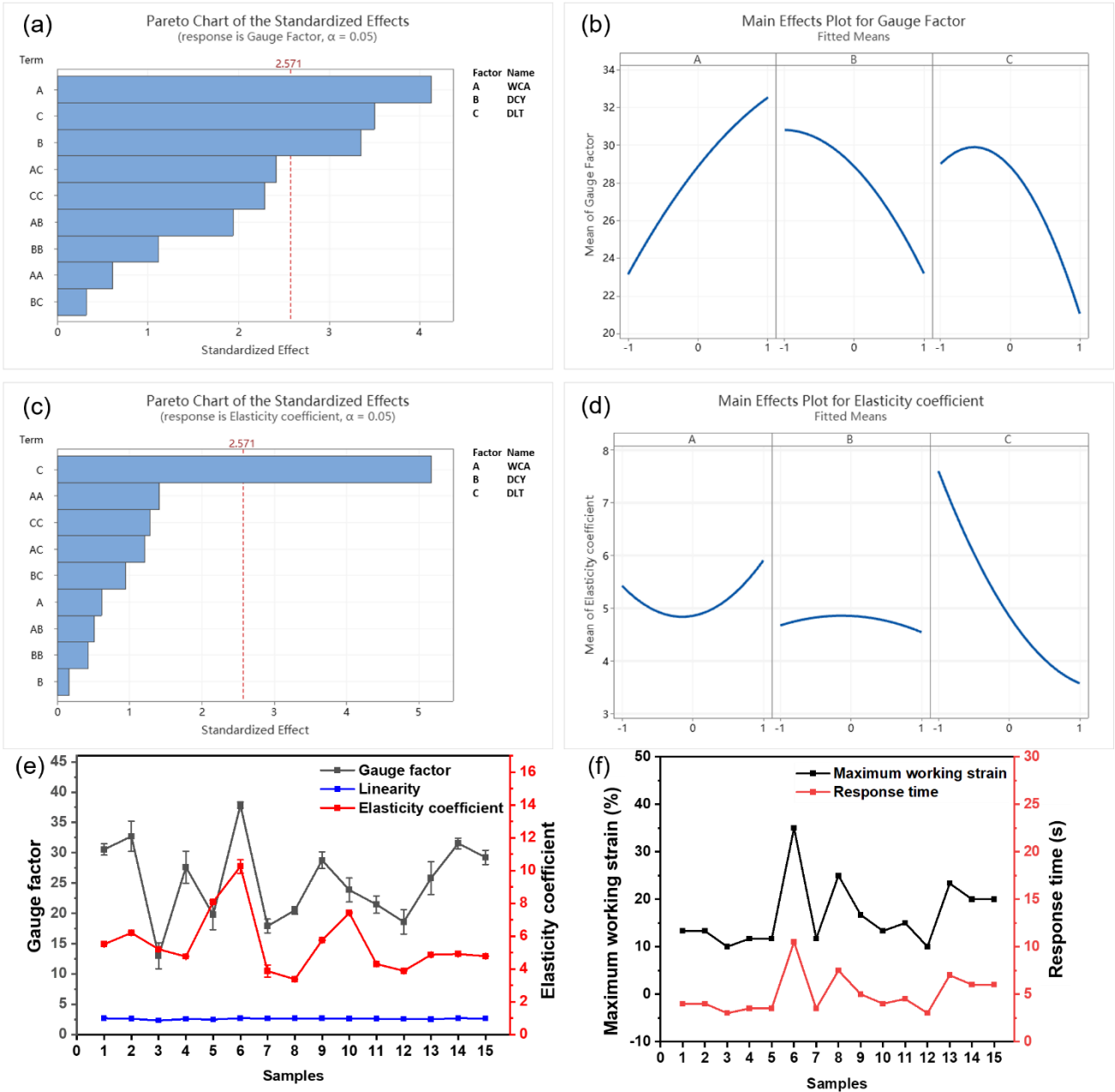


Figure 6-2. Factorial analysis of the sensor's design effects on GF and EC. (a) Significant effects for GF. (b) Main effects plot of factors impacts on GF. (c) Significant impact on EC. (d) Main effects plot of factor C on EC. (e) Mean and SD of GF, EC and linearity of each sensor samples. (f) Mean of maximum working strain, response time of each sensor samples.

In order to detect respiratory signals by measuring strain changes of chest during inhale and exhale, the strain sensor should have the highest GF with the lowest EC. Based on the regression models in response surface design analyse, response optimization analysis was performed in Minitab 19 software with the combination goal of maximized GF and minimized

EC, and the result was shown in Table 6-3. Multiple variables analysis of response optimization prediction can be found in Supporting Figure S6-3.

Table 6-3. Solution and multiple response prediction for requested optimization

Solution			Response of GF		Response of EC	
A	B	C	Fit	95% CI	Fit	95% CI
-0.01	-1	0.01	30.745	(25.55, 35.94)	4.652	(2.873, 6.431)

Ten samples of HESS were embroidered with advised design parameters, which were 10 mm width of conductive area, conductive yarns filling with 0.3 mm, and 2 mm distance between elastane thread placement. The average GF and EC were 29.37 ± 2.25 and 4.04 ± 0.79 respectively, which were in the 95% CI of predictions. This embroidered strain sensor was used to evaluate electromechanical performance and carry out respiration measurement test.

6.3.2 Electromechanical performance and working mechanism of the embroidered strain sensor

The relative resistance change ($\Delta R/R_0$) of HESS plotted against the applied strain is shown in Figure 6-3(a). The $\Delta R/R_0$ increased linearly at first and then displayed an exponential dependency upon applied external strain. Ten samples of HESS presents the maximum GF of 34.2 ($0 < \varepsilon < 40\%$), and minimum GF of 23.4 ($0 < \varepsilon < 25\%$). The HESS in the tensile range shows excellent linearity that the R^2 was 0.992 and 0.988 respectively. Figure 6-3(b) shows the required external force to stretch HESS. The EC of HESS samples were in 3.54 to 4.12, which is highly flexible and can be easily stretched. Since this HESS was targeted for respiratory measurement, this elasticity performance was proper to measure the changes of chest circumference during breathing.

The elastic recovery and mechanical hysteresis play a fundamental role in sensor reproducibility and reliability [190]. Taking advantage mechanical property of elastane fibres, the HESS shows great elastic recovery and little hysteresis, as displayed in Supporting Figure S6-3. The relative resistance change of HESS was measured when it was stretched to 5%, and

were then released to the original length at a strain rate of 1 mm/s. The HESS was subsequently stretched under the stepwise elongations of 10%, 15%, 20% and 25%. Figure 6-3(c) shows the stretching and releasing paths of curves were identically at 5%, 10%, 15% and 20% elongation. It is noted that the path of curves was different at 25% elongation. This is due to the separation and deformations of conductive yarns stitches during stretching. At the small range of stretching, the stitches of conductive yarns were stable and the contacts of adjacent conductive lines separated and return back to attach during relaxation. Thus, the stitches of conductive yarns cross over elastane threads was deformed by the external force and the polyester stitches in frame sections.

Most of durability evaluation for strain sensors was at low level strain, such as 3% in [40], and 10% in [45]. For really daily life, the strain of e-textiles wearable was far more than 10% strain. In this study, 30%, which was 75% of the working scope was used to test the durability of HESS at a strain rate of 9 mm/s. The long-time stability under 30% strain over 1000 cycles were shown in Figure 6-3(d). Even though the resistance response to the stretch-releasing cycles with a stepwise increase was noted, the HESS exhibited clear and precise relative resistance change according to applied strain. This indicates the reliability of HESS in sensing changes of strain.

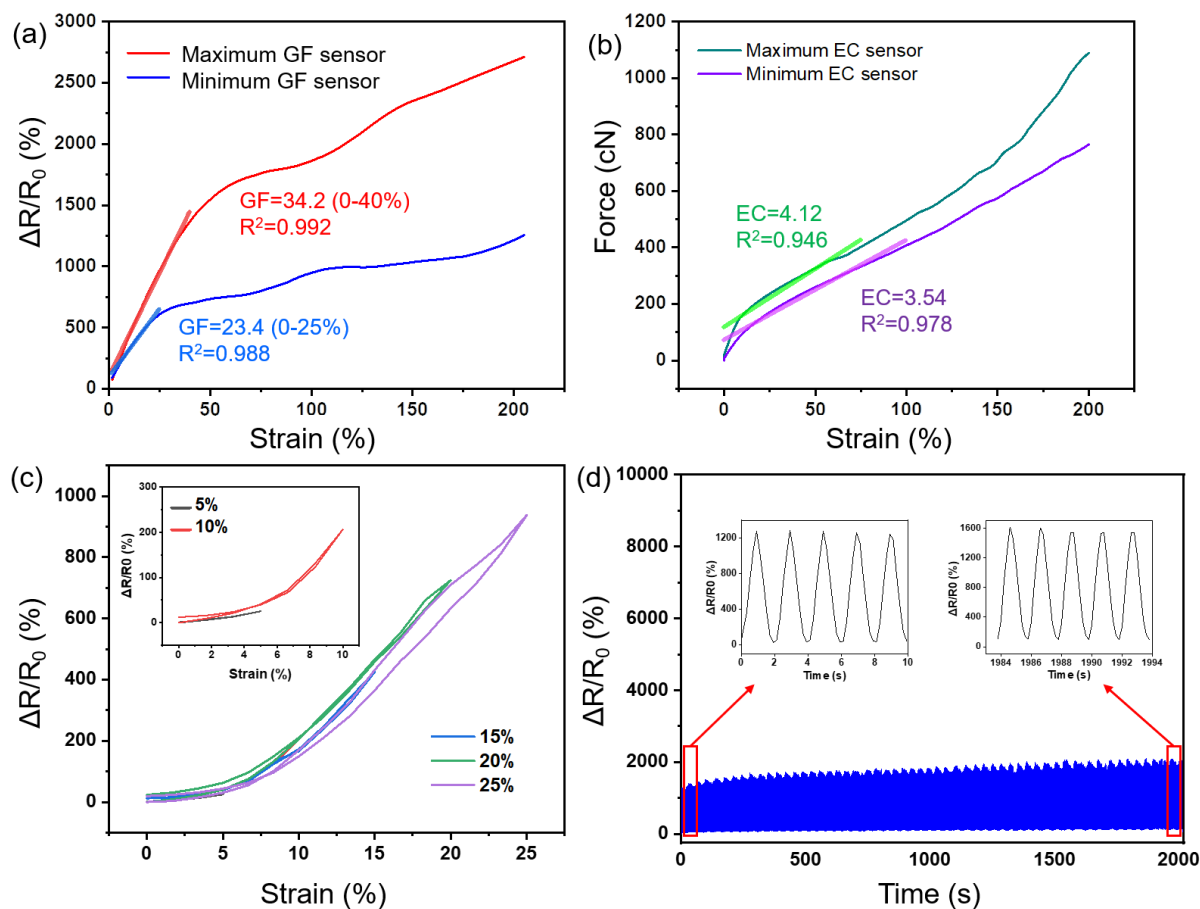


Figure 6-3. Electro-mechanical behaviour of the HESS. (a) The relationships between relative resistance change ($\Delta R/R_0$) and applied strain for the strain sensor. (b) Typical force-strain curves of sensors with maximum and minimum EC value. (c) Electro-mechanical hysteresis for one stretching-releasing cycle: the inset is the amplified cycle at 5% and 10%. (d) 1000 stretching-releasing cycles from 0 to 30%, with insets above being signals of the initial and last five cycles.

To interpret the electromechanical properties of the HESS, the structure of HESS and changes of structures during the stretching-releasing was presented in Figure 6-4. The HESS was embroidered with polyester thread and conductive yarns HC 40 by lock stitch techniques, as shown in Figure 6-4(a), W is the width of designed conductive section. Figure 6-4(b) shows the HC 40 was stitched cross over the elastane thread and form conductive meander tracks according width in design. Figure 6-4(c) illustrated the sensing mechanism of HESS. When the PVA substrate was dissolved, the pre-strain in the HESS is released and a balance between the

strain energy stored in the substrates and the deformation energy in the embroidery was established. After HESS was dry, adjacent tracks came into electrical contact, electrically shorting the meander, and the resistance measured along its length was reduced. Applying external force to HESS causes the contacting tracks to separate, and reducing the contact area. As a result, the measured resistance of HESS increased until saturation, where there was no contact area between meander tracks.

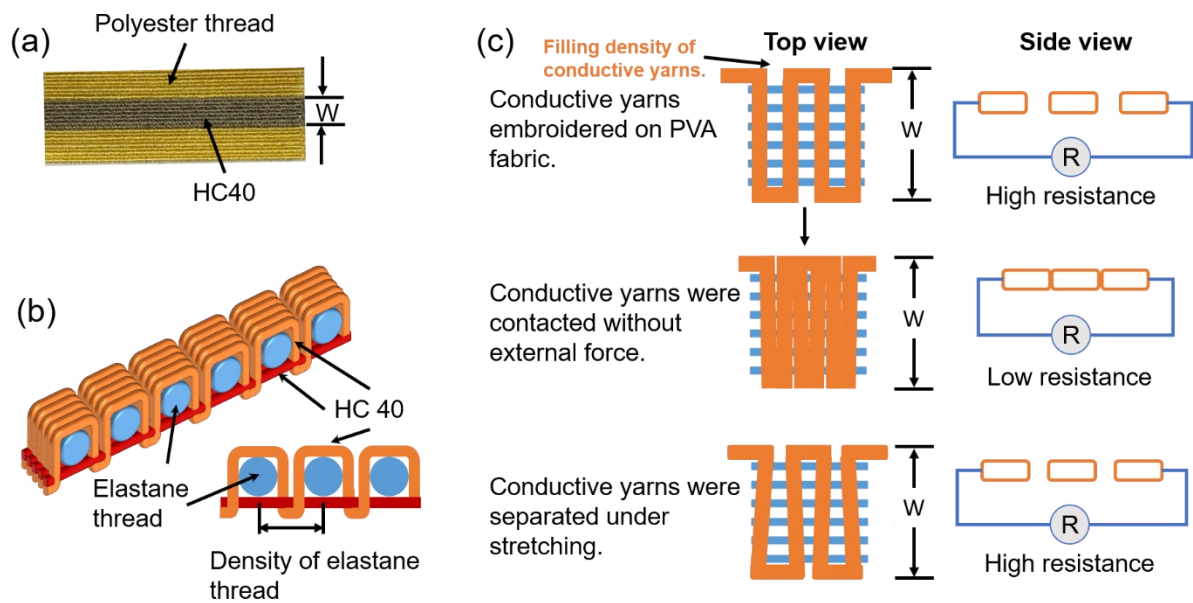


Figure 6-4. Image and schematic diagram of HESS. (a) Face image of HESS. (b) The conductive section's illustration with conductive tracks contacted in proposed HESS. (c) Operating principle of conductive section in HESS. Conductive yarns were shown in orange, and the blue lines represented elastane threads.

Holm's contact theory [191] was used to calculate contact resistance by the following equation:

$$R_c = \frac{\rho}{2} \sqrt{\frac{\pi \cdot H}{nP}} \quad (6 - 1)$$

where:

R_c = contact resistance;

ρ = electrical resistivity;

H = material hardness;

n = number of contact points;

P = contact pressure.

The electrical resistivity and material hardness are constant for a given material but the number of contact points and the contact pressure are variable depending on the strain sensor design. Higher contact pressure and the increase of contact points between conductive tracks could reduce the contact resistance. In the design of proposed HESS, contact pressure between conductive tracks was provided by the elastane thread used in TFP. The number of contact points between conductive tracks depends on the width design of conductive section, the density of filling conductive stitches, and the level of applied force to stretch the HESS. The conductive mechanism of HESS were foundations of design parameters for this type of strain sensors. The resistance range, and the sensitivity of HESS can be tailored according to requirement of application.

6.3.3 Respiration measurement test

Figure 6-5 shows three-pattern representative respiratory signals measured with HESS and pressure sensor. The HESS was able to express resistance changes with breathing but the performance in breathing measurement was varied with respiration patterns. The resistance changes of HESS were clear and regular according to the normal and deeply slow breathing. As shown in Figure 6-5(a) and (b), there was no significant baseline drift or artifact noise in the measurements. The mechanism of HESS was to measure the circumference changes of chest in breathing. The peak of resistance changes represents the inhalation (sensor stretching), and valleys represent the exhalation (sensor relaxing). Comparing with normal breathing, the deep breathing is done with expansion of chest to inhale more air into the lungs. This was reflected in the resistance changes of HESS increased up to 80% in deep breathing. For shallow

and fast rate respiration measurement, Figure 6-5(c) shows the inhalation of minimal breath mainly into the chest, and the changed of chest area gently. The resistance changes of HESS in shallow breathing were similar to the normal breathing, but the waveform of HESS was fluttered and this could be the motion artifact influence from chest in fast rate respiration. The referred pressure sensor was more sensitive to this motion artifact in breathing measurement. The artifact noise can be noticed in normal and deep breathing, and it was seriously in shallow and fast pace breathing. The result of shallow breathing measurement of HESS is similar to the previous study [45], since intercostal muscles in chest area were more likely to be affected by irregular noise generated during shallow respiration.

Figure 6-5(d) shows the frequency spectrum of normal breathing signal measured in normal breathing with HESS and pressure sensor have similar distributions. The calculated respiratory rates of participants were statistically studied by two-sample t-Test. The results shown in Figure 6-5(e) proved the respiratory rate measured by HESS in normal breathing was the same with the measurement from pressure sensor, and the p-value can reach as high as 0.99.

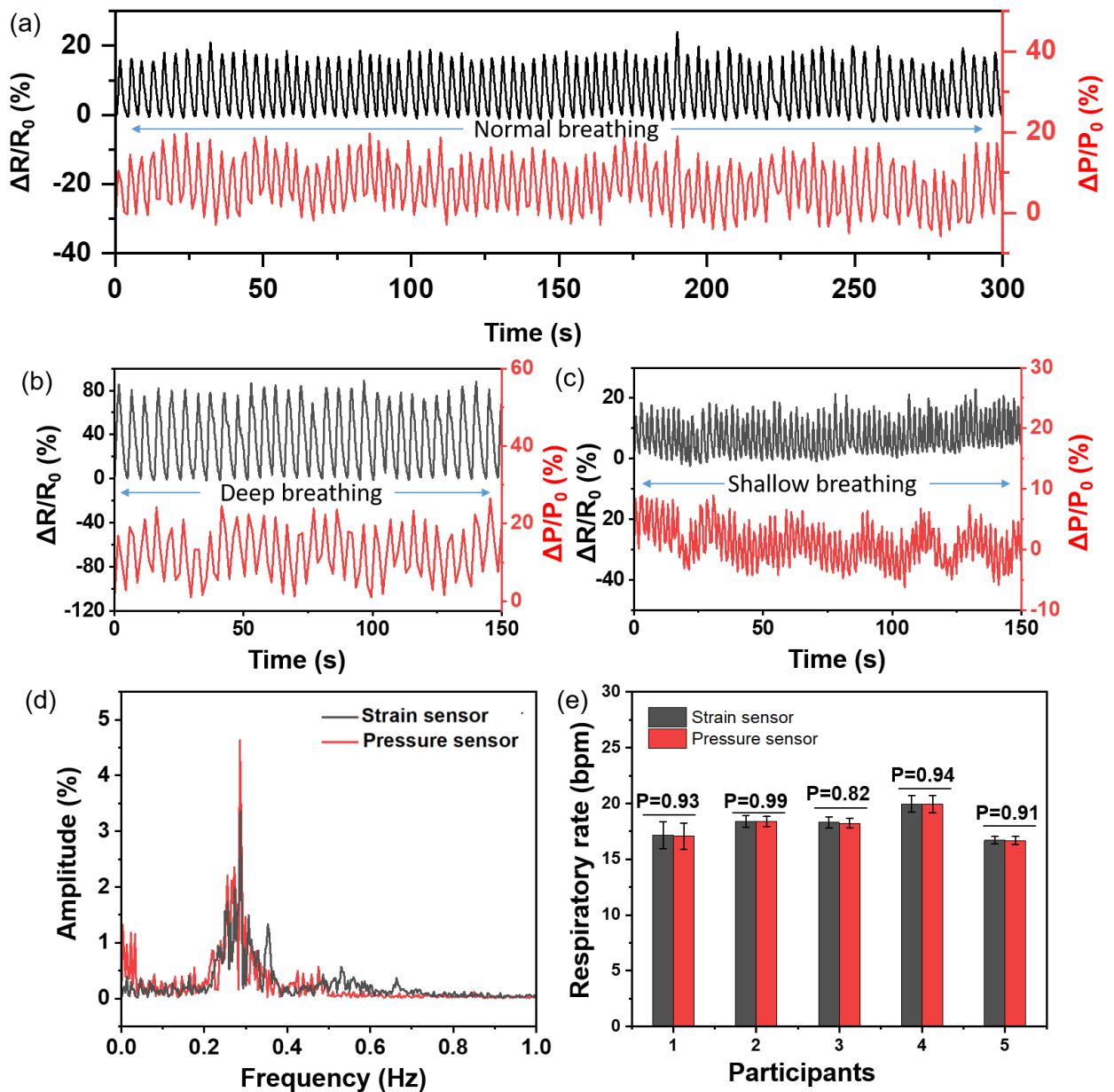


Figure 6-5. Respiratory signal from HESS (colour in read) and pressure sensor (colour in black). (a) Normal breathing, (b) deep and slow breathing at 12 bpm, and (c) shallow and fast breathing at 30 bpm. (d) Frequency spectrum of respiration of normal pattern breathing. (e) Comparison of respiratory rate measured from two types of sensors.

6.4 Conclusion

In this research, a novel textile-based strain sensor was developed to monitor human respiration. The HESS was fabricated with elastane thread and conductive yarns using combination of two

embroidery techniques. Unlike other strain sensors relying on stretch property from silica gel, such as PDMS, this HESS can be sewn onto clothing directly by delicate combination design of elastane thread, polyester thread and conductive threads. Since the working mechanism of the sensor was based on the separation of the conductive contact points in response to applied strain, the effects of design parameters on electrical performance of sensors were investigated. After that, the HESS with optimised design variables was fabricated to assess the electromechanical performance and durability. The application of real time respiration monitoring was performed under three breathing patterns. The HESS presents highly uniform signal patterns in normal breathing and deep breathing at slow rate. It was able to use in shallow and fast breathing conditions, but the signals were drifted due to motion artifacts. Future work will to analyse the wearing pressure impact, and develop the smart wearables with a system to wirelessly monitor real time data.

Supporting information

Table S6-1. Detailed Box-Behnken experimental design

Sample No.	A-Width of conductive area (mm)	B-Filling density of conductive yarns (mm)	C-Density of elastane threads (mm)
1	5	0.3	2
2	15	0.3	2
3	5	0.7	2
4	15	0.7	2
5	5	0.5	1.5
6	15	0.5	1.5
7	5	0.5	2.5
8	15	0.5	2.5
9	10	0.3	1.5
10	10	0.7	1.5
11	10	0.3	2.5
12	10	0.7	2.5
13	10	0.5	2
14	10	0.5	2
15	10	0.5	2

Table S6-2 Information of participants for respiration measurement

Participant	Gender	Height (cm)	Weight (kg)	Age
1	Male	182	75	28
2	Male	178	72	20
3	Male	175	69	23
4	Male	173	63	27
5	Male	170	65	30

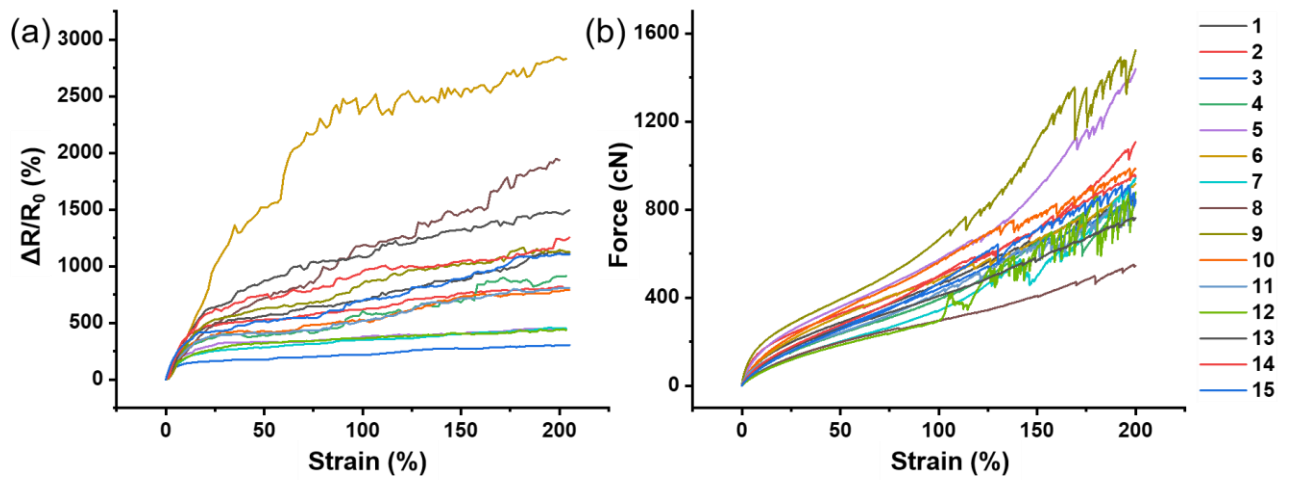


Figure S6-1. (a) Relationships between relative resistance change and applied strain for each typical strain sensor samples. (b) Tensile-strain curves of typical samples to present elasticity coefficient of sensors. The colour for each sample is the same in two figures.

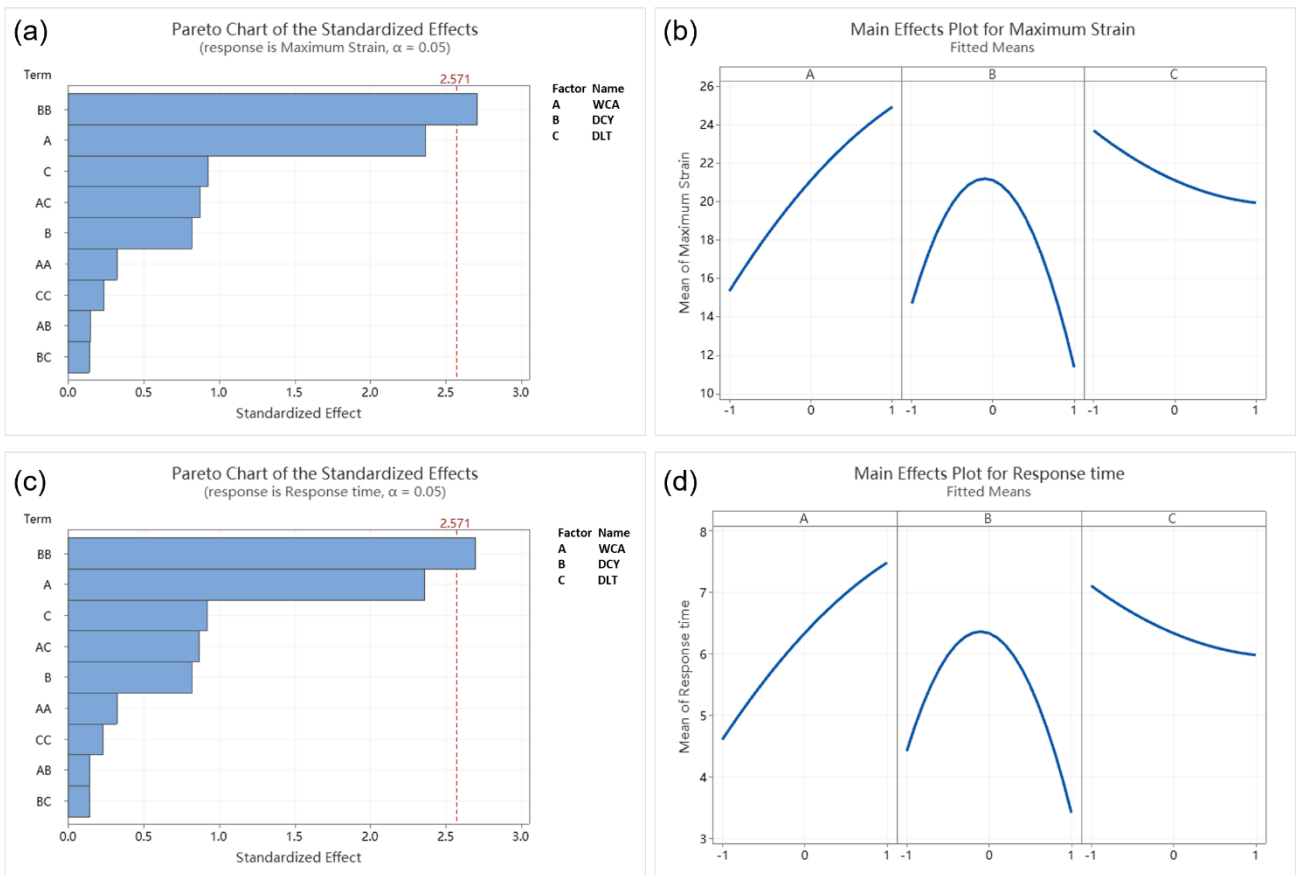


Figure S6-2. (a) Significance analysis of design parameters impact on maximum strain of sensors. (b) Main effects plot of factor B impact on maximum strain. (c) Significance analysis of design parameters impact on response time of sensors. (d) Main effects plot of factor B on response time.

Table S6-3. Summary of ANOVA response for gauge factor

Source	DF	Adj SS	Adj MS	F-Value	P-Value
Model	9	582.397	64.711	6.27	0.029
Linear	3	417.530	139.177	13.48	0.008
A	1	175.688	175.688	17.01	<u>0.009</u>
B	1	115.596	115.596	11.19	<u>0.020</u>
C	1	126.246	126.246	12.23	<u>0.017</u>
Square	3	64.714	21.571	2.09	0.220
A*A	1	3.895	3.895	0.38	0.566
B*B	1	12.803	12.803	1.24	0.316
C*C	1	54.150	54.150	5.24	0.071
2-Way	3	100.154	33.385	3.23	0.119
Interaction					
A*B	1	38.875	38.875	3.76	0.110
A*C	1	60.218	60.218	5.83	0.060
B*C	1	1.061	1.061	0.10	0.762
Error	5	51.631	10.326		
Lack-of-Fit	3	34.994	11.665	1.40	0.442
Pure Error	2	16.637	8.318		
Total	44	634.028			

Table S6-4. Summary of ANOVA response for elasticity coefficient

Source	DF	Adj SS	Adj MS	F-Value	P-Value
Model	9	40.5656	4.5073	3.72	0.081
Linear	3	32.8206	10.9402	9.04	0.018
A	1	0.4594	0.4594	0.38	0.565
B	1	0.0324	0.0324	0.03	0.876
C	1	32.3288	32.3288	26.72	<u>0.004</u>
Square	3	4.5574	1.5191	1.26	0.383
A*A	1	2.4175	2.4175	2.00	0.217
B*B	1	0.2204	0.2204	0.18	0.687
C*C	1	1.9834	1.9834	1.64	0.257
2-Way	3	3.1877	1.0626	0.88	0.512
Interaction					
A*B	1	0.3226	0.3226	0.27	0.628
A*C	1	1.7782	1.7782	1.47	0.280
B*C	1	1.0868	1.0868	0.90	0.387
Error	5	6.0507	1.2101		

Lack-of-Fit	3	6.0417	2.0139	448.60	0.002
Pure Error	2	0.0090	0.0045		
Total	44	46.6163			

Table S6-5. Summary of ANOVA response for maximum strain

Source	DF	Adj SS	Adj MS	F-Value	P-Value
Model	9	507.414	56.379	1.72	0.286
Linear	3	233.610	77.870	2.37	0.187
A	1	183.361	183.361	5.58	0.065
B	1	22.012	22.012	0.67	0.450
C	1	28.238	28.238	0.86	0.396
Square	3	247.417	82.472	2.51	0.173
A*A	1	3.483	3.483	0.11	0.758
B*B	1	240.089	240.089	7.31	<u>0.043</u>
C*C	1	1.868	1.868	0.06	0.821
2-Way	3	26.387	8.796	0.27	0.846
Interaction					
A*B	1	0.722	0.722	0.02	0.888
A*C	1	25.000	25.000	0.76	0.423
B*C	1	0.664	0.664	0.02	0.892
Error	5	164.237	32.847		
Lack-of-Fit	3	156.844	52.281	14.14	0.067
Pure Error	2	7.393	3.696		
Total	44	671.651			

Table S6-6. Summary of ANOVA response for response time

Source	DF	Adj SS	Adj MS	F-Value	P-Value
Model	9	45.6458	5.0718	1.71	0.288
Linear	3	21.0625	7.0208	2.36	0.188
A	1	16.5313	16.5313	5.56	0.065
B	1	2.0000	2.0000	0.67	0.449
C	1	2.5312	2.5312	0.85	0.398
Square	3	22.2083	7.4028	2.49	0.175
A*A	1	0.3141	0.3141	0.11	0.758
B*B	1	21.5641	21.5641	7.26	<u>0.043</u>
C*C	1	0.1603	0.1603	0.05	0.826
2-Way	3	2.3750	0.7917	0.27	0.847

Interaction					
A*B	1	0.0625	0.0625	0.02	0.890
A*C	1	2.2500	2.2500	0.76	0.424
B*C	1	0.0625	0.0625	0.02	0.890
Error	5	14.8542	2.9708		
Lack-of-Fit	3	14.1875	4.7292	14.19	0.067
Pure Error	2	0.6667	0.3333		
Total	44	60.5000			

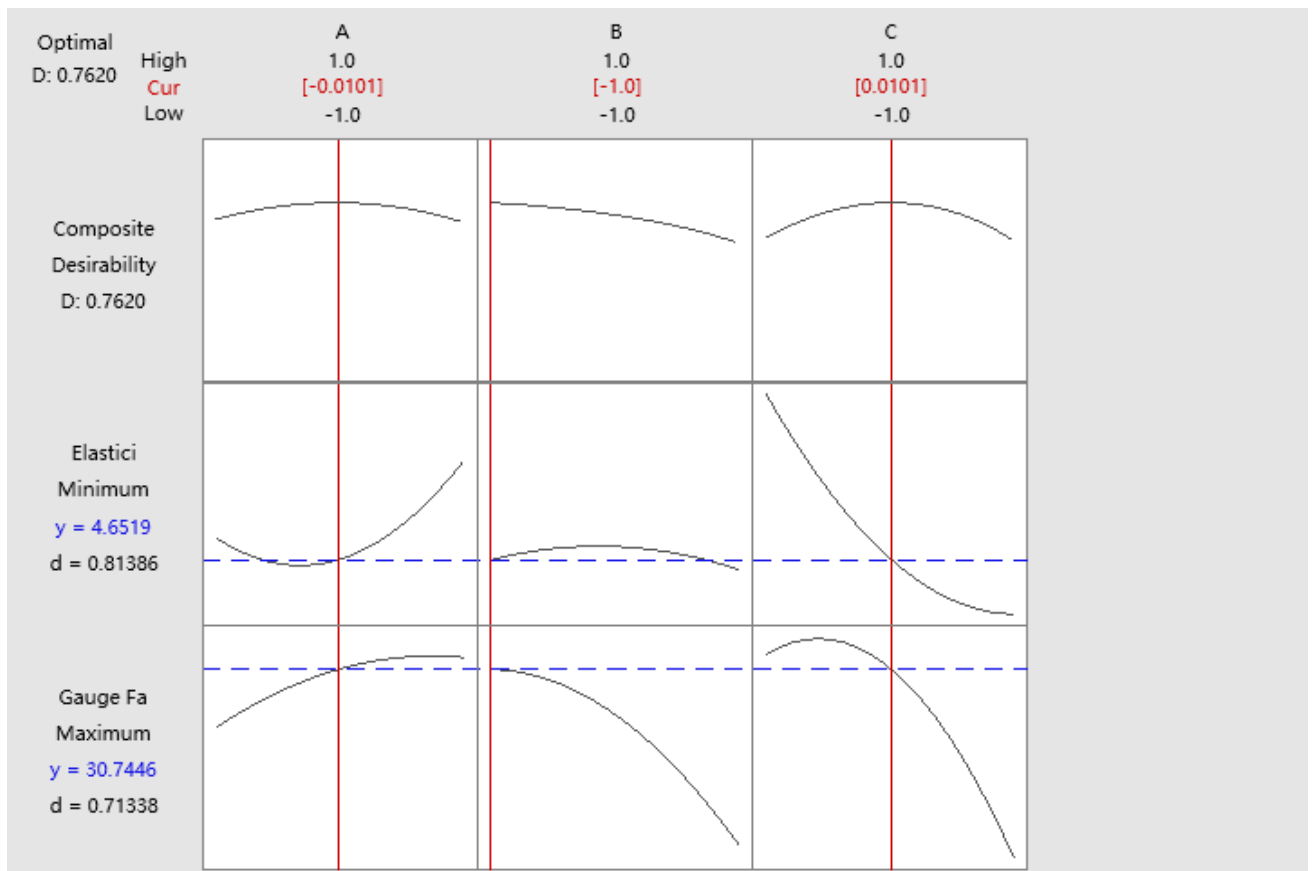


Figure S6-3. Response optimization prediction with multiple variables analysis.

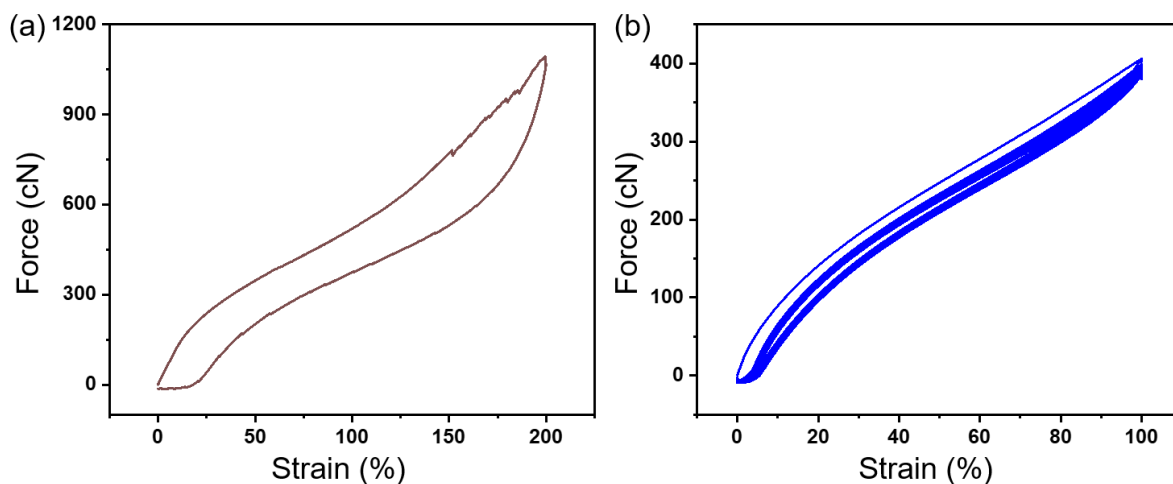


Figure S6-4. Force-strain curves of HESS. (a) The force-strain curve of the sensor under maximum stretching-releasing strain, and (b) the force-strain curve of the sensor under 20 repeated stretching-releasing strain of 100%, showing the little mechanical hysteresis.

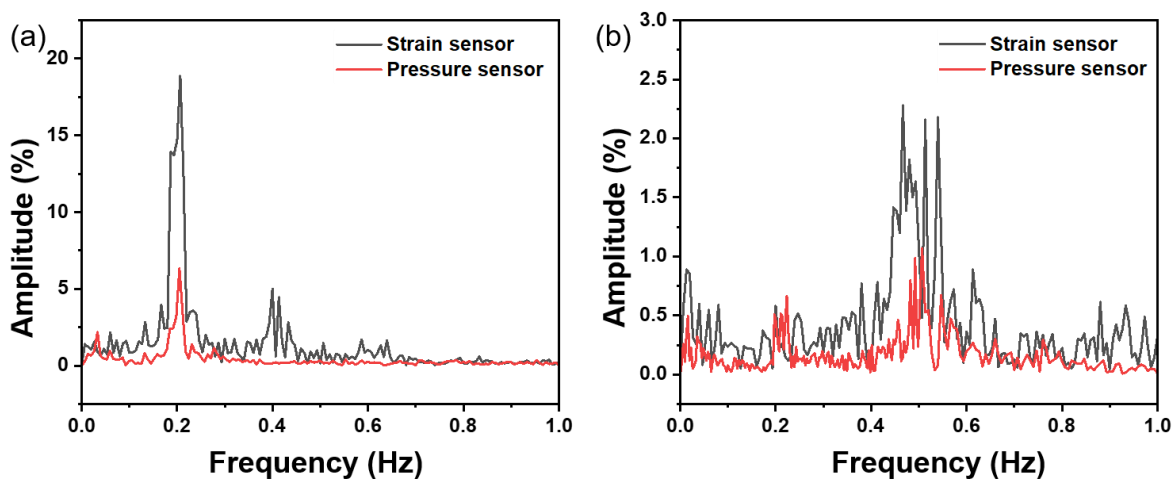


Figure S6-5. Frequency spectrum of respiration for the pattern of breathing and sensors. (a) Deep breathing at 12 bpm, and (b) Shallow breathing at 30 bpm.

CHAPTER 7. EFFECTS OF WEARING PRESSURE AND BODY MOVEMENTS ON THE ECG AND RESPIRATION PATTERN DETECTION OF EMBROIDERED TEXTILE ELECTRODES AND STRAIN SENSORS

This chapter focuses on completing objective 5 collaborating with external research partners.

Authors: Yan Zheng, Lu Jin, Tim Jun Li, Hai Guo, Boan Ying, Jing Qi and Yi Li

Targeted journal: International Journal of Clothing Science and Technology, submitted

Statement of own contributions: Main research idea, embroidered electrodes and strain sensors fabrication and evaluation, subject tests protocol and implement; data analysis and modelling; preparation of prototype, tables, figures, and manuscript.

Statement of co-author contributions: Lu Jin supports in respiratory rate analysis. Hai Guo and Tim Jun Li support in electronics development of the smart band prototype. Boan Ying and Jing Qi help in subject test. Yi Li initiated project idea and provided supervision and guidance in research methodology, the design of experiment, data analysis and interpretation, and paper revision.

7.1 Introduction

The customized smart e-textile wearables related to bio-signals monitoring are getting more attention in researchers and product developers with the “Big Data” concept application in health care systems [192]. The first step in harnessing the big data is acquisition of the bio-signals from multitude of individuals, such as heart rate, respiration rate, electrocardiogram, body temperature, etc. The process needs the individual data is continuously monitored during the various daily activities, and the data can be collected, stored and transmitted. Smart e-textile wearables are favourite solutions since it is based on textiles and the wearable is lightweight,

less discomfort, and the form factor can be customised to suit the user [116]. Most of research prototypes and wearable products in the healthcare application have multi-functions that can monitor more than one biological parameter, including measurement of ECG, heart rate, respiratory rate, temperature, SpO₂, and activity monitoring [121, 193–196]. However, in practical applications, the smart e-textile wearables tailored for individuals to assist clinical analysis is still undergoing research. For example, the cardiologist diagnoses heart disease according real-time ECG waveforms from different leads. E-textile wearables collecting bio-signals from designated position of body is crucial for health care systems since current clinical diagnosis are based on bio-signals from designated location.

Embroidery techniques have been widely used in e-textile wearables development, including electrodes [12, 14, 31, 95], sensors [18, 20, 100], antenna [197] and interconnects [198] because this technique is easy to integrate electrical conductive functions on fabric and enables more customization in the design. Function part of e-textile wearable embroidered with conductive yarns are reliable after domestic machine washing [12, 199]. Motion artefacts are the main factor to influence the quality of measured signals. Some studies [31, 200, 201] have found the sweat have effect on reducing the contact impedance of dry electrodes, which can increase signal quality detected by textile-based dry electrodes. The performance evaluation of embroidered electrodes for ECG acquisition was investigated in static [13, 202] and dynamic [48, 93] status. However, the effects of motion artefacts with various wearing pressure on real-time monitoring quality of ECG and respiratory signals were still under investigated. The sweating in daily walking and effects on ECG monitoring quality of e-textile wearables need to study quantitatively.

In this paper, a smart band prototype was developed with embroidered electrodes and a strain sensor to record physiological signals, including ECG, respiratory rate, temperature and humidity in real time, and all data can be monitored and saved by a tailored Android APP through Bluetooth. The performance of smart band for respiratory rate and ECG signal monitoring were evaluated under three levels of wearing pressure, which were 0.5 kPa, 1.5 kPa

and 2.5 kPa. The participants were recruited to wearing the smart band in static conditions (sitting and standing) and dynamic conditions with various arms motions and body torso twist. The recorded respiratory rate was compared with referred surface pressure gauge, and the quality of ECG signals was evaluated in terms of sensitivity and accuracy comparing with the commercial ECG measurement system (Biopac MP160 system). Moreover, the performance of developed smart band for physiological signal monitoring in daily life walking was assessed by a participant walking on a tread mill at five appointed speeds.

7.2 Materials and methods

7.2.1 Embroidered electrodes and strain sensor

The embroidered electrodes were fabricated with 2-ply Madeira HC 12, which is 100% polyamide core coated with silver conductive thread. This is specifically developed for embroidery applications based on Statex silver coated Shieldex thread 235/36-2ply. Figure 7-1(a) shows the electrode, 20 mm width with 40 mm length, embroidered on knitted fabrics, which is officially permitted for manufacturing firefighter T-shirt in Europe. The electrodes were embroidered with satin stitch that can keep stable conductivity for ECG signal monitoring. The strain sensor was embroidered with 2-ply Madeira HC 40 conductive thread as the conductive part, as shown in Figure 7-1(b). The stretchable polyamide yarn twisted around Elastane fibres were used to provide stretchability and polyester thread were embroidered to develop stretchable textile substrate structure for sewing. Figure 7-1(c) shows changes in resistance of a strain sensor based on tensile stress. When the strain sensor is stretched by an external force, tension is applied to the conductive area, thereby increasing the resistance. When the external force applied to the sensor is removed, the conductive yarns return to contact status, and the resistance decrease. During perspiration, the chest circumference increases and decrease with inhalation and exhalation. The strain sensor can reflect respiratory rate according to resistance changes caused by chest circumference changes of inhalation and exhalation.

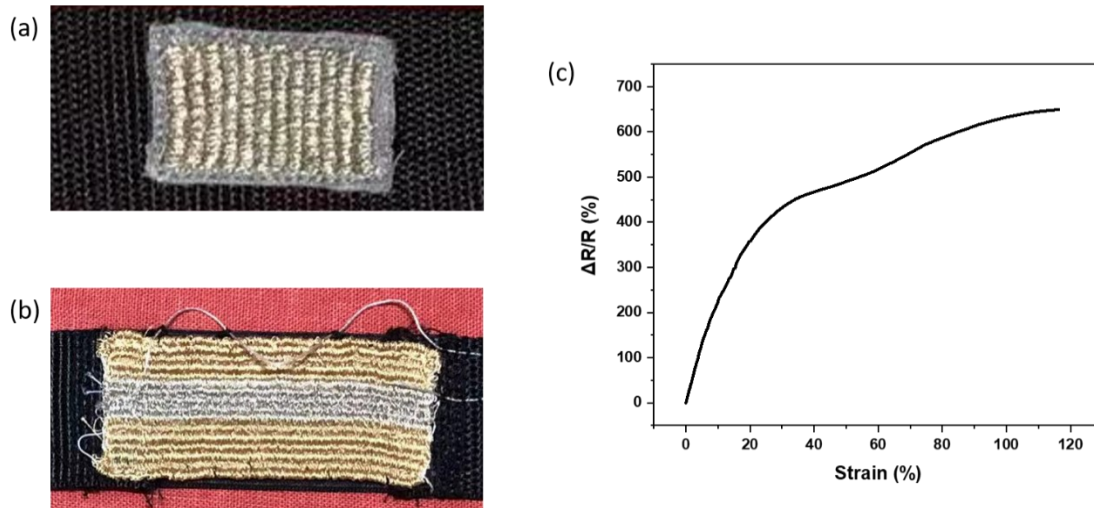


Figure 7-1. Image of the embroidered electrode and strain sensor. (a) The embroidered electrodes used for the ECG monitoring. (b) The strain sensor connected for the breath rate monitoring. (c) The changes in resistance of the strain sensor.

7.2.2 Prototype development

The customised smart band with two embroidered electrodes and a textile-based strain sensor was prototyped using a braided band, as shown in Figure 7-2(a) and (b). The strain sensor was sewed on an elastic band to keep its stretch ability during breathing. Two embroidered electrodes were sewed on the band according to the ECG measurement requirements. The strain sensor was sewed on the left side of the body to measure the rib part changes during breath. To record the physiological data, a digital temperature and humidity sensor (SHT75 from Sensirion AG) was connected to measure temperature and humidity of body-band microclimate. Figure 7-2(c) shows a Bluetooth electronic module with an interfacing circuit board was developed by the 3rd partner. The SHT75 sensor is detachable and easy to replace in case it was damaged. The wire helps the sensor to flexibly allocate with measurement requirements. The rechargeable electronic module is detachable for protection from potential washing damage.

A process flow of the data acquisition and transmission system was shown in Figure 7-2(d). ECG signal was measured by two embroidered electrodes and processed by the ECG single channel IC (MAX30003 from Maxim Integrated) connected to the microcontroller (Cortex M4, from Nordic nRF52832QFAA). The resistance value of strain sensor, temperature and humidity

value from commercial SHT 75 sensor were processed by this microcontroller in the meantime. The frequency of ECG signal recording and resistance of strain sensor measurement are 100 Hz and 50 Hz, respectively. The system measures temperature and humidity every 10 seconds. These data were then outputted in real time through Bluetooth antenna to the cell phone. The developed Android APP (Figure 7-2e) collect and save continuous real-time measurement data. The electronic module and Android App of smart band is provided by Digital Clothing Ltd, Hong Kong, China.

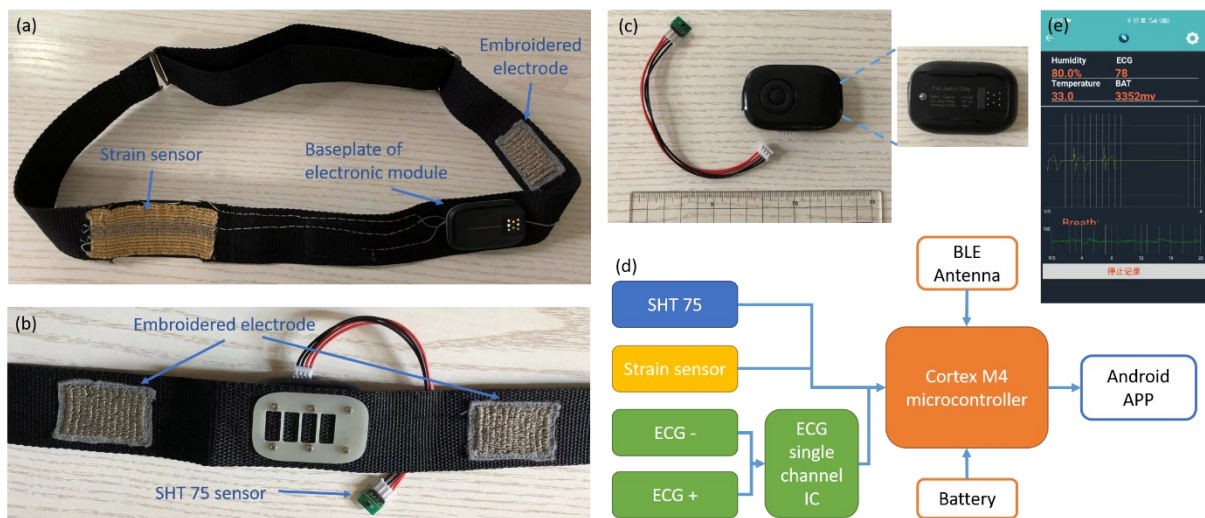


Figure 7-2. Image of the smart band and accessories. (a) Image of the smart band and connections to baseplate of electronic module. (b) The inside image of the smart band with electrodes and the humidity/temperature digital sensor. (c) Front view of the electronic module with a detachable sensor. The exploded image on the right shows the rare view of the module. (d) Schematic of the electronic structure for the module to process signals. (e) Interface of Android APP in smart phone for the subject test.

7.2.3 Experimental protocol

This experimental protocol was approved by the ethics committee of University of Manchester (2019-5112-12512). Prior informed consent form was obtained from all participants. Three healthy male participants were recruited for this laboratory study according to the specification in ASTM F2668-2016 (Standard Practice for Determining the Physiological Responses of the Wearer to Protective Clothing Ensembles). The participants were non-smokers with no known history of cardiovascular disease. The average age was 26 ± 5.29 years, height 1.8 ± 0.06 m,

weight 75.2 ± 6.43 kg. Demographic information and major body measurements are listed in Table 7-1.

Table 7-1. Demographic information and body measurements of participants

Participant	Gender	Age (years)	Height (m)	Body Weight (kg)	Chest Circumference (cm)
1	Male	24	1.73	67.5	88.5
2	Male	22	1.85	80.5	90.5
3	Male	30	1.75	70.5	89.0

The developed smart band was put on the chest of participants. The centre of electrodes on left and right aim to the C1 and C2 points. As shown in Figure 7-3(a), C1 point is the intersection of the fourth ICS and mid-clavicular line. C2 point is the symmetric point of C1. Two clinical proved gel Ag/AgCl electrodes were pasted close to the C1 and C2 points. Figure 7-3(b) shows the Biopac ECG adaptor, wireless connected to Biopac MP160 system (Biopac Inc., Goleta, CA, USA), was connected with Ag/AgCl electrodes to record ECG signal as reference. To evaluate the respiratory measurement performance, a comparative experiment with a standard air-pack type contact surface pressure measuring system AMI 3037-2 (AMI Techno CO., LTD. TOKYO, JAPAN) was employed. As a reference sensor to measure respiration rates, the air-pack sensor (round shape with 2 cm diameter) was stick on the skin of right ribcage to detect pressure through expansion and contraction of the chest during respiration. The wiring tube of the air-pack sensor was fixed onto the skin with tape to prevent motion disturbance when participants perform activities, which was shown in Figure 7-3(c).

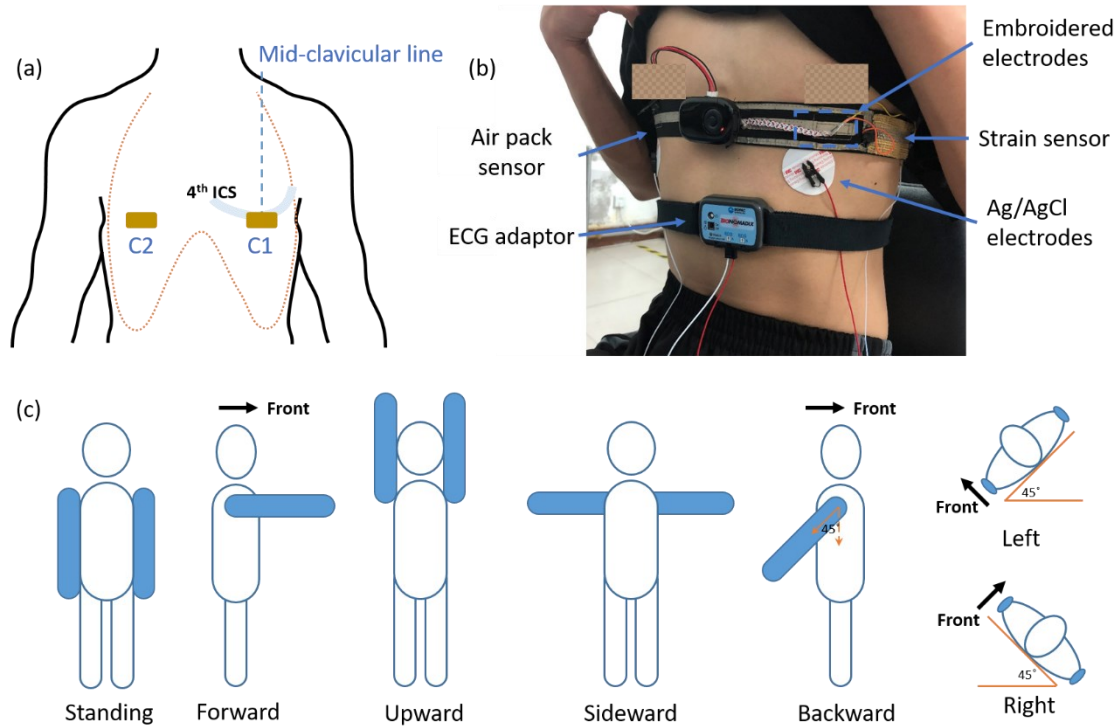


Figure 7-3. Images for the subject test. (a) Positioning of electrodes for ECG measurement. (b) Participant wearing the smart band and reference system. (c) Activities protocols for the experiment.

To evaluate electrocardiogram (ECG), heart rate (HR) and respiratory rate (RR) monitoring performance of smart band with three level wearing pressure, 0.5 kPa, 1.5 kPa and 2.5 kPa wearing pressure were respectively tested. Participants were asked to perform two static and six controlled dynamic measurement conditions, representing daily body movements that may introduce motion artefacts into the electrodes and sensor signal.

1) Sitting still and relax for 3 minutes, then start to record physiological signal for 150 seconds.

2) Standing still and relax for 1 minute, then start to record physiological signal for 150 seconds.

After standing still and relax for 1 minute, start to perform arm and body activities:

3) Raising arms forward in 10 seconds, then drop down, repeat 3 times.

4) Raising arms upward in 10 seconds, then drop down, repeat 3 times.

5) Raising arms sideward to horizontal level of shoulder in 10 seconds, then drop down, repeat 3 times.

6) Waving arms backward in 10 seconds, then drop down, repeat 3 times.

7) Rotating the torso left in 10 seconds, then drop down, repeat 3 times.

8) Rotating the torso right in 10 seconds, then drop down, repeat 3 times.

To investigate the ability of smart band for physiological signal monitoring in walking situation, one male participant was invited to perform walking test on treadmill at different pace. The wearing pressure of the band was 1.5 kPa based on results of previous analysis. After sitting still and relax for 3 minutes, the participant was asked to remain relaxed in standing on the still treadmill to collect 60 seconds physiological signals recordings. When the participant is ready, he was asked to walk on a treadmill with following speed continuously: 2km/h for 8 minutes, 4 km/h for 8 minutes, 6 km/h for 8 minutes, 4 km/h for 8 minutes, and 2 km/h for 8 minutes.

7.2.4 Data analysis

After collecting the data, the performance of the proposed smart band system was verified by comparing its measured ECG signal with that of Biopac system, and respiration signal acquired by strain sensor with surface pressure measurement systems. To calculate the respiration rate, the frequency spectrum of the respiratory signal obtained through fast Fourier transformation (FFT) was used. To qualitative evaluate recorded ECG signals, the durations of all data were manually examined to determine the shapes of QRS waves and to identify artefacts. Two statistical indices, the sensitivity and the overall accuracy, were calculated using a modification of Lee's method [203], which were determined as follows:

$$\text{Sensitivity (\%)} = \frac{TP}{TP + FN} \times 100 \quad (7 - 1)$$

$$\text{Accuracy (\%)} = \frac{TP}{TP + FP + FN} \times 100 \quad (7 - 2)$$

where *TP* represents true positive, which is a quantification of the correctly detected QRS complex; *FN* represents false negative, which is a quantification of the missed QRS complex; and *FP* represents false positive, which is a quantification of false detection of an QRS complex error during the normal non-QRS-wave duration.

Table 7-2 shows experimental design to analyse difference of signal index calculated between the proposed smart band and referenced measurement systems in static and dynamic measuring conditions (MC). Three levels of wearing pressure (WP), 0.5 kPa, 1.5 kPa and 2.5 kPa are applied respectively. A two-way analysis of variance (ANOVA) was used to compare respiration rate, statistic indices of ECG signals calculated from the smart band with referenced system. A *p* value <0.05 was considered significant.

Table 7-2. Design of selected evaluation parameters and levels for the experiment

Experiment condition	Evaluation factors		Levels				
Static	WP (kPa)	0.5	1.5		2.5		
	MC	Sitting	Standing				
Dynamic	WP (kPa)	0.5	1.5		2.5		
	MC	AF	AU	AS	AB	TL	TR

AF: arms forward; AU: arms upward; AS: arms sideward; AB: arms backward; TL: torso left; TR: torso right.

7.3 Results and discussion

7.3.1 Effects of wearing pressure on respiratory rate measurements

7.3.1.1 Performance of respiration measurement in static conditions

Figure 7-4 shows a representative frequency spectrum of the respiratory signal of subject 1 measured by smart band and surface pressure gauge during sitting and standing status at three levels of wearing pressure. After analysing the frequency content of the signals through FFT, the respiratory component was filtered by a band-pass filter with a 0.05-0.8 Hz passband[45].

Figure 7-4(a) to (c) show a 60 s respiratory signal examples of subject 1 from smart band

compared to the surface pressure gauge in sitting and standing measurement conditions at different wearing pressure. Signals shown in the figure were filtered respiration curve for better visualization and processing with its corresponding surface pressure gauge signal. Overall, the proposed smart band could similarly detect each phase of respiration peaks as well as the referenced surface pressure gauge. The performance of the measurement varied with different wearing pressure. As seen in Figure 7-4(a), the respiratory waveform of the surface pressure gauge at 0.5 kPa wearing pressure irregular shape. The respiratory waveform of the smart band in 1.5 kPa wearing pressure showed matching peak and shapes compared to surface pressure gauge, as shown in Figure 7-4(b). For proposed smart band, Figure 7-4(c) shows the strain sensor will be more sensitive to motion in 2.5 kPa, and the signal amplitude was small or spiked noise was generated in the measurements. The developed smart band showed a continuous change in resistance to stretch, which resulted in less saturation than in the surface pressure gauge.

The spectrum of respiration had similar frequency characteristics and the peak with a higher amplitude at frequency from 0.3 Hz to 0.4 Hz. Figure 7-4(d) and (f) show these two measurement systems have similar distributions, but different shapes for the peak. The spectrum of surface pressure gauge has peaks with a higher amplitude than that from smart band when wearing in 0.5 kPa and 2.5 kPa. However, the spectrum of these two measurement systems shows exactly the same frequency and amplitude in Figure 7-4(e). In the spectral analysis, the smart band showed a similar respiration measurement performance in static conditions (sitting and standing) with 1.5 kPa wearing pressure.

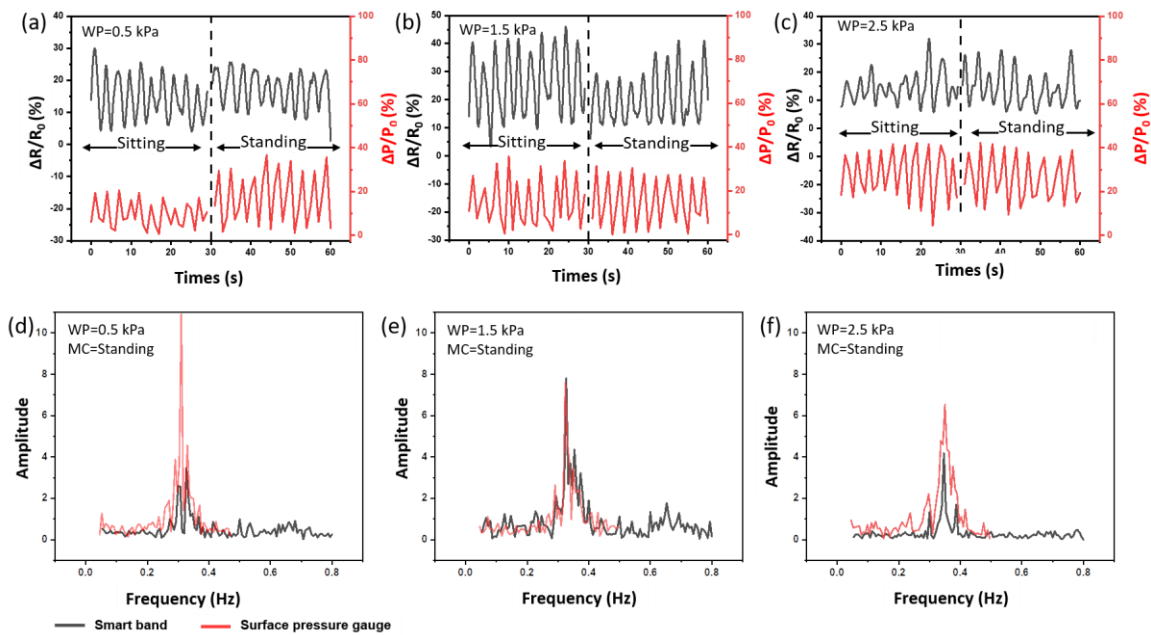


Figure 7-4. Respiration waveform and frequency spectrum of Subject 1 in sitting and standing. Respiration waveform with WP (a) 0.5 kPa, (b) 1.5 kPa, (c) 2.5 kPa. Frequency spectrum of respiration according to the type of measurement systems with WP (d) 0.5 kPa, (e) 1.5 kPa, and (f) 2.5 kPa.

Figure 7-5 shows respiratory rate calculated from textile strain sensor measurement in smart band prototype and surface pressure gauge of three subjects. A two-way analysis of variance (ANOVA) found no significant difference between periods calculated from the smart band and surface pressure gauge across all respiration rate for each subject in sitting and standing. There was no significant difference of RR detection between smart band and reference pressure gauge in sitting and standing status under 0.5 kPa, 1.5 kPa and 2.5 kPa wearing pressure. The p-value of MC and measurement systems for each participant is listed in Supplementary Table S7-1.

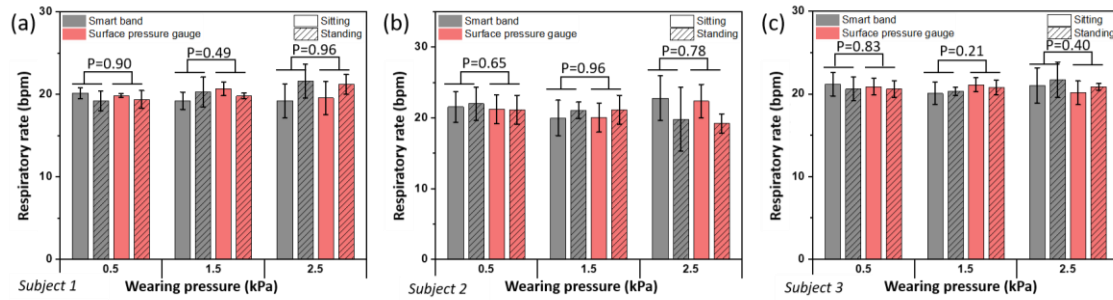


Figure 7-5. Respiratory rate value statistics in static measurement of (a) Subject 1, (b) Subject 2, (c) Subject 3.

7.3.1.2 Performance of respiration measurement during up body dynamic conditions

The detection of respiration signal of proposed smart band was different according wearing pressure in dynamic status. With wearing pressure 0.5 kPa, detected breathing peaks with signal noise caused by movement of arms were observed in Figure 7-6(a). Since the principle of smart band to monitor breathing is the extension and contraction of embroidered strain sensor, the movement of arms have effects on the strain of the sensor and cause the noise during breathing. Meanwhile, the slippage of smart band with the movement of arms is significant under lower wearing pressure. As shown in Figure 7-6(b), the peak of frequency spectrum in FFT were diluted in AF, AU, AS and AB motions, while the frequency of movement noise when rotating the torso left and right were lower than respiratory rate. The peak of respiratory rate was visible and identical to the reference pressure gauge.

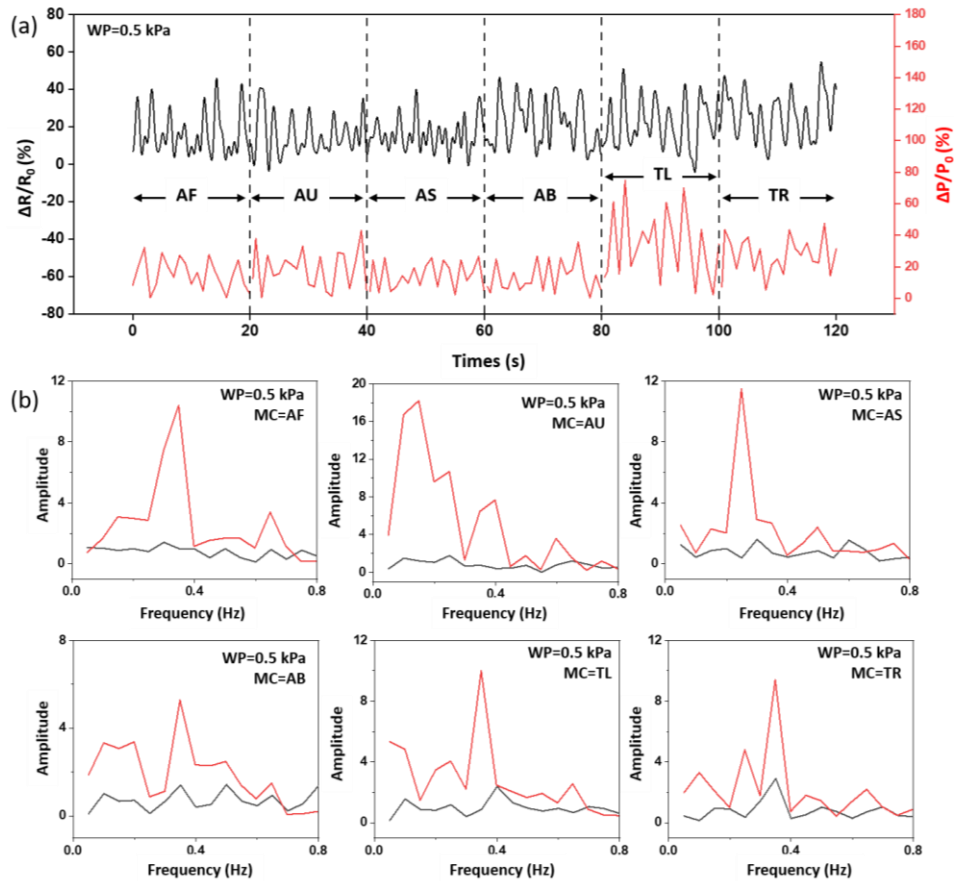


Figure 7-6. Respiratory waveform and frequency domain of Subject 1 started waving arms with 0.5 kPa WP. (a) Detrended outputs, and (b) frequency domain for the respiration rate measured from the smart band (presented in black lines), and surface pressure gauge (presented in red).

The respiration monitoring under 1.5 kPa wearing pressure are presented in Figure 7-7. The waveform of breathing in Figure 7-7(a) shows motion artefacts when raising arms forward, up, side, and back. The FFT analysis in Figure 7-7(b) indicates that the proposed smart band can detect respiratory rate that similar with the signal detected by reference surface pressure gauge. But there was difference of respiratory rate when raising arms forward, upward, and side. The peak of frequency spectrum in arms back action and body torso turning left and right were identical.

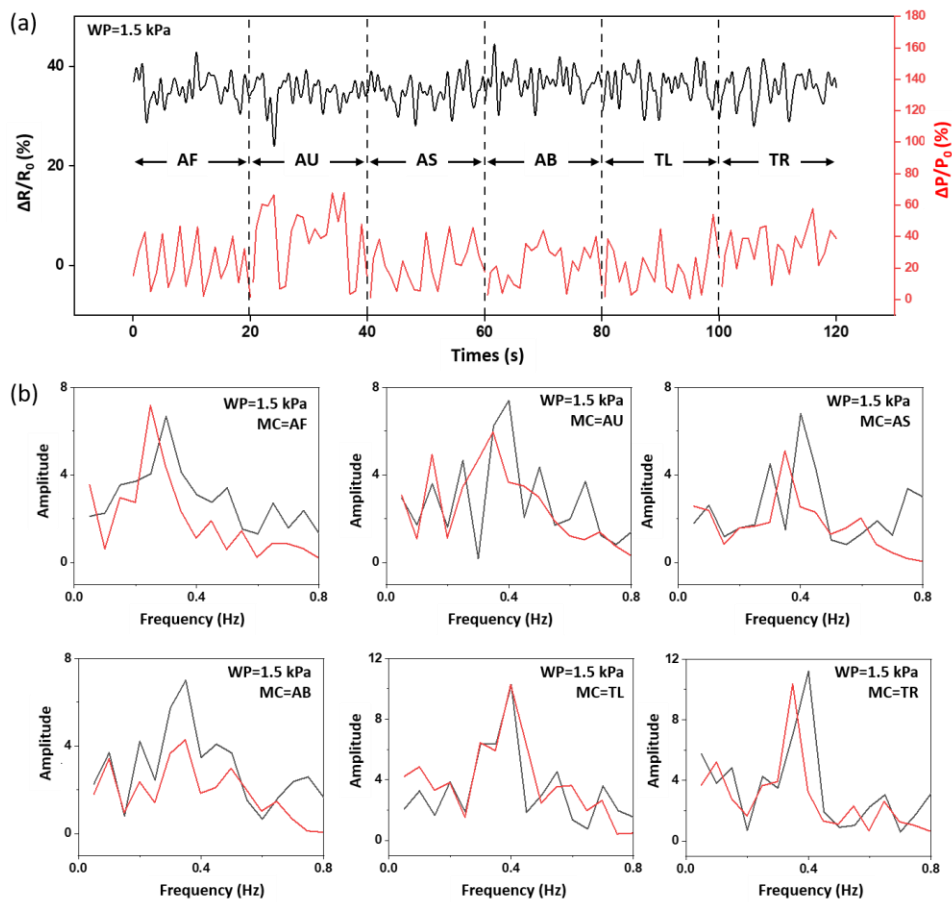


Figure 7-7. Respiratory waveform and frequency domain of Subject 1 started waving arms with 1.5 kPa WP. (a) Detrended outputs, and (b) frequency domain for the respiration rate measured from the smart band (presented in black lines), and surface pressure gauge (presented in red).

Figure 7-8 shows the breathing pattern with different motion under 2.5 kPa wearing pressure. Figure 7-8(a) shows the respiration signals were clear and distinguishable with arms motions. The six pattern of frequency spectrum of FFT are presented in Figure 7-8(b). The peak of respiratory rate from proposed smart band were identical with compared surface pressure gauge in raising arms forward, up, side, and body torso twist. Motions of waving arms up and back cause artefact noise to the respiration signal.

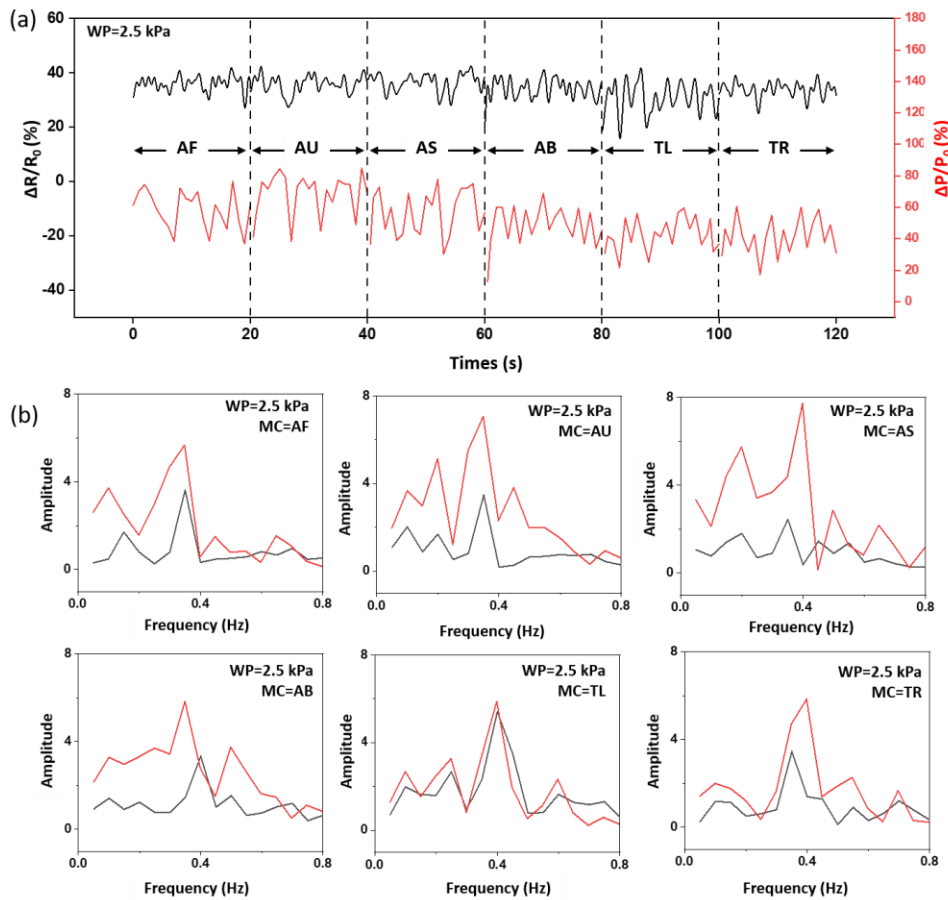


Figure 7-8. Respiratory waveform and frequency domain of Subject 1 started waving arms with 2.5 kPa WP. (a) Detrended outputs, and (b) frequency domain for the respiration rate measured from the smart band (presented in black lines), and surface pressure gauge (presented in red).

Figure 7-9 shows respiratory rate calculated from proposed smart band prototype and reference surface pressure gauge of three subjects. A two-way ANOVA found there was significant difference of respiratory rate between proposed smart band and referenced systems under 0.5 kPa wearing pressure. The respiratory rate calculated from the smart band are similar to the referenced surface pressure gauge with wearing pressure of 1.5 kPa and 2.5 kPa. But raising arms up have artefact effects on breathing signal monitoring in 1.5 kPa wearing pressure. There was no significant difference of RR detection in six motions under 2.5 kPa wearing pressure. The p-value of MC and measurement systems for each participant is listed in Supplementary Table S7-1 as well.

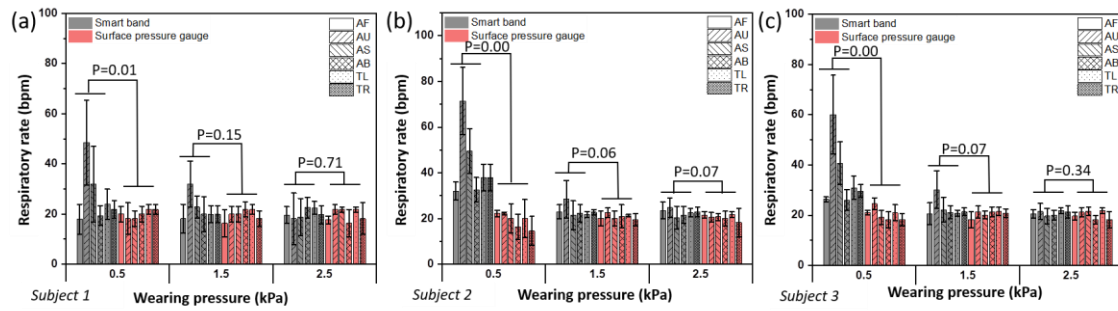


Figure 7-9. Respiratory rate value in dynamic measurement of (a) Subject 1, (b) Subject 2, and (c) Subject 3.

7.3.2 Effects of wearing pressure on ECG measurements

7.3.2.1 Performance of ECG measurements in static conditions

Figure 7-10 shows the representative P, QRS, and T waves were comparable between smart band and the Biopac system of participant 1 in sitting and standing status with three levels of wearing pressure. There were no false positive peaks in all static measurement conditions. Figure 7-10(a) shows false negative peaks were observed and there were QRS complex missed with wearing pressure of 0.5 kPa. There was drift in the base line of the signals in standing status. There were no false negative peaks and no drift in the base line in sitting and standing status in 1.5 kPa and 2.5 kPa wearing pressure, as shown in Figure 7-10(b) and (c). But the drift of the base line in standing status was observed under 2.5 kPa wearing pressure as shown in Figure 7-10(c). This base line drift caused by the chest movement noise during breathing in higher wearing pressure.

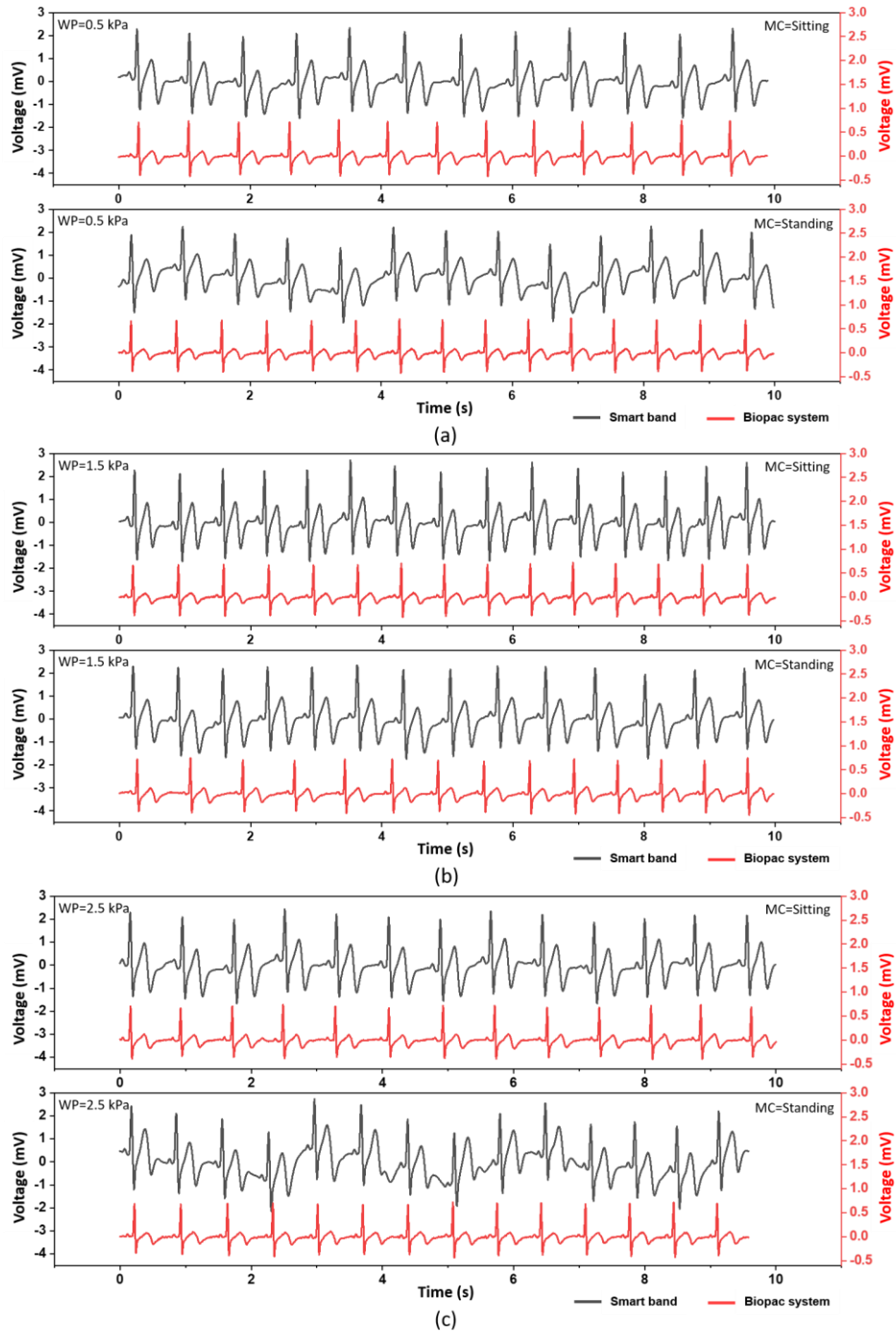


Figure 7-10. Representative ECG signals of Subject 1 in sitting and standing with different wearing pressure. (a) 0.5 kPa; (b) 1.5 kPa; (c) 2.5 kPa. (Black: proposed smart band; Red: reference Biopac system).

The statistical results for three subjects in 150 seconds measurement are presented in Supporting Table S7-2. The sensitivity and accuracy of QRS detection were the same since there was no false negative peak in sitting and standing status. As shown in Figure 7-11 and

Table S7-3 in supporting, the sensitivity and accuracy enhanced with the increase of wearing pressure. On average, the proposed smart band had a QRS complex detection accuracy in static measurement conditions were over 96% under 1.5 kPa wearing pressure and reach 99% wearing in 2.5 kPa, respectively.

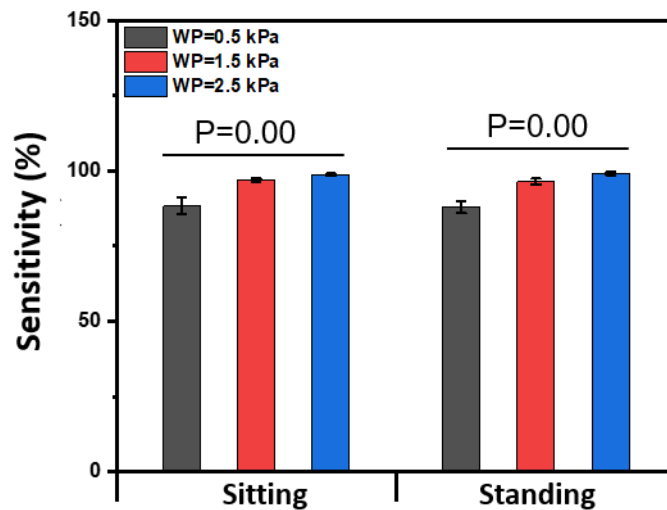


Figure 7-11. Sensitivity of QRS detection in static measurement condition.

7.3.2.2 Performance of ECG measurements in dynamic conditions

Figure 7-12 shows representative ECG waveform of Subject 1 in dynamic measurement conditions at 0.5 kPa wearing pressure. The ECG waveform were fluctuated with arm movements, and the R peak of ECG signals was hard to classified during arm upward, arms side and arm back. The QRS peak in ECG cycle was clear when raise arm forward, turn body left and turn body right. But the QRS peak bias with body movements. There were clearly fluctuated waveforms caused by motions.

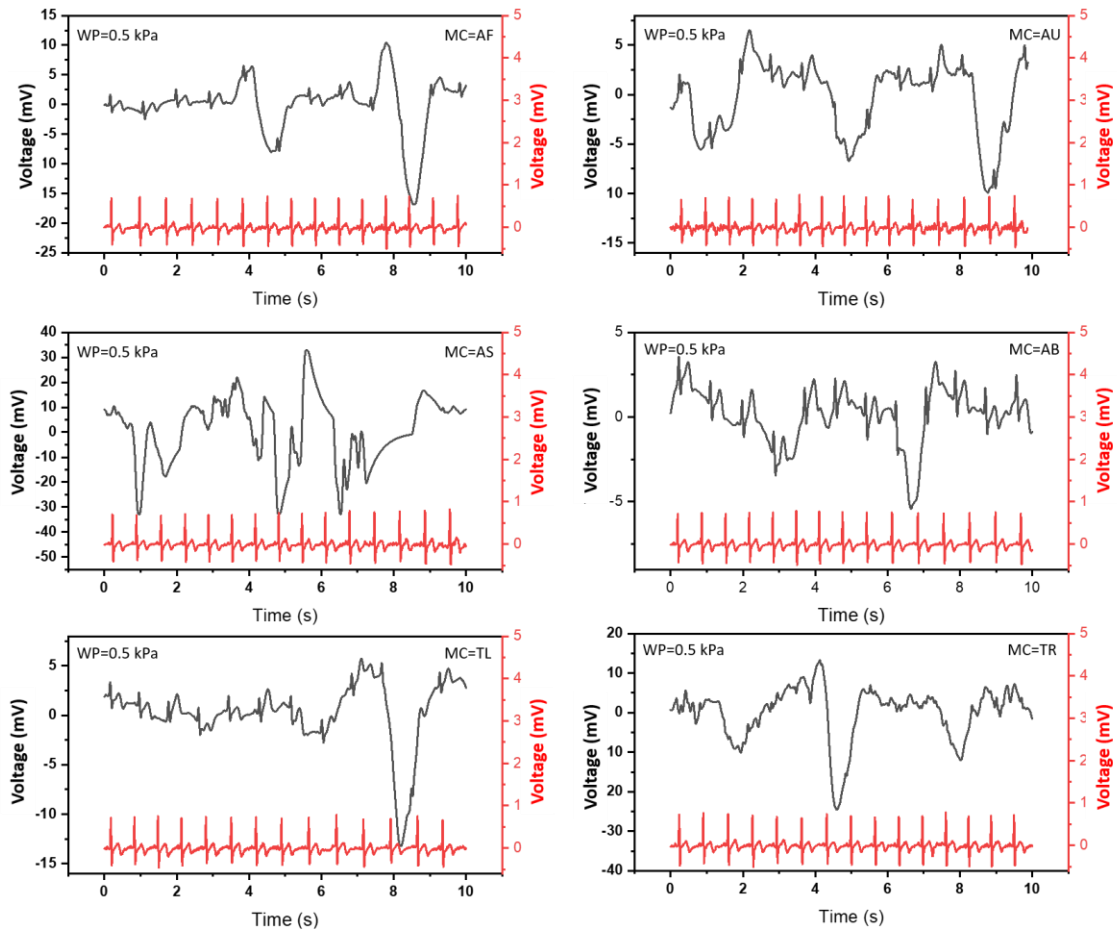


Figure 7-12. Representative ECG signals of Subject 1 in dynamic measurement conditions at 0.5 kPa wearing pressure. (Black: proposed smart band; Red: reference Biopac system).

When the wearing pressure increased to 1.5 kPa, the ECG wave form was clear and QRS peak can be recognised clearly, as shown in Figure 7-13. The QRS and T waves were comparable between the smart band and Biopac system. But there was waveform fluctuated when raise arms in body side. This trend was not linear dependent when wearing pressure increased to 2.5 kPa. As shown in Figure 7-14, the ECG waveforms were acutely fluctuated with arms movement, except wave arms backward. Turing body left and right have little effects on ECG wave forms, and the QRS peak was clear only some baseline shift in the pattern. The fluctuation and shift of ECG waveform showed effects of movement artifacts on signal quality. The ECG recording of the smart band was worst when arms raised forward, up and side, since the motion cause the skin and muscles movement in the chest part, which results in the motion artifacts noise covered the signal of ECG.

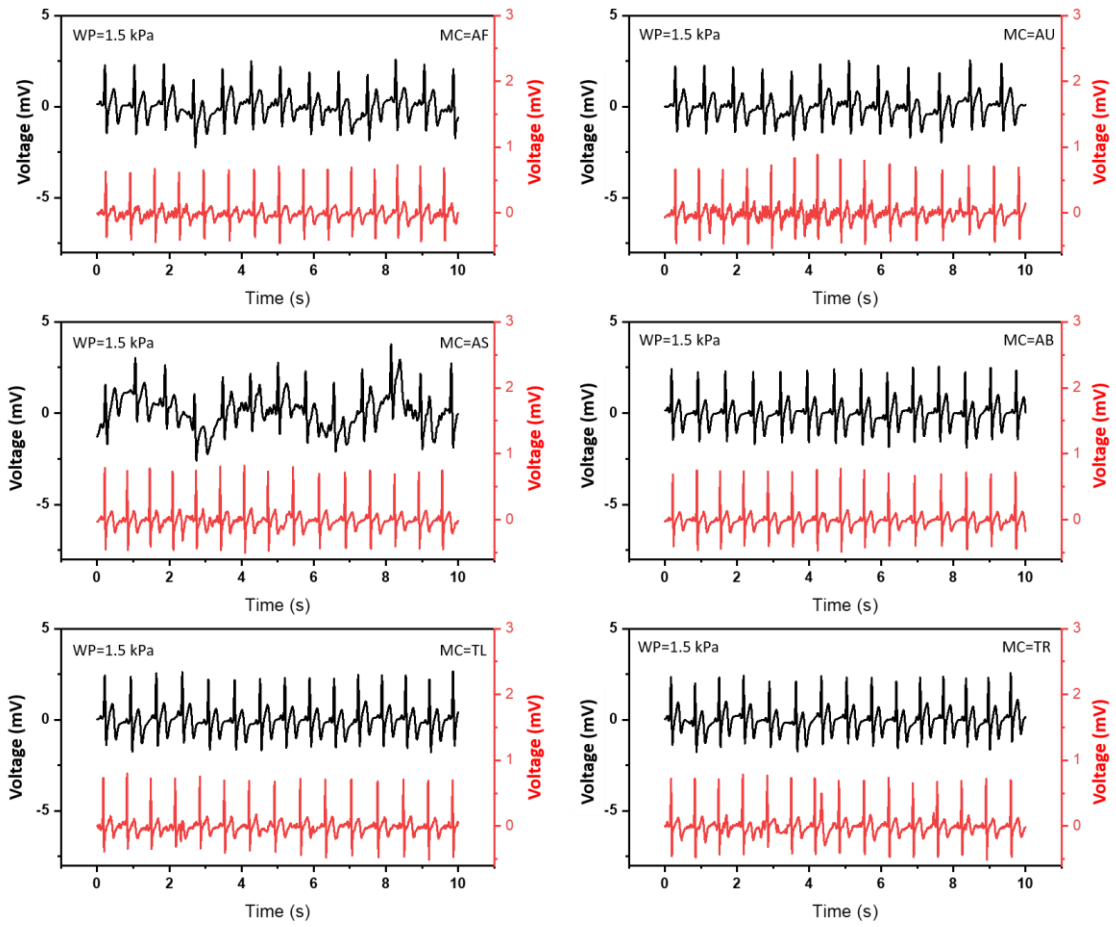


Figure 7-13. Representative ECG signals of Subject 1 in dynamic measurement conditions at 1.5 kPa wearing pressure. (Black: proposed smart band; Red: reference Biopac system).

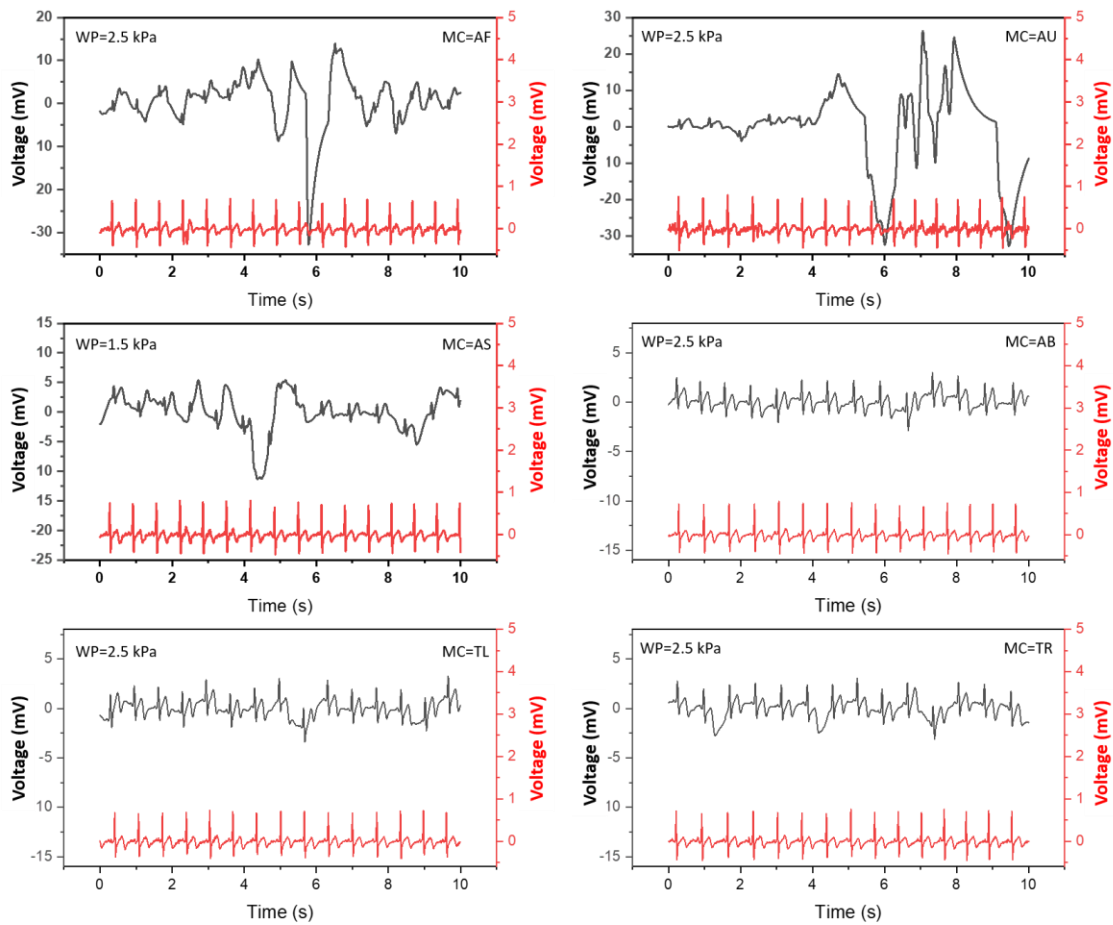
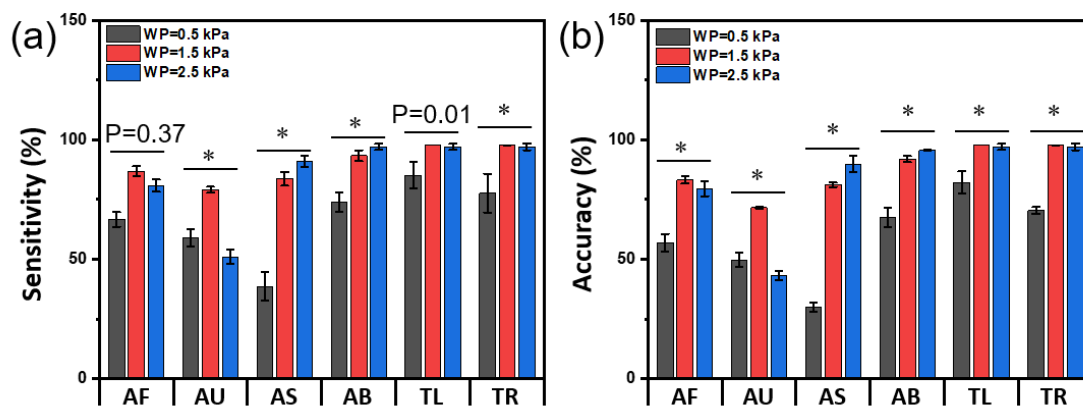


Figure 7-14. Representative ECG signals of Subject 1 in dynamic measurement conditions at 2.5 kPa wearing pressure. (Black: proposed smart band; Red: reference Biopac system).

The statistical sensitivity and accuracy for QRS detection in dynamic MC of three subjects can be found in supporting Table S7-4. Figure 7-15 and Supporting Table S7-5 show a one-way ANOVA result of sensitivity and accuracy of QRS detection. When monitoring ECG signal in dynamic measurement conditions, most of the sensitivity and accuracy of QRS detection enhanced with wearing pressure, except raising arms forward and upward. Particularly, the movement artifacts noise from motion of skin and muscles during raising arms upward were significant and has negative impact on QRS detection at 2.5 kPa wearing pressure. Turning torso left and right have less effects on QRS detection, and the sensitivity and accuracy were over 97% at 1.5 kPa and 2.5 kPa wearing pressure. Increased wearing pressure could improve the sensitivity and accuracy when raising arms sideward and backward. For ECG monitoring in dynamic measure conditions, the 1.5 kPa wearing pressure was proper for QRS detection

since the sensitivity and accuracy were over 80%.



The * in the graph represents p value is 0.00.

Figure 7-15. Difference of QRS detection in static measurement condition (a) sensitivity and (b) accuracy.

7.3.3 Performance of physiological signal monitoring in walking

One male subject was invited to walking continuously on the treadmill at the specified speeds with this proposed smart band and T-shirt made with polyester. According results from ECG measurement, the band was worn at 1.5 kPa pressure. Before and after walking test, the subject was asked to stand still for 1 minute to record ECG signals in static status. Figure 7-16 shows selected ECG recordings during the test, ECG waveforms of five seconds in each minute were selected to represent ECG signals when the subject walking from slow (2 km/h) to fast (6 km/h), then return back to walk slow (2 km/h). The quality of ECG signals was worse when start to walking at 2 km/h, and heart beats signals (QRS complex) were covered by motion artefacts in walking. This artefact has negative impact on ECG signal qualities with the increase of walking speed. From walking speed 2 km/h to 4 km/h, high-frequency noise and a baseline shift were noted. The worst signal was found at the beginning of walking at 6 km/h with increased base line noise caused by movement of the arms and body at high-speed walking. However, the heart beats signals returned regularly and the P wave was clearly detectable after walking 1300 seconds. The P, QRS, and T waves were clearly recognised after walking 1500 seconds, and

perfect ECG signals can be easily found after 1920 seconds when walking at 2 km/h. As shown in Figure 7-17(a), the humidity in skin-clothing microclimate was increased significantly after 960 seconds walking. This relative humidity reached over 50% after walking 1300 second, which helped to increase ECG monitoring performance of proposed textile electrodes.

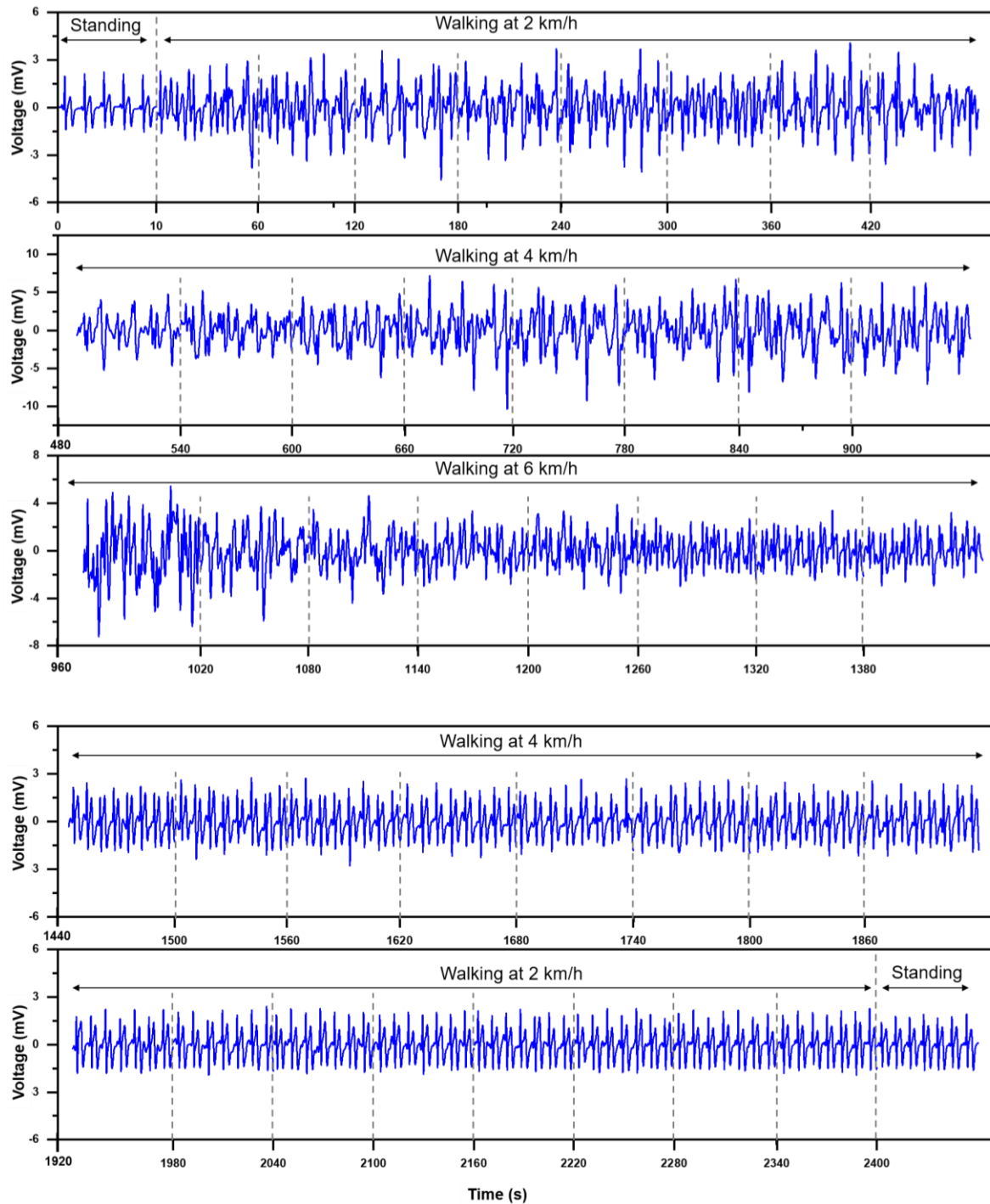


Figure 7-16. Representative plots of raw ECG waveforms from the smart band while the subject is standing stationary, walking on a treadmill at 2 km/h, 4 km/h, 6 km/h, 4 km/h, and 2 km/h in 40 minutes. In each section, five seconds ECG signals were selected to represent variation trend.

The proposed smart band can measure temperature and humidity of skin-clothing microclimate successfully. Figure 7-17 shows the change of temperature and humidity while the subject walking at the specified speeds wearing two types of clothing. The fleeced hoodie is fit for keeping warm with the fluffy fabric structures. The T-shirt is made of texture thin and soft polyester fibres, which can absorb sweat quickly during sports and exercises. The temperature and humidity sensor in the smart band recorded the temperature and humidity changes during walking, and the difference impacts of clothing wearing can be detected successfully. While walking at speed of 6 km/h, the subject intended to sweat and humidity increased significantly. During this period, a gradually decline of temperature can be noticed since the inapparent sweating helped to exhaust body heat. After the subject walking returned to 2 km/h, the fast-dry T-shirt helped to absorb the moisture and the relative humidity declined progressively, as shown in Figure 7-17(a). However, Figure 7-17(b) shows the hygroscopicity performance of fleeced hoodie seems to be weak and the relative humidity still at higher level when the subject slow down the walking speed.

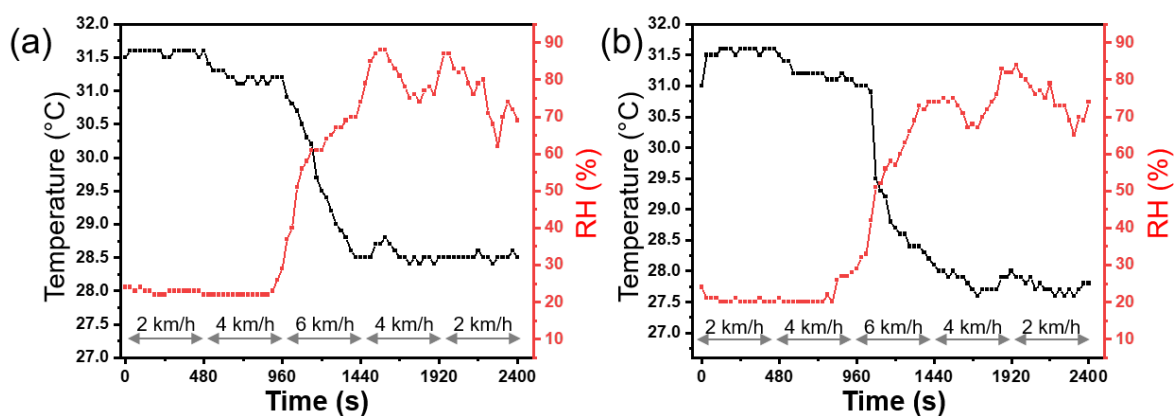


Figure 7-17. The body-clothing microclimate temperature(°C) and relative humidity (%) during the walking test with the participant wearing (a) T-shirt and (b) fleeced hoodie.

In order to understand the smart band’s performance for respiration rate monitoring under

motion, the subject 1 was asked to perform normal respiration procedures while walking at 2 km/h, 4 km/h, 6 km/h, 4 km/h, and 2 km/h on a treadmill. A low pass filter at 1 Hz was used to remove the motion artifact, which has a higher frequency, from the strain sensor data in smart band. Figure 7-18 shows the representative waveform of the strain sensor resistance after filtering. The filtered signals indicated the increase of respiration rate and intensity from standing to walking from slow to fast, then gradually walking slow down. This change of resistance caused by chest expansion and contraction during breathing, and the body naturally increases air intake during walking were captured. As the subject transitioned from standing to increase walking speed gradually, the frequency and depth of respiration increased, which results in the increase of resistance changes of the strain sensor caused by movements of the chest from respiration. The respiration returned back to steady after walking at 2 km/h, and the waveform of respiratory changes was similar to the beginning of standing after standing stationary for several minutes. The waveform of the strain sensor resistance can be used to calculate respiration rate, and volume while walking.

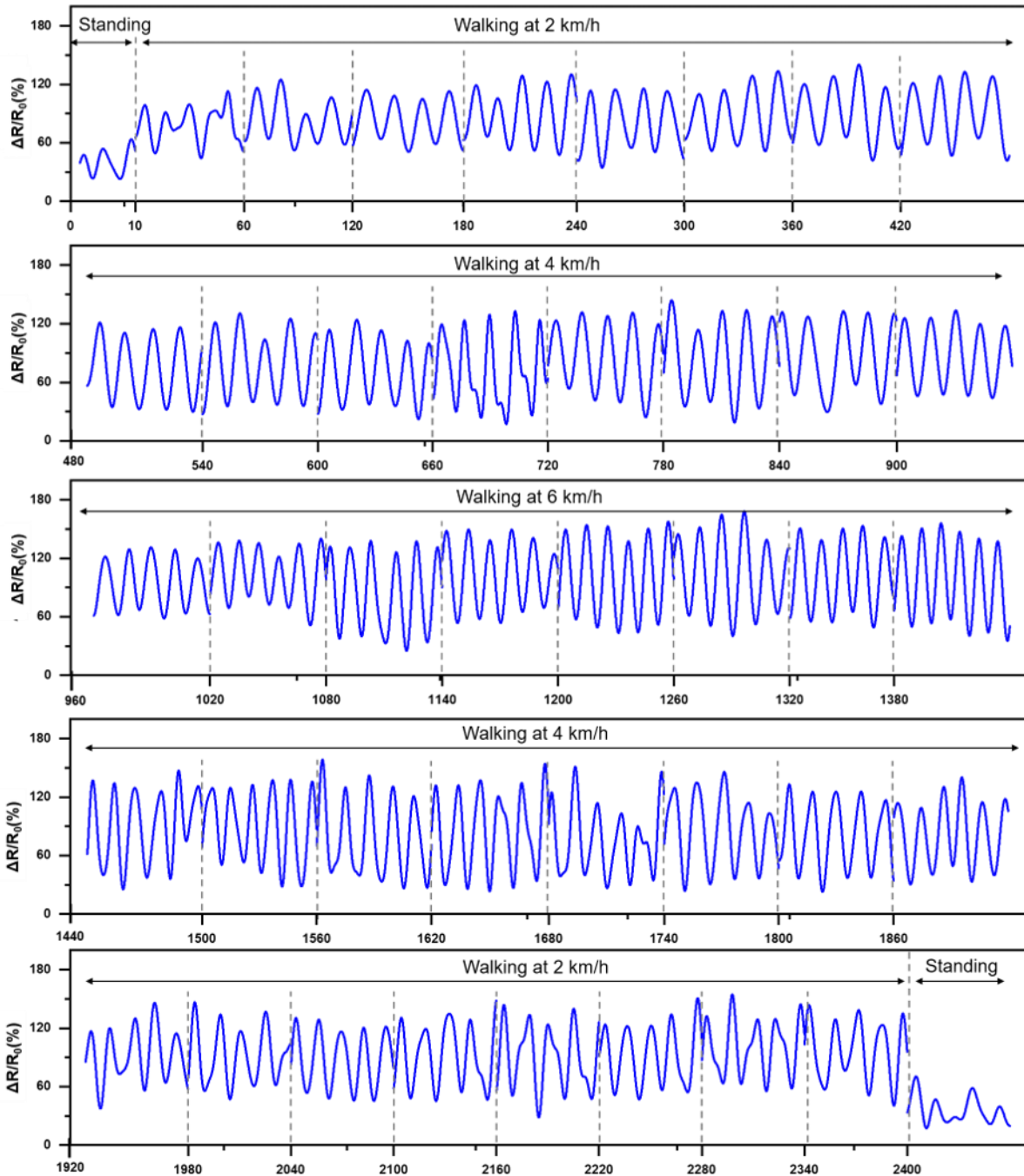


Figure 7-18. Plots of the filtered resistance changes measured from the smart band while the subject is standing stationary, walking on the treadmill at 2 km/h, 4 km/h, 6km/h, 4km/h, 2 km/h, and back to standing. In each section, 10 seconds changes of resistance were selected to represent respiration rate and intensity.

7.4 Conclusion

In this study, a smart band integrated with embroidered electrodes and the strain sensor was

developed to monitor ECG and respiration pattern. The effects of three levels wearing pressure on the signal quality were investigated in static status and six dynamic conditions. And then, the performance of the smart band in walking for monitoring body temperature, humidity, ECG and respiratory rate was evaluated. The results showed that ECG waveforms and respiratory signals were recorded completely in sitting and standing measurement conditions, and there was no significant difference between three levels of wearing pressure. The tracking signals of respiration and ECG had similar morphology to those of reference systems. In dynamic measurement, the signal quality was less likely to be influenced by motion artefacts under 1.5 kPa wearing pressure. Moreover, the walking tests demonstrated that the smart band was able to measure representative respiratory and ECG waveform features, body temperature and humidity in various levels of treadmill speed with 1.5 kPa wearing pressure. Also, this study confirmed that the increased humidity in body-clothing microclimate could enhance the ECG monitoring performance of dry electrodes. Since the proposed system has not yet been verified for users with various gender, ages and physiological characteristics, it needs to be generalized through follow-up experiments involving more diverse subjects. The comfort, durability and resistance to laundering of proposed smart band is also required to explore in future study.

Supporting information

Table S7-1. The p-value from the two-way ANOVA analysis

Wearing pressure Two-way ANOVA		Static measurement			Dynamic measurement		
		0.5 kPa	1.5 kPa	2.5 kPa	0.5 kPa	1.5 kPa	2.5 kPa
Subject 1	Measuring conditions	0.19265	0.90333	0.09993	0.03659	0.08906	0.8491
	Measurement systems	0.89846	0.48788	0.96423	0.00834	0.14806	0.70912
	Interaction	0.66614	0.18531	0.72752	0.0072	0.18599	0.54429
Subject 2	Measuring conditions	0.87081	0.36627	0.12191	0.00012	0.36792	0.75689
	Measurement systems	0.64604	0.96198	0.77768	2.94E-10	0.06433	0.07072
	Interaction	0.84654	0.97539	0.96526	0.00129	0.88293	0.78195
Subject 3	Measuring conditions	0.57018	0.94818	0.48527	0.00003	0.06915	0.30836
	Measurement systems	0.82965	0.21289	0.40018	4.18E-08	0.06765	0.33491
	Interaction	0.84023	0.59419	0.98813	0.00126	0.19793	0.45940

The p-value is listed for the different respiration rate for each subject.

Table S7-2. Statistical results for QRS complex detection in static measurement conditions.

Subject	WP (kPa)	MC	TP (Beats)	FN (Beats)	FP (Beats)	Sensitivity (%)	Accuracy (%)
Subject 1	0.5	Sitting	182	20	0	90.10	90.10
		Standing	199	23	0	89.64	89.64
	1.5	Sitting	185	6	0	96.86	96.86
		Standing	216	7	0	96.86	96.86
	2.5	Sitting	195	3	0	98.48	98.48
		Standing	227	2	0	99.13	99.13
Subject 2	0.5	Sitting	165	29	0	85.05	85.05
		Standing	187	31	0	85.78	85.78
	1.5	Sitting	189	5	0	97.42	97.42
		Standing	207	6	0	97.18	97.18
	2.5	Sitting	194	2	0	98.98	98.98
		Standing	211	1	0	99.53	99.53
Subject 3	0.5	Sitting	179	21	0	89.50	89.50
		Standing	193	25	0	88.53	88.53
	1.5	Sitting	184	7	0	96.34	96.34
		Standing	187	9	0	95.41	95.41
	2.5	Sitting	193	2	0	98.97	98.97
		Standing	205	3	0	98.56	98.56

Table S7-3 ANOVA results for QRS complex detection in static measurement conditions.

MC	WP (kPa)	Sensitivity (%)		P value
		Mean	SD	
Sitting	0.5	88.22	2.76	1.03E-09
	1.5	96.87	0.54	
	2.5	98.81	0.29	
Standing	0.5	87.98	1.99	1.03E-9
	1.5	96.48	0.94	
	2.5	99.07	0.49	

Table S7-4. Statistical results for QRS complex detection in dynamic measurement conditions.

Subject	WP (kPa)	MC	TP (Beats)	FN (Beats)	FP (Beats)	Sensitivity (%)	Accuracy (%)
Subject 1	0.5	AF	30	15	5	66.67	60.00
		AU	27	19	7	58.70	50.94
		AS	15	29	5	34.09	30.61
		AB	32	11	3	74.42	69.57
		TL	36	9	1	80.00	78.26
		TR	32	12	1	72.73	71.11
	1.5	AF	39	7	0	84.78	84.78
		AU	35	10	4	77.78	71.43
		AS	37	9	0	80.43	80.43
		AB	41	4	0	91.11	91.11
		TL	42	1	0	97.67	97.67
		TR	43	1	0	97.73	97.73
	2.5	AF	37	8	0	82.22	82.22
		AU	22	24	8	47.83	40.74
		AS	44	3	0	93.62	93.62
		AB	43	2	0	95.56	95.56
		TL	44	1	0	97.78	97.78
		TR	42	2	0	95.45	95.45
Subject 2	0.5	AF	30	13	9	69.77	57.69
		AU	27	16	9	62.79	51.92
		AS	16	28	14	36.36	27.59
		AB	32	14	5	69.57	62.75
		TL	38	7	2	84.44	80.85
		TR	33	12	3	73.33	68.75

Subject 3	1.5	AF	40	5	3	88.89	83.33	
		AU	35	9	5	79.55	71.43	
		AS	37	6	2	86.05	82.22	
		AB	42	3	1	93.33	91.30	
		TL	42	1	0	97.67	97.67	
		TR	42	1	0	97.67	97.67	
	2.5	AF	37	8	1	82.22	80.43	
		AU	25	23	9	52.08	43.86	
		AS	40	4	1	90.91	88.89	
		AB	45	1	1	97.83	95.74	
		TL	46	1	0	97.87	97.87	
		TR	44	1	0	97.78	97.78	
	Subject 3	0.5	AF	28	16	9	63.64	52.83
			AU	25	20	9	55.56	46.30
AS			20	24	20	45.45	31.25	
AB			35	10	5	77.78	70.00	
TL			41	4	2	91.11	87.23	
TR			40	6	10	86.96	71.43	
1.5		AF	40	6	3	86.96	81.63	
		AU	36	9	5	80.00	72.00	
		AS	38	7	2	84.44	80.85	
		AB	43	2	1	95.56	93.48	
		TL	42	1	0	97.67	97.67	
		TR	43	1	0	97.73	97.73	
2.5		AF	35	10	1	77.78	76.09	
		AU	25	22	9	53.19	44.64	
	AS	40	5	1	88.89	86.96		
	AB	44	1	1	97.78	95.65		
	TL	44	2	0	95.65	95.65		
	TR	45	1	0	97.83	97.83		

Table S7-5 ANOVA results for QRS complex detection in dynamic measurement conditions.

MC	WP	Sensitivity			Accuracy		
		Mean	SD	p-value	Mean	SD	p-value
AF	0.5	66.69	3.07		56.84	3.66	
	1.5	86.88	2.05	3.68E-01	83.25	1.58	6.58E-05
	2.5	80.74	2.57		79.58	3.16	
AU	0.5	59.01	3.63	4.18E-05	49.72	3.01	7.58E-06

	1.5	79.11	1.17		71.62	0.33	
	2.5	51.03	2.83		43.08	2.06	
	0.5	38.64	6.01		29.82	1.96	
AS	1.5	83.64	2.89	8.37E-06	81.17	0.94	1.39E-07
	2.5	91.14	2.37		89.82	3.43	
	0.5	73.92	4.13		67.44	4.07	
AB	1.5	93.33	2.22	1.15E-04	91.96	1.31	1.61E-05
	2.5	97.05	1.30		95.65	0.09	
	0.5	85.19	5.59		97.10	1.26	
TL	1.5	97.67	0.00	5.88E-03	82.12	4.62	7.13E-04
	2.5	97.10	1.26		97.67	0.00	
	0.5	77.67	8.05		70.43	1.46	
TR	1.5	97.71	0.03	3.14E-03	97.71	0.03	1.62E-07
	2.5	97.02	1.36		97.02	1.36	

CHAPTER 8. CONCLUSIONS AND SUGGESTIONS FOR FUTURE WORK

8.1 Conclusions

Based on the investigation of sewing ability of conductive yarns for embroidery techniques, this thesis has explored the characterization of conductive tracks fabricated with lock-stitch embroidery techniques. Technical methodologies of stretchable interconnects, electrodes for ECG monitoring, and a strain sensor with advanced hybrid embroidery techniques for respiration measurement were investigated and evaluated. Along with a smart band prototype development and subject experiments, the impact of wearing pressure and body movements on real-time ECG and respiratory rate monitoring was explored.

The first objective has been achieved by evaluation of various conductive yarns sewing ability and performance of conductive tracks embroidered on knitted fabrics, which was fulfilled in Chapter 3. After tensile test and sewn with 602 type stitch, the silver-coated conductive yarns were found can be used as needle thread for lock-stitch embroidery since their tenacity was fit for small radius loop formation. The equation to calculate needle size was achieved based on the diameter of conductive yarns. Moreover, the analysis of conductive tracks with multi-direction lock-stitch embroidery indicated ED and SL significantly affect size shrinkage, SL and ES significantly affect resistance of conductive tracks. An optimal embroidery condition (SL=4 mm, ES=200 rpm, NTP=30 gf) to embroider conductive tracks that trade off the lower resistance and size shrinkage.

The second objective is to investigate optimal embroidery parameters for enhanced conductivity and stretchability of interconnects, which was completed in Chapter 4. Using conductive threads in needle and bobbin together results in the highest conductivity, and resistance value of interconnects reduced 50% than original yarns. There was no significant difference between stitch types of 301, 304 and 308. Based on the results, zigzag-shaped and

horseshoe-shaped were designed and embroidered by lock-stitch and TFP techniques respectively. The horseshoe-shaped interconnect proposed in this study ($R = 5\text{mm}$ and $\theta = 45^\circ$) shows significant elongation over 130% and can remain stable resistance during stretching. Besides, the embroidered interconnects were applied as conductive interconnects in a LED circuit to demonstrate the stretchability for fitting arm and leg movement requirements of smart clothing.

The third object is to design and evaluate in time ECG signal monitoring performance of textile-based electrodes embroidered with silver coated polyamide threads, which is accomplished in Chapter 5. Embroidered electrodes with area size of $20\text{ mm} \times 40\text{ mm}$, 1 mm filling density, single layer and 304 stitch types have lower skin-electrodes contact impedance at 1 Hz frequency. The subject test for ECG monitoring found electrodes embroidered with EP2 pattern has the highest CC value ($r=0.959$) compared with Ag/AgCl electrodes under 2.5 kPa wearing pressure. In details, the RR, QRS intervals, PH and RH of 200 s ECG waveforms measured by EP2 are exactly the same with Ag/AgCl electrodes. Additionally, it has been explored that the EP2 pattern electrodes could reach the lowest surface resistance under 2.5 kPa wearing pressure since the conductive threads overlapped in filling stitch structures.

To achieve the fourth objective, a strain sensor hybrid embroidered with elastane yarns, conductive yarns and polyester threads was developed to monitor human respiration, which is presented in Chapter 6. The design parameters, which were 10 mm width of conductive area, conductive yarns filling with 0.3 mm, and 2 mm between elastane yarns, has been drawn with best balance of GF and EC. The electromechanical performance of optimal sample shows 32.4 GF at 40% elongation. Taking advantage of elastane threads in substrate, the sensor shows less electro-mechanical hysteresis with 5%, 10% and 15% strain and stable stretching-releasing performance within 1000 cycles. Moreover, the tests with an elastic band integrated the sensor to measure respiration signals found the normal breathing and deeply slow breathing can be detected clearly and accurately. A base line drift was found in shallow fast breathing since the noise impact from motion artefact in chest.

To address application for smart e-textile wearables for physiological signal monitoring, a smart band prototype has been developed by embroidery techniques in Chapter 7, which achieve the fifth objective. The smart band integrated embroidered electrodes for ECG monitoring, an embroidered strain sensor for respiratory rate measurement, and the electronic temperature & humidity sensor. Analysing the data collected by a tailored Android APP through Bluetooth, ECG waveforms and respiratory signals were similar to referred measurement systems in static measurement conditions at each level of wearing pressure. Wearing pressure at 1.5 kPa can ensure the quality of ECG and respiratory signals in six body dynamic measurement conditions. Additionally, the walking tests demonstrated that the smart band under 1.5 kPa wearing pressure was able to measure representative respiratory and ECG waveform features, body temperature and humidity at various levels of treadmill speed. Also, this study confirmed that the increased humidity in body-clothing microclimate could significantly improve the ECG signal quality monitored by dry electrodes.

8.2 Limitation

Due to limited time and resources, the limitations in the research work of the thesis are:

- 1) Cardiologists may feel difficult to interpret the ECG signals monitored by embroidered electrodes since the contact impedance of embroidered electrodes was higher than Ag/AgCl electrodes. The clinical application of embroidered electrodes has not been investigated in this thesis.
- 2) Material types of clothing could affect the sensitivity of HESS since the functional area of sensors were directly exposed without any shielding. The performance of HESS after laundry was not investigated in this thesis.
- 3) Participants to attend the wear trials were postponed and limited due to the COVID-19 pandemics.

8.3 Suggestions for future work

Although the objectives have been completed, there are still some limitations in the current work. Therefore, several suggestions for future work are recommended as follows.

- 1) Investigating clinical application of developed smart band and update the functions of bio-signal real time monitoring.
- 2) Verifying the performance of developed smart band for diverse users at different ages, genders, BMI and body shapes, etc.
- 3) Exploiting skin friendly materials integration on the smart band to improve dynamic monitoring performance.
- 4) Follow-up experiments of laundry reliability since the embroidery techniques are versatile to design detachable and changeable electrodes and sensors.

REFERENCES

- [1] Trung TQ, Lee NE. Flexible and Stretchable Physical Sensor Integrated Platforms for Wearable Human-Activity Monitoring and Personal Healthcare. *Adv Mater* 2016; 28: 4338–4372.
- [2] Amjadi M, Pichitpajongkit A, Lee S, et al. Highly stretchable and sensitive strain sensor based on silver nanowire-elastomer nanocomposite. *ACS Nano* 2014; 8: 5154–5163.
- [3] Lee YH, Kim Y, Lee TI, et al. Anomalous Stretchable Conductivity Using an Engineered Tricot Weave. *ACS Nano* 2015; 9: 12214–12223.
- [4] Yun J, Song C, Lee H, et al. Stretchable array of high-performance micro-supercapacitors charged with solar cells for wireless powering of an integrated strain sensor. *Nano Energy* 2018; 49: 644–654.
- [5] Kim D, Kim D, Lee H, et al. Body-Attachable and Stretchable Multisensors Integrated with Wirelessly Rechargeable Energy Storage Devices. *Adv Mater* 2016; 28: 748–756.
- [6] Magenes G, Curone D, Caldani L, et al. Fire Fighters and rescuers monitoring through wearable sensors: The ProeTEX project. *2010 Annu Int Conf IEEE Eng Med Biol Soc EMBC'10* 2010; 3594–3597.
- [7] Notley SR, Flouris AD, Kenny GP. On the use of wearable physiological monitors to assess heat strain during occupational heat stress. *Appl Physiol Nutr Metab* 2018; 5: 869–881.
- [8] Feese S, Arnrich B, Troster G, et al. CoenoFire: Monitoring Performance Indicators of Firefighters in Real-world Missions Using Smartphones. In: *Proceedings of the 2013 ACM International Joint Conference on Pervasive and Ubiquitous Computing*. Zurich, Switzerland, pp. 83–92.
- [9] Tao X. *Handbook of smart textiles*. Singapore: Springer Science & Business Media, 2015. Epub ahead of print 2015. DOI: 10.1007/978-981-4451-45-1.
- [10] Selm B a R, Bischoff B, Seidl R. 12 Embroidery and smart textiles. In: Tao XM (ed) *Smart Fibres, Fabrics and Clothing*. Cambridge: Woodhead Publishing Limited and CRC Press LLC, pp. 218–225.
- [11] Hahner J, Hinüber C, Breier A, et al. Adjusting the mechanical behavior of embroidered scaffolds to lapin anterior cruciate ligaments by varying the thread materials. *Text Res J* 2015; 85: 1431–1444.
- [12] Trindade IG, da Silva JM, Miguel R, et al. Design and evaluation of novel textile wearable systems for the surveillance of vital signals. *Sensors* 2016; 16: 1573.

- [13] Kannaian T, Neelaveni R, Thilagavathi G. Design and development of embroidered textile electrodes for continuous measurement of electrocardiogram signals. *J Ind Text* 2012; 42: 303–318.
- [14] Shafti A, Ribas Manero RB, Borg AM, et al. Embroidered Electromyography: A Systematic Design Guide. *IEEE Trans Neural Syst Rehabil Eng* 2017; 25: 1472–1480.
- [15] Vališevskis A, Briedis U, Juchnevičienė Ž, et al. Design improvement of flexible textile aluminium- air battery. *J Text Inst* 2019; 0: 1–6.
- [16] Post ER, Orth M, Russo PR, et al. E-broidery: Design and fabrication of textile-based computing. *IBM Syst J* 2000; 39: 840–860.
- [17] Linz T, Simon EP, Walter H. Modeling embroidered contacts for electronics in textiles. *J Text Inst* 2012; 103: 644–653.
- [18] Martínez-Estrada M, Moradi B, Fernández-García R, et al. Impact of conductive yarns on an embroidery textile moisture sensor. *Sensors (Switzerland)*; 19. Epub ahead of print 2019. DOI: 10.3390/s19051004.
- [19] Roh J-S. Textile touch sensors for wearable and ubiquitous interfaces. *Text Res J* 2014; 84: 739–750.
- [20] Roh J-S, Kim S. All-fabric intelligent temperature regulation system for smart clothing applications. *J Intell Mater Syst Struct* 2016; 27: 1165–1175.
- [21] Hesarian MS, Najari SS, Shirazi RS. Design and fabrication of a fabric for electromagnetic filtering application (Experimental and modeling analysis). *J Text Inst* 2018; 109: 775–784.
- [22] Agcayazi T, Chatterjee K, Bozkurt A, et al. Flexible Interconnects for Electronic Textiles. *Adv Mater Technol* 2018; 3: 1–32.
- [23] Lou CW, He CH, Lin JH. *Manufacturing techniques and property evaluations of conductive elastic knits*. 2019. Epub ahead of print 2019. DOI: 10.1177/1528083718791343.
- [24] Li Q, Tao X. A stretchable knitted interconnect for three-dimensional curvilinear surfaces. *Text Res J* 2011; 81: 1171–1182.
- [25] Yokus MA, Foote R, Jur JS. Printed Stretchable Interconnects for Smart Garments: Design, Fabrication, and Characterization. *IEEE Sens J* 2016; 16: 7967–7976.
- [26] Lee WJ, Park JY, Nam HJ, et al. The development of a highly stretchable, durable, and printable textile electrode. *Text Res J* 2019; 89: 4104–4113.
- [27] Jin H, Matsuhisa N, Lee S, et al. Enhancing the Performance of Stretchable Conductors for E-Textiles by Controlled Ink Permeation. *Adv Mater*; 29. Epub ahead

- of print 2017. DOI: 10.1002/adma.201605848.
- [28] Linz T, Kallmayer C, Aschenbrenner R, et al. Embroidering electrical interconnects with conductive yarn for the integration of flexible electronic modules into fabric. *Proc - Int Symp Wearable Comput ISWC* 2005; 2005: 86–89.
- [29] Roh J-S. All-fabric interconnection and one-stop production process for electronic textile sensors. *Text Res J* 2017; 87: 1445–1456.
- [30] Daniel IH, Flint JA, Seager R. Stitched transmission lines for wearable RF devices. *Microw Opt Technol Lett* 2017; 59: 1048–1052.
- [31] Weder M, Hegemann D, Amberg M, et al. Embroidered electrode with silver/titanium coating for long-term ECG monitoring. *Sensors* 2015; 15: 1750–1759.
- [32] Pola T, Vanhala J. Textile electrodes in ECG measurement. *Proceedings of the 2007 International Conference on Intelligent Sensors, Sensor Networks and Information Processing, ISSNIP 2007*; 635–639.
- [33] Cömert A, Honkala M, Hyttinen J. Effect of pressure and padding on motion artifact of textile electrodes. *Biomed Eng Online* 2013; 12: 1–18.
- [34] Yamada T, Hayamizu Y, Yamamoto Y, et al. A stretchable carbon nanotube strain sensor for human-motion detection. *Nat Nanotechnol* 2011; 6: 296–301.
- [35] Kayser L V., Lipomi DJ. Stretchable Conductive Polymers and Composites Based on PEDOT and PEDOT:PSS. *Adv Mater* 2019; 1806133: 1806133.
- [36] Yin B, Wen Y, Hong T, et al. Highly Stretchable, Ultrasensitive, and Wearable Strain Sensors Based on Facilely Prepared Reduced Graphene Oxide Woven Fabrics in an Ethanol Flame. *ACS Appl Mater Interfaces* 2017; 9: 32054–32064.
- [37] Atalay O, Kennon WR, Demirok E. Weft-knitted strain sensor for monitoring respiratory rate and its electro-mechanical modeling. *IEEE Sens J* 2015; 15: 110–122.
- [38] Wang J, Soltanian S, Servati P, et al. A knitted wearable flexible sensor for monitoring breathing condition. *J Eng Fiber Fabr*; 15. Epub ahead of print 2020. DOI: 10.1177/1558925020930354.
- [39] Wang X, Li Q, Tao X. Sensing mechanism of a carbon nanocomposite-printed fabric as a strain sensor. *Compos Part A Appl Sci Manuf* 2021; 144: 106350.
- [40] Cai G, Yang M, Xu Z, et al. Flexible and wearable strain sensing fabrics. *Chem Eng J* 2017; 325: 396–403.
- [41] Fu YF, Li YQ, Liu YF, et al. High-Performance Structural Flexible Strain Sensors Based on Graphene-Coated Glass Fabric/Silicone Composite. *ACS Appl Mater Interfaces* 2018; 10: 35503–35509.

- [42] Seyedin S, Zhang P, Naebe M, et al. Textile strain sensors: A review of the fabrication technologies, performance evaluation and applications. *Mater Horizons* 2019; 6: 219–249.
- [43] Wang C, Li X, Gao EL, et al. Carbonized silk fabric for ultrastretchable, highly sensitive, and wearable strain sensors. *Adv Mater* 2016; 28: 6640–6648.
- [44] Park S, Ahn S, Sun J, et al. Highly Bendable and Rotational Textile Structure with Prestrained Conductive Sewing Pattern for Human Joint Monitoring. *Adv Funct Mater* 2019; 29: 1–12.
- [45] Park J, Park S, Ahn S, et al. Wearable Strain Sensor Using Conductive Yarn Sewed on Clothing for Human Respiratory Monitoring. *IEEE Sens J* 2020; 3000923.
- [46] Hunter AL, Shah ASV, Langrish JP, et al. Fire simulation and cardiovascular health in firefighters. *Circulation* 2017; 135: 1284–1295.
- [47] Cho H, Lim H, Cho S. Efficacy research of electrocardiogram and heart rate measurement in accordance with the structure of the textile electrodes. *Fibers Polym* 2016; 17: 2069–2077.
- [48] Tsukada YT, Tokita M, Murata H, et al. Validation of wearable textile electrodes for ECG monitoring. *Heart Vessels* 2019; 34: 1203–1211.
- [49] Amjadi M, Kyung KU, Park I, et al. Stretchable, Skin-Mountable, and Wearable Strain Sensors and Their Potential Applications: A Review. *Adv Funct Mater* 2016; 26: 1678–1698.
- [50] Gonçalves C, Ferreira da Silva A, Gomes J, et al. Wearable E-Textile Technologies: A Review on Sensors, Actuators and Control Elements. *Inventions* 2018; 3: 14.
- [51] Locher I. *Technologies for system-on-textile integration*. SWISS FEDERAL INSTITUTE OF TECHNOLOGY ZURICH. Epub ahead of print 2006. DOI: 10.3929/ETHZ-B-000225616.
- [52] Xiao X, Pirbhulal S, Dong K, et al. Performance Evaluation of Plain Weave and Honeycomb Weave Electrodes for Human ECG Monitoring. *J Sensors* 2017; 2017: 1–13.
- [53] Zysset C, Kinkeldei T, Münzenrieder N, et al. Combining electronics on flexible plastic strips with textiles. *Text Res J* 2013; 83: 1130–1142.
- [54] Li L, Au WM, Li Y, et al. A Novel Design Method for an Intelligent Clothing Based on Garment Design and Knitting Technology. *Text Res J* 2009; 79: 1670–1679.
- [55] Atalay O, Kennon W. Knitted Strain Sensors: Impact of Design Parameters on Sensing Properties. *Sensors* 2014; 14: 4712–4730.

- [56] Paul G, Torah R, Beeby S, et al. Novel active electrodes for ECG monitoring on woven textiles fabricated by screen and stencil printing. *Sensors Actuators, A Phys* 2015; 221: 60–66.
- [57] Grabham NJ, Li Y, Clare LR, et al. Fabrication Techniques for Manufacturing Flexible Coils on Textiles for Inductive Power Transfer. *IEEE Sens J* 2018; 18: 2599–2606.
- [58] Linz T, Viero R, Dils C, et al. Embroidered Interconnections and Encapsulation for Electronics in Textiles for Wearable Electronics Applications. *Adv Sci Technol* 2008; 60: 85–94.
- [59] Polanský R, Soukup R, Řeboun J, et al. A novel large-area embroidered temperature sensor based on an innovative hybrid resistive thread. *Sensors Actuators, A Phys* 2017; 265: 111–119.
- [60] Bonaldi RR. *Electronics used in high-performance apparel—Part 1/2*. Elsevier Ltd. Epub ahead of print 2018. DOI: 10.1016/B978-0-08-100904-8.00014-6.
- [61] Forster Rohner. Illuminated Textiles - Forster Rohner Textile Innovations, <http://www.frti.ch/en/technology/illuminated-textiles.html> (accessed 18 June 2018).
- [62] Mecnika V, Scheulen K, Anderson CF, et al. 7 Joining technologies for electronic textiles. In: Dias T (ed) *Electronic Textiles: Smart Fabrics and Wearable Technology*. Cambridge: Woodhead Publishing Limited, 2015, pp. 133–153.
- [63] ZSK. ZSK Special Embroidery Machines. www.zsk.de, <https://www.zsk.de/special-embroidery-machines.html> (2018, accessed 18 June 2018).
- [64] Mecnika V, Hoerr M, Krievins I, et al. Technical Embroidery for Smart Textiles: Review. *Mater Sci Text Cloth Technol* 2014; 9: 56–63.
- [65] Bosowski P, Hoerr M, Mecnika V, et al. 4 Design and manufacture of textile-based sensors. In: Dias T (ed) *Electronic Textiles: Smart Fabrics and Wearable Technology*. Cambridge: Woodhead Publishing Limited, 2015, pp. 75–107.
- [66] Eberle H. *Clothing technology : from fibre to fashion*. 5th ed. Haan-Gruiten : Europa-Lehrmittel, 2008.
- [67] Radavičienė S, Juciene M. Influence of embroidery threads on the accuracy of embroidery pattern dimensions. *Fibres Text East Eur* 2012; 92: 92–97.
- [68] Roh JS, Chi YS, Lee JH, et al. Characterization of embroidered inductors. *Smart Mater Struct*; 19. Epub ahead of print 2010. DOI: 10.1088/0964-1726/19/11/115020.
- [69] Yang JH, Cho HS, Lee JH. An analysis on the luminance efficiency of the machine embroidery method applied to flexible plastic optical fiber for realization of the textile display. *Text Res J*. Epub ahead of print 2017. DOI: 10.1177/0040517517703197.

- [70] A.Schwarz, I.Kazani, L.Cuny, et al. Electro-conductive and elastic hybrid yarns-The effects of stretching, cyclic straining and washing on their electro-conductive properties. *Mater Des* 2011; 32: 4247–4256.
- [71] Locher I, Klemm M, Kirstein T, et al. Design and Characterization of Purely Textile Patch Antennas. *IEEE Trans Adv Packag* 2006; 29: 777–788.
- [72] Schwarz A, Hakuzimana J, Westbroek P, et al. How to Equip Para-aramide Yarns with Electro-conductive Properties. In: *2009 Sixth International Workshop on Wearable and Implantable Body Sensor Networks*. 2009, pp. 278–281.
- [73] Oh KW, Park HJ, Kim SH. Stretchable Conductive Fabric for Electrotherapy. *J Appl Polym Sci* 2003; 88: 1225–1229.
- [74] Schwarz A, Cuny L, Hertleer C, et al. Electrical circuit model of elastic and conductive yarns produced by hollow spindle spinning. *Materials Technology* 2011; 26: 121–127.
- [75] Radavičiene S, Juciene M, Juchnevičiene Ž, et al. The influence of the properties of embroidery threads on buckling of fabric inside of the embroidered element. *Mater Sci* 2012; 18: 373–378.
- [76] Orth M. Defining Flexibility and Sewability in Conductive Yarns. *Mater Res Soc Symp Proc* 2003; 736: 37–48.
- [77] Radostina A. Angelova; Daniela Sofronova VN. A Case Study on the Defects in Industrial Manufacturing of Embroidered Textiles. *J Multidiscip Eng Sci Technol* 2016; 3: 6373–6376.
- [78] Daukantienė V, Laurinavičiūtė I. The synergism of design and technology for the optimisation of embroidery motifs in clothing. *Int J Cloth Sci Technol* 2013; 25: 350–360.
- [79] El-Kateb SN. an investigation of factors affect ends-down rate in embroidery machine. *J Am Sci* 2015; 11: 39–42.
- [80] Juchnevičienė Ž, Jucienė M, Radavičienė S. The Research on the Width of the Closed-Circuit Square-shaped Embroidery Element. *Mater Sci* 2017; 23: 186–190.
- [81] Juchnevičienė Ž, Briedis U, Vališevskis A, et al. Electrical conductivity of a closed-circuit embroidery element. *Proc Est Acad Sci* 2018; 67: 158–164.
- [82] Wang F, Zhu B, Shu L, et al. Flexible pressure sensors for smart protective clothing against impact loading. *Smart Mater Struct*; 23. Epub ahead of print 2014. DOI: 10.1088/0964-1726/23/1/015001.
- [83] Li Q, Tao X. Three-dimensionally deformable, highly stretchable, permeable, durable and washable fabric circuit boards. *Proc R Soc A Math Phys Eng Sci* 2014; 470: 20140472–20140472.

- [84] Xu S, Zhang Y, Jia L, et al. Soft Microfluidic Assemblies of for the Skin. *Science* (80-) 2014; 344: 70–74.
- [85] Tao X, Koncar V. 25 Textile electronic circuits based on organic fibrous transistors. In: *Smart Textiles and Their Applications*. 2016, pp. 569–598.
- [86] Brosteaux D, Axisa F, Gonzalez M, et al. Design and fabrication of elastic interconnections for stretchable electronic circuits. *IEEE Electron Device Lett* 2007; 28: 552–554.
- [87] Hsu Y-Y, Gonzalez M, Bossuyt F, et al. Design and analysis of a novel fine pitch and highly stretchable interconnect. *Microelectron Int* 2010; 27: 33–38.
- [88] Gonzalez M, Axisa F, Bulcke M Vanden, et al. Design of metal interconnects for stretchable electronic circuits. *Microelectron Reliab* 2008; 48: 825–832.
- [89] Gonzalez M, Vandeveldel B, Christiaens W, et al. Design and implementation of flexible and stretchable systems. *Microelectron Reliab* 2011; 51: 1069–1076.
- [90] Plovie B, Vanfleteren J, Vervust T, et al. Design Automation of Meandered Interconnects for Stretchable Circuits. *IEEE Trans Comput Des Integr Circuits Syst* 2019; 38: 1648–1660.
- [91] Fan Z, Zhang Y, Ma Q, et al. A finite deformation model of planar serpentine interconnects for stretchable electronics. *Int J Solids Struct* 2016; 91: 46–54.
- [92] Coyle S, Diamond D. 10 Medical Applications of Smart Textiles. In: Langenhove L va. (ed) *Advances in Smart Medical Textiles: Treatments and Health Monitoring*. Cambridge: Woodhead Publishing, 2016, pp. 215–237.
- [93] Majumder S, Mondal T, Deen M. Wearable Sensors for Remote Health Monitoring. *Sensors* 2017; 17: 130.
- [94] Bystřický T, Moravcova D, Kaspar P, et al. A comparison of embroidered and woven textile electrodes for continuous measurement of ECG. *Proc Int Spring Semin Electron Technol* 2016; 2016-Sept: 7–11.
- [95] Ankhili A, Zaman S uz, Tao X, et al. Washable embroidered textile electrodes for long-term electrocardiography monitoring. *Text leather Rev* 2019; 2: 126–135.
- [96] Xu PJ, Liu H, Zhang H, et al. Electrochemical Modification of Silver Coated Multifilament for Wearable ECG Monitoring Electrodes. *Adv Mater Res* 2011; 332–334: 1019–1023.
- [97] Zhang H, Li W, Tao X, et al. Textile-structured human body surface biopotential signal acquisition electrode. *Proc - 4th Int Congr Image Signal Process CISP 2011* 2011; 5: 2792–2797.

- [98] Mecnika V, Jockehoefel S, Schwarz-pfeiffer A. Preliminary Study on Textile Humidity Sensors. In: *Smart SysTech*. Aachen, Germany, 2015, pp. 1–9.
- [99] Meyer J, Lukowicz P, Tröster G. Textile pressure sensor for muscle activity and motion detection. *Proc - Int Symp Wearable Comput ISWC 2006*; 69–74.
- [100] Liu X, Lillehoj PB. Embroidered electrochemical sensors on gauze for rapid quantification of wound biomarkers. *Biosens Bioelectron* 2017; 98: 189–194.
- [101] Seesaard T, Lorwongtragool P, Kerdcharoen T. Development of fabric-based chemical gas sensors for use as wearable electronic noses. *Sensors (Switzerland)* 2015; 15: 1885–1902.
- [102] Vena A, Koski K, Moradi E, et al. An Embroidered Two-Dimensional Chipless Strain Sensor for Wireless Structural Deformation Monitoring. *IEEE Sens J* 2013; 13: 4627–4637.
- [103] Liu Y, Yu M, Xia B, et al. E-Textile Battery-Less Displacement and Strain Sensor for Human Activities Tracking. *IEEE Internet Things J* 2021; 8: 16486–16497.
- [104] Martínez-Estrada M, Gil I, Fernández-García R. An Alternative Method to Develop Embroidery Textile Strain Sensors. *Textiles* 2021; 1: 504–512.
- [105] Bubonia JE. Thread Specifications. In: Janace E. Bubonia (ed) *Apparel Production Terms and Processes*. New York: Fairchild Books, 2017, pp. 102–109.
- [106] Rudolf A, Geršak J. Study of the relationship between deformation of the thread and built-in fibres. *Int J Cloth Sci Technol* 2001; 13: 289–300.
- [107] Bedeloglu A, Sunter N, Yildirim B, et al. Bending and tensile properties of cotton/metal wire complex yarns produced for electromagnetic shielding and conductivity applications. *J Text Inst* 2012; 103: 1304–1311.
- [108] Stylios GK, Zhu R. The Mechanism of Sewing Damage in Knitted Fabrics. *J Text Inst* 1998; 89: 411–421.
- [109] Laing RM (Raechel), Webster J. 5 Surface characteristics and appearance of seams. In: *Stitches and seams*. Manchester, UK: The Textile Institute, 1998, pp. 51–65.
- [110] Hayes SG, McLoughlin J. 10 Technological advances in sewing garments. In: Catherine Fairhurst (ed) *Advances in Apparel Production*. Woodhead Publishing Limited and CRC Press LLC, 2008, pp. 197–221.
- [111] Sewing machine needles for the apparel industry. *Groz-Beckert KG*, www.groz-beckert.com.
- [112] ASTM D8007-15: Standard Test Method for Wale and Course Count of Weft Knitted Fabrics.

- [113] Choudhary AK, Sikka MP, Bansal P. The study of sewing damages and defects in garments. *Res J Text Appar* 2018; 22: 109–125.
- [114] Morton WE, Hearle JWS. 17 Directional effects. In: Boca Raton (ed) *Physical Properties of Textile Fibres*. Cambridge: Woodhead Publishing Limited and CRC Press LLC, 2008, pp. 414–457.
- [115] Trung TQ, Lee NE. Flexible and Stretchable Physical Sensor Integrated Platforms for Wearable Human-Activity Monitoring and Personal Healthcare. *Adv Mater* 2016; 28: 4338–4372.
- [116] Shi J, Liu S, Zhang L, et al. Smart Textile-Integrated Microelectronic Systems for Wearable Applications. *Adv Mater* 2019; 31: 1901958: 1–37.
- [117] Barker L, Burnstein B, Mercer J. Acceleration profile of an acrobatic act during training and shows using wearable technology. *Sport Biomech* 2018; 31(1): 1–12.
- [118] Tao X, Huang T-H, Shen C-L, et al. Bluetooth Low Energy-Based Washable Wearable Activity Motion and Electrocardiogram Textronic Monitoring and Communicating System. *Adv Mater Technol* 2018; 3: 1700309.
- [119] Gopalsamy C, Park S, Rajamanickam R, et al. The Wearable Motherboard: The first generation of adaptive and responsive textile structures (ARTS) for medical applications. *Virtual Real* 1999; 4: 152–168.
- [120] Sahin O, Kayacan O, Bulgun EY. Smart textiles for soldier of the future. *Def Sci J* 2005; 55: 195–205.
- [121] Curone D, Secco EL, Tognetti A, et al. Smart garments for emergency operators: The ProeTEX project. *IEEE Trans Inf Technol Biomed* 2010; 14: 694–701.
- [122] Helmer RJN, Mestrovic MA, Farrow D, et al. Smart Textiles: Position and Motion Sensing for Sport, Entertainment and Rehabilitation. *Adv Sci Technol* 2009; 60: 144–153.
- [123] Radavičienė S, Jucienė M, Juchnevičienė Z, et al. Analysis of Shape Nonconformity between Embroidered Element and Its Digital Image. *Mater Sci* 2014; 20: 84–89.
- [124] Juchnevičienė Ž, Meškuotienė A, Jucienė M, et al. The evaluation of the uncertainty of the research method on the geometrical parameters of the embroidery elements. *J Text Inst* 2019; 110: 1202–1209.
- [125] Chui YT, Yang CX, Tong JH, et al. A systematic method for stability assessment of Ag-coated nylon yarn. *Text Res J* 2016; 86: 787–802.
- [126] Black S. 1 Trends in smart medical textiles. In: Van Langenhove L (ed) *Smart textiles for medicine and healthcare: Materials, systems and applications*. Cambridge: Woodhead Publishing Limited, 2007, pp. 3–26.

- [127] de Kok M, de Vries H, Pacheco K, et al. Failure modes of conducting yarns in electronic-textile applications. *Text Res J* 2015; 85: 1749–1760.
- [128] Audzevičiūtė-Liutkienė I, Masteikaitė V, Jucienė M, et al. Analysis of knitted fabrics deformations non-uniformity. *J Text Inst* 2019; 110: 1051–1058.
- [129] Swielam EM, Eltopshy SM, Sobhy SK, et al. Impact of the Fabrication Parameters on the Performance of Embroidered E-clothes. *Egypt J Chem* 2019; 62: 109–117.
- [130] Madeira. HC high conductive threads for industrial embroidery machines, <https://www.madeira.co.uk/embroidery-threads/hc/>.
- [131] H.MYERS RCM. 3. Two-level factorial designs. In: Balding DJ (ed) *Response surface methodology: process and product optimization using designed experiment*. New York: WALTER A. SHEWHART, 2016, pp. 81–160.
- [132] H.MYERS RCM. 7. Multiple response optimization. In: Balding DJ (ed) *Response surface methodology: process and product optimization using designed experiment*. New York: WALTER A. SHEWHART, 2016, pp. 325–368.
- [133] Guler SD. Chapter 4: Cutting and Sewing. In: Gannon M, Sicchio K (eds) *Crafting Wearables : Blending Technology with Fashion*. New York: Apress, 2016, pp. 33–44.
- [134] Baum TC, Ziolkowski RW, Ghorbani K, et al. Embroidered Active Microwave Composite Preimpregnated Electronics-Pregronics. *IEEE Trans Microw Theory Tech* 2016; 64: 3175–3186.
- [135] Wesley DS, Rengasamy RS. Changes in tensile properties of needle thread in lock stitch sewing. *Fibers Polym* 2017; 18: 390–399.
- [136] Kang SW, Choi H, Park H Il, et al. The development of an IMU integrated clothes for postural monitoring using conductive yarn and interconnecting technology. *Sensors* 2017; 17: 1–10.
- [137] Ghahremani M, Babaei M, Latifi M. Evaluating silver tracks conductivity on flexible surfaces. *J Ind Text* 2016; 46: 530–548.
- [138] Ruppert-Stroescu M, Balasubramanian M. Effects of stitch classes on the electrical properties of conductive threads. *Text Res J* 2017; 88: 2454–2463.
- [139] Kim I, Shahariar H, Ingram WF, et al. Inkjet Process for Conductive Patterning on Textiles: Maintaining Inherent Stretchability and Breathability in Knit Structures. *Adv Funct Mater* 2019; 29: 1–12.
- [140] Petersen P, Helmer R, Pate M, et al. Electronic textile resistor design and fabric resistivity characterization. *Text Res J* 2011; 81: 1395–1404.
- [141] Hsu YY, Gonzalez M, Bossuyt F, et al. In situ observations on deformation behavior

- and stretching-induced failure of fine pitch stretchable interconnect. *J Mater Res* 2009; 24: 3573–3582.
- [142] Norhidayah AA, Saad AA, Sharif MFM, et al. Stress Analysis of a Stretchable Electronic Circuit. *Procedia Eng* 2017; 184: 625–630.
- [143] Li X, Ruan X, Yao W, et al. Large-area, kirigami topology structure-induced highly stretchable and flexible interconnects: Directly printing preparation and mechanic mechanism. *Sci China Mater* 2019; 62: 1412–1422.
- [144] Fan JA, Yeo WH, Su Y, et al. Fractal design concepts for stretchable electronics. *Nat Commun* 2014; 5: 1–8.
- [145] Ma Q, Cheng H, Jang KI, et al. A nonlinear mechanics model of bio-inspired hierarchical lattice materials consisting of horseshoe microstructures. *J Mech Phys Solids* 2016; 90: 179–202.
- [146] Han S, Kim MK, Wang B, et al. Mechanically Reinforced Skin-Electronics with Networked Nanocomposite Elastomer. *Adv Mater* 2016; 28: 10257–10265.
- [147] Zhang Y, Fu H, Xu S, et al. A hierarchical computational model for stretchable interconnects with fractal-inspired designs. *J Mech Phys Solids* 2014; 72: 115–130.
- [148] Nasreldin M, Delattre R, Marchiori B, et al. Microstructured electrodes supported on serpentine interconnects for stretchable electronics. *APL Mater*; 7. Epub ahead of print 2019. DOI: 10.1063/1.5085160.
- [149] Bossuyt F, Vervust T, Vanfleteren J. Stretchable electronics technology for large area applications: Fabrication and mechanical characterization. *IEEE Trans Components, Packag Manuf Technol* 2013; 3: 229–235.
- [150] Vanfleteren J, Loehner T, Gonzalez M, et al. SCB and SMI: two stretchable circuit technologies, based on standard printed circuit board processes. *Circuit World* 2012; 38: 232–242.
- [151] Rahimi R, Ochoa M, Yu W, et al. A sewing-enabled stitch-and-transfer method for robust, ultra-stretchable, conductive interconnects. *J Micromechanics Microengineering* 2014; 24: 95018.
- [152] Rahimi R, Yu W, Parupudi T, et al. A low-cost fabrication technique for direct sewing stretchable interconnections for wearable electronics. *2015 Transducers - 2015 18th Int Conf Solid-State Sensors, Actuators Microsystems, TRANSDUCERS 2015* 2015; 1350–1353.
- [153] Li Q, Tao X. A stretchable knitted interconnect for three-dimensional curvilinear surfaces. *Text Res J* 2011; 81: 1171–1182.
- [154] Ramasamy S, Balan A. Wearable sensors for ECG measurement: a review. *Sens Rev*

- 2018; 38: 412–419.
- [155] Xu PJ, Zhang H, Tao X. Textile-structured electrodes for electrocardiogram. *Text Prog* 2008; 40: 183–213.
- [156] Coosemans J, Hermans B, Puers R. Integrating wireless ECG monitoring in textiles. *Sensors Actuators, A Phys* 2006; 130–131: 48–53.
- [157] Trindade IG, Martins F, Miguel R, et al. Design and Integration of Wearable Devices in Textiles. *Sensors & Transducers* 2014; 183: 42–47.
- [158] An X, Stylios G. A Hybrid Textile Electrode for Electrocardiogram (ECG) Measurement and Motion Tracking. *Materials (Basel)* 2018; 11: 1887.
- [159] Marozas V, Petrenas A, Daukantas S, et al. A comparison of conductive textile-based and silver/silver chloride gel electrodes in exercise electrocardiogram recordings. *J Electrocardiol* 2011; 44: 189–194.
- [160] Beckmann L, Neuhaus C, Medrano G, et al. Characterization of textile electrodes and conductors using standardized measurement setups. *Physiol Meas* 2010; 31: 233–247.
- [161] Taji B, Chan ADC, Shirmohammadi S. Effect of Pressure on Skin-Electrode Impedance in Wearable Biomedical Measurement Devices. *IEEE Trans Instrum Meas* 2018; 67: 1900–1912.
- [162] Cho H, Lee JH. A Study on the Optimal Positions of ECG Electrodes in a Garment for the Design of ECG-Monitoring Clothing for Male. *J Med Syst*; 39. Epub ahead of print 2015. DOI: 10.1007/s10916-015-0279-2.
- [163] Joutsen AS, Kaappa ES, Karinsalo TJ, et al. Dry electrode sizes in recording ECG and heart rate in wearable applications. In: *IFMBE Proceedings*. FINLAND: SPRINGER-VERLAG PTE LTD, 2017, pp. 735–738.
- [164] Assambo C, Baba A, Dozio R, et al. Determination of the parameters of the skin-electrode impedance model for ECG measurement. In: *Proceedings of the 6th WSEAS International Conference on Electronics Hardware Wireless and Optical Communications*. 2007, pp. 90–95.
- [165] Yapici MK, Alkhidir T, Samad YA, et al. Graphene-clad textile electrodes for electrocardiogram monitoring. *Sensors Actuators, B Chem* 2015; 221: 1469–1474.
- [166] Celik N, Manivannan N, Strudwick A, et al. Graphene-Enabled Electrodes for Electrocardiogram Monitoring. *Nanomaterials* 2016; 6: 156.
- [167] Medrano G, Ubl A, Zimmermann N, et al. Skin Electrode Impedance of Textile Electrodes for Bioimpedance Spectroscopy. *13th Int Conf Electr Bioimpedance 8th Conf Electr Impedance Tomogr* 2007; 260–263.

- [168] Xiong F, Chen D, Chen Z, et al. Impedance Characteristics of the Skin-Electrode Interface of Dry Textile Electrodes for Wearable Electrocardiogram. In: Fortino G, Wang Z (eds) *Advances in Body Area Networks I*. Cham: Springer International Publishing, 2017, pp. 343–356.
- [169] Tadesse MG, Harpa R, Chen Y, et al. Assessing the comfort of functional fabrics for smart clothing using subjective evaluation. *J Ind Text* 2018; 1–17.
- [170] Thiel D V. 4 Statistical analysis. In: *Research Methods for Engineers*. CAMBRIDGE UNIVERSITY PRESS, 2014, pp. 114–155.
- [171] Albulbul A, Chan ADC. Electrode-skin impedance changes due to an externally applied force. In: *MeMeA 2012 - 2012 IEEE Symposium on Medical Measurements and Applications, Proceedings*. IEEE, 2012, pp. 61–64.
- [172] Taji B, Shirmohammadi S, Groza V. Measuring skin-electrode impedance variation of conductive textile electrodes under pressure. In: *Conference Record - IEEE Instrumentation and Measurement Technology Conference*. 2014, pp. 1083–1088.
- [173] Decaens J, Vermeersch O. 12 Specific testing for smart textiles. In: *Advanced Characterization and Testing of Textiles*. Elsevier Ltd., 2018, pp. 351–374.
- [174] Blau PJ. The significance and use of the friction coefficient. *Tribol Int* 2001; 34: 585–591.
- [175] De Luca G, Johansson A, Roy SH, et al. Sweat Test for Electro-mechanical Stability of the EMG Electrode-skin Interface.
- [176] Daňová R, Olejnik R, Slobodian P, et al. The piezoresistive highly elastic sensor based on carbon nanotubes for the detection of breath. *Polymers (Basel)*; 12. Epub ahead of print 2020. DOI: 10.3390/polym12030713.
- [177] Chu M, Nguyen T, Pandey V, et al. Respiration rate and volume measurements using wearable strain sensors. *npj Digit Med* 2019; 2: 1–9.
- [178] Li XA, Stepaniak C, Gore E. Technical and dosimetric aspects of respiratory gating using a pressure-sensor motion monitoring system. *Med Phys* 2006; 33: 145–154.
- [179] Brady S, Dunne LE, Tynan R, et al. Garment-based monitoring of respiration rate using a foam pressure sensor. In: *Ninth IEEE International Symposium on Wearable Computers (ISWC'05)*. 2005, pp. 214–215.
- [180] Guay P, Gorgutsa S, LaRochelle S, et al. Wearable Contactless Respiration Sensor Based on Multi-Material Fibers Integrated into Textile. *SENSORS*; 17. Epub ahead of print 2017. DOI: 10.3390/s17051050.
- [181] Fobelets K. Knitted coils as breathing sensors. *Sensors Actuators, A Phys* 2020; 306: 111945.

- [182] Liu Y, Wang M, Yu M, et al. Embroidered Inductive Strain Sensor for Wearable Applications. In: *2020 IEEE International Conference on Pervasive Computing and Communications Workshops, PerCom Workshops 2020*. 2020, pp. 12–17.
- [183] Jiang P, Zhao S, Zhu R. Smart Sensing Strip Using Monolithically Integrated Flexible Flow Sensor for Noninvasively Monitoring Respiratory Flow. *Sensors* 2015; 15: 31738–31750.
- [184] Dinh T, Phan H-P, Nguyen T-K, et al. Solvent-free fabrication of biodegradable hot-film flow sensor for noninvasive respiratory monitoring. *J Phys D Appl Phys* 2017; 50: 215401.
- [185] Kwon S, Kwon Y-T, Kim Y-S, et al. Skin-conformal, soft material-enabled bioelectronic system with minimized motion artifacts for reliable health and performance monitoring of athletes. *Biosens Bioelectron* 2020; 151: 111981.
- [186] Folke M, Cernerud L, Ekström M, et al. Critical review of non-invasive respiratory monitoring in medical care. *Med Biol Eng Comput* 2006; 41: 377–383.
- [187] Araromi OA, Graule MA, Dorsey KL, et al. Ultra-sensitive and resilient compliant strain gauges for soft machines. *Nature* 2020; 587: 219–224.
- [188] Myers RH. 6. THE ANALYSIS OF SECOND-ORDER RESPONSE SURFACES. In: *Response Surface Methodology: Process and Product Optimization Using Designed Experiments*. John Wiley & Sons, Inc., 2016, pp. 273–324.
- [189] Li T, Wang X, Jiang S, et al. Study on electromechanical property of polypyrrole-coated strain sensors based on polyurethane and its hybrid covered yarns. *Sensors Actuators, A Phys* 2020; 306: 111958.
- [190] Wang X, Meng S, Tebyetekerwa M, et al. Highly sensitive and stretchable piezoresistive strain sensor based on conductive poly(styrene-butadiene-styrene)/few layer graphene composite fiber. *Compos Part A Appl Sci Manuf* 2018; 105: 291–299.
- [191] Holm R. *Electric contacts; theory and application*. 4th ed. New York: NY, USA: Springer-Verlag, 1967.
- [192] Park S, Jayaraman S. The wearables revolution and Big Data: the textile lineage. *J Text Inst* 2017; 108: 605–614.
- [193] Gao W, Emaminejad S, Nyein HYY, et al. Fully integrated wearable sensor arrays for multiplexed in situ perspiration analysis. *Nature* 2016; 529: 509–514.
- [194] Paradiso R, Loriga G, Taccini N. A wearable health care system based on knitted integrated sensors. *IEEE Trans Inf Technol Biomed* 2005; 9: 337–344.
- [195] Yetisen AK, Martinez-Hurtado JL, Ünal B, et al. Wearables in Medicine. *Adv Mater* 2018; 30: 1–26.

- [196] Khan Y, Ostfeld AE, Lochner CM, et al. Monitoring of Vital Signs with Flexible and Wearable Medical Devices. *Adv Mater* 2016; 28: 4373–4395.
- [197] Chen X, Liu A, Wei Z, et al. Experimental study on strain reliability of embroidered passive UHF RFID textile tag antennas and interconnections. *J Eng (United States)*; 2017. Epub ahead of print 2017. DOI: 10.1155/2017/8493405.
- [198] Noda A, Shinoda H. Frequency-division-multiplexed signal and power transfer for wearable devices networked via conductive embroideries on a cloth. *IEEE MTT-S Int Microw Symp Dig* 2017; 537–540.
- [199] Ankhili A, Tao X, Cochrane C, et al. Washable and reliable textile electrodes embedded into underwear fabric for electrocardiography (ECG) monitoring. *Materials (Basel)* 2018; 11: 1–11.
- [200] Peng HL, Liu JQ, Dong YZ, et al. Parylene-based flexible dry electrode for bio-potential recording. *Sensors Actuators, B Chem* 2016; 231: 1–11.
- [201] Pani D, Dessi A, Saenz-Cogollo JF, et al. Fully Textile, PEDOT:PSS Based Electrodes for Wearable ECG Monitoring Systems. *IEEE Trans Biomed Eng* 2016; 63: 540–549.
- [202] Gwon D, Cho H, Shin H. Feasibility of a waistband-type wireless wearable electrocardiogram monitoring system based on a textile electrode: Development and usability study. *JMIR mHealth uHealth* 2021; 9: 1–16.
- [203] Lee J, Heo J, Lee W, et al. Flexible Capacitive Electrodes for Minimizing Motion Artifacts in Ambulatory Electrocardiograms. *Sensors* 2014; 14: 14732–14743.

APPENDICES

Appendix 1. Data of conductive tracks embroidered with HC 12 and HC 40 for performance evaluation

ES	SL	NTP		ED	Size Shrinkage (%)		Electrical resistance (Ohm/10 cm)		Floated stitch numbers (number/10 cm)	
		HC12	HC 40		HC 12	HC 40	HC 12	HC 40	HC 12	HC 40
200	1.5	30	20	Wale	2.22	3.89	21.25	110.35	5.68	5.20
600	1.5	30	20	Wale	2.78	3.89	21.49	120.40	3.43	15.03
200	4	30	20	Wale	3.33	3.89	12.64	57.69	0.00	0.58
600	4	30	20	Wale	3.33	5.00	12.36	81.40	0.00	7.60
200	1.5	50	40	Wale	3.89	2.22	21.56	58.86	0.00	0.00
600	1.5	50	40	Wale	1.11	3.33	25.06	76.32	0.00	0.00
200	4	50	40	Wale	5.00	2.78	12.46	60.11	0.00	0.00
600	4	50	40	Wale	3.89	3.33	23.82	93.16	0.00	0.00
200	1.5	30	20	Course	6.00	3.00	21.70	105.46	10.64	6.19
600	1.5	30	20	Course	5.00	5.00	23.58	128.74	21.05	8.42
200	4	30	20	Course	5.00	5.00	11.26	68.00	3.16	1.05
600	4	30	20	Course	4.00	7.00	12.50	89.89	3.13	3.23
200	1.5	50	40	Course	3.00	7.00	23.40	77.74	0.00	0.00
600	1.5	50	40	Course	7.00	6.00	27.10	153.51	0.00	0.00
200	4	50	40	Course	5.00	8.00	14.74	95.00	0.00	0.00
600	4	50	40	Course	7.00	7.00	22.37	81.29	0.00	0.00
200	1.5	30	20	Wale	3.33	1.67	21.03	94.58	1.15	13.56
600	1.5	30	20	Wale	2.22	1.67	20.97	76.67	1.14	0.00
200	4	30	20	Wale	3.89	2.78	11.68	67.66	0.00	0.57
600	4	30	20	Wale	4.44	2.78	12.62	57.83	0.00	0.00
200	1.5	50	40	Wale	3.33	2.78	22.82	74.23	0.00	0.00
600	1.5	50	40	Wale	2.78	2.78	26.11	93.60	0.00	0.00
200	4	50	40	Wale	3.89	3.89	15.61	44.80	0.00	0.00
600	4	50	40	Wale	5.00	3.33	14.97	69.43	0.00	0.00
200	1.5	30	20	Course	7.00	7.00	22.37	85.48	12.90	4.30
600	1.5	30	20	Course	6.00	7.00	23.94	76.56	10.64	3.23
200	4	30	20	Course	7.00	5.00	12.15	64.95	2.15	0.00
600	4	30	20	Course	6.00	5.00	12.13	49.26	2.13	0.00
200	1.5	50	40	Course	6.00	6.00	28.30	92.87	3.19	0.00
600	1.5	50	40	Course	4.00	5.00	26.25	113.26	0.00	0.00
200	4	50	40	Course	5.00	6.00	14.53	54.68	0.00	0.00
600	4	50	40	Course	5.00	6.00	17.26	79.68	0.00	0.00
200	1.5	30	20	Wale	2.22	0.56	19.09	88.32	2.84	14.53
600	1.5	30	20	Wale	1.67	0.56	20.96	77.54	0.00	2.23
200	4	30	20	Wale	2.78	1.67	10.40	55.54	0.00	0.00
600	4	30	20	Wale	2.78	3.89	11.26	51.73	0.00	0.58

200	1.5	50	40	Wale	2.78	1.11	20.74	80.73	0.00	0.00
600	1.5	50	40	Wale	1.67	2.22	24.92	103.07	0.00	0.00
200	4	50	40	Wale	4.44	3.33	12.91	59.89	0.00	0.00
600	4	50	40	Wale	3.89	3.33	13.99	60.52	0.00	0.00
200	1.5	30	20	Course	6.00	8.00	21.81	72.50	8.51	2.17
600	1.5	30	20	Course	7.00	7.00	23.98	96.56	5.38	2.15
200	4	30	20	Course	6.00	9.00	12.98	59.67	0.00	0.00
600	4	30	20	Course	8.00	8.00	12.72	62.07	0.00	0.00
200	1.5	50	40	Course	5.00	8.00	26.95	92.07	0.00	0.00
600	1.5	50	40	Course	7.00	2.00	27.10	100.82	0.00	0.00
200	4	50	40	Course	7.00	8.00	15.38	83.04	0.00	0.00
600	4	50	40	Course	8.00	4.00	15.76	79.27	0.00	0.00
400	2.75	40	30	Wale	3.33	4.44	15.92	108.31	0.00	0.00
400	2.75	40	30	Course	6.00	8.00	12.77	99.13	0.00	0.00
400	2.75	40	30	Wale	2.22	5.00	12.90	64.85	0.00	0.00
400	2.75	40	30	Course	7.00	5.00	14.62	65.37	0.00	0.00
400	2.75	40	30	Wale	4.44	4.72	12.44	86.94	0.00	0.00
400	2.75	40	30	Course	4.00	9.00	13.44	79.89	3.13	0.00
400	2.75	40	30	Wale	3.33	3.33	12.59	79.08	0.00	0.00
400	2.75	40	30	Course	6.00	8.00	13.51	67.61	2.13	0.00

Appendix 2. Resistance of conductive tracks for interconnects with HC 12 and HC 40

Factors			Resistance (Ohm/m)	
A	B	C	HC 12	HC 40
301	Needle	1	118.519	674.332
301	Needle	3	110.337	558.653
301	Bobbin	1	63.636	196.244
301	Bobbin	3	75.587	307.656
301	Both	1	40.518	171.724
301	Both	3	41.315	146.296
304	Needle	1	184.901	920.185
304	Needle	3	160.648	698.039
304	Bobbin	1	65.962	180.000
304	Bobbin	3	67.606	263.146
304	Both	1	46.528	151.389
304	Both	3	50.231	172.454
308	Needle	1	179.254	917.931
308	Needle	3	165.621	730.796
308	Bobbin	1	63.369	212.311
308	Bobbin	3	68.779	288.502
308	Both	1	47.356	138.391
308	Both	3	47.945	179.108

Appendix 3. Mechanical and electrical data of zigzag-shaped interconnects

Arm length	Opening angle	Strain at change of force (%)	Strain at breaking (%)	Breaking force (N)	Electrical resistance before change (Ohm/m)	Strain at change of resistance (%)	E1	E2	ER1	ER2
2	45	8.642	28.610	30.680	45.833	11.754	0.196	1.512	0.282	10.560
4	45	17.926	39.360	28.930	44.167	18.736	0.076	1.332	0.203	6.587
2	60	42.215	67.810	31.190	56.667	45.533	0.099	1.042	0.091	5.572
4	60	75.581	104.920	28.300	58.333	83.205	0.058	0.783	0.109	2.636
2	45	13.226	30.510	31.140	46.667	10.929	0.126	1.750	0.092	7.730
4	45	13.922	37.770	30.890	48.333	9.157	0.074	1.288	0.101	5.412
2	60	32.235	55.380	28.680	56.667	25.176	0.078	1.131	0.016	4.887
4	60	49.006	72.480	28.680	59.167	45.575	0.066	1.105	0.028	4.821
2	45	11.170	29.560	30.910	47.500	10.519	0.155	1.641	0.286	7.655
4	45	16.170	38.565	29.910	45.000	10.286	0.086	1.324	0.131	5.951
2	60	38.556	61.595	29.935	57.500	32.534	0.091	1.165	0.020	5.041
4	60	62.600	88.700	28.490	65.000	54.554	0.057	0.956	0.025	3.758

Appendix 4. Mechanical and electrical data of horseshoe-shaped interconnects

Inner radius	Turning angle	Strain at change of force (%)	Strain at breaking (%)	Breaking force (N)	Electrical resistance before change (Ohm/m)	Strain at change of resistance (%)	E1	E2	ER1	ER2
5	0	41.435	73.240	43.025	82.500	58.885	0.113	1.162	0.006	5.617
10	0	55.216	90.160	51.443	89.167	65.776	0.077	1.575	0.009	8.924
5	45	122.323	187.210	73.925	148.333	138.440	0.089	0.950	0.001	0.854
10	45	113.355	174.020	84.710	165.000	129.839	0.106	1.181	0.001	1.118
5	0	43.164	71.530	41.865	75.000	45.881	0.082	1.351	0.001	11.248
10	0	55.452	91.800	52.677	90.000	62.654	0.086	1.579	0.003	10.685
5	45	121.103	195.080	86.420	145.833	126.680	0.102	1.053	0.000	0.899
10	45	111.726	170.600	78.470	159.167	125.329	0.128	1.089	0.010	1.404
5	0	39.871	72.385	42.445	74.167	46.112	0.093	1.142	0.004	10.620
10	0	54.284	90.980	52.060	76.667	62.300	0.081	1.498	0.003	10.764
5	45	112.889	191.145	80.172	148.333	116.619	0.096	0.855	0.001	0.842
10	45	106.870	172.310	81.590	160.000	121.114	0.118	1.014	0.010	1.493

Appendix 5. Contact impedance at 1 Hz of embroidered electrodes

Factors				Contact impedance at 1 Hz	Factors				Contact impedance at 1 Hz	Factors				Contact impedance at 1 Hz
A	B	C	D		A	B	C	D		A	B	C	D	
4	1	1	301	801655.5	4	1	1	301	1718616.5	4	1	1	301	2144343.5
8	1	1	301	377601.4	8	1	1	301	475049.3	8	1	1	301	299080.85
4	2	1	301	845624	4	2	1	301	1448958.5	4	2	1	301	1215736.5
8	2	1	301	735371	8	2	1	301	1401523.5	8	2	1	301	1972084.5
4	1	2	301	3917651	4	1	2	301	4239252	4	1	2	301	4143387
8	1	2	301	2251122.5	8	1	2	301	2296248.5	8	1	2	301	2298172.5
4	2	2	301	4810589.5	4	2	2	301	4698132.5	4	2	2	301	4940128.5
8	2	2	301	2803199.5	8	2	2	301	2759207.5	8	2	2	301	2628456
4	1	1	304	665125.5	4	1	1	304	405350.55	4	1	1	304	1224353
8	1	1	304	817725	8	1	1	304	1314841.5	8	1	1	304	1623196
4	2	1	304	2307216	4	2	1	304	2815632.5	4	2	1	304	3055908
8	2	1	304	1737773	8	2	1	304	1713728.5	8	2	1	304	1879667
4	1	2	304	2787853.5	4	1	2	304	3024436.5	4	1	2	304	3010282
8	1	2	304	1476182.5	8	1	2	304	1477943	8	1	2	304	1513774.5
4	2	2	304	2933133	4	2	2	304	3429052.5	4	2	2	304	3336878.5
8	2	2	304	1817069	8	2	2	304	1890317.5	8	2	2	304	1877545.5

Appendix 6. Coefficient of friction and resistance of embroidered electrodes

Applied Force	Electrodes Type	SCF	DCF	Resistance (Ohm/m)	Applied Force	Electrodes Type	SCF	DCF	Resistance (Ohm/m)
0.5 kPa	EP1	0.765	0.637	3	1.5 kPa	EP3	0.552	0.340	4.4
0.5 kPa	EP2	1.020	0.701	3.5	1.5 kPa	EP4	0.680	0.595	5.1
0.5 kPa	EP3	1.020	0.765	4.3	2.5 kPa	EP1	0.510	0.408	3.5
0.5 kPa	EP4	1.020	0.637	6	2.5 kPa	EP2	0.561	0.459	2.8
1.5 kPa	EP1	0.340	0.297	3.3	2.5 kPa	EP3	0.561	0.408	4.4
1.5 kPa	EP2	0.552	0.510	3.4	2.5 kPa	EP4	0.612	0.408	4.6
1.5 kPa	EP3	0.510	0.404	4.3	0.5 kPa	EP1	0.714	0.765	3.2
1.5 kPa	EP4	0.595	0.510	5.5	0.5 kPa	EP2	1.020	0.765	3.5
2.5 kPa	EP1	0.459	0.357	3.1	0.5 kPa	EP3	1.147	0.765	4.2
2.5 kPa	EP2	0.459	0.446	2.8	0.5 kPa	EP4	1.020	0.765	6.7
2.5 kPa	EP3	0.459	0.382	4.2	1.5 kPa	EP1	0.382	0.340	3.1
2.5 kPa	EP4	0.510	0.446	5.2	1.5 kPa	EP2	0.595	0.510	3.3
0.5 kPa	EP1	0.841	0.510	3.4	1.5 kPa	EP3	0.595	0.425	4.4
0.5 kPa	EP2	0.765	0.637	3.6	1.5 kPa	EP4	0.637	0.425	5.3
0.5 kPa	EP3	0.969	0.765	4.3	2.5 kPa	EP1	0.510	0.306	3.3
0.5 kPa	EP4	1.071	0.765	6.8	2.5 kPa	EP2	0.561	0.459	2.8
1.5 kPa	EP1	0.382	0.340	3	2.5 kPa	EP3	0.612	0.357	4.2
1.5 kPa	EP2	0.595	0.425	3.2	2.5 kPa	EP4	0.612	0.459	4.9

Appendix 7. Coefficient of friction and resistance of embroidered electrodes

Width of conductive area (mm)	Filling density of conductive yarns (mm)	Filling density of elastane threads (mm)	Gauge Factor	Elasticity Coefficient	Maximum strain (%)	Response time (s)
5	0.3	2	30.56	5.51	13.3	4
15	0.3	2	32.71	6.203	13.3	4
5	0.7	2	13.01	5.2	10	3
15	0.7	2	27.63	4.757	11.7	3.5
5	0.5	1.5	19.75	8.085	11.7	3.5
15	0.5	1.5	37.87	10.252	35	10.5
5	0.5	2.5	17.91	3.871	11.7	3.5
15	0.5	2.5	20.51	3.371	25	7.5
10	0.3	1.5	28.78	5.755	16.7	5
10	0.7	1.5	23.86	7.421	13.33	4
10	0.3	2.5	21.46	4.304	15	4.5
10	0.7	2.5	18.6	3.885	10	3
10	0.5	2	25.81	4.866	23.33	7
10	0.5	2	31.54	4.912	20	6
10	0.5	2	29.25	4.78	20	6